JAERI-M
93-047

JAERI TIARA ANNUAL REPORT Vol. I(1992)

APRIL 1991 - MARCH 1992

March 1993

Department of Advanced Radiation Technology

日本原子力研究所
Japan Atomic Energy Research Institute

JAERI-Mレポートは，日本原子力研究所が不定期に公刊している研究報告書です。
入手の問合わせは，日本原子力研究所技術情報部情報資料課（〒319－11茨城県那珂郡東海村）あて，お申しこしください。なお，このほかに財団法人原子力弘済会資料センター（〒319-11茨城県那珂郡東海村日本原子力研究所内）で複写による実費頒布をおこなっております。

JAERI-M reports are issued irregularly.
Inquiries about availability of the reports should be addressed to Information Division, Department of Technical Information, Japan Atomic Energy Research Institute, Tokai-mura, Naka-gun, Ibaraki-ken 319-11, Japan.

編集兼発行　日本原子力研究所
印　　刷　日立高速印刷株式会社

JAERI-M 93-047

JAERI TIARA Annual Report Vol. 1 (1992)
April 1991 - March 1992

Department of Advanced Radiation Technology

Takasaki Radiation Chemistry Research Establishment
Japan Atomic Energy Research Institute
Watanuki-cho, Takasaki-shi, Gunma-ken

(Received February 5, 1993)

This annual report describes research activities which have been performed with the JAERI TIARA (Takasaki Ion Accelerators for Advanced Radiation Application) facilities from April 1, 1991 to March 31, 1992, and also gives an outline of the ion accelerators and surrounding apparatus which have been constructed and prepared for various experiments.

As well as an outline of the characteristics of AVF cyclotron, 3 MV tandem electrostatic accelerator and other ones, included are 25 summary reports on preparation of experimental apparatus and on the preliminary results of experimental studies using the 3 MV tandem accelerator in the different research fields of beam technology, materials for space environment and nuclear fusion reactor, organic and inorganic functional materials, biology, medicine, radiation chemistry, radioisotope production and nuclear chemistry. Lists of publication, staff of TIARA and cooperated researchers are also given.

Keywords : JAERI TIARA, Ion Accelerators, Solid State Physics, Radiation Effects in Materials, Materials for Space, Nuclear Fusion Reactor, Functional Materials, Radiation Chemistry, Radiation Biology, Nuclear Medicine, Biotechnology, Radioisotope Production, Nuclear Chemistry

---

Editors : Isao Ishigaki, Isamu Nashiyama, Hiroshi Naramoto, Hideki Omichi
Ryuichi Tanaka, Hiromasa Watanabe, Hiroshi Watanabe

JAERI-M 93-047

原研イオン照射研究施設平成3年度年次報告

日本原子力研究所高崎研究所
放射線高度利用研究推進室

(1993年2月5日受理)

本年次報告は，原研イオン照射研究施設で，1991年4月1日から1992年3月31日までの間に行われた研究活動，及び本施設で整備が進められてきたイオン加速器設備や内装実験装置の概要をまとめたものである。

AVFサイクロトロン，タンデム型静電加速器等の設備と性能の概要とともに，ビーム技術，宇宙環境・核融合炉用材料，有機及び無機新機能材料，生物・医学，放射線化学，ラジオアイソトープ製造・核化学の分野にわたる25編の実験装置整備やタンデム加速器について先行した利用実験研究の報告，公表された文献，TIARAのスタッフ，協力者等のリスト，並びに共同研究及び協力研究のリストを収録する。

高崎研究所：〒370－12 群馬県高崎市綿貫町1233

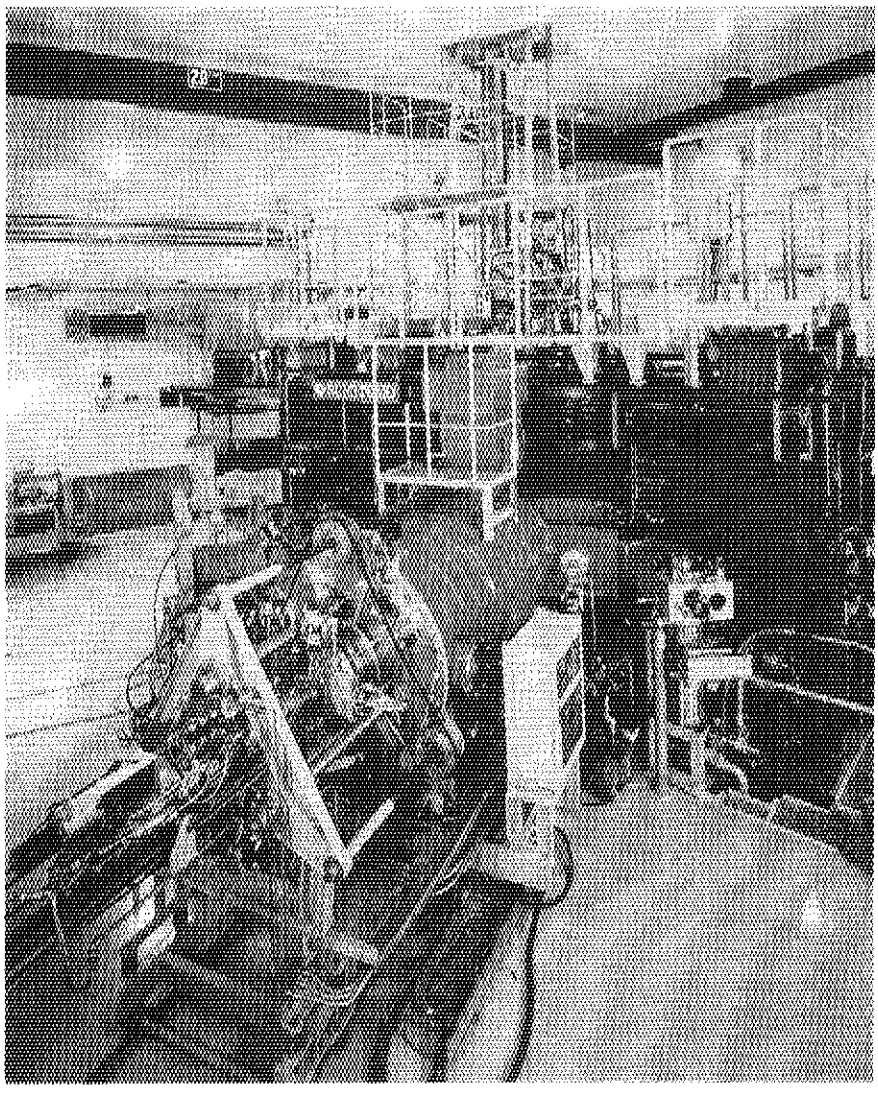

JAERI AVF Cyclotron

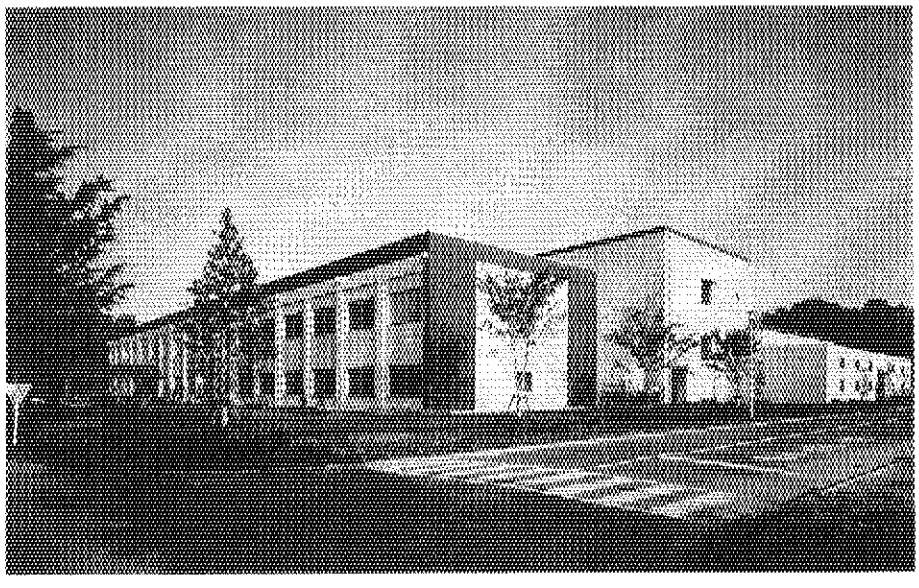

TIARA Facilities

PREFACE

It is our great pleasure to publish the first issue of the "TIARA Annual Report". We sincerely hope that this series of report will grow into a prosperous "tiara" decorated with many valuable fruits of the facilities.

The TIARA facilities (Takasaki Ion Accelerators for Advanced Radiation Application) have been constructed at the Takasaki Radiation Chemistry Research Establishment under the 6-year program from 1987. The first phase of the construction including those of an AVF cyclotron and a 3 MV tandem accelerator was completed in October 1991.

The planning of the facilities and the research program have been made on the base of discussions at "Consultative Committee for the Advanced Radiation Technology" chaired by the late Professor Keichi Oshima, who was succeeded by Professor Yoneho Tabata, and at six subcommittees. The members of the committee and subcommittees have been authorities from universities, national and public research institutes and industries, in addition to the members from JAERI. I wish to express sincere thanks to all members for their earnest discussions.

Appreciation should also be extended to members of 19 "Advisory Groups" who all actively cooperated in planning of each research subject and designing of experimental apparatus such as target chambers and measuring instruments for various research fields.

This first issue of the annual report covers the outline and the results of test operation of accelerator facilities, the preparation of experimental apparatus in TIARA, and preliminary results of research activities on materials science. The research activities made use of the TIARA facilities in the test operation stage, operated by JAERI staff and some of the researchers from other institutions until March 1992, although official start of the joint research was in April 1992.

We appreciate also advices of the "TIARA Program Committee", which was organized in October 1991 for investigating research proposals, experimental plans and schedule of the accelerator operations.

Shoichi Sato
Director General
Takasaki Radiation Chemistry
Research Establishment

Contents

1. AVF CYCLOTRON

Kazuo ARAKAWA, Yoshiteru NAKAMURA, Watalu YOKOTA,
Mitsuhiro FUKUDA, Takayuki NARA, Takashi AGEMATSU,
Susumu OKUMURA, Ikuo ISHIBORI, Tomihiro KAMIYA,
Ryuichi TANAKA, Toshiki TACHIKAWA*, Keizou HOSHIKA*,
Masanori TACHIBANA*, Yukio KUMATA*, Yoshihiro HAYASHI*,
Koichi ISHII*, Masami SANO*, Keiji ISO*, Tsuneo TORII**,
Kazuyuki SUZUKI**, Junki SAGAWA** and Tsuneyuki TONOOKA**

Ion Accelerator Division, JAERI, *Sumitomo Heavy Industries,Ltd.,
**Hitachi,Ltd.

1.1 Introduction

Large AVF cyclotrons have been used mostly for fundamental nuclear physics and medical application to radiation therapy and radioisotope production so far. The JAERI AVF cyclotron[1,2] is the first one dedicated to R & D in materials science and other irradiation purposes. The cyclotron facility was planned mainly on the basis of valuable experience in accelerator development and parasitic beam utilization which have been accumulated in accelerator facilities for research of fundamental physics.

The application of the cyclotron to various fields of R & D in materials science requires acceleration of ion particles in wide ranges of mass and energy. Recent development of electron cyclotron resonance(ECR) type ion sources and the axial beam injection system allowed to meet the requirement considerably. Cyclotron operation in high harmonic modes also allowed to extend the lower limit of the acceleration energy for heavy ions.

The above application also requires a wide variety of beam utilization such as uniform irradiation of high-energy and high-intensity beams over a wide area, pulsed beam irradiation by beam chopping, a wide range of beam intensity, secondary produced neutron beams, etc.. Some of these additional functions were already satisfied at the commissioning stage, and the other ones were under development.

The dedication to R & D in materials science also requires easy control and efficient operation of the accelerators and reproducible setting of beam parameters. Computer control and assist systems are expected to play an important role to fulfill these requirements.

This chapter describes the AVF cyclotron system and the result of the test performance and the first year's operation.

REFERENCES

1) R.Tanaka, K.Arakawa, W.Yokota, Y.Nakamura, T.Kamiya, M.Fukuda, T.Agematsu, H.Watanabe, N.Akiyama, S.Tanaka, T.Nara, M.Hagiwara, S.Okada and M. Maruyama, "JAERI AVF Cyclotron for Research of Advanced Radiation Technology," presented at the 12th International Conference on Cyclotrons and Their Applications, Berlin, Germany, May 8-12, 1989.

2) K.Arakawa, Y.Nakamura, W.Yokota, M.Fukuda, T.Nara, T.Agematsu, S.Okumura, I.Ishibori, T.Karasawa, R.Tanaka, A.Shimizu, T.Tachikawa, Y.Hayashi, K.Ishii and T.Satoh, "Construction and First Year's Operation of the JAERI AVF cyclotron," presented at the 13th International Conference on Cyclotrons and Their Applications, Vancouver, Canada, July 6-10, 1992.

1.2 AVF Cyclotron

I. DESIGN AND CONSTRUCTION

(1) General description

The JAERI AVF cyclotron is of the model 930 of Sumitomo Heavy Industries, Ltd.(SHI), the same model as the CYCLONE (Universite Catholique de Louvain, BELGIUM), the IRE cyclotron (Institut National des Radioelements, BELGIUM) and the NIRS-Chiba cyclotron (National Institute of Radiological Sciences, JAPAN). The latter three cyclotrons have movable-panel type resonators with a peak rf voltage of 50 kV. The JAERI cyclotron employed a movable-short type resonator in order to make allowance for generating a higher maximum dee voltage of 60 kV, which is required for accelerating 90 MeV protons in the constant-orbit mode.

In order to meet technical requirements in the research plan of the ART(Advanced Radiation Technology) project, we modified or improved the design of the accelerator system as follows; 1) The system is equipped with two external ion sources,[1] an ECR source for generating heavy ions and a multicusp source for generating light ions. 2) The system is equipped with a beam chopping system[2] for pulsed beam operation and beam scanning systems for uniform irradiation to the wide area of target samples. 3) A distributed computer control system is introduced for rapid and reliable control of operation parameters.[3] 4) In order to reduce the radiation exposure of operators, the cyclotron is equipped with automatic changing systems for inflector and puller electrodes. A remote controlled conveying system makes a deflector remove from the cyclotron and guide to a cooling room.

At the end of 1986 it was approved by the Science and Technology Agency to construct a medium scale cyclotron for multipurposes and its accommodations at JAERI Takasaki in the period of 1987-1992 fiscal years.

The construction of the cyclotron was started in 1988. The field mapping for the main magnet was carried out from December 1988 to March 1989 and the performance of the rf system[4] was tested from October 1989 to March 1990 at the Niihama works of SHI. The cyclotron was installed at JAERI, Takasaki, in July 1990. The beam generation test has been started from March 1991.

(2) Outline of AVF cyclotron

Figure 1 shows a photograph of the cyclotron. A schematic drawing of the cyclotron is shown in Fig. 2 and the major characteristics of the JAERI AVF cyclotron are shown in Table 1.

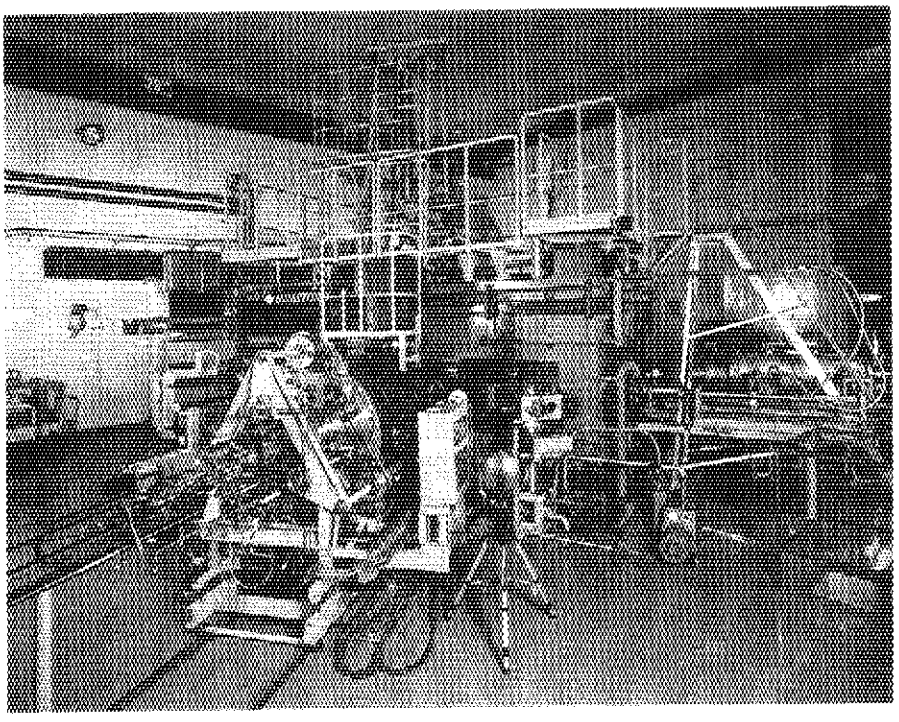

Fig.1 Photograph of the JAERI AVF cyclotron.

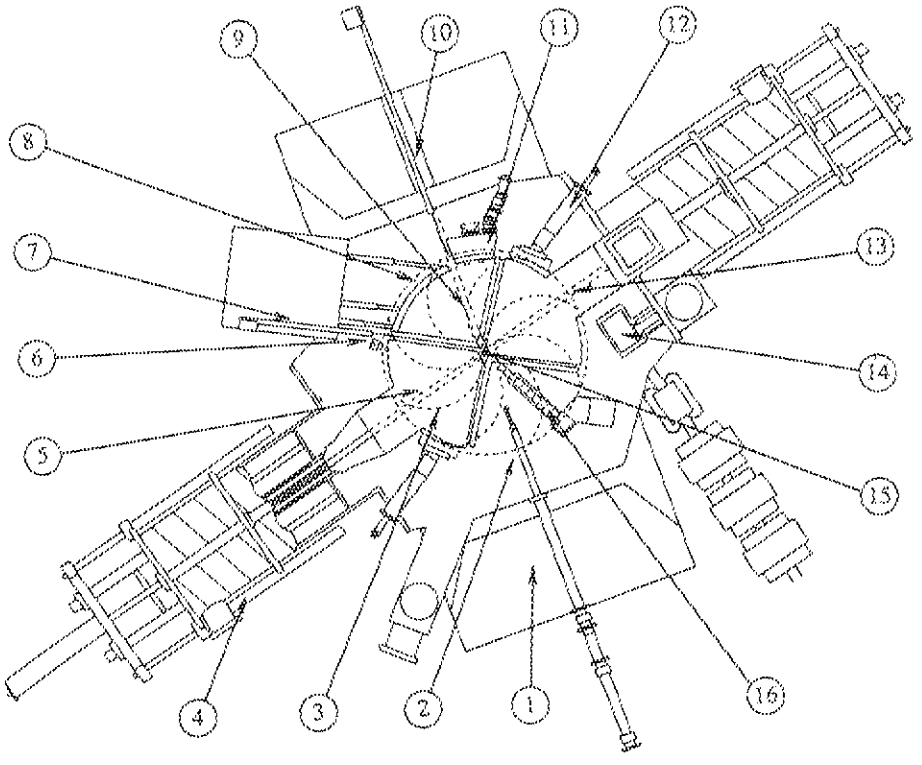

Fig.2 Schematic drawing of the cyclotron. (1)Yoke, (2)Main radial probe, (3)Spiral sector, (4)Resonator, (5)Puller, (6)Dee voltage pickup, (7)Deflector probe, (8)Deflector, (9)Phase slit II, (10)Magnetic channel probe, (11)Magnetic channel, (12)Capacitive fine frequency tuner, (13)Phase slit I, (14)Gradient corrector, (15)Inflector, (16)Phase probe.

Table 1 Parameters of JAERI AVF cyclotron.

MAGNET	
Maximum average field	16.7 kG at extraction radius
Maximum hill field	20.4 kG
Number of sectors	4
Spiral angle in degrees	53°
Number of circular trim coils	12 pairs
Number of harmonic coils	8 pairs (4 pairs in central region) (4 pairs in extraction region)
Magnet size	5.19 m long, 2.31 m wide, 2.6 m high
Magnet weight	229 ton
Extraction radius	923 mm
Power,maximum	
Main coils	250 kW
Trim coils	52 kW
Maximum main coil current	900 A
Pole diameter	2156 mm
Pole gap	405 mm
Sector gap	166 mm
Bending limit	110 MeV
Focusing limit	95 MeV
RF SYSTEM	
Number of dees	2
Dee angle	86°
Frequency range	10.6 ~ 22.0 MHz
Frequency stability	$\pm 10^{-6}$
Resonator	$\lambda/4$ coaxial type with movable short
Full relative frequency change $\Delta f/f$	1.6 %
Fine tuning	Capacitive panel
Maximum dee voltage	60 kV
Harmonic number	1, 2, 3
Phase stability	$\leq \pm 0.5°$
Voltage stability	$\leq \pm 1 \times 10^{-3}$
Vertical aperture inside dee	40 mm
Gap between dee and ground plate	42 mm
Movable range of shorting plate	1350 mm
Inner tube diameter	300 mm
Inside diameter of outer tube	1000 mm
Pre-amplifier	EIMAC 4CW800B
Final amplifier	EIMAC 4CW50,000E
Power feeder	Inductive coupling
Maximum output power	50 kW × 2

Table 1 Continued.

VACUUM SYSTEM	
Cryogenic pump	4000 ℓ/sec × 4
Turbo molecular pump	2000 ℓ/sec × 1
	160 ℓ/sec × 1
Rotary pump	5000 ℓ/min × 1
	1300 ℓ/min × 1
	240 ℓ/min × 1
	93 ℓ/min × 1
	47 ℓ/min × 1
BEAM PROBES	
Main radial probe	Integral and differential 3-finger
Deflector probe	Single head
Magnetic channel probe	Single head
EXTRACTION SYSTEM	
First channel	Electrostatic deflector
Second channel	Electromagnetic coil
Focusing channel	Passive-type field gradient corrector
ION SOURCE	
For light ions	Multicusp
For heavy ions	ECR (OCTOPUS)
INJECTION SYSTEM	Axial injection with spiral inflector

The cyclotron is a 4-sectored variable-energy AVF machine with an extraction radius of 923 mm. The acceleration electrodes consist of a couple of 86-degree dees, each connected with a resonant cavity. Beams of protons, deuterons and helium ions are available with maximum energies of 90, 53 and 108 MeV, respectively. Heavy ion beams can be accelerated to an energy range of (2.5×A) MeV to (110×Q^2/A) MeV, where A is mass number and Q is charge state. Acceleration harmonic numbers of 1, 2 and 3 are available.

(3) Magnet

The cyclotron magnet is of an H-type with a pole diameter of 2156 mm and four spiral sectors. Twelve pairs of circular trim coils are wound concentrically on the sectors. Four pairs of harmonic valley coils are placed in the central region for centering the off-centered beam. The other four pairs of harmonic valley coils are placed in the extraction region for fine adjustment of turn separation.

The procedure for the excitation of the magnet is as follows. 1) The magnet is excited up to a maximum field level at a main coil current of 900 A. 2) The magnet is de-excited down to a low field level at 50 A. 3) The main coil current is set up to a higher level by 1 % than the required field level. 4) The current is set down to a lower

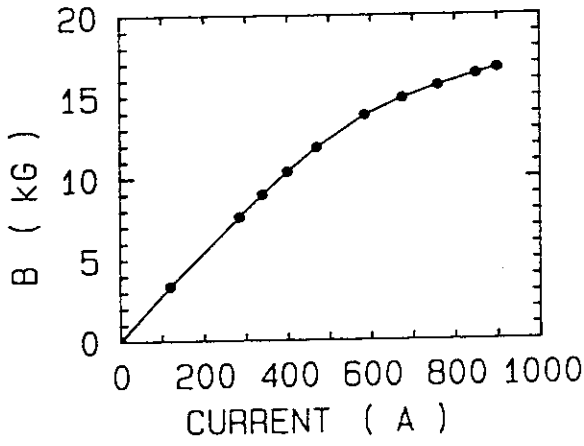

Fig.3 Excitation curve of the cyclotron magnet at an extraction radius of 923 mm.

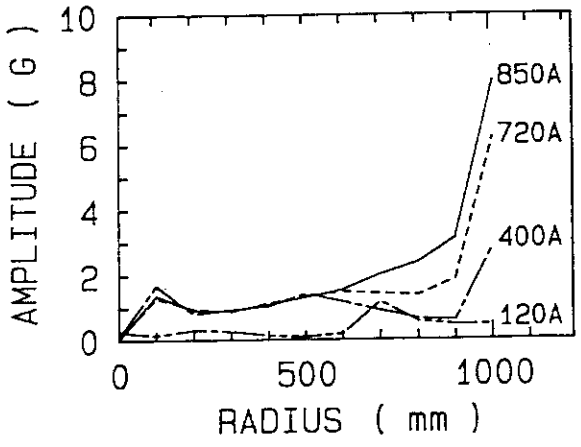

Fig.4 Radial Distributions of the first harmonic amplitude at four base field levels.

level by 1 % than the required current. 5) The current is set up to the required level. 6) Finally the currents of the circular trim coils and harmonic coils are set up to the preset ones. It takes around 30 minutes for the excitation.

The median plane magnetic fields were measured for the main coil, circular trim coils and harmonic coils in polar coordinates of (r,θ). A Hall generator, Siemens SBV 601-S1, is placed in a 50 mm long-, 34 mm wide- and 20 mm thick housing made of polymethylmethacrylate. The inside of the housing were kept at a constant temperature by a temperature regulator. The housing was moved by 2 cm steps in r and 1.8 degree steps in θ.

The excitation curve at an extraction radius of 923 mm is shown in Fig. 3, which is obtained for ten excitation levels. The maximum average field strength at the extraction radius is 16.7 kG. The first harmonic amplitude was less than 4G over the entire operating range as shown in Fig. 4. The first harmonic field can be modified by optimizing the harmonic coil field. The circular trim coil field strongly depends on the base field level because of field saturation. The field strength at a base field level of 850 A is weakened down to nearly 50 % of that at 120 A. Two pairs of the harmonic coils are excited with opposite polarity. The maximum first harmonic amplitudes at r=200 mm and r=860 mm at a base field level of 850A are 17G and 27G, respectively.

(4) Rf system

The $\lambda/4$ coaxial type resonator with a movable shorting plate was adopted for JAERI AVF cyclotron. The symmetrical structure of the coaxial cavity has a great advantage of uniform distribution of the current density on the stem. The Q-value

of the coaxial cavity, therefore, is higher than that of the movable-panel type cavity. Consequently, the output power of the amplifier is reduced to 30 kW.

A schematic view of the coaxial cavity is shown in Fig. 5. The two dees and the cavity are made of 10 mm thick oxygen free copper(OFC). The dee is connected through the transition section to the inner coaxial line. The one end of the inner line is supported with a ceramic rod and the other end is supported with the end plate of the cavity. The length of the cavity is approximately 2000 mm. The stroke of the shorting plate is 1350 mm so as to cover the required frequency range from 10.6 MHz to 22.0 MHz. The shorting plate has many contact fingers made of the Be-Cu. They are pressed to the inner and outer coaxial line with the pneumatic bellows.

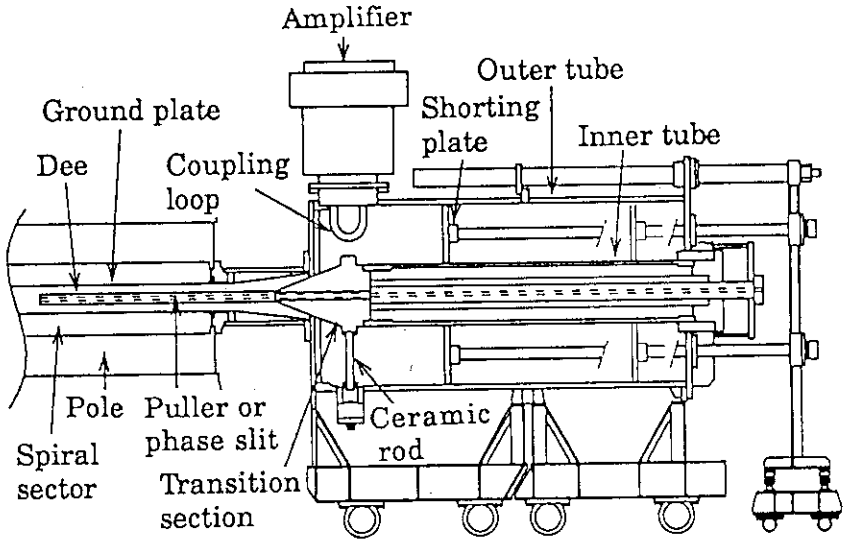

Fig.5 Schematic view of the coaxial resonator with a movable shorting plate.

The capacitive fine frequency tuner is located on the outer side of the dee. The tuner gap is adjustable from 8 mm to 50 mm automatically. The maximum frequency change adjusted by the fine tuner is 1.6 % of the fundamental frequency. The dee voltage is detected with a capacitive divider of which the ratio is around 1/1000.

The final amplifier is directly mounted on the front part of the outer cavity and is coupled with the resonator through a loop coupling. A couple of the cryogenic pumps(4000 ℓ/s each) are mounted on the bottom of the cavity. An rf shield consisting of copper pipes was attached on the each pumping port to shield the leakage of rf power from the cavity to the pump.

The measured Q-value and the shunt impedance are shown in Fig. 6 and Fig. 7 as a function of resonant frequency. The properties of the resonator were calculated with the one-dimensional transmission line approximation. Three quarter of the calculated values are indicated in Fig. 6 and 7, and is well consistent with measured values. The

measured values of the movable panel type cavity are also shown in Fig. 6 and 7. The shunt impedance in higher frequency region has been much improved by approximately 4 times.

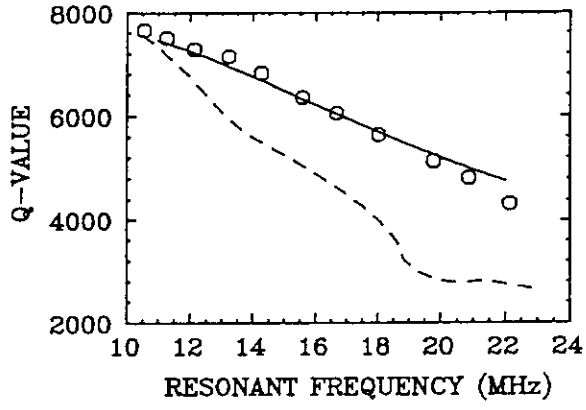

Fig.6 Frequency dependence of Q-value. The solid line shows 75 % of the calculated value based on one-dimensional transmission-line approximation. The dashed line shows the measured value of the movable-panel type cavity.

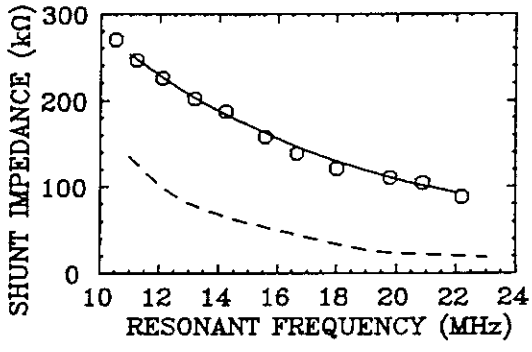

Fig.7 Frequency dependence of shunt impedance. The solid line shows 75 % of the calculated value based on one-dimensional transmission-line approximation. The dashed line shows the measured value of the movable-panel type cavity.

The amplifier is composed of one solid-state amplifier and two stage tetrodes (EIMAC 4CW800B and 4CW50,000E). They are used as grounded-cathode configuration to obtain higher power gain. A variable vacuum capacitor connected parallel to the loop is used for the adjustment of the coupling impedance.

The power test has been carried out successfully in the frequency range of 10.6 MHz to 22.0 MHz. The maximum voltage of 60 kV has been achieved at 21.14 MHz with a lower power consumption of 22 kW than that of the movable-panel type resonator. The voltage and phase stability are better than $\pm 1 \times 10^{-3}$ and ± 0.5 degrees respectively over the whole frequency range. The dee voltage ripple is less than 1×10^{-3} and the phase ripple 0.3 degrees.

(5) Injection, central region, extraction

Low-energy beams from the ion sources, located in the basement, are axially injected upward into the median plane of cyclotron through the hole of the bottom yoke. The layout of the axial injection system is shown in Fig. 8. Four Glazer lenses and a steering magnet are placed inside the hole. The injected beam is guided to the median plane through a spiral inflector and a puller, which are prepared separately for each acceleration harmonic number from 1 to 3. The inflector is inserted downward through the hole of the upper yoke. The layout of the central region is shown in Fig. 9. Two movable phase-defining slits are set inside the dee and the dummy dee.

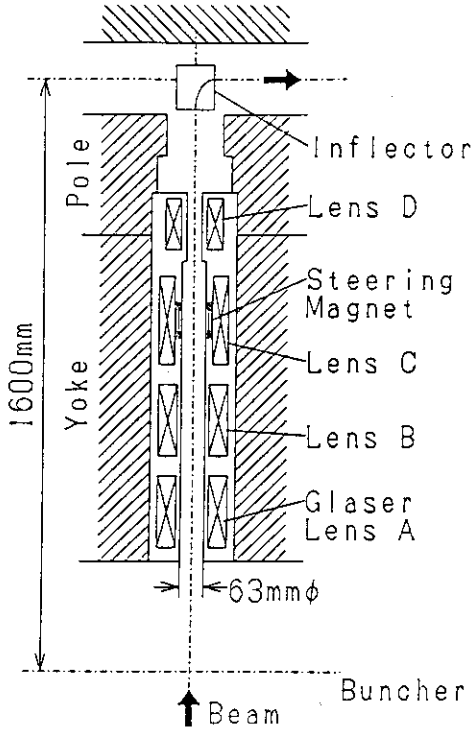

Fig.8 Layout of the axial injection system.

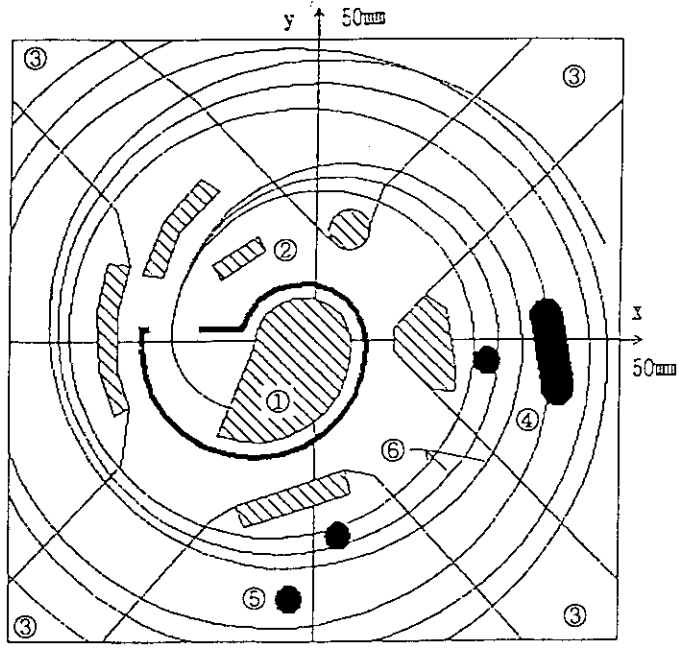

Fig.9 Schematic drawing of the central region of the cyclotron. (1)Inflector, (2)Puller, (3)Dee gap, (4)Phase slit II, (5)Phase slit I, (6)Beam trajectories(dee voltage of 40, 50 and 60 kV).

The beam extraction system consists of an electrostatic deflector and a magnetic channel and also of a field gradient corrector to focus the beam horizontally. For the purpose of minimizing the deflector voltage to extract 90 MeV protons, the maximum field of magnetic channel was improved from 3.5 kG to 4.3 kG by adding a chilling unit in the water cooling system.

(6) Beam diagnostics

A main radial probe, a deflector probe, a magnetic channel probe and a set of phase probes are placed inside of the acceleration chamber of the cyclotron for beam diagnostics. The main probe is inserted through a hole of the side yoke and its stroke covers 1150 mm (r=40-1190 mm). The main radial probe is equipped with three finger-like electrodes to measure the beam current differentially and integrally.

The phase probes consist of ten pairs of rectangular pickup electrodes to measure the relative phase of beams on different turns (r=236-893 mm). The electrodes made of 2.5 mm thick OFC are installed in the radial direction as shown in Fig. 1. The electrode are radially 58 mm long and azimuthally 40 mm wide for the inner threes, 60 mm for the middle fours and 93 mm for the outer threes. The amount of field correction necessary for outer 10 circular coils are calculated by using the phase differences measured with this probe.

A baffle slit system consisting of four leaves is placed just before the entrance of the inflector. Other baffle slit systems are placed at the entrance of the magnetic channel and the field gradient corrector. Another baffle slit system is also placed at the extraction hole of the acceleration chamber.

II. RESULTS OF FIRST YEAR'S OPERATION

(1) Extraction current and transmission

The first beam, 50 MeV $^4He^{2+}$, was extracted from the cyclotron in March 1991. The beam acceleration tests have been conducted for H^+(10, 45, 70 and 90 MeV), D^+(10, 35 and 50 MeV), $^4He^{2+}$(20, 50 and 100 MeV), $^{40}Ar^{8+}$(175 MeV), $^{40}Ar^{13+}$(460 MeV) and $^{84}Kr^{20+}$(520 MeV). The result of the beam acceleration test are summarized in Table 2.[5] Protons and deuterons are generated by the multicusp ion source, and other ions by the ECR ion source.

The 90 MeV protons were successfully extracted with a beam current of 10 μA. The stability of extracted beam for light ions is typically $\pm$5 %. The beam transmission efficiency between before injection and after extraction is typically 4-5 %. The best transmission and extraction efficiency was 15 % ($^4He^{2+}$ 50 MeV) and 89 % (H^+ 70 MeV), respectively. The extraction efficiency is the beam intensity ratio of the main probe at r=900 mm to the magnetic channel probe (just after deflector). The phase

slit I on the opposite side of the puller is effective to optimize the extraction efficiency. The transmission from cyclotron entrance to r=200 mm is about 20 %. This is limited mainly by the rf phase acceptance and the efficiency of a beam buncher installed at the entrance of cyclotron. A typical value of measured bunching efficiency is about 2.5. The transmission is estimated at 21(= 2.5 × 30/360) % assuming that the phase acceptance is 30 degrees.

Table 2 Results of extracted intensity and transmission. (*:Phase slit I is inserted.)

Ion	Energy (MeV)	Harmonic number	Frequency (MHz)	Injection voltage (kV)	Extracted intensity (eμA)	Extraction Efficiency (%)	Overall Transmission(%)
H^+	10	2	14.97	3.10	10	54	3.8
	45	1	15.46	8.64	30	85*	4.0
	90	1	21.14	15.11	10	53*	2.0
D^+	10	2	10.63	3.10	11	45	3.7
	35	2	19.70	11.00	41	71*	4.6
	50	1	11.76	9.53	21	64*	7.2
$^4He^{2+}$	20	2	10.67	3.40	5.7	55	11
	50	2	16.77	8.53	20	82*	15
	100	1	11.81	10.15	10	51*	6.4
$^{40}Ar^{8+}$	175	3	15.14	10.06	3.0	60	5.7
$^{40}Ar^{13+}$	460	2	16.24	11.71	0.011	26	2.8
$^{84}Kr^{20+}$	520	2	11.98	8.81	0.004	17	1.0

(2) Correction of isochronous field by phase probe

Deviation of magnetic field from the isochronous one can be corrected by using the phase probe. A typical pickup signal induced by ion beams is shown in Fig. 10. The signal voltage was adjusted by a variable attenuator and a 40 dB fast amplifier. Relative phase difference from the pickup signal of the second electrode were detected by a digital storage oscilloscope. Current correction for each circular trim coil was made by a least-square fitting method so as to minimize the field deviation from the isochronous field. The phase deviations can be finally reduced within ±5 degrees after a few times iterative corrections.

(3) Emittance

The phase space configuration of extracted beams can be measured by an emittance monitor at the exit of cyclotron. The emittance monitor consists of two sets of beam defining slits and position-sensitive multiwire electrodes for measuring horizontal and vertical emittance. The slits are made of 12 mm thick copper. The electrodes are composed of 48 gold-plated tungsten wires with a diameter of 0.1 mm. The drift length

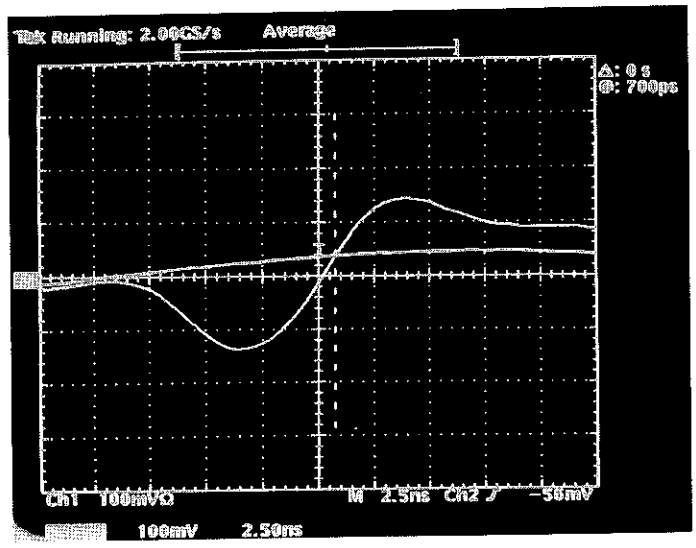

Fig.10 Pickup signal of the phase probe induced by ion beams.

between the slits and detectors is 1.6 m. The horizontal and vertical emittance for $^{40}Ar^{8+}$ 175 MeV are 14.0π mm·mrad and 9.9π mm·mrad, respectively.

(4) Buncher

The beam buncher is placed at 1581.6 mm below the medium plane of the cyclotron. The buncher is of two-gap klystron type with $\lambda/2$ mode. A high-voltage electrode is placed between two grounded electrodes. The electrode gap is 29 mm. The electrode has a beam aperture of 30 mm diam. The resonant frequency range of sinusoidal voltage is 11 to 22 MHz. The bunching efficiency of 2.5 to 3 has been obtained for all ions.

REFERENCES

1) W.Yokota, K.Arakawa, Y.Nakamura, T.Nara, M.Fukuda, T.Agematsu, S.Okumura, I.Ishibori, T.Tachikawa, Y.Hayashi and K.Ishii, "Operation of ion sources and beam transport to JAERI AVF cyclotron," presented at the 13th International Conference on Cyclotrons and Their Applications, Vancouver, Canada, July 6-10, 1992.

2) W.Yokota, K.Arakawa, M.Fukuda, T.Tachikawa, Y.Hayashi, Y.Kumata, "Performance of beam chopping system for JAERI AVF cyclotron," presented at the 13th International Conference on Cyclotrons and Their Applications, Vancouver, Canada, July 6-10, 1992.

3) S.Okumura, T.Agematsu, W.Yokota, T.Kamiya, M.Fukuda, Y.Nakamura, T.Nara, I.Ishibori, K.Arakawa, M.Maruyama, K.Iso, K.Hoshika and M.Tachibana, "Control system for JAERI AVF cyclotron," presented at the 13th International Conference on Cyclotrons and Their Applications, Vancouver, Canada, July 6-10, 1992.

4) Y.Kumata, Y.Fukumoto, M.Fukuda, K.Arakawa, T.Karasawa and A.Shimizu, "Modified RF system for JAERI AVF cyclotron," presented at the 13th International Conference on Cyclotrons and Their Applications, Vancouver, Canada, July 6-10, 1992.

5) K.Arakawa, Y.Nakamura, W.Yokota, M.Fukuda, T.Nara, T.Agematsu, S.Okumura, I.Ishibori, T.Karasawa, R.Tanaka, A.Shimizu, T.Tachikawa, Y.Hayashi, K.Ishii and T.Satoh, "Construction and First Year's Operation of the JAERI AVF cyclotron," presented at the 13th International Conference on Cyclotrons and Their Applications, Vancouver, Canada, July 6-10, 1992.

1.3 Ion Sources and Injection Line

I. ION SOURCES

Two ion sources, a multi-cusp ion source for light ions and an ECR ion source for heavy ions, were installed for the JAERI AVF cyclotron. The sources were manufactured at Ion Beam Applications s.a. in Belgium in 1989. Test operation and connection with the computer control system were carried out at Niihama works of Sumitomo Heavy Industries, Ltd. in 1990. Operation of the sources at JAERI started in February 1991. The ability of ion generation required for beams injected into the cyclotron has been attained. Ion beams are transported through the injection line and axially injected into the cyclotron.

(1) ECR Ion Source

The JAERI ECR ion source is of model OCTOPUS and the basic design is almost identical to the first OCTOPUS, which was constructed in 1985 at the Centre de Recherches du Cyclotron in Louvain-la-Neuve (Belgium).[1] The performance of the first OCTOPUS has been improved through some modifications such as reduction of the bore diameter of the multi-pole magnets and change of RF feeding into the 2nd stage chamber from radial to axial, etc.[2] The JAERI ECR ion source is equipped with the RF frequency of 6.4 GHz for the 2nd stage and the pumps of turbomolecular type, while those for the first OCTOPUS are 8.5 GHz and oil diffusion type, respectively. It was found that the gas pressure in a typical tuning is close in both sources, while the pressure at the extraction stage is lower for the JAERI ECR ion source by factor 3. The characteristics of the JAERI ECR ion source is summarized in Table 1 and the cross section is shown in Fig. 1.

Table 1 Design parameters of the JAERI ECR ion source.

1st stage	
ECR frequency	14.3 GHz
RF power; maximum	2 kW
typical	80 - 200 W
2nd stage	
length between mirros	60 cm
diameter	18 cm
multipole	octupole (SmCo)
RF frequency	6.4 GHz
ECR field	0.2291 T
RF power: maximum	3 kW
typical	0.6 - 1.5 kW
RF feed	axial
vacuum pump	turbomolecular
typical pressure in operation	
1st stage	$1.0 - 2.0 \times 10^{-3}$ Pa
2nd stage	$0.7 - 1.0 \times 10^{-4}$ Pa
extraction stage	$1.0 - 3.0 \times 10^{-5}$ Pa

The source is provided three identical gas feed and flow control systems allowing independent operation. One feeds a main gas into the 2nd stage, the other two feed support gases into the 1st and the 2nd stages. A low temperature oven and a rod in-

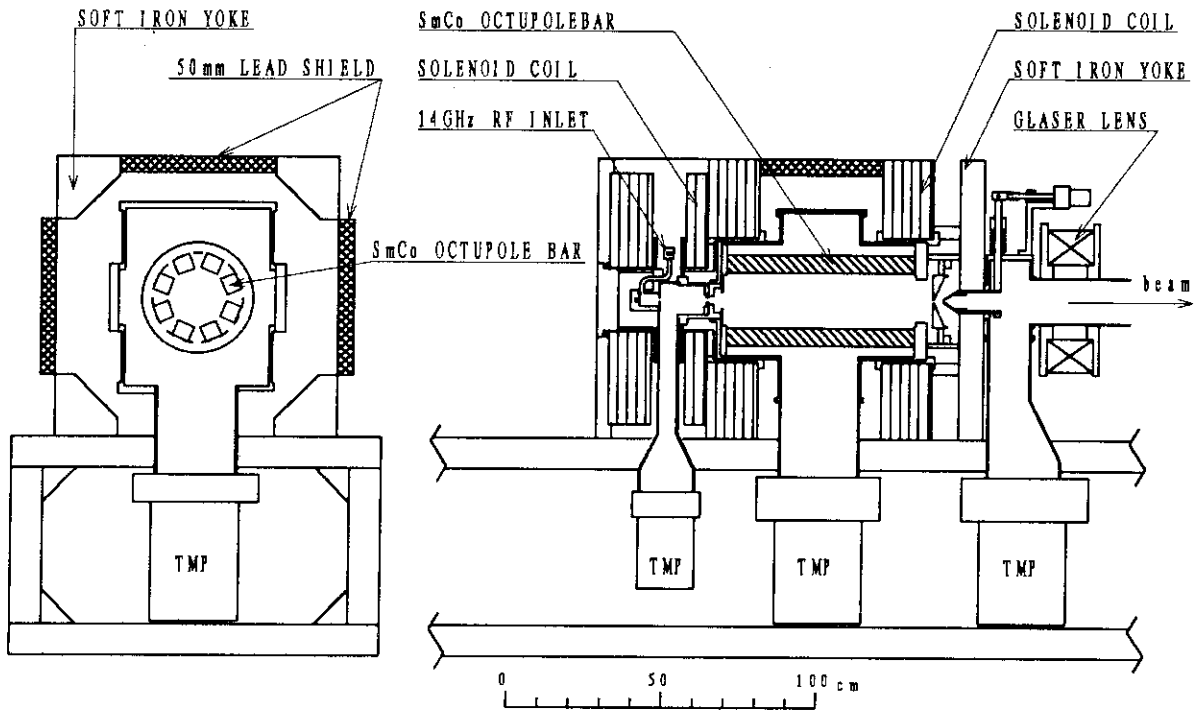

Fig.1 Cross section of the JAERI ECR ion source.

sertion mechanism prepared for producing ions of metal elements can be installed in the 2nd stage chamber. The operating parameters for ion production are four mirror coil currents, RF powers, gas flow rates, extraction and puller voltages and puller position. They are operated and monitored through a computer control system of the AVF cyclotron.

The ion generation test at JAERI has been made for O^{6+}, Ar^{8+}, Ar^{13+} and Kr^{20+} to ensure generation of beam currents more than 1 eμA. The test was successful for every ion species. The beams except for O^{6+} were injected into the cyclotron, and acceleration and beam extraction tests have been carried out. The maximum ion beam currents are listed in Table 2. It turned out from the data of the JAERI ECR ion source that the currents were improved at lower charge states, but reduced at higher charge states in comparison with the first OCTOPUS.[3] The difference may be due to the lower RF frequency of the 2nd stage of the JAERI ECR ion source.

Emittance for 80 % current density of Ar^{8+} ion beam was measured at an extraction voltage of 10 kV in a wide range of mirror coil currents by an emittance monitoring system, at a diagnosis chamber after the analyzing system, consisting of a pair of a slit and a multi-wired detector. The measured emittance varied in a range from 100 to 170π mm·mrad depending on mirror coil currents and was a quarter to half of the beam acceptance of the injection line.

Table 2 Beam currents extracted from the JAERI ECR ion source. (eμA)

charge state	He	C	N	O	Ne	Ar	Kr	Xe
1		83	170	370	140			
2	325	121	128	300	147			
3		70	140	190	136	113		
4		50	97		92	102		
5		7	93	116				
6			18	120	58	78		
7				10	20	95		4
8						115	35	10
9						85	44	17
10							47	19
11						13	38	18
12						4		19
13						1	31	19
14						0.2		18
15								17
16								17
17								13
18								12
19								10
20								8
21								4.8
22								3.5
23								1.5

For designing radiation shield of the source, the X-ray leakage outside the source was measured in terms of dose-rate equivalent by an ionization chamber as functions of the RF power of the 2nd stage and the thickness of shielding material when generating Ar and Kr ions. The X-ray shield was designed so that the dose-rate outside the shield should be below 6μSv/h under operation of the source. The 2nd stage chamber, the main X-ray source, was covered by a laminate lead of 50 mm thick. Large gaps between coils and an iron yoke or turbomolecular pumps were filled by lead. To shield the residual X-ray leak from these local shields, an iron cage of 22 mm thick was installed around the source.

The highest dose-rate of 37 μSv/h, however, was observed when the source parameters were optimized to generate O^{6+} at the 2nd stage power of 700 W. Much less dose-rate of about 5 μSv/h was observed for Ar^{8+} and Kr^{13+} generation at the 2nd stage RF powers of 900 and 1200 W, respectively. Additional shield may be necessary for different source parameters.

(2) Multicusp Ion Source

The specification of the multicusp ion source and its side view are shown in Fig. 2 and Table 3, respectively. The cylindrical source chamber, 15 cm in length, 10 cm in diameter, is made of copper. A tungsten filament, 15cm in length, is set along the central axis in the chamber. The arc plasma is confined by magnetic field of four rows of ten SmCo magnets mounted on the outer side of the chamber and six SmCo magnets at the end of the chamber. The beam extraction system consists of an extraction and a movable puller electrode, and the gap between the electrodes is variable. The source can be simply operated mainly by arc voltage, arc current, gas flow, puller voltage and puller position. They are operated and monitored through the computer control system of the cyclotron. It covers a wide extraction voltage range of 3 kV to 20 kV to meet the acceleration energy range of the cyclotron.

Table 3 Characteristics of the multi-cusp ion source.

chamber	
diameter	10 cm
length	15 cm
magnet	
material	SmCo
number of pieces	46
filament	
voltage	0 - 15 V
current	0 - 100 A
arc	
voltage	0 - 400 A
current	0 - 15 A

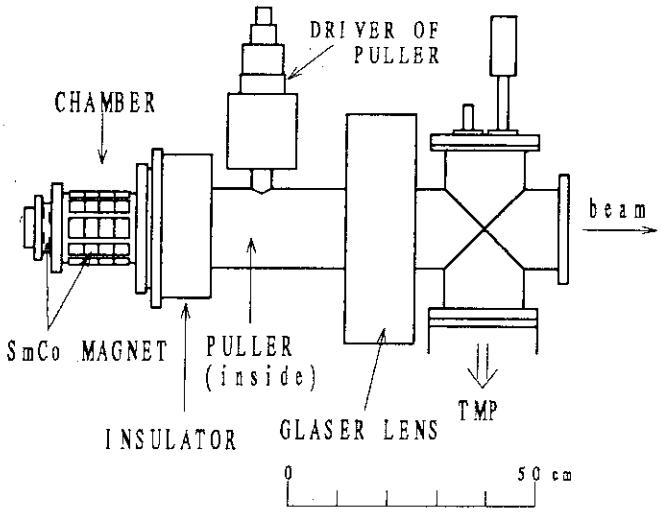

Fig.2 Side view of the multi-cusp ion source.

The beam current from the source was not sufficient at low extraction voltages for the original extraction and puller electrodes with a single hole of 6.5 mm diameter. A large amount of beam current was lost around the puller electrode because of a large divergence of the extracted beam. To reduce the divergence by a smaller aspect ratio of the diameters to the gap between the extraction and the puller electrodes, they were replaced by multi-hole type electrodes with nineteen holes of 1.8 mm diameter. This increased beam current by ten times at an extraction voltage of 3 kV. The maximum beam currents of H^+ (1.3 emA) and D^+ (1.0 emA) were stably extracted, in which the short term flutter was less than 5 % by peak-to-peak. The multi-hole puller electrode is damaged by beam sputtering, however, and its effect turned out to be serious when high

current of He^{2+} beam was extracted. Therefore now we generate He^{2+} beam usually by the ECR source.

II. INJECTION LINE

Ion beams generated by the multi-cusp and the ECR ion sources are transported to the cyclotron through the injection line and axially injected into the cyclotron. The line was designed to accept beams with large emittance by adopting large diameter of beam ducts and wide pole gaps of bending magnets. A schematic layout of the ion

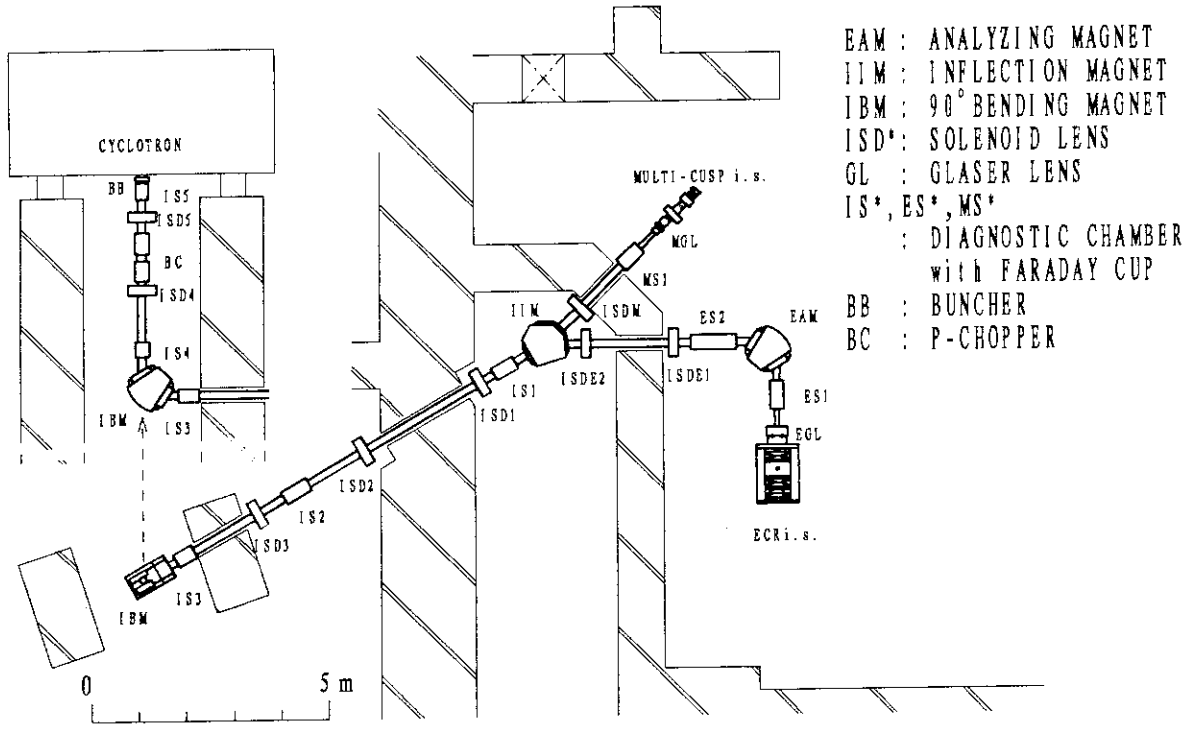

Fig.3 Schematic layout of the ion sources and the injection line.

sources and the injection line to the cyclotron is shown in Fig. 3. The injection line consists of a 90° analyzing magnet (EAM) for the ECR source, an inflection magnet (IIM) as an analyzer for the multi-cusp source, a 90° bending magnet (IBM) for vertical injection into the cyclotron and eight solenoid lenses which were chosen to focus beams with large diameters. The magnets EAM and IBM are of double-focusing, having 102 mm pole gap and 400 mm radius of curvature, and were designed to minimize the contribution of sextupole magnetic field. The injection line is also equipped with eight chambers for beam diagnosis, each of which is provided with a Faraday cup, X-Y slits and a three-wired beam profile monitor. The diameter of the beam ducts is 152.4 mm. A beam buncher and a pulse voltage chopper (P-chopper) are set near the entrance of the cyclotron yoke.

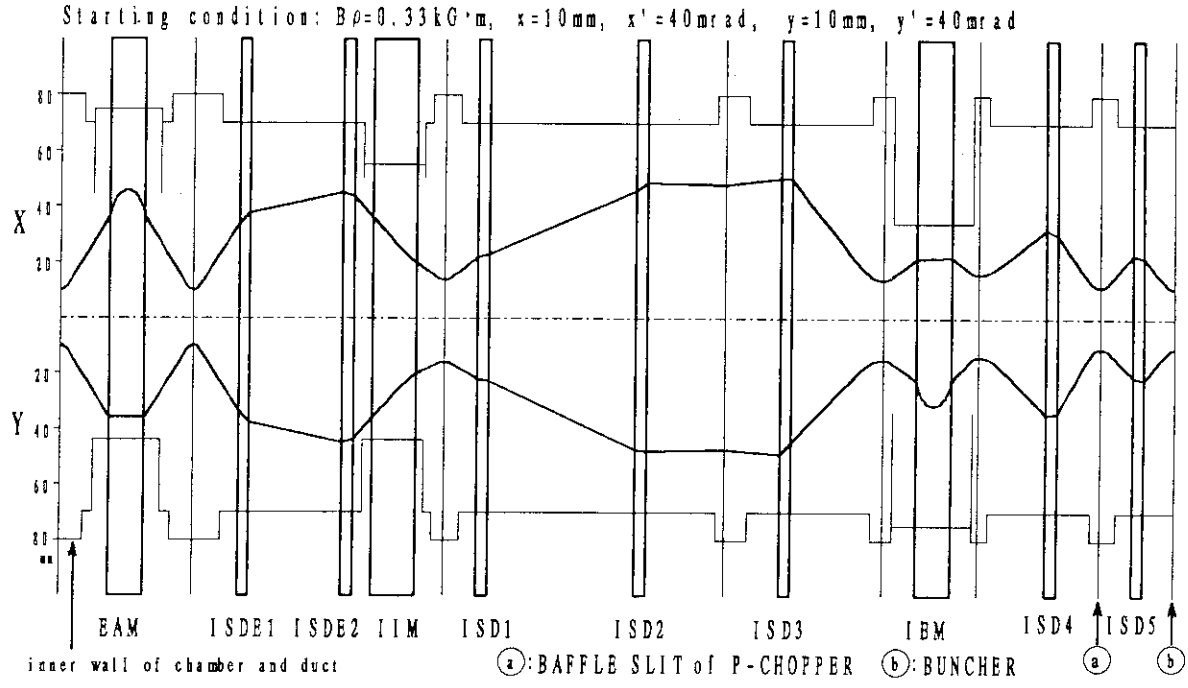

Fig.4 Beam envelope for the JAERI ECR ion source.

The beam emittance of ECR ion sources has been reported at 200π mm·mrad or less.[4–6] It is desirable, however, to assume emittance larger than the reported value to maximize beam transmission, since there are intrinsic difficulties to optimize design parameters of the extraction lens under the strong magnetic field of the ECR ion source. The beam optics calculation was made using a code 'TRANSPORT' assuming that emittance value is 400π mm·mrad (beam diameter: 10 mm at the focus of the Glaser lens EGL). Solenoid lens and quadrupole lens were examined in the beam optics calculation, and the former showed better focusing.[7] Therefore we adopted solenoid lenses in spite of the large amount of electric power. The beam emittance of the multi-cusp ion source was assumed at 300π mm·mrad with a beam diameter 10 mm at the focus of the Glaser lens MGL. The beam envelope using solenoid lenses is shown in Fig. 4 for the ECR ion source. The beam size is large between IIM and IBM to reduce the effect of space charge. The buncher and a baffle slit of the P-chopper are set at beam waists. In actual beam transport to the cyclotron, the beam transmission has been improved by careful optimization of beam transport. Examples of the transmission are listed in Table 4. The transmission of the ECR source beams is less dependent on ion species and beam current. The measured emittance for 80 % current density of the beams from the JAERI ECR ion source is a quarter to a half of the acceptance and the transmission expected to be improved up to 95 %, which may be limited by collision with residual gases in the

Table 4 Beam transmission from the ion sources to the cyclotron.

a) ECR ion source

ion	Vex (kV)	ES2	IS1	IS3	IS5	I at ES2(eμA)
Ar^{8+}	10.0	1.00	0.91	0.83	0.78	58
He^{2+}	8.5	1.00	0.94	0.92	0.84	255
	8.5	1.00	0.91	0.91	0.86	22

b) Multi-cusp ion source

ion	Vex (kV)	IS1	IS3	IS5	I at IS1(eμA)
H^+	12.5	1.00	0.99	0.96	16
	8.7	1.00	1.00	0.94	1.6
	8.7	1.00	0.84	0.58	760
	3.1	1.00	0.79	0.68	96
	3.1	1.00	0.60	0.48	500

line. The transmission of the beam from the multi-cusp source strongly depends on the extraction voltage and beam current as seen in Table 4-b. It is higher than 90 % for low beam current and at high extraction voltage, while it is very low along the injection line at low extraction voltage and high beam current. This is attributed to large beam divergence beyond the beam acceptance of the line, which is caused at the extraction region. The origination of the divergence, however, has not been clarified so far.

REFERENCES

1) Y. Jongen, G. Ryckewaert, IEEE Trans. on Nucl. Sci., **NS-32**, No.5 (1985), pp.1817-1819.
2) J.-L. Bol, A Chevalier, Y. Jongen and M. Lacroix, Proc. of 11th Int. Con. on Cyclotrons and their Applications, 1987, Tokyo, pp.90-93.
3) C. Dupont, Y. Jongen, K. Arakawa, W. Yokota, T. Satoh and T. Tachikawa, Rev. Sci. Instr. (1990) pp.265-266.
4) D.J.Clark, Y.Jongen, C.M.Lyneis, IEEE Trans. Nulc. Sci. (1984) 133.
5) G.Bellmo, Proc. of Eleventh Int. Conf. on Cyclotron and their Applications, 1986, Tokyo, Japan, pp.503-506.
6) R.K.Bhandari, J.Reich, Proc. of Ninth Conf. on Cyclotron and their Applications, 1981, Cean, France, pp.261-265.
7) T.Kamiya, W.Yokota, K.Arakawa and E.Minehara, Proc. of the 6th Symposium on Accelerator Science and Technology, 1987, Tokyo, Japan, pp.281-283.

1.4 Beam Transport System

(1) Outline of the System

A beam transport system illustrated in Fig. 1 was constructed for the AVF cyclotron (K=110) facilities in which various irradiation experiments using high-energy light and heavy ion beams were planned on the separate beam courses.

The transport system consists of bending and focusing magnets, beam monitors, beam scanners, rotary beam shutters, etc.. There are 9 bending magnets, 85 quadrupole magnets and 10 beam steering magnets in 10 horizontal and 4 vertical beam courses which transport ion beams to 17 target ports on the ways or at the ends of the beam courses located in the 8 ion rooms. There are also 27 Faraday cups, 27 profile monitors, 25 alumina monitors, 25 beam slit systems, an emittance monitor and a non- destructive current monitor to monitor beam current and/or beam profile for adjusting parameters of magnets. They have been mounted on the chambers called "diagnostic stations", located at the focusing points or the ends of the beam lines. An achromatic and telescopic beam transport system was designed for high transmission efficiency of ion beams and good adjustability of the magnet parameters using the beam optics calculation program TRANSPORT.[1)]

(2) Beam Optics

Ion beams extracted from an AVF cyclotron have large emittance and energy variation in comparison with electrostatic accelerators. To transport such ion beams without any beam loss in the beam ducts, the transport system was designed achromatically. Ion beams with large momentum spread are dispersed by one dipole magnet system and achromatized by another dipole magnet system. The analyzing magnet (TAM) and the switching magnet(TSM) form achromatic system in the horizontal beam courses except LD, HC and HD in which deflecting angles at TSM are much smaller than that at TAM(80 degree). In HE course which branches from HC course, achromatic system also can be formed by an analyzing magnet(TAMHE). A dispersive beam is formed in LE course by a 25 degree bending magnet and in vertical courses HX, HY and HZ by their 90 degree bending magnets. Achromatic beams are transported in LX course with a couple of 45 degree bending magnets. Specifications of magnets are shown in table 1.

The beam transport system was divided into small sections so that the number of adjusting parameter is reduced and beam image of the entrance is exactly the same as of the exit. The layout and parameters of magnets in each section were adjusted to form simple and telescopic transport system. The waist of the beam envelope is formed at the end of each section at which a beam diagnostic station or target port is located.

An example of beam envelopes for HE course is shown in Fig.2.

(3) Beam Monitors

A typical diagnostic station is equipped with a Faraday cup, a beam profile monitor, an alumina monitor and a beam slit system.

The Faraday cup is used as a beam current monitor and also as a beam stopper in the interlock system of the cyclotron facility. The cup is made of copper and cooled by purified water. To measure beam current accurately, it has a secondary electron suppressing plate at which -500V is applied.

The beam profile monitor has three wires for monitoring of the projected profile of beam current density in three directions: vertical, horizontal and an oblique(45 deg.) directions. The position of the wires, driven along the 45 deg. direction by an air cylinder, is detected by a rotary-encoder and indicated graphically.

The alumina monitor is used for observation of the cross-sectional beam shape, which is monitored by a TV camera system.

The beam slit system is composed of the horizontal and the vertical slits, independently mounted at 45 deg. ports of the diagnostic station. The beam current can be monitored separately at each slit tip, made of copper and cooled by water. Each tip is driven by a stepping motor and the position is detected by counting control pulses of the motor.

For measurement of the beam emittance, a beam emittance monitor is equipped. The monitor is a combination of a slit system and a multi-wire system. The former system has a couple of 0.25mm gaps in x- and y- directions. The latter system has two sets of isolated 48 wire sensors for measurement of the beam distribution in x- and y- directions. These systems are driven by different stepping motors and the position is detected in the same way as the beam slit system. The horizontal and the vertical emittance can be measured with only one scan. The distribution in the divergence-position phase space is indicated graphically.

For measurement of the beam current without interrupting most of the beam current, a non-destructive current monitor is used. The monitor has a tungsten rod 0.5mm in diameter, which rotates at 60 - 200 rpm across the beam. The beam current is calibrated with the Faraday cup.

REFERENCES

1) K.L.Brown, SLAC-91, 1977.

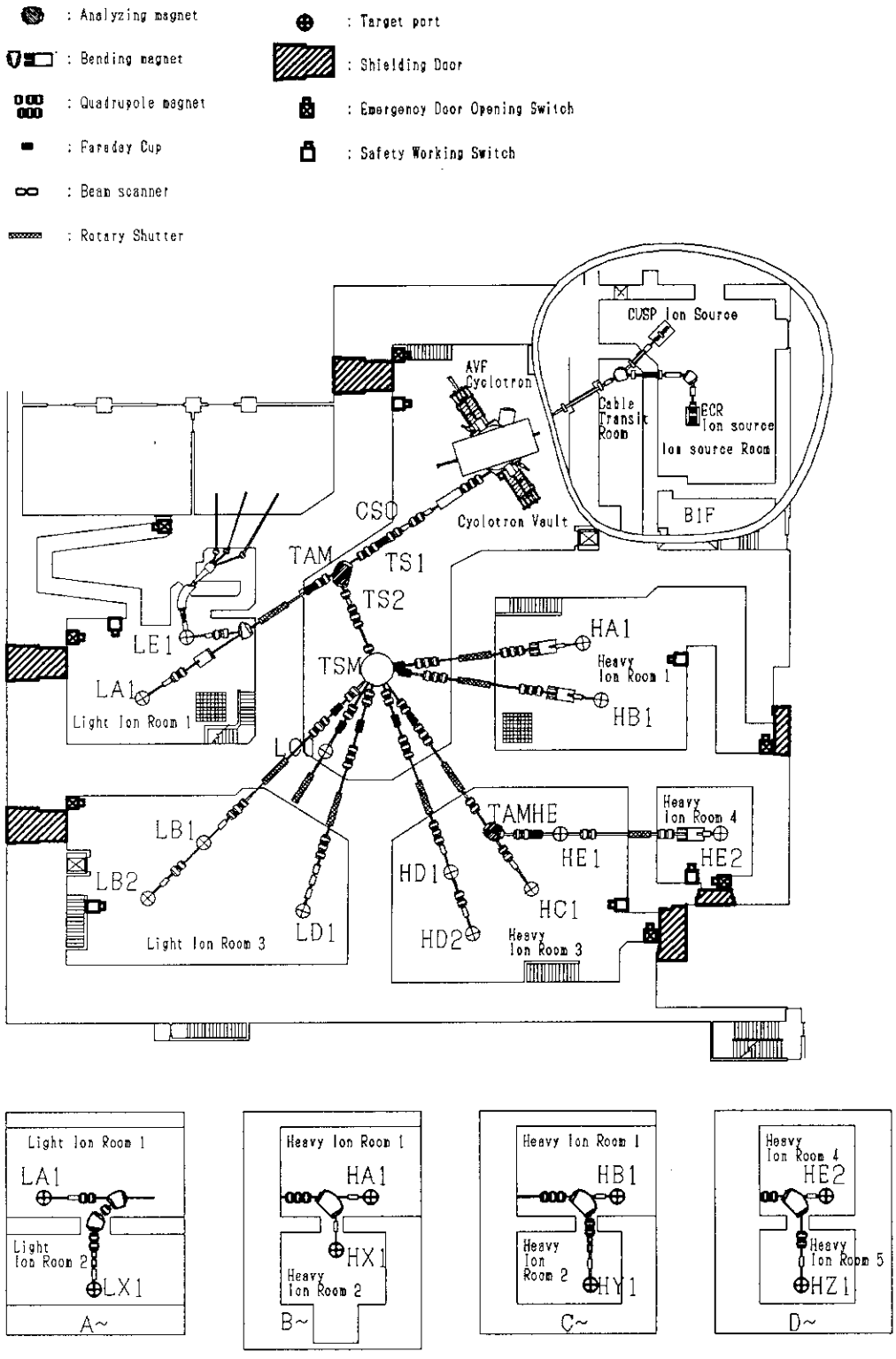

Fig. 1 Beam transport system.

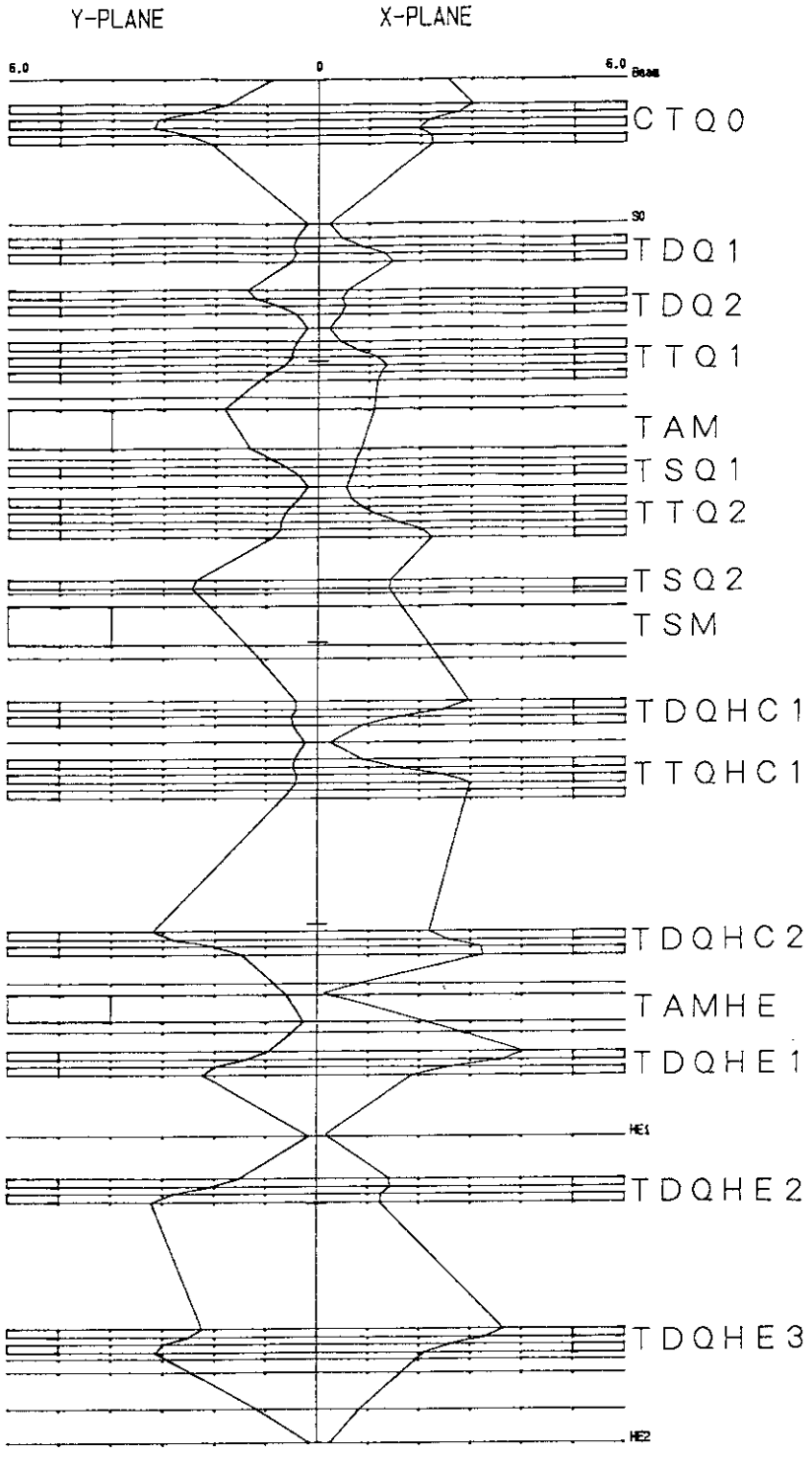

Fig. 2 Beam envelope of HE course.

Table 1 Specifications of magnets

SWITCHING MAGNET

Shape of pole tip	circular
Pole gap (mm)	70
Maximum field (T)	1.7
Maximum deflection angle (deg.)	74
Maximum excitation current (A)	525
Maximum voltage (V)	155

ANALYZING MAGNET

	TAM	TAMHE
Deflection angle (deg.)	80	55
Curvature radius (m)	1	1
Maximum field (T)	1.6	1.6
Entrance angle (deg.)	+31.5	+14.6
Exit angle (deg.)	+31.5	+14.6
Pole gap(mm)	60	60
Maximum excitation current (A)	290	290
Maximum voltage (V)	160	125
Stability of current (/8hrs)	$<10^{-5}$	$<10^{-5}$

QUADRUPOLE MAGNET

Shape of pole tip	hyperbolic
Pole gap (mm)	115
Pole length (mm)	260
Maximum field gradient (T/m)	10
Maximum excitation current (A)	213
Maximum voltage (V)	37

1.5 Beam Chopping System

The JAERI AVF cyclotron provides various ion beam characteristics in order to meet a number of requirements for beam utilization in the research program and pulsed beam irradiation is one of the important characteristics. The chopping system was designed and made to reduce repetition of naturally bunched beam from the cyclotron (11 MHz $\sim$ 22 MHz) down to 1 kHz $\sim$ 1MHz.[1] A pulse voltage chopper (P-chopper) was installed in the injection line to chop DC beams from the ion sources into pulse beams with intervals of 1 μs $\sim$ 1 ms and with duration several times the RF period of the cyclotron. This results in extraction of trains of plural beam pulses from the cyclotron. To extract a single pulse from a train, a sinusoidal voltage chopper (S-chopper) was installed after the exit of the cyclotron.

(1) Beam Chopping Process

A pair of parallel-plate electrodes were adopted for both choppers and their voltage waves synchronize with the cyclotron RF. The schematic arrangement of the choppers in the cyclotron system is shown in Fig. 1, and the chopping process is illustrated in Fig.2. The beam pulse after the P-chopper has a total time width T several times the cyclotron RF period τ_c. The zero volt period of the P-chopper voltage τ_p is chosen so that the duration at the maximum beam current equals to the effective bunching phase t_b (assumed at 150° of τ_c) ; $\tau_p - t_l = t_b$, where t_l is the ion transit time through the P-chopper electrodes. The resultant beam pulse is modulated by the buncher into plural bunches, followed by injection into the cyclotron. A bunch is separated into a pulse train, which consists of several pulses, by natural bunching during the acceleration. Each pulse is further divided into plural pulses (n pulses) by multi-turn extraction at the deflector. The time length of the extracted beam train is longer than the beam pulse width after the P-chopper, resulting from additional pulses from the multi-turn extraction.

The period of the sinusoidal voltage wave is $2m\tau_c$ ($1/m$: reduction rate), and the length of a beam pulse train must be shorter than the period to extract a single beam pulse from the train. This is realized when T is shorter than $T_{max} = 2m\tau_c - (n-1)\tau_c - t_b$, as illustrated in Fig. 2.

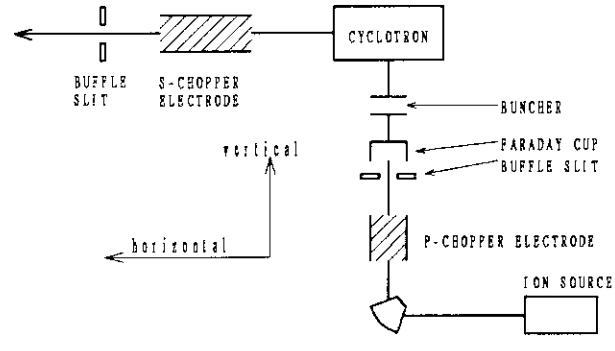

Fig.1 Schematic layout of beam chopping system.

(2) Optimization of Parameters

The design of beam transport optics and the arrangement of optical elements around the choppers restrict the parameters concerning the chopper geometry. On the other hand, we are allowed to choose a maximum value of the P-chopper voltage V_{pmax} within a limitation of high voltage application. If we choose a large value of m, a large T and a small V_{pmax} are allowed. Contrary to that, however, the S-chopper voltage applied on k-1 and k+1 th pulses are lower for larger m (see Fig. 2-h,i) and the maximum S-chopper voltage V_{smax} is required to be smaller than 40 kV to avoid dielectric breakdown. There is another restriction on the S-chopper that the frequency can cover a range within a factor three because of a limitation on the capacitance of the tuning condenser. The essential point for the optimization is to search a combination of reasonable values of V_{pmax} and m. In consideration of practical allowance we required a strict condition that the deviation should be larger than 1.5 time the slit gap for both choppers. The number of multi-turn extraction n was not defined and we assumed it at five.

It was found that 1.5 kV was practically reasonable for the maximum value of V_{pmax} and resulted in reasonable choice of T value of the S-chopper for almost all ion species and energies.

As a result of above consideration

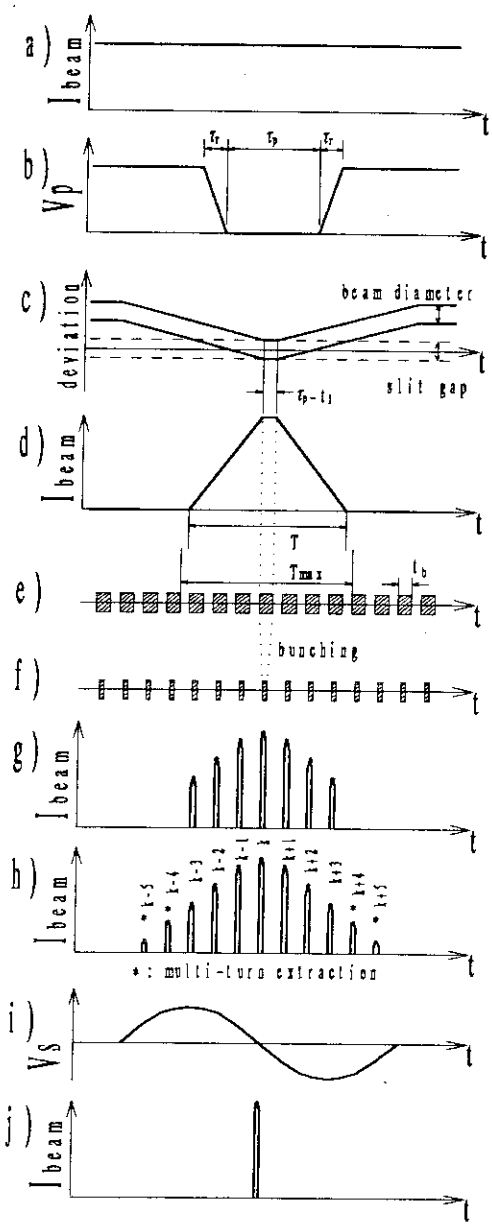

Fig.1 Diagram of beam chopping process (an example for chopping rate 1/6).
a)D.C beam current from ion sources.
b)P-chopper voltage wave.
c)Beam deviation at P-chopper baffle slit.
d)Beam pulse after passing through P-chopper.
e)Effective buncher phase.
f)Acceleration phase.
g)A group of plural beam pulses in cyclotron.
h)A train of plural beam pulses extracted from cyclotron.
i)S-chopper voltage wave.
j)Beam pulse after S-chopper.

we chose 4, 5 and 6 as the number m, and 1 to 3 MHz for the S-chopper frequency range. Finally optimized parameters are listed in Table 1. H^+ beam with energy higher than 75 MeV can not be chopped into a single beam pulse because of technical limitation in choice of small T value.

Table 1 Design parameter of the chopping system.

	P-chopper	S-chopper
electrode length (cm)	13	120
electrode gap (cm)	8	4
drift length (cm)	60	80
slit gap (cm)	2.4	0.4
maximum voltage (V)	1.5	40
frequency (MHz)	0.001 - 1.0	1.0 - 3.0
reduction rate 1/m	-	1/4, 1/5, 1/6

(3) Test Operation

The chopping system was tested with He^{2+} beams at extraction voltage of 8.5 kV and an acceleration energy 50 MeV. We observed beam pulse signals detected by Faraday cups after the P- and the S-choppers using an oscilloscope. The signals after the P-chopper were clearly observed in the same duration as that of the P-chopper voltage. Several signals were observed after the cyclotron, corresponding to one signal of them. However, the correct number of the pulses and the number of multi-turn extraction were not determined because of the poor signal to noise ratio. When the S-chopper was on and P-chopper off, one of every six beam pulses was observed after the S-chopper. We ensured that the pulse interval was the same as that of the P-chopper voltage with both choppers on, and finally a single pulse was extracted from a pulse train.

REFERENCES

1) W. Yokota, K. Arakawa, Y. Nakamura, T. Kamiya, M. Fukuda, T. Tachikawa, T. Mita and T. Satoh, Proc. of Twelfth Int. Conf. on Cyclotrons and their Applications, 1989, Berlin, Germany, pp.388-391.

1.6 Beam Scanners

Uniform irradiation of high-energy intense ion beams over a wide area is one of the most characteristics beam applications required from different fields of R&D in the ART project. Two-dimensional beam scanners have been designed and constructed for the cyclotron by using horizontal and vertical bending electromagnets feeded with alternating excitation current in triangular wave form. To avoid the power loss caused by the eddy current, these magnets are made of stacked thin iron plates. An ion beam is scanned in a fixed frequency of 50 Hz in one direction, and also scanned simultaneously in different frequencies of 0.5, 1.0, 2.5, 5.0 Hz in the normal direction. The maximum scanned area of 100×100 mm is available at the beam line LD for various accelerated energies within 50 MeV in proton beams. Beam scanners were installed on three beam lines(HY,LX and LD). The specifications of beam scanners are shown in Table 1.

Two-dimensional relative dose distributions of the irradiation by beam scanners were measured with cellulose-triacetate(CTA) film dosimeters.[1] The dosimetry is based on the linear dose response of radiation-induced optical densities at 280nm. An example of measured dose distributions in the irradiated film is shown in Fig. 1. In this case, the dose uniformity is within ±10% in the center area of 20×20 mm. There are three peaks along the x-axis: on the left hand side,the middle and the right hand side. These peaks cause inhomogeneity in the distribution. This feature of the distribution is common to most of irradiation results. This is because time-dependent magnetic field of the scanning magnet has distortions as shown in Fig. 2. The distortion near the peak is caused by the induced electromotive force and the one near the zero- cross point is caused by the transistor-off period for polarity change. In this experiment, the homogeneity is independent of scanning frequency but a little dependent on the beam size.

REFERENCES

1) Sunaga,H., et al., Radioisotopes,**Vol.37**,P84-87 (1988).

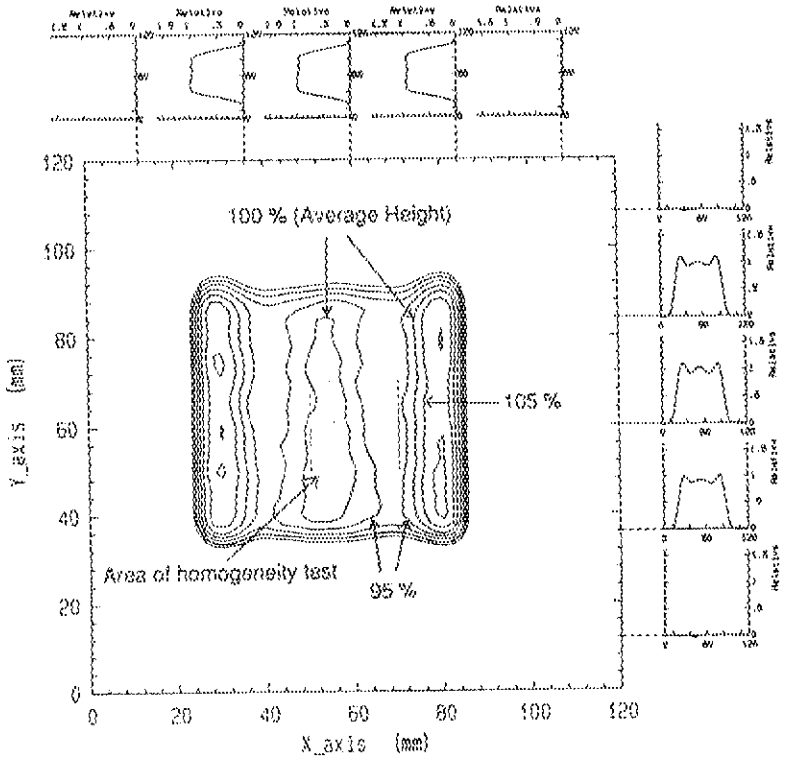

Fig. 1 Example of relative dose distribution.
(H 45MeV, LD1 port)

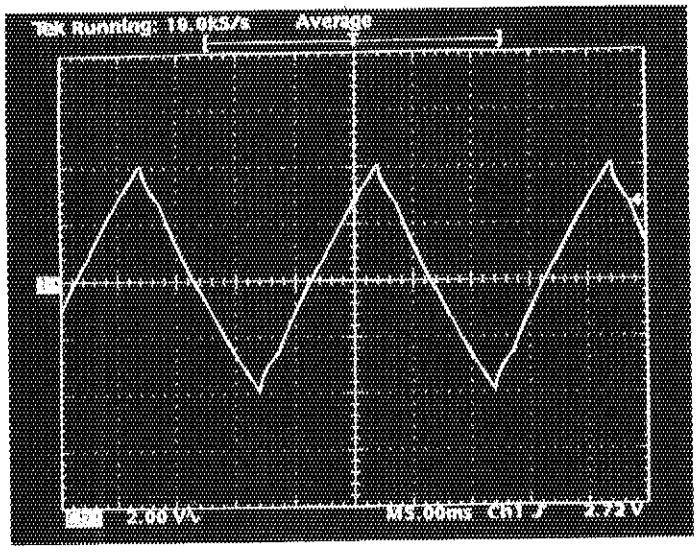

Fig. 2 Wave form of varying current supplied to the magnet.
(X direction, LD1 port)

Table 1 Specifications of beam scanners for the cyclotron.

Target Port	LD1	LX1	HY1
Direction of irradiation	horizontal	vertical	vertical
Scanned area of irradiation (mm)	20×20～100×100	10×10～20×20	20×20～50×50
One scanning period (sec)	0.1, 0.25, 0.5, 1.0	0.1, 0.25, 0.5, 1.0	0.1, 0.25, 0.5, 1.0
Frequency of magnetic field (Hz)	x:50 y:0.5, 1.0, 2.5, 5.0	x:50 y:0.5, 1.0, 2.5, 5.0	x:0.5, 1.0, 2.5, 5.0 y:50

1.7 Vacuum System

(1) General Description

The vacuum system for JAERI AVF cyclotron[1] has been designed based on a plan as follows:

1) Whole vacuum system is divided into 25 vacuum sections as shown in Fig. 1. Each section is managed independently and systematically.

2) The vacuum system is controlled separately from cyclotron control, and operated in remote or local mode.

3) Aluminum ducts, metal gaskets and all-metal gate valves were adopted to reduce outgassing from the vacuum components, because high transmission rate of ion beams is required mainly for heavy ion acceleration.

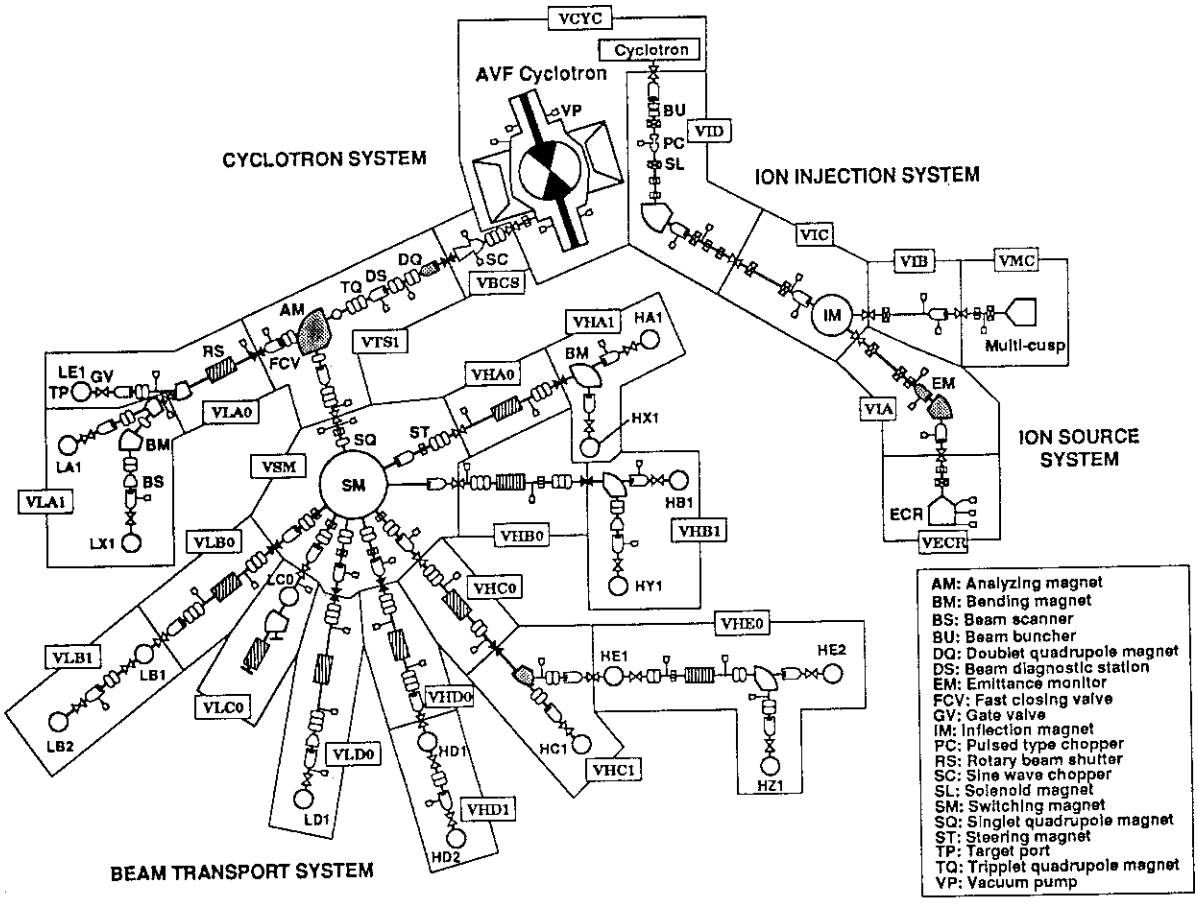

Fig.1 General construction and division of vacuum sections on the vacuum system for JAERI AVF cyclotron.

4) Sputter ion pumps (IP) and cryogenic pumps (CRYO) were chosen for simple composition and oil-free condition of the system. Magnetic suspended turbo molecular pumps (MSTMP) were used for auxiliary evacuation.

5) Some parts of the vacuum controllers sensitive against radiation exposure were installed at the places where the radiation level is relatively low.

(2) Pressure Required and Beam Transmission

Beam current loss depends on the total path length of the ion, the residual gas pressure and the cross section of charge exchange reaction with the gas, since the contribution of Coulomb scattering to the total beam current loss is generally much smaller than that of charge exchange reaction.

In the cyclotron, as the total number of turn N is much larger than 1, the total path length X is expressed by

$$X = \sum_{n=1}^{N} L_n = \frac{2\pi R_{ex}}{\sqrt{N}} \sum_{n=1}^{N} \sqrt{n} = 2\pi R_{ex} \left(\frac{2}{3}N + \frac{1}{2}\right), \tag{1}$$

where R_{ex} is the extraction radius, L_n the traveling distance of accelerated ions at n-th turn in the cyclotron. The average orbit radius is equal to about 2/3 of the extraction radius.

And, N is written as

$$N = \frac{K}{4eV_D \sin\left(\frac{h\theta}{2}\right) \sin\left(\phi_0 + \frac{h\theta}{2}\right)} \cdot \frac{Q}{M}, \tag{2}$$

where K is the K-number of the cyclotron, e unit charge, V_D (MV) the dee voltage, h the harmonic number, θ the dee angle, ϕ_0 the acceleration phase, Q the charge state and M the mass number.

For the maximum energy (295 MeV) of $^{84}Kr^{15+}$ in the JAERI AVF cyclotron, N is evaluated at 210 for h=3 and $V_D = 33.5 \times 10^{-3}$, and X is calculated at 815 m for R_{ex}=0.923 m. Assuming the pressure in the vacuum chamber (P) is 6.7×10^{-5} Pa and the cross section of the charge exchange[2] (σ_T) is 9.1×10^{-17} cm^2, the transmission rate of $^{84}Kr^{15+}$ in the vacuum chamber is estimated at 0.88 by using the equation: $f_T = \exp(-2.47 \times 10^{14} \cdot P \cdot \sigma_T \cdot X)$.

The transmission rate of $^{84}Kr^{15+}$ in the ion injection system is evaluated at f_T=0.93 for the 24 m beam-line, assuming that σ_T[3] is 1.7×10^{-14}cm^2, which is given for 100 keV, and that the pressure of the injection beam-line is 6.7×10^{-6} Pa.

To estimate the beam transmission rate in the beam transport system, σ_T is written by the equation[4]:

$$\sigma_T = \sigma_L + \sigma_C = 9 \times 10^{-19} Q^{-0.4} \beta^{-2} + 3 \times 10^{-28} Q^{2.5} \beta^{-7}, \tag{3}$$

where σ_L is the cross section of electron loss, σ_C that of electron capture and β the velocity ratio of ion beam to light. For 310 MeV $^{129}Xe^{27+}$, the equation (3) gives $1.7 \times 10^{-16}cm^2$ where σ_L is $4.6 \times 10^{-17}cm^2$ and σ_C is $1.2 \times 10^{-16}cm^2$. The beam loss at 6.7×10^{-5} Pa is estimated at only 1.5 % for the longest beam-line of 54 m length, and that for 2.5 MeV protons is almost the same as that for 310 MeV $^{129}Xe^{27+}$.

From the above results, the beam loss due to the interaction of ions with residual gases at the pressure required is expected to be 20 % at the maximum for heavy ion beams.

(3) Vacuum System

The main specifications of the vacuum system are shown in Table 1. Each vacuum section is partitioned off the gate valves so that the restoration work for vacuum failure can be localized. The cyclotron is protected from vacuum accidents by eight fast closing gate valves (closing time:16 msec) installed in several beam-lines. Figure 2 illustrates the vacuum system of the cyclotron. The main pumps are four CRYO's (4000 ℓ/s), each pair of them is directly mounted at the bottom of each resonator, and a MSTMP (2000 ℓ/s) is connected with the vacuum chamber. Differential evacuation systems are provided to easily exchange the inflector and puller electrodes, and to pull out the main and deflector probes without breakdown of high vacuum.

Table 1 Number of pumps, valves and gauges.

Sputter ion pump	33
Cryogenic pump	10
Magnetic suspended turbo molecular pump	15
Rotary pump	22
Gate valve (more than 4 in.)	45
Gate valve (fast closing, 4 in.)	8
Right angle valve (4 in.)	45
Ionization gauge	4
Portable evacuation unit	5

In the ion injection system, the evacuation system consists of CRYO's (1600 ℓ/s) and MSTMP's (270 ℓ/s) which were installed at the beam diagnostic stations. A thick beam-line duct of 6 in. in diameter was selected for the ion injection to minimize the beam loss resulting from the large beam emittance.

An example of vacuum sections in the beam transport system after extraction from the cyclotron is shown in Fig. 3. The beam-line duct of 4 in. in diameter is made of aluminum alloy (A6063) to reduce outgassing and radioactivation. The arrangement and result of measuring outgassing rate of the aluminum duct is shown in Fig. 4. The measured value agrees with the designed one.

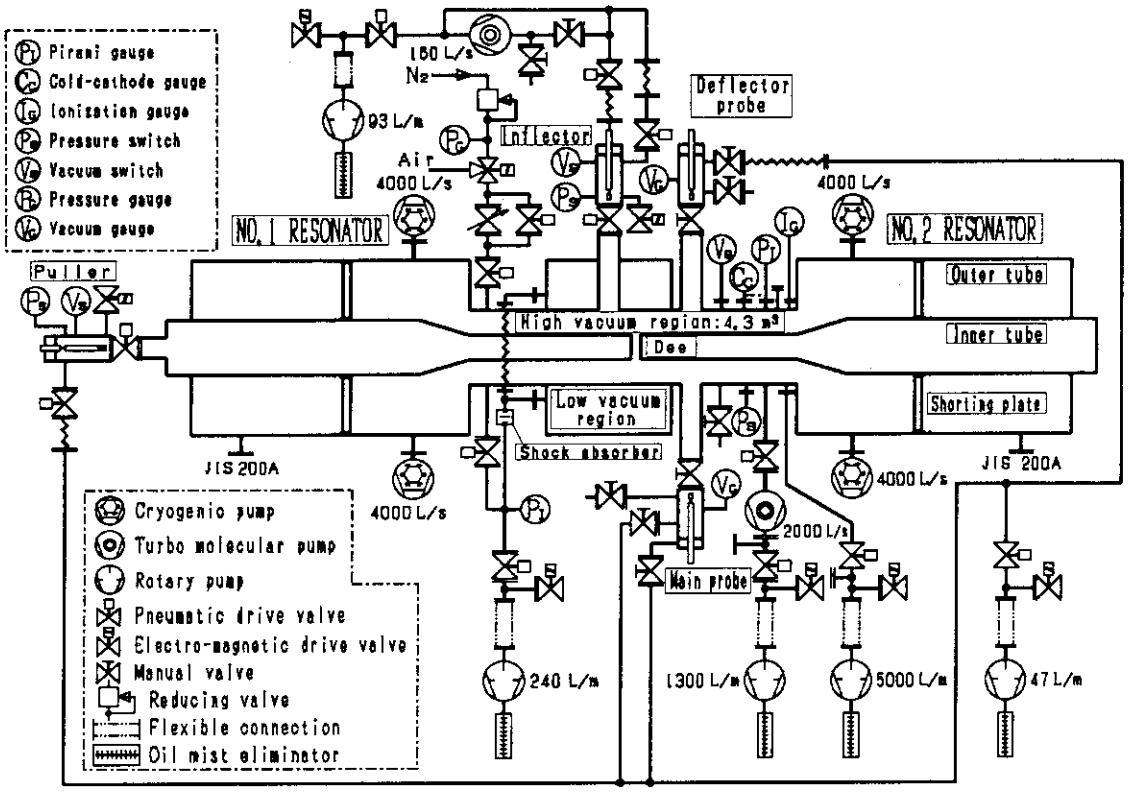

Fig.2 Vacuum system of the JAERI AVF cyclotron.

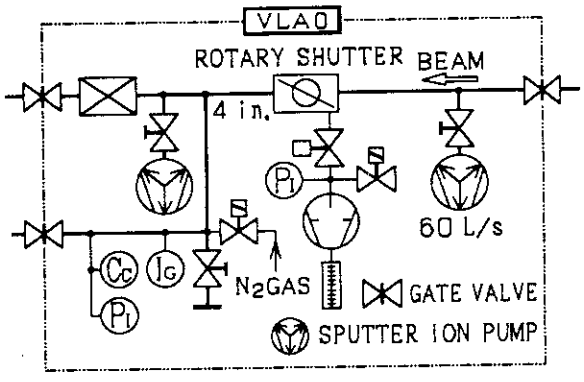

Fig.3 Construction of a vacuum section in the beam transport system.

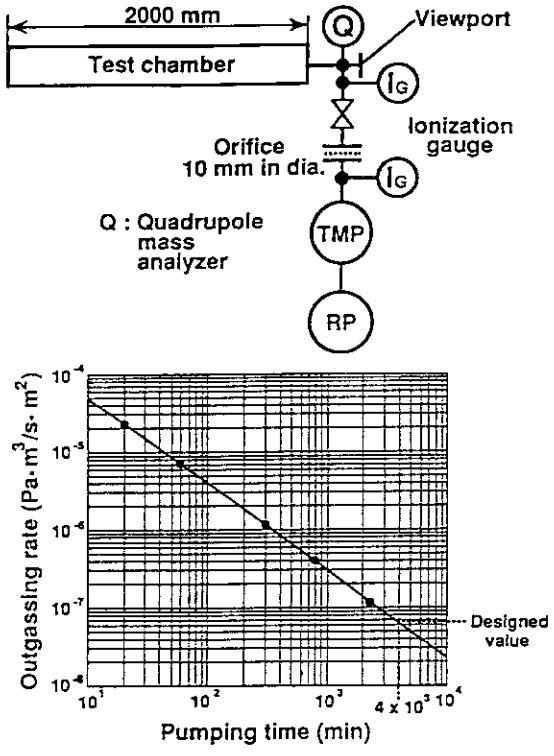

Fig.4 Arrangement and result of measuring outgassing rate of the aluminum duct.

The vacuum section is roughly evacuated by a portable unit consisting of a MSTMP and a rotary pump. High vacuum condition is held by two IP's (60 ℓ/s) in the section. A rotary pump was installed to exclusively evacuate the narrow space where an axial vacuum seal is used around the driving shaft of a rotary beam shutter, inserted in a penetration beam-line duct across the radiation shielding wall. Each vacuum section is also equipped with a wide-range vacuum gauge consisting of a pair of a Pirani and a cold-cathode gauge, and also provided with the leak lines for dry nitrogen gas and the open air.

The pressure distribution is estimated based on the outgassing rate[5] from component materials and geometrical structures. Figure 5 shows the calculated pressure distribution in the cyclotron. The total outgassing load was evaluated at 1.6×10^{-5}Pa$\cdot$m^3/s, and the pressure was estimated at 2.8×10^{-5} Pa at the top of the dee, and 7.3×10^{-5} Pa at the bottom in the perpendicular injection hole.

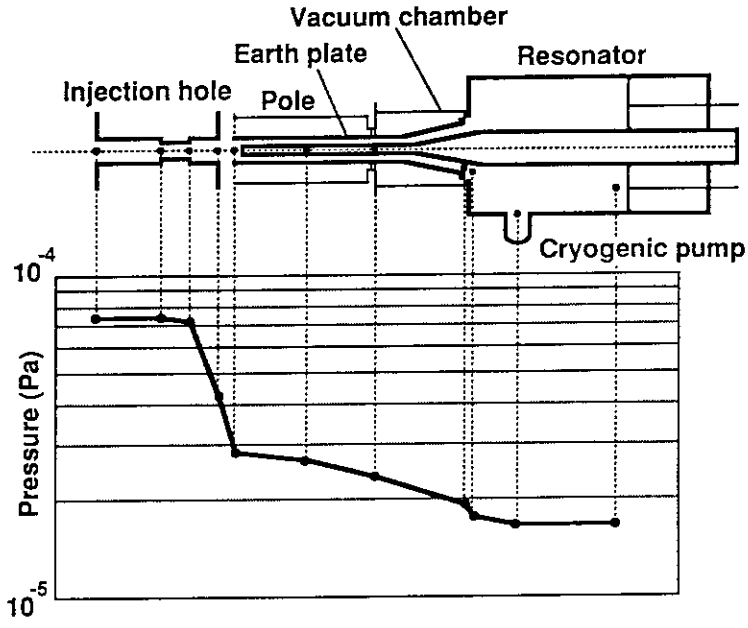

Fig.5 Pressure distribution in the JAERI AVF cyclotron.

(4) Present Status

There has been no serious trouble in the vacuum system since the start of evacuation in October, 1990. After a year passed, the pressure is 2 to 3 $\times 10^{-6}$ Pa in the ion injection system, 1 to 2 $\times 10^{-5}$ Pa in the vacuum chamber of the cyclotron and 0.4 to 6×10^{-5} Pa in the greater part of beam transport system.

The vacuum condition of the cyclotron system is going up to a steady state gradually, and the pressure required in whole vacuum sections will be also satisfied in near future.

REFERENCES

1) K.Arakawa, Y. Nakamura, W. Yokota, M. Fukuda et al., Proc. 8th Symp. Accel. Sci. Technol., Saitama, Japan (1991).
2) Private communication, Universite Catholique de Louvain.
3) J. L. Belmont, Rapport Interne, ISN 86-106, ISN Grenoble (1986).
4) H. C. Hseuh, I. Feigenbaum, M. Manni, P. Stattel, R. Skelton, IEEE Trans. Nucl. Sci., **NS-32**, No. 5 (1985).
5) Private communication, ULVAC, Corp.

1.8 Utility

I. COOLING SYSTEM

(1) General Description

The cooling system of the JAERI AVF cyclotron consists of three separate closed loop : ion sources and injection loop, cyclotron loop and beam transport loop. Each loop provides a mechanically sealed water pump, heat-exchanger and demineralizers so as to isolate the primary cooling water with low electric conductivity from the secondary one.

This system was designed according to several technical criteria as follows;

1) it has excellent durability so that the system can be continuously operated for a long time,

2) the temperature of circulating water is constant in the primary loop,

3) radioactivity in the primary loop dose not release into the environment,

4) the electrical conductivity of the primary water is enough low to insulate high-voltage devices such as dees and deflector electrodes.

(2) Design

Figure 1 shows a block diagram of the cooling system. The water temperature at the outlet of the heat-exchanger is monitored by a resistance thermometer, of which the signal is fed back to a temperature controller. The water temperature is controlled by changing the flow rate into the heat-exchanger. The primary cooling water is regulated at a constant temperature of 30°C.

All of the components and water pipes are made of stainless steel to minimize metal dissolution into the primary loop. A number of water connection nylon hoses are used for mechanical flexibility and electric insulation. The low-conductivity water is supplied by mixed-bed demineralizers and each split stream (about 10% of total flow rate) is recycled through a demineralizer to keep the conductivity less than 1 μS/cm except a vacuum cooling loop.

A couple of demineralization towers (DT), in serial connection,each of which is filled with ion exchange resin are installed in each loop. The flow sequence from one tower to another can be changed easily by valve operation. This coupling system is effective to reduce the volume of the radioactive resin waste. The cooling towers (CT) in the secondary loops are installed on the roof of the cyclotron building to cool the primary water by the heat exchangers. To protect the secondary water from extraneous

contaminations, a closed type cooling towers were adopted for the secondary cooling loops. A chilled water vessel (CWV,1000 m^3) to supply water (12°C) cooled by a turbo refrigerator was provided to keep the temperature of the primary loop constant in hot season. The expansion tank (EXT,1.5 m^3) is also auxiliary provided to supply demineralized water. The characteristics of the primary cooling system are shown in Table 1. The amount of the ion exchange resin was estimated on the basis of data on the corrosive metallic ions which are solved into purified water. The total surface area of stainless steel and copper in contact with purified water were 54 m^2 for the ion sources and the injection system, 256 m^2 the cyclotron system and 653 m^2 the beam transport system. The corrosion thickness for copper was empirically estimated at about 2 μm/year.[1] If the value is the same as that for stainless steel, the life time of the ion exchange resin is estimated to be about one year from the total surface area and the corrosion thickness. The values of the resin volume required are listed in Table 1. A mixture consisting of the same volume of anion (IRN-77) and cation (IRN-78) resins is actually used for the ion exchange resin.

Since the vacuum cooling system dose not require demineralization of water, raw water cooled by a chiller unit is only circulated in the primary loop. Rotary pumps, turbo molecular pumps, and cryogenic pumps in the vacuum system are cooled by a separate system which is operated independently. The information of the operational status of the cooling system is indicated graphically on the operation panel in the pump room. The operational status can be monitored at the graphic panel in the cyclotron control room.

Table 1 Characteristics of primary cooling system.

COOLING SYSTEM	Cooling capacity (kW)	Pressure loss (kg/cm^2)	Pump pressure (kg/cm^2)	Ion exchange resin volume (L)	Main pipe diameter
Ion source injection	139	6.0	9.5	30×2	40A
Cyclotron	778	12.0	15.0	135×2	125A
Beam transport	471	6.0	9.0	340×2	150A
Vacuum pump	19	2.0	5.0	-	25A

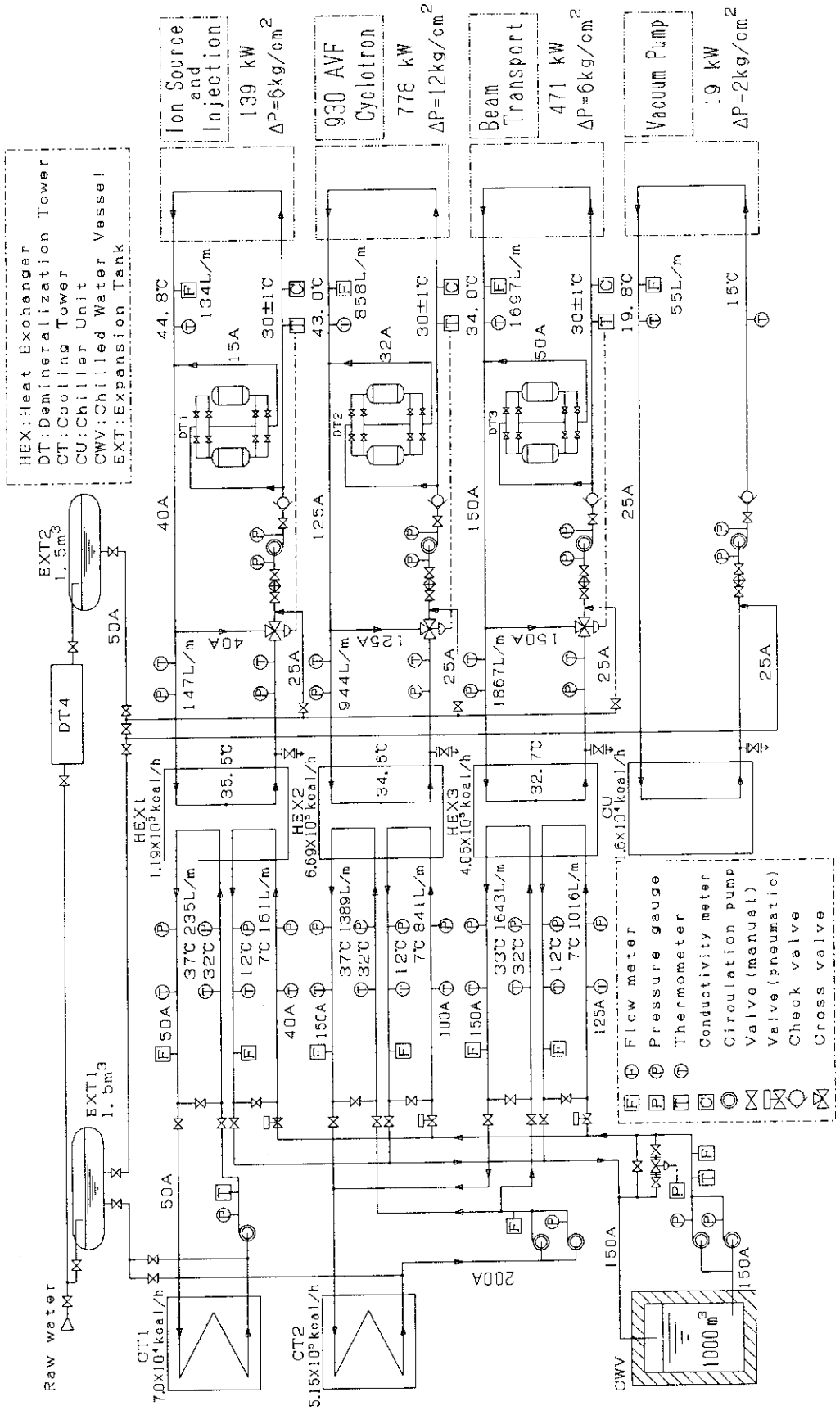

Fig. 1 Block diagram of cooling system

II. POWER SUPPLY SYSTEM

(1) General Description

Basic considerations for power supply system of JAERI AVF cyclotron are as follows.

1) Power supplies consist of saturable-core reactors and power transistors because it has been pointed out[2] that the noise due to large surge ON-state current from SCR may affect other circuits.

2) Stability of the magnet power supplies is regulated depending on the stability of their magnetic fields. Their current capacity has 10 % allowance.

3) To save the construction cost of the power supply system, several power supplies for common use were installed, each of which can feed electricity to plural magnets through a load selector.

4) A grounding conductor of the first class was prepared exclusively for many devices with large current capacity. The measured earth resistance was 0.8 Ω with copper grounding electrode 105 m deep.[3]

5) A smoke detector was mounted in each power supply box to prevent the firing damage, of which the signal is always monitored in the cyclotron control room.

6) A radiation-resistant and flame-retardant cable (FSR-PHCT,[4,5] ethylene-propylene rubber insulated hypalon sheathed flexible cable) was selected as a power cable for the magnets.

(2) Construction of Power Supply

AC 415 and AC 200 V of three-phases, AC 100 V of single-phase power are supplied to 4 switchboards located in the cyclotron power supply room, the ion source room, the water cooling room and the cyclotron control room. Electric power is supplied to each power supply through a magnetic circuit breaker (MCB) or an earth leakage breaker. Figure 2 shows a circuit diagram of 415 V lines as a typical example. In this diagram, MCB's of 500, 200 and 125 A are arranged in CYC_POW_10, _20 and _30 power supply boxes, respectively.

The block diagram of the power supply for each magnet is shown in Fig. 3. Three-phases AC input voltage is dropped down by the transformer, and rectified in full-wave mode. After the DC output is smoothed down by using a LC circuit, it is stabilized and controlled at a constant current by a transistor bank, and finally fed to loading elements. The transistor bank is equipped with many power transistors (2SD873), each

of which has 8 A of I_C and 140 V of V_{CB} as DC characteristics. The power supply of the cyclotron main coil with a rated-current of 900 A is composed of 340 transistors divided into 10 banks.

The power supplies are controlled and monitored by universal device controllers (UDC).[6] The monitoring signals of the output current through a shunt resistor and line-to-line voltage are transmitted to the UDC via a 4 channel ADC. The control data from

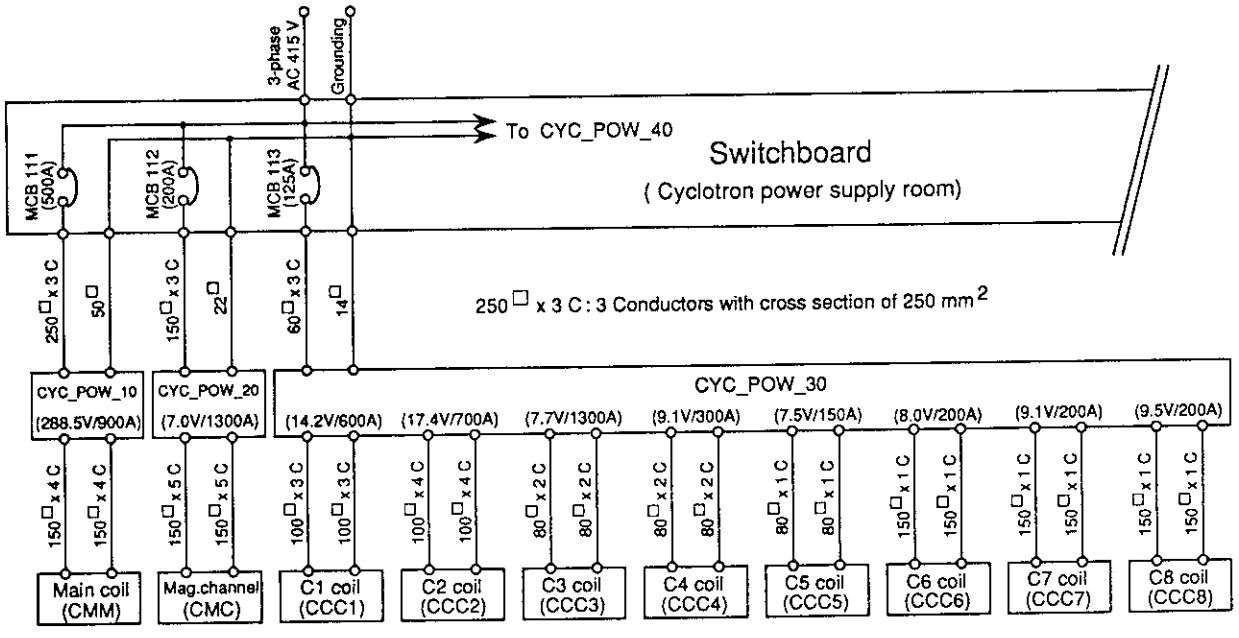

Fig. 2 Circuit diagram of three-phases 415 V lines for the power supplies of AVF cyclotron.

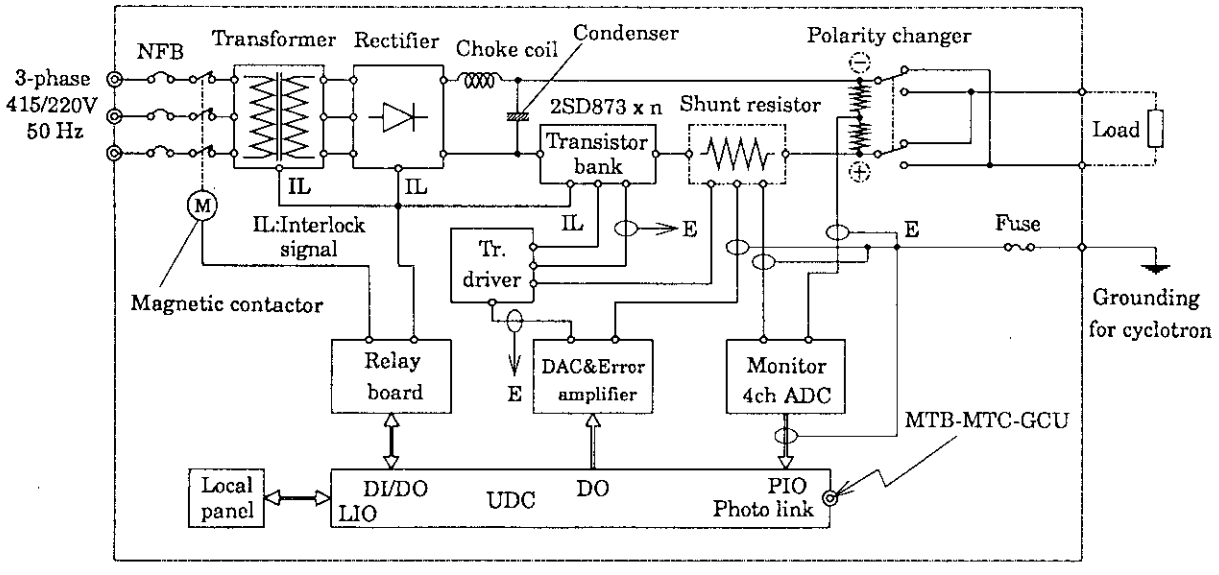

Fig. 3 Block diagram of a power supply for each magnet.

a group control unit (GCU) or a local panel are send to a DAC and an error amplifier through the UDC. The safety interlock signals from the transformer, the rectifier unit and the transistor bank, are also transmitted to the UDC.

The current stability was given depending on the required stability of the magnetic fields. The main coil of the cyclotron and the 80° analyzing magnets need a very high stability within $\pm 1 \times 10^{-5}$. In this power supply, the temperature of the shunt resistor enclosed in a cylinder tube is controlled to regulate stably the load current of magnets. The circular trimming coils for the cyclotron, solenoid lenses and quadrupole magnets for beam lines allow relatively low stability within $\pm 1 \times 10^{-4}$.

An example of measured stability data for the cyclotron main coil is shown in Fig. 4. The stability during 4 hours was estimated at $\pm 5.8 \times 10^{-6}$. The current ripple was also regulated at 1.3×10^{-6}, which was much less than the required value.

A 5 kVA uninterruptible power supply was connected with computer control lines so that short time failures of commercial electric power do not affect the computer system.

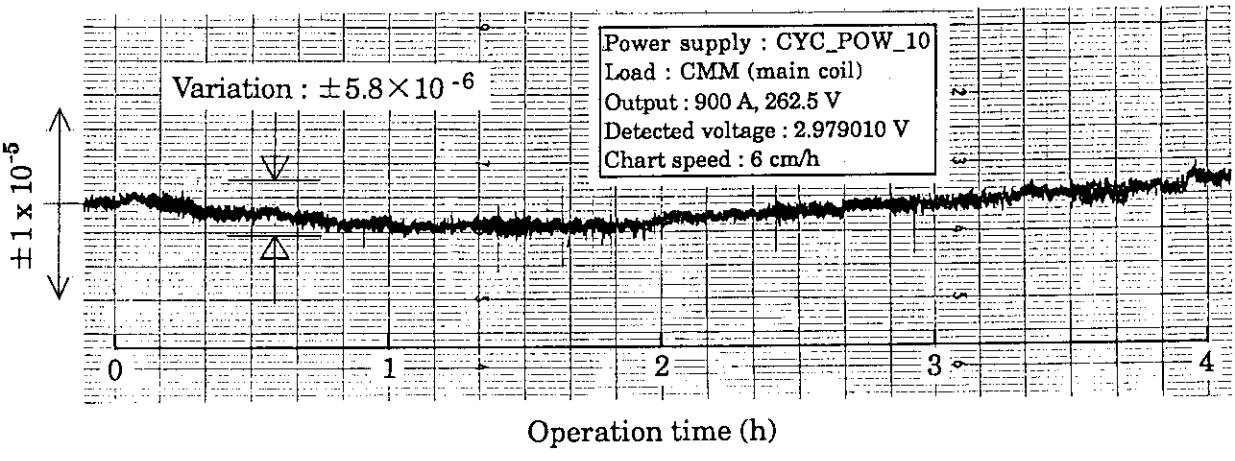

Fig. 4 Measured stability of the power supply when 900 A current was supplied to the cyclotron main coil.

(3) Power Consumption

The maximum amount of power consumption for whole cyclotron system was initially estimated at 1800 kVA in midsummer. The currents through the feeders during cyclotron operation were measured by using a digital clump meter (HIOKI, 3261) in early June, when an accelerated beam of 460 MeV $^{40}Ar^{+13}$ was transported to the

experiment port HE2 at the end of the second longest beam course. The measured current of each feeder was 1140 A for 415 V lines (820 kVA), 990 A for 200 V lines (340 kVA) and 140 A for 100 V lines (14 kVA), respectively. The total power consumption in the whole cyclotron system was evaluated at 1180 kVA which was 66 % of the initially estimated value.

(4) Cabling

A number of cables were laid along the beam courses. Many bent sleeves for cable penetration were installed under building construction, and were filled with the cables, occupying 30 % of their opening space for the radiation shielding.

The temperature rise due to the cable heating in the sleeve was estimated at 65°C at the maximum current. This value is tolerable because the limiting hottest-spot temperature of the PHCT cable is 80°C.

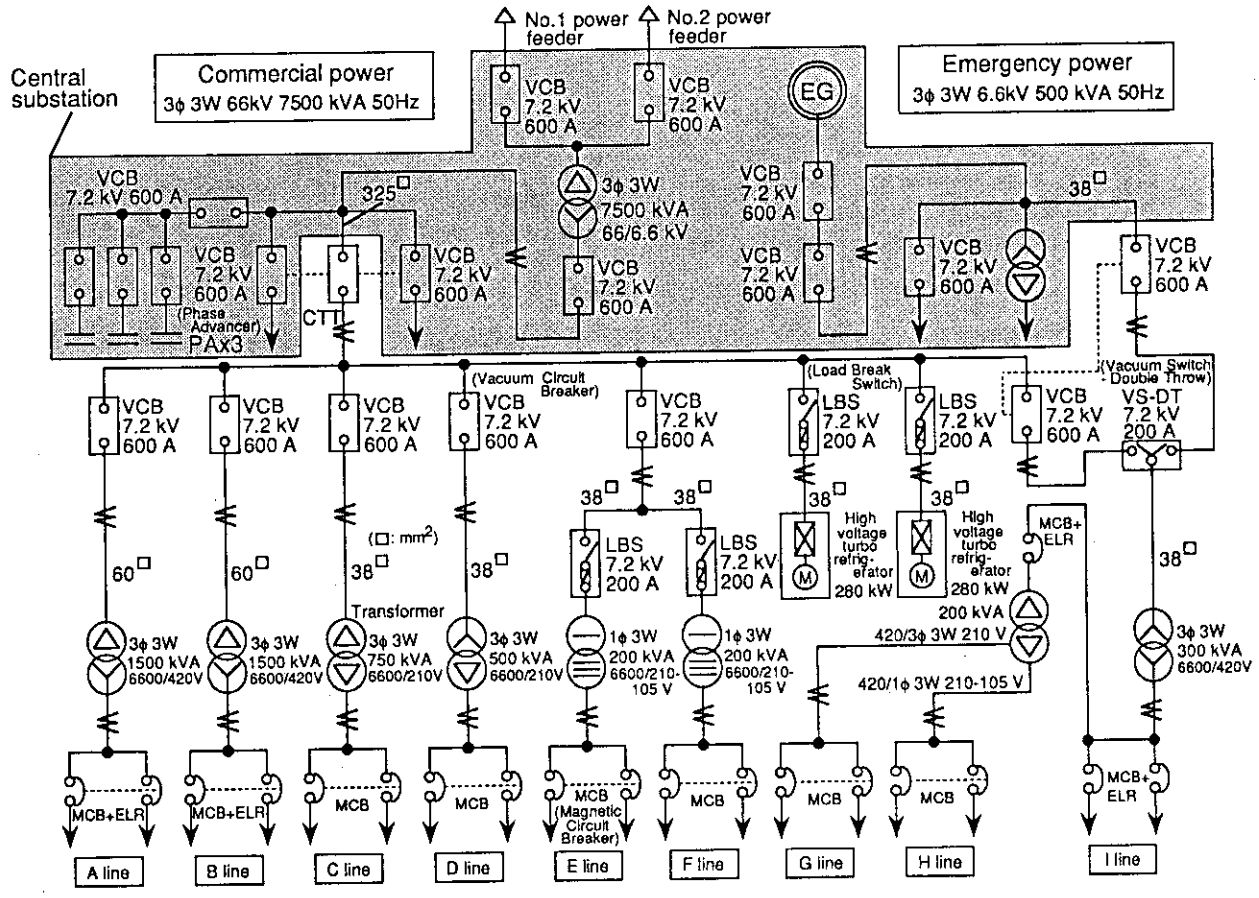

Fig. 5 Trunk connection diagram of the electric-supply lines for ion beam research facility.

(5) Electric-Supply Lines

Electric-supply lines of 66 kV extra-high voltage were replaced with the 6.6 kV high voltage electric-supply lines because of limitation of the power capacity. The trunk connection diagram[7] of the electric-supply lines is shown in Fig. 5. The cyclotron system has been operated smoothly without any failure during the first year's operation, although power failures were induced sometimes by lightnings which struck 6.6 kV lines in our site in summer.

REFERENCES

1) Y. Torikoshi, T. Ichino, M. Nakano, Bousyoku Gizyutu, 28, p343-347 (1979).
2) M. Fujioka, Private communication.
3) N. Akiyama, Private communication.
4) M. Hagiwara, Y. Morita, A. Udagawa, E. Oda, et al., Furukawa Denko Jihou, No.75 (1985).
5) Furukawa Denko, Catalog "Furukawa Super Radiation Resistance Cable" (1987).
6) S. Okumura, T. Agematsu, W. Yokota, T. Kamiya, et al., Proc. 8th Symp. Accel. Sci. Technol., Saitama, Japan (1991).
7) K. Fukuda, Private communication.

1.9 Control System

(1) Introduction

The computer control system of the cyclotron was designed so that an inexperienced operator can control devices smoothly without special knowledge about computers and programming. Using a man-machine interface and automated sequential programs, the operator can turn the cyclotron on or off and adjust device parameters efficiently. Such functions contribute to the reduction of the beam production time.

For the cyclotron operation, a knowledge based expert system has been developed to assist an operator with theoretical and empirical knowledges, which are required for the efficient beam production and transport.

(2) System Architecture

The system composed of computer networks like a tree structure is divided into three layers, as shown in Fig. 1. In the top layer, a central computer named system control unit(SCU) manages the whole system and serves operators with man-machine interfaces and operation functions. In the middle layer, two subcomputers named group control unit(GCU) control several groups of devices. In the bottom layer, universal device controllers(UDC's), single-board computers, are installed in each device for specific control.

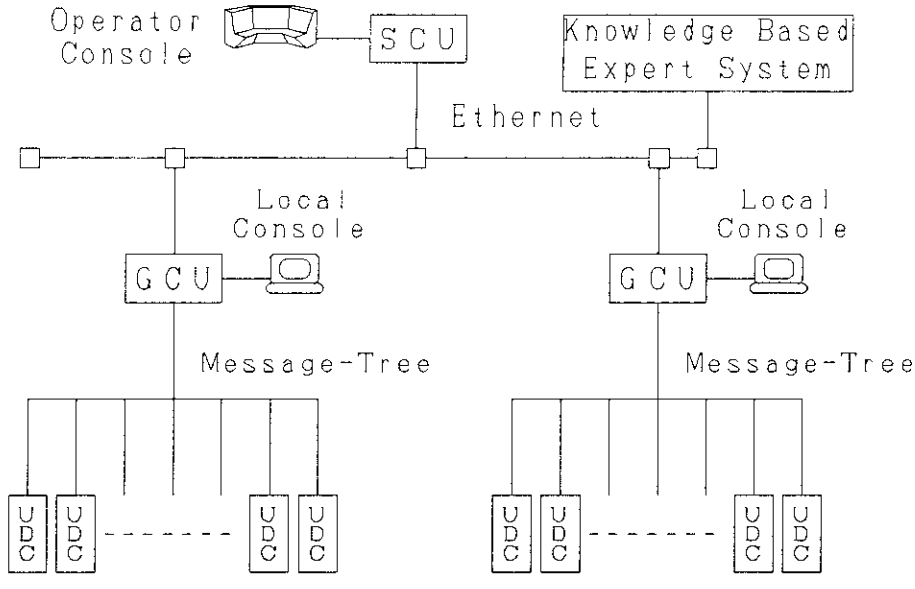

Fig.1 Architecture of the cyclotron control system.

SCU, GCU's and the knowledge based expert system are connected to each other

through an Ethernet. GCU communicates with UDC's through a signal-multiplexed communication system named Message-Tree.

SCU comprises a central processing unit(Micro VAX 3500), two hard disks, and several kinds of interface devices. Using touch-screens, rotary-encoders and graphic displays provided from SCU, the operator can control devices smoothly. Communicating with GCU's, SCU manages device conditions and control processes. Various files such as program and parameter files are stored and maintained in SCU. For a new beam production, SCU calculates a new set of parameters from stored parameter files on accelerated beams.

Two GCU's(rt VAX1000) execute the control sequences for each group of devices according to commands of SCU. All devices are divided into four groups: ion sources, the injection system, the cyclotron, and the beam transport system. One GCU manages the first three groups, and the other manages the last group through Message-Tree. Local consoles can connect with a GCU to control devices directly.

A UDC is an eight-bit single-board computer standardized for easy development and maintenance. 420 UDC's are used in the whole system. System and application softwares are programed and installed into two ROM's. A UDC controls each devices intelligently by executing eight tasks at the maximum capacity. Devices can be operated directly using a local panel connected with a UDC. The local panel indicates preset and actual values of the device,and provides several buttons for operation.

A Message-Tree is a signal-multiplexed communication system between GCU and UDC's, and consists of an interface board installed in GCU, named message tree communicator(MTC), a signal distributor named message tree brancher(MTB) and UDC's. Fifty UDC's can be connected to a MTC through a Message-Tree, and five MTC's can be connected to a GCU.

Message-Tree is a polling-addressing communication system; a MTC is a master and UDC's are slaves. MTC sends order message to all UDC's through a MTB. A MTB distributes the messages to all connected UDC's. UDC's receive the message identified by the UDC number and send response messages including only changed status data to reduce communication loads. These communications are executed every 100 ms. The major features of Message-Tree are the following:

- electromagnetic noise immunity by using optical-fiber cables;
- transmission speed of 375 kbit/s;
- transmission capability of 2.6 km;
- synchronous data-link control(SDLC) protocol.

(3) Operation

The cyclotron is normally operated using an operator console in the control room. The operator console consists of a pair of identical control units, and a monitor unit composed of a monitor TV for beam diagnostics, a 400 MHz oscilloscope for fast-signal measurement, etc. Each control unit provides a display-panel(20-inch CRT), an operation-panel(14-inch CRT), an adjustment-panel(14-inch CRT), the touch-screens on these panels, and four rotary-encoders. An operator can control devices by touching color-coded cells on the displays in combination with four rotary-encoders. The response time from a change of parameter to the display of the actual changed parameter is about 250 ms. The cyclotron is operated efficiently using two control units simultaneously.

When a fault occurs, a fail-safe sequence is executed automatically and the alarm is given as a sound signal and on display. An operator can receive information about the fault to clear up the causes.

Various data on every run of beam acceleration, such as ion species, acceleration energy and device parameters, are recorded in a log-file which is useful to refer records on past operations.

(4) Software

The operating system is VMS for SCU, and VAXELN for GCU, and C language is mainly used in these systems. Since GCU has no magnetic disk, the control programs and the device information stored in SCU are loaded into GCU's at system start-up.

The programs for GCU are described in a concurrent interpretive language for sequence control of accelerators, named OPELA(OPEration Language for Accelerator).[1] These programs can be debugged and modified easily and executed fast by using the intermediate codes. In these programs devices are treated as logic names to set and refer to parameter values.

The operating system of UDC(UDC44) has been developed for multitask programming to control devices. UDC44 consists of a kernel, a basic I/O system(BIOS) and a serial interface unit(SIU) handler. The kernel can manage eight tasks, and the BIOS manages communication registers and input-output ports. The SIU handler is a communication task for Message-Tree. Application programs can be written in a high-level language PL/M51.

(5) Knowledge Based Expert System

The knowledge based expert system assists operators in adjusting parameters with operational sequences. This system is programed by OPS83. These sequences, written in the IF-THEN form, are stored in the knowledge base and referred according to the operational condition. The operational sequences are divided into eight blocks from

axial injection to extraction of the cyclotron, so that even an inexperienced operator can understand the sequences clearly. This system can be useful by acquiring the knowledges of operations from experienced operators.

REFERENCES

1) Iso,K., et al., "A concurrent interpretive language for sequence control of accelerators", in proceedings of first workshop on control systems, Tsukuba, Japan, 1987, pp.100-103.

1.10 Safety Interlock System

The main tasks of the safety interlock system for the JAERI AVF cyclotron is to protect a person from the hazards due to unexpected radiations. The system mainly consists of hard wired and electromechanical relays. When high-energy ions are generated and/or transported in a radiation-shielded room, no one can enter the room by the interlock system. To generate high-energy ions safety in the cyclotron room, the status of the safety interlock system are requested as following conditions:

1) No one is in the room.

2) Shielding doors for entrance and exit are closed.

3) Radiation level in the working area outside the radiation shield is not over the safety limit.

4) The room is ventilated.

5) A safety working switch is not operated.

The safety interlock system enables to operate the cyclotron. The status of "Operation" is defined as the condition in which the RF voltage is generated on the dee electrodes. The RF voltage can be generated, when all of the interlock conditions are satisfied completely. If one of the interlock conditions is broken, the RF voltage can not be generated, or RF voltage generation is stopped immediately.

The operation of the cyclotron is divided into two modes. One is termed 'Adjustment Mode' in which the operating parameters are adjusted while ion beams are stopped at a Faraday cup just after the cyclotron. The other is termed 'Irradiation Mode' in which the ion beams are transported to the ion rooms for experiment. Details of the interlock conditions are shown in Fig. 1.

The limit of neutron generation in the ion rooms should depends on the capability of radiation shielding of each ion room. This means permissible neutron generation rate differs with each ion room. Since the neutron yield depends on ion particle, its energy and beam current, the permissible maximum beam current is given for each particle as a function of its energy. If the beam current exceeds the limit value of the room, the beam transport in the injection line is stopped automatically according to the interlock sequence. In consideration of neutron induced the activation of air in the cyclotron vault and in the light ion rooms, ventilation speed can be changed with the ion species and energies.

Now in the cyclotron facility, radiation field due to induced radioactivity is still in low level. However, the radiation level is expected to be steadily increased in the circumference of accelerated beam lines because light ions with high-energy and intense beam currents are requested for research experiments.

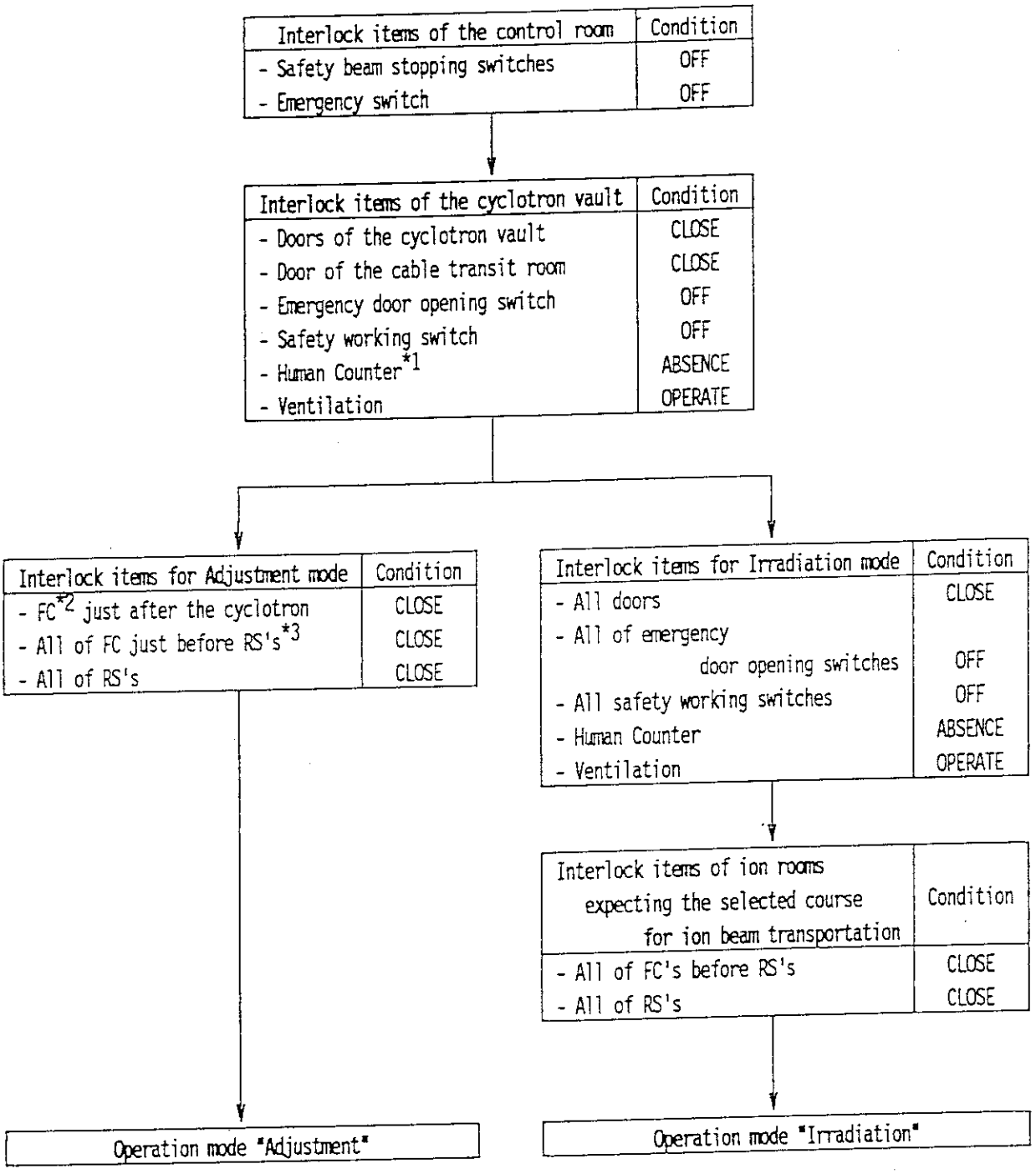

Fig.1 Interlock Condition of Cyclotron Operation.

*1 Human Counter: A system called "Non-Touch Cards" are human counters to detect whether anyone is in the rooms.

*2 FC: Faraday Cup

*3 RS: Rotary Shutter

2. ELECTROSTATIC ACCELERATORS

2.1 3MV Tandem Electrostatic Accelerator

Satoshi TAJIMA, Isao TAKADA, Kiyoshi MIZUHASHI,
Yuichi SAITO, Sadanori UNO, Kiyonori OKOSHI,
Yasuyuki ISHII, Masahiro ISHII, Keiichi YOTSUMOTO
and Ryuichi TANAKA

Department of Advanced Radiation Technology
Japan Atomic Energy Research Institute

I. INTRODUCTION

As a source of heavy ion beam covering an energy range from 0.8 to 21 MeV for the advanced radiation technology project, the model 9SDH-2 of Pelletron tandem accelerator (National Electrostatics Corp., USA)[1] was selected. The Installation of the accelerator and the beamline components started in December 1990. The first beam of 15 MeV Ni ions was accelerated on February 22, 1991. The accelerator completed at the end of March 1991 after acceptance tests.

This report outlines the accelerator system, the performance, and the initial operation for experiments.

II. ACCELERATOR SYSTEM

The tandem accelerator consists of a 3MV high voltage generator, two negative ion sources, a beam transport system and a control system. A layout of the accelerator system is shown in Fig.1.

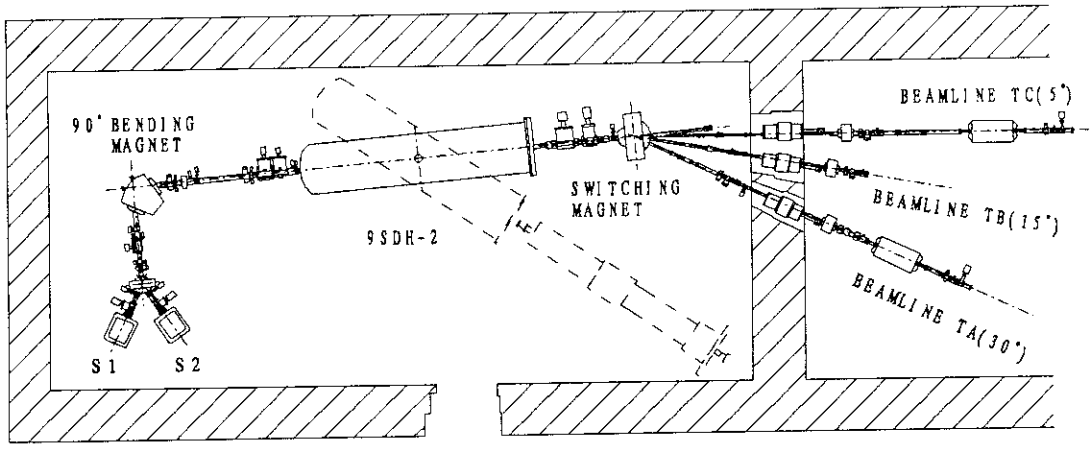

Fig.1 Layout of the 3MV Tandem Accelerator System, S1 and S2 are Negative Ion Sources.

(1) 3MV High Voltage Generator

The insulating column structure of the generator, shown in Fig.2, consisting of a low energy column, a high voltage terminal and a high energy column is housed in a pressure vessel. The pressure vessel, 5.64m in length and 1.22m in diameter, was designed at the maximum SF_6 gas pressure of 8.8kg/cm^{2}G. There are two Pelletron chains in the high energy column to deliver the maximum charging current of 250μA from ground to the terminal. The low and high energy accelerating tubes are placed in the low and high energy column, respectively. Both tubes are assembled by six units, and the maximum voltage load is 500kV/unit. Each unit has eighteen accelerating gaps with the maximum voltage load of 27.8kV. To make the uniform voltage distribution along the tubes, the grading resistors are fixed over each gap.

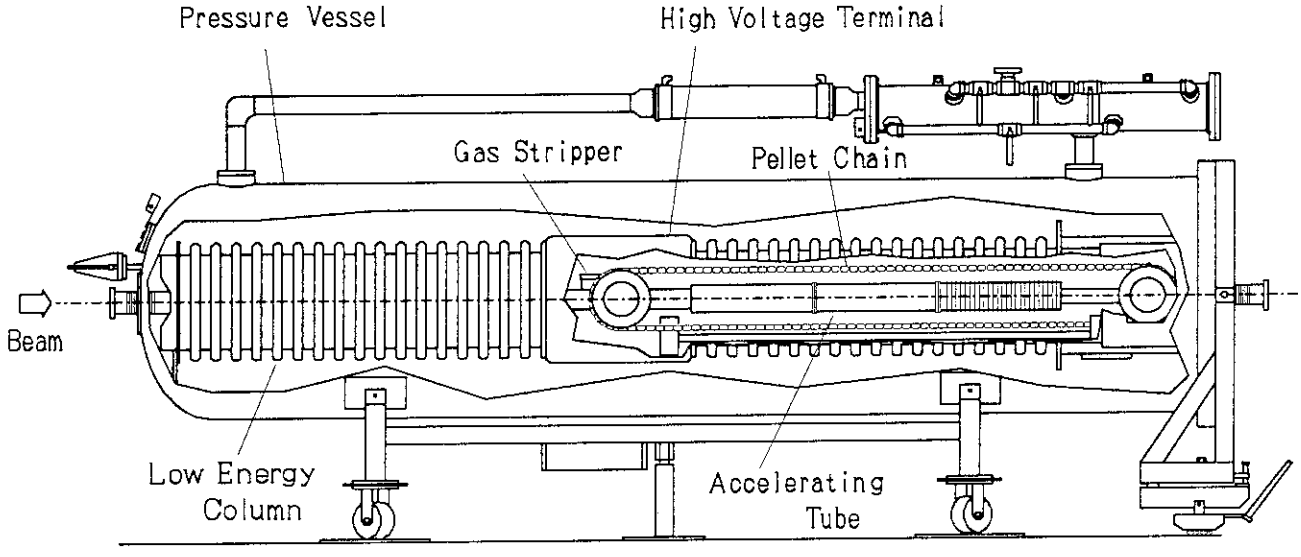

Fig.2 Structure of the 3MV Tandem Accelerator.

A gas stripper for exchanging negative ions to positive ones and a turbomolecular pump to recirculate nitrogen gas in the stripper are located in the high voltage terminal. The recirculation was very effective to prevent the gas load in the accelerating tubes. The recirculation efficiency was about 80%.

A corona probe system is provided to stabilize the terminal voltage which is determined by the balance between the charging current and the load current consisting of beam current, accelerating tube grading current and corona probe current. The probe keeps the balance by increasing or

decreasing the corona current so that the terminal voltage or beam energy may maintain the preset value. A generating voltmeter to measure the terminal voltage is located on the accelerator vessel and a energy slit to detect the beam energy is placed in each beamline behind a switching magnet.

(2) Negative Ion Sources

Two different type of negative ion sources are connected with the tandem accelerator; one is a charge exchange RF ion source, and the other a cesium sputter ion source. The former one (NEC, ALPHATROSS [S1]) is operated exclusively for generating helium ions. It consists of two stages. In the first stage the helium plasma is made by RF and magnetic fields in a quartz tube. He^+ ions are pushed out from the plasma to second stage by 6kV probe in the quartz tube. In the second stage He^- ions are produced by charge exchange collisions between He^+ ions and rubidium vapor. Finally, He^- yield of about 1.5μA can be extracted from the source.

The latter one (NEC, SNICS [S2]) produces a wide variety of the high intensity negative ions from hydrogen to bismuth except several ion species such as rare gases. The negative ions are generated from the cathode, containing the element of interest, sputtered by cesium ions. Various ion species, H (30μA), D (14), C (230), O (16), Si (16), Fe (2.4), Ni (98) and Au (75) have been available so far from the source.

(3) Beam Transport System

The beam transport line consists of three parts, a injection beamline, a post-acceleration beamline and three target beamlines. The beamline consists of oil-free vacuum components to prevent the organic contaminations.

The injection beamline is equipped with two bending magnets; one is a 30 degree switching magnet for selecting an ion source of S1 or S2, and the other is a 90 degree mass analyzing magnet. The mass energy product of both magnets were designed at 16 amu·MeV allowing to bend 80keV negative ions with masses from 1 to 200amu. The switching magnet equipped with five beam ports is located at the end of the post-acceleration beamline to select a target beamline of TA, TB, TC and TD of which the bending angle is 30, 15, 5 and -40 degree, respectively. The mass energy product

of the magnet is 150 amu・Mev at 30 degree. TD line is to be completed in the 2nd phase construction of TIARA.

Three experimental apparatuses were installed at the end of the three beamlines in the target room No.1. A heavy ion microbeam apparatus is located on TB line. An apparatus for heavy ion irradiation to cells in air with penetration depth control was connected with TC line.

(4) Control System

Two microcomputers (Heuricon Corp. 25MHz 68030) in a VME crate take care of management and development of a software and of digital real-time communication between a control console and local devices[2]. The accelerator system has about 800 input/output signals to control or readback by the control computer. These are interfaced to CAMAC. The control console consists of two main operator terminals, a touch panel terminal, a facility display terminal, eight analog assignable meters, a CRT for beam profile monitor and a digital oscilloscope for analyzing beam profiles. The parameters for normal operation can be controlled on the graphic display of the main operator terminal by using a mouse and a keyboard, and also can be controlled on the touch panel terminal.

(5) SF_6 Gas Handling System

The SF_6 gas handling system were installed in the air conditioning machine room No.1. SF_6 gas transfer can be operated automatically only pushing a button of recovery or filling. It takes 4.4hrs for gas transfer between the accelerator vessel and a storage tank located on the roof of the Cyclotron Building, when the pressure of the accelerator vessel is $6kg/cm^2G$.

(6) Safety system

The safety system for accelerator operation are basically the same for the tandem accelerator and the cyclotron. The interlock system for the tandem accelerator was designed so that the accelerator system can be operated when persons are outside the accelerator room and the door is closed, and also accelerated beams can be transported to the target room when target room is in the same conditions. If any one of interlock conditions breaks, the accelerator operation should be stopped immediately.

The accelerator room and target room are equipped with a couple of

radiation monitors for gamma rays and fast neutrons. The shielding door does not open if the measured values of the monitors exceed the preset alarm values.

III. PERFORMANCE OF THE ACCELERATOR

The acceptance tests of the accelerator system were carried out successfully from the end of February to March in 1991. Their performance are summarized in Table 1. The training of the operation and the accumulation of various operation data for the experiments were also conducted till the end of October 1991. The results of acceptance tests and some operation data are described below.

To determine the acceleration energy the generating voltmeter (GVM) was calibrated by using the nuclear reaction, $^{7}Li(p, n)^{7}Be$ of which the threshold energy is 1.880 MeV. Figure 3 shows neutron counts from the Li target with increasing proton energy gradually. The correction value for the GVM reading was 0.947.

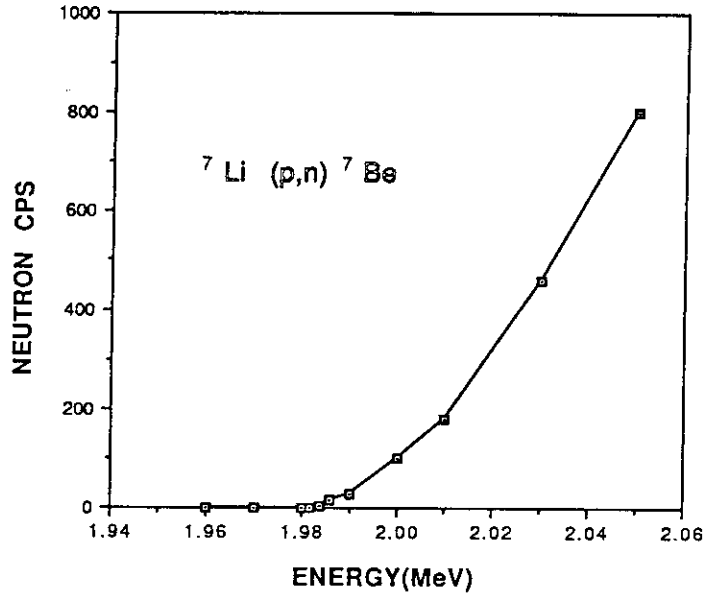

Fig.3 Measurement of the Threshold Proton Energy in the Nuclear Reaction $^{7}Li(p,n)$ for Calibration of the Generating Voltmeter.

The high voltage ripples (peak to peak value) at the terminal were measured by capacitive pick-off (CPO), which is located on the accelerator vessel against the terminal and calibrated with reference ripples. The ripples at the terminal voltage of 3MV were less than 600V in GVM mode

operation and less than 800V in slit mode operation, which satisfied the guaranteed value of the stability, 3×10^{-4}.

After the test of beam transmission, the acceptance tests of beam current measurement at the ends of beamlines were carried out. The measured beam currents exceeded the guaranteed beam current values for all the tested ion species and energies, listed in Table 1. The typical values of beam current at the ends of beamlines measured in the machine time (3-1) are listed in Table 2.

Table 1 Performance of the Tandem Accelerator.

Acceleration voltage:	0.4～3.0 MV (variable)	
Voltage stablility:	3×10^{-4} (P-P)	
Ion mass for acceleration:	1～200 amu	
Maximum charging current:	250 μA	
Maximum injection energy:	80 keV	
Acceleration energy:	1+ ion	0.8～ 6.0 MeV
	2+ ion	1.2～ 9.0 MeV
	3+ ion	1.6～12.0 MeV
	4+ ion	～15.0 MeV
	5+ ion	～18.0 MeV
Beam intensity on target:	H^+ 0.8 MeV	2.5 μA
	H^+ 6.0 MeV	5.0 μA
	He^{1+} 0.8 MeV	0.5 μA
	He^{2+} 9.0 MeV	1.0 μA
	C^{3+} 12.0 MeV	10.0 μA
	Ni^{4+} 15.0 MeV	4.0 μA
	Au^{3+} 12.0 MeV	15.0 μA

Table 2 Typical Beam Currents at the End of Beamline.

ION	ENERGY (MeV)	BEAM CURRENT (eμA)	BEAMLINE
p	0.9	0.73	TA
p	2.5	0.63	TA
p	3.75	0.50	TA
d	1.25	0.60	TA
He^{1+}	2.0	0.041	TA
He^{2+}	6.0	0.47	TC
He^{2+}	9.0	0.50	TC
C^{1+}	0.8	0.80	TA
C^{3+}	12.0	8.0	TC
C^{4+}	15.0	0.45	TB
O^{5+}	18.0	1.13	TA
S^{4+}	15.0	2.6	TA
Ni^{2+}	3.0	0.21	TA
Ni^{2+}	6.0	0.33	TA
Ni^{2+}	9.0	1.11	TA
Ni^{4+}	15.0	3.7	TB
Au^{2+}	3.0	0.65	TA
Au^{3+}	7.2	0.56	TA
Au^{6+}	21.0	0.24	TA

The charge distribution of positive ions after passing through the stripper gas depends on ion species, acceleration energy and gas pressure. The distributions were measured as a function of the gas pressure and the terminal voltage for different ions. The charge distribution of carbon, nickel and gold at 3MV are shown in Fig.4. The relation between measured beam current of different ion species and gas pressure are plotted in Fig.5. It indicates the stripper gas pressure at the maximum beam current depend on ion species.

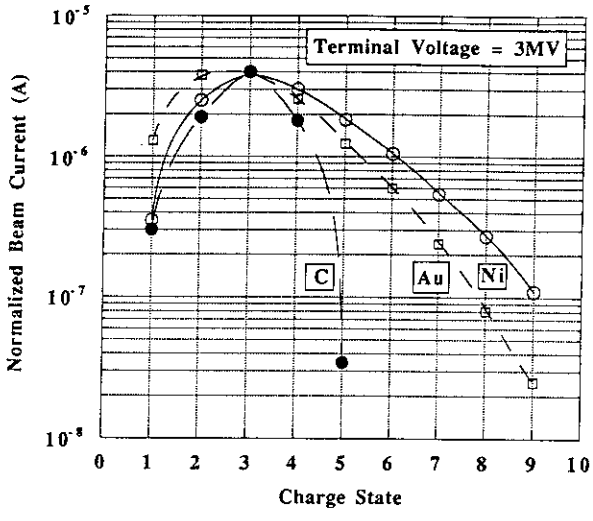

Fig.4 Charge State Distributions of C, Ni and Au Ions at 3MV after Passing Through the Stripper Gas.

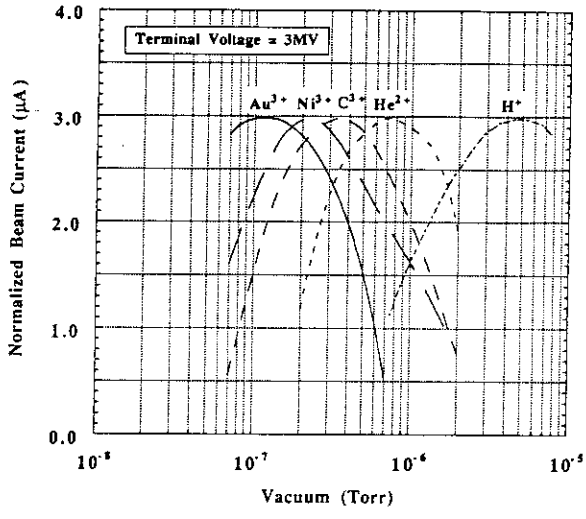

Fig.5 Beam Currents Measured for Several Ion Species at 3MV as a Function of Stripper Gas Pressure.

IV. OPERATION

The accelerator operation test was followed by the acceptance and the installation of experimental apparatuses at the beamline ends in the target room No.1, the heavy ion microbeam apparatus, the apparatus for heavy ion irradiation to cells in air with penetration depth control, and a chamber for ion implantation and ion beam analysis.

The tandem accelerator was smoothly operated for the first machine time (3-1) for experiment from November 1991 to March 1992 except a machine trouble. It was a break off of an insulating rod in the accelerator vessel, delivering rotating power to a terminal generator. The rod was replaced with new one. The break down time due to the trouble was only a week. Other miner machine troubles did not disturb the scheduled opera-

tion.

The main experiments were development of heavy ion microbeam technique (TB), measurement of single-event current transients in integrated circuits using the microbeam (TB), ion implantation and ion beam analysis for inorganic materials (TA), and development of irradiation technique for biological samples (TC).

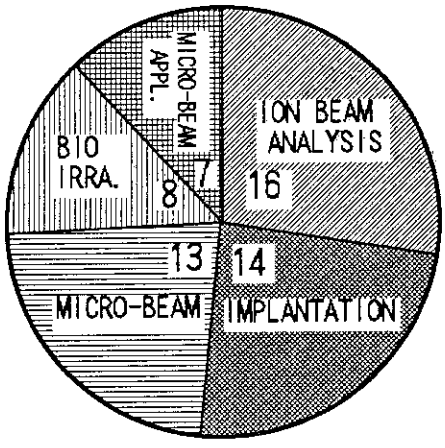

Fig.6 Contribution of Each Experimental Field in the Machine Time(3-1).

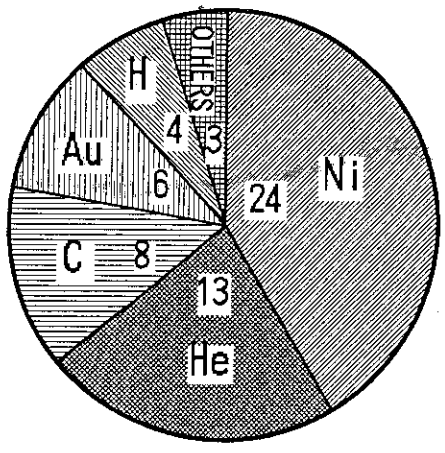

Fig.7 Contribution of Each Supplied Ion Species in the Machine Time(3-1).

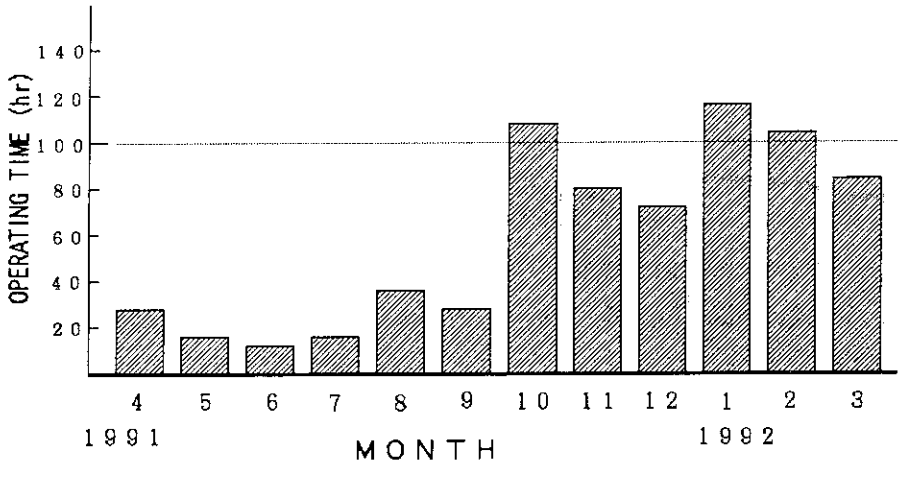

Fig.8 Monthly Operation Hours in 1991 Fiscal Year.

The contribution of each field of experiment in the operation time is summarized in Fig.6. The contribution of each supplied ion species in the yearly operation time for experiments are also summarized in Fig.7.

Supplied ion species were ^{1}H, ^{2}H, ^{4}He, ^{12}C, ^{16}O, ^{32}S, ^{58}Ni and ^{197}Au. The yearly operation time of the tandem accelerator for the fiscal year 1991 was 705 hours. Monthly operation hours throughout the year are shown in Fig.8.

REFERENCE

1) S.Tajima,I.Takada,K.Mizuhashi,Y.Saito,K.Yotsumoto,R.Tanaka, Proc. 4th Workshop on Tandem Accelerator and Technology, Takasaki(1991) p.27
2) R.D Rathmell, R.L Kitchen, Nucl. Instr. and Meth. B56/57 (1991)996

2.2 Multiple Ion Beam Irradiation Facility of the TIARA

Keiichi Yotsumoto, Satoshi Tajima, Isao Takada, Kiyoshi Mizuhashi, Tomihiro Kamiya, Yuichi Saitoh, Sadanori Uno, Kiyonori Ohgoshi

Department of Advanced Radiation Technology, JAERI

I. Introduction

The second phase construction work for the TIARA started in 1991 after completion of the AVF Cyclotron and the 3 MV Tandem accelerator facilities. Both of a 3MV and a 400 kV electrostatic accelerators are installed in a new building adjacent to the 3 MV Tandem accelerator facility which was completed in the first phase of the construction work.

A salient feature of the TIARA is to combine different ion beams from the electrostatic accelerators on target. In the triple-beam irradiation all the three accelerators are operated simultaneously and different ion beams are introduced to a target chamber. Since these accelerators can be operated independently and simultaneously three different combinations of dual-beam irradiation are also possible. These multiple ion beam irradiation technique will be effectively applied for simulating radiation damage of materials for nuclear fusion reactor. This paragraph outlines of the new ion beam irradiation facility being under construction.

II. Accelerators

3 MV D.C. accelerator is of a multi stage cascade rectifier type manufactured by NISSIN HIGH VOLTAGE CO., LTD.(N H V). Schematic layout of the accelerator is shown in Fig.1. The high voltage generator is separated from the acceleration section in the pressure vessel which is 2.5 m in diameter and 7.1 m in length. In order to control the terminal voltage a capacitive-resistor type high voltage measuring circuit is mounted in parallel with the acceleration tube. The circuit signal is led to the high-frequency power supply of the high voltage generator to regulate the terminal voltage. This system often has been applied to electron microscope so far and provides an extremely high voltage stability of 1×10^{-5} at the acceleration terminal. The ion source is of an RF type and can produce either positive ions or electrons.

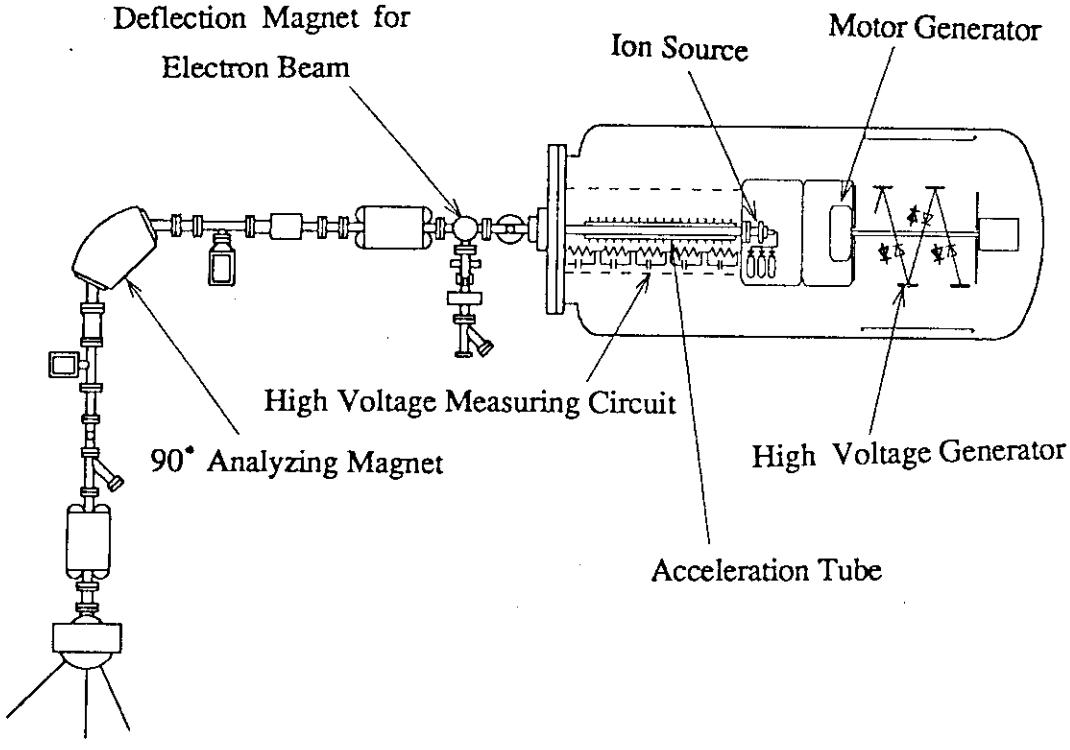

Fig. 1. General layout of the 3 MV D.C.Accelerator

To minimize beam instability the acceleration terminal is designed only to house the RF source with three source-gas bottles, and the power supply of which the motor generator is driven by a rotating shaft is incorporated in the high voltage generator. The electron beam from the RF source can be accelerated by changing the polarity of the high voltage generator. The output characteristics of the accelerator are shown in Table 1.

Table 1. Output characteristics of the 3MV D.C. accelerator

Acceleration voltage :	± 0.4 MV ~ 3.0 MV			
Voltage stability	± 1 x 10^{-5}			
Ion beam currents :	H	300	μA	(at 3MV)
	H	100		(at 0.4 MV)
	He	200		(at 3MV)
	He	50		(at 0.4 MV)
electron beams	e^-	100		(at 3MV)

The 400 kV D.C. accelerator is an air open of Cockcroft-Walton type also manufactured by N H V. The general view of the accelerator is shown in Fig.2. The high voltage terminal, 1.6 meter square and 0.84 m in height, is supported on four insulated ceramic columns surrounding the high voltage generator.

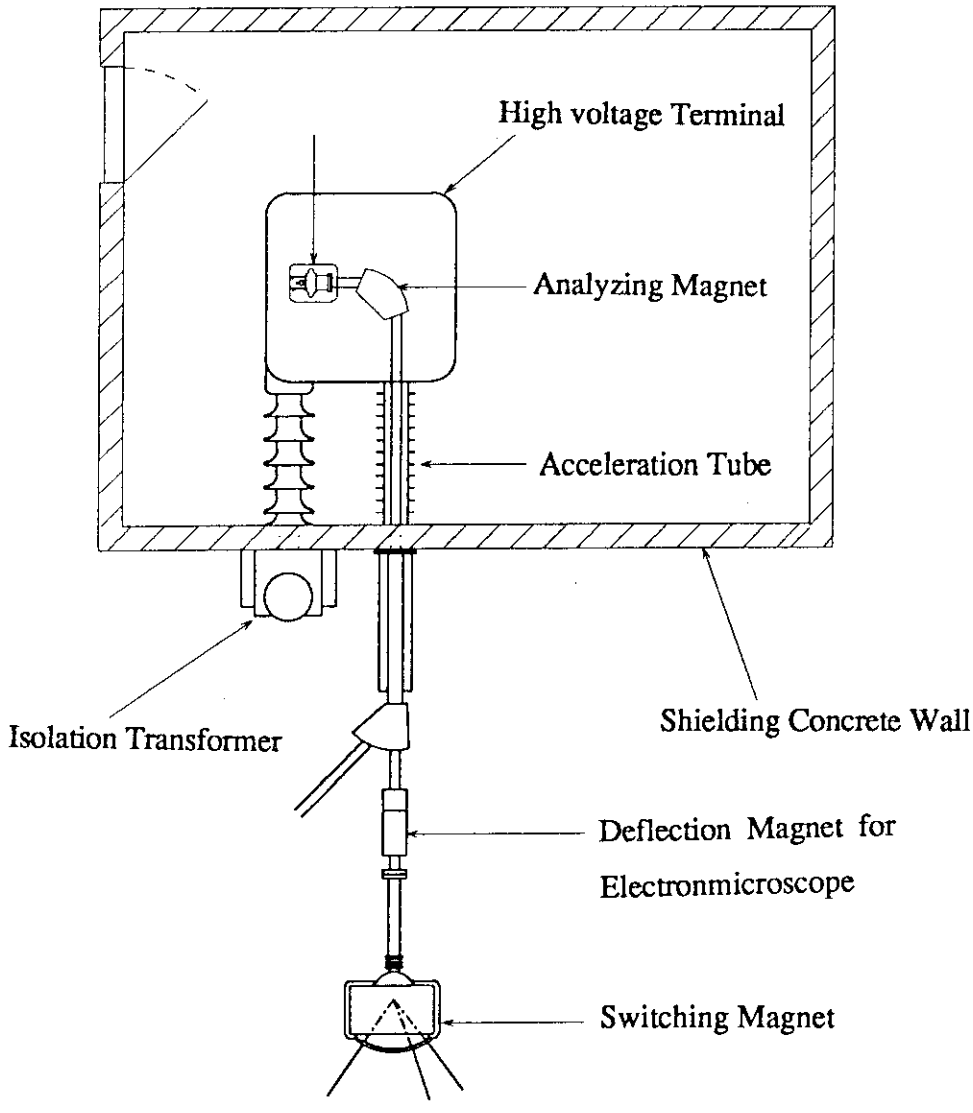

Fig.2. General layout of the 400 kV D.C. Accelerator

The ion source is of a Freeman type with a sputtering electrode and an oven, which produces ions in a wide range of mass. A 90° analyzing magnet with a mass resolution of more than 100 is located between the ion source and the acceleration section. The oil filled isolating transformer supplies electric power to the high voltage terminal through a special transmission line in parallel with the acceleration tube. The output characteristics of the accelerator are shown in Table.2.

Table.2. The output characteristics of the 400 kV D.C. accelerator

Acceleration voltage : 10 kV ~ 400 kV			
Voltage stability : $\pm 3 \times 10^{-3}$			
Beam currents :	Typical value on the target		
B	30 μA	Si	30 μA
P	30	As	30
Ar	30	Ag	4

III. Beam lines

A general layout of the accelerator irradiation facilities is shown in Fig.3. Three target chambers for the multiple ion beam irradiation will be installed in the target room No.2. An new beam line from 3 MV tandem accelerator manufactured by National Electrostatic Corporation (NEC) is also provided in the room through the shielding wall in which beam line-shield is embedded. Three different ion beams enter the chamber at an angle of 15 between the lines. To lead the ion beam down into an electron microscope with multianalytical functions,which will be installed in the target room No.4 in the basement a 50° deflection magnet is installed between the outlet of the 400 kV D.C.accelerator and a switching magnet.

A microprobe system is installed in the target room No.3 on the beam line from the 3 MV D.C. A 90° focussing uniform field magnet is located in the 3 MV D.C. accelerator's room at a distance of 8.6 m from the exit of the accelerator to achieve a focussed beam size of submicron level. This magnet has a mass energy product of 48 and a mean deflection radius of 1.5 m. To direct the electron beams down to the target room No.5 the electron deflection and beam line system is installed at the exit of the accelerator.

IV. Summary

The building construction work will be completed in March 1993 followed by the installation of accelerators and beam lines.The acceptance test operation will be done in July 1993.

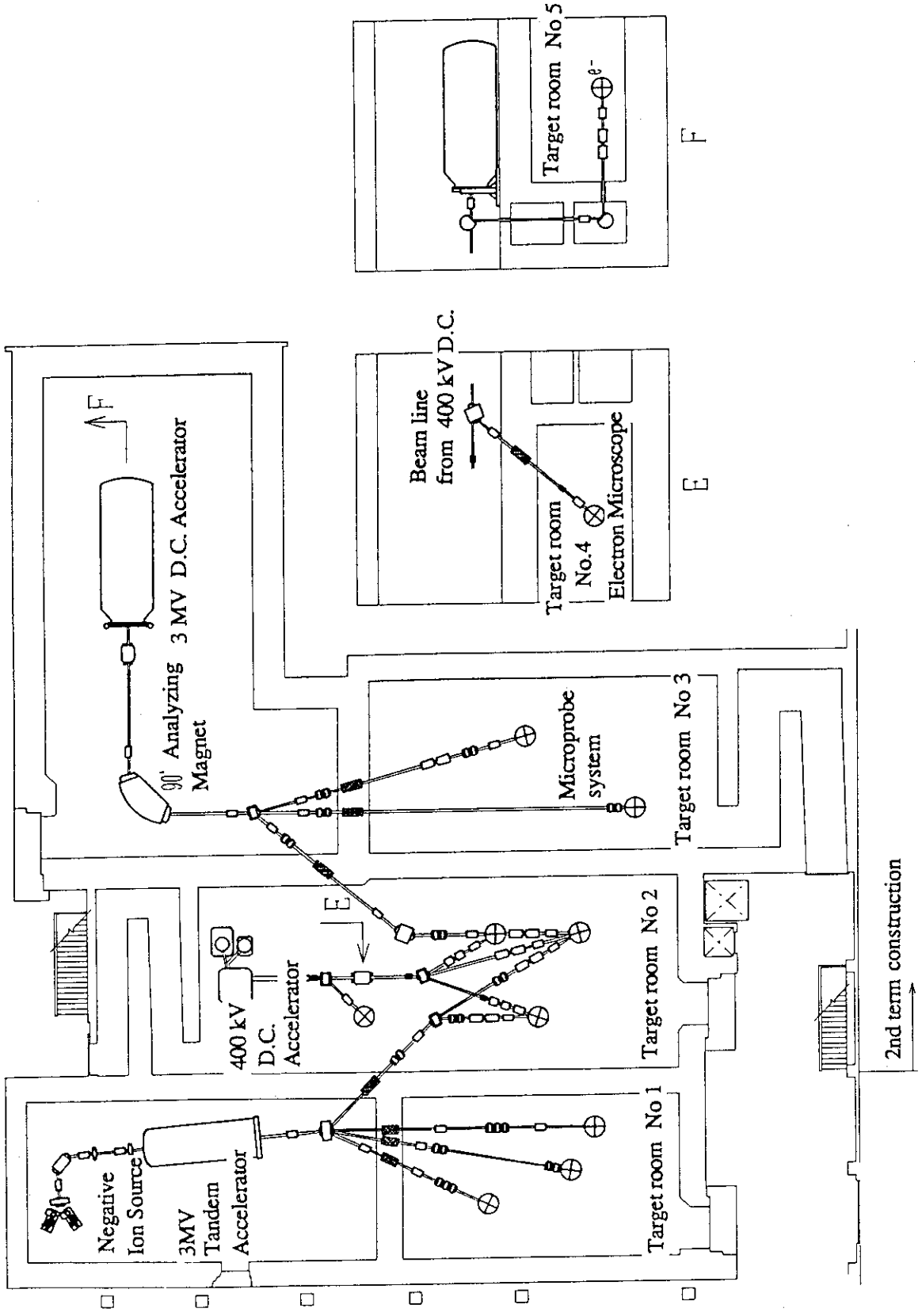

Fig.3. General layout of the multiple ion beam irradiation facilities

3. BEAM TECHNOLOGY

3.1 The Computer System for Experimental Data Handling

Koichi NISHIMURA, Sohei OKADA*, Watalu YOKOTA**, Mitsuhiro FUKUDA**, Yoshimasa OBA*** and Hiromasa WATANABE

Ion Beam Research Administration Division, *Irradiation Service Division,**Ion Accelerator Division, JAERI, ***RIKEI Co.Ltd.

Introduction

A wide variety of experiments for research on materials is proposed at TIARA. Many sorts of measurements are carried out for analyses of atomic structures by RBS, structural changes by time-resolved X-ray spectroscopy and electronic/defect structures by positron annihilation spectroscopy control. The computer system for device control, data acquisition and handling is required for the analyses.

This system enables remote control, data transfer and visualization through a fiber optic network free from RF noises and otherr disturbances.

Network

The network is constructed by use of fiber optic Ethernet conforming to IEEE802.3. The protocols of TCP/IP and DECnet are supported. Fig. 1 schematically shows the network topology. The network is available at various places in the Ion Beam Irradiation Research Building such as a computer room, experiment preparation rooms and terminal rooms. It is also connected to JAERInet, which makes it possible to access host computers (FACOM M-780 and VP-260) at JAERI Tokai. Functions of mail, remote-login and file transfer from/to some universities through TISN are equipped.

A software named Gator Share is installed in order to connect the network to Machintosh personal computer and Laser Writer. It is connected to Ethernet via Cyman's GatorBoxCS which acts as protcol converter between Apple Tolk and TCP/IP.

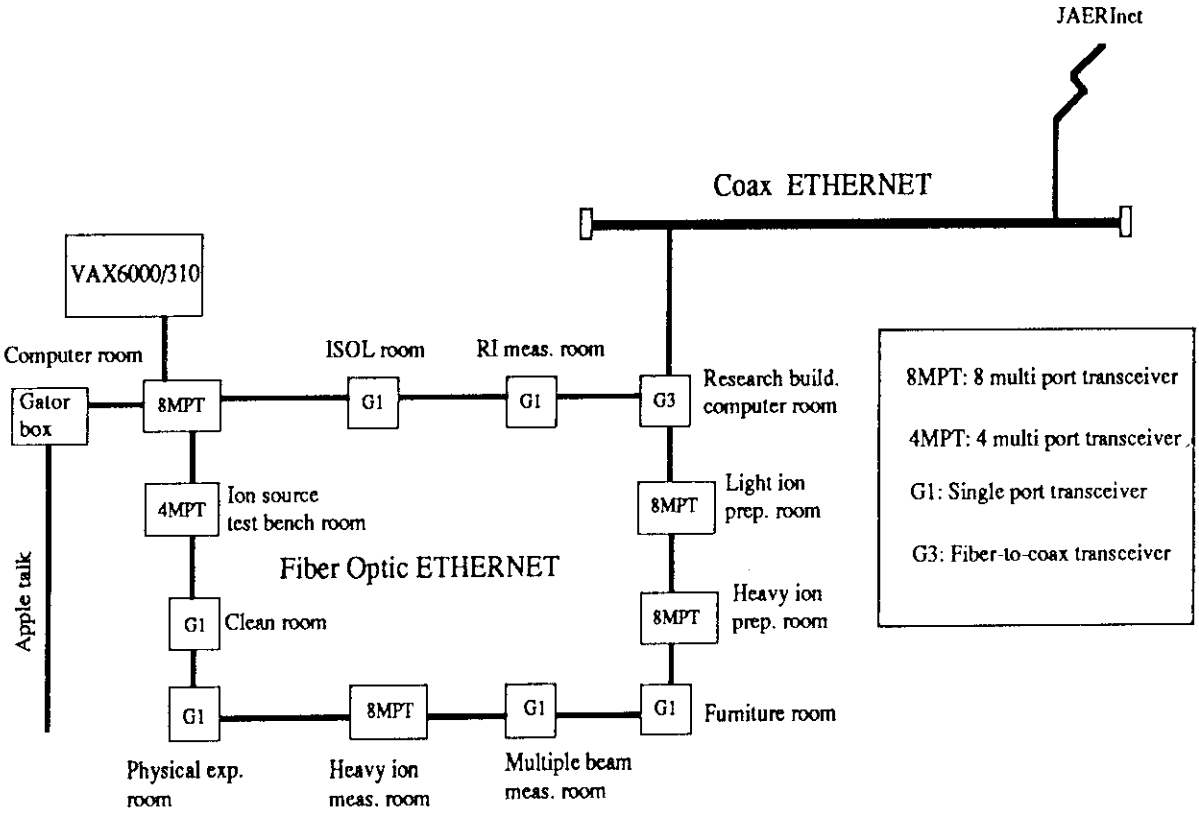

Fig. 1 Network topology at TIARA

Computer System

The computer system architecture is shown in Fig. 2. The computer is 32-bit operated VAX6000/310 of Digital Equipment Corp. It is equipped with a 32MB memory, a magnetic disk drive with 3.6GB capacity, an array processor AP500 , a system console terminal and a laser printer. The graphic displays are DEC station5000/200 and VT286.

Software

The operating systems of the VAX6000/310 and DECstation5000/200 are VAX/VMS and ULTRIX, respectively. The application programs are installed as graphic, digital signal processing and scientific subroutine library. The graphics routines are composed of UNIRAS package and DEC GKS. The digital signal processing routine uses ILS, and the scientific subroutine library IMSL.

An graphic program for data analysis was developed. Data can be displayed in different ways such as two dimensional event graph, two dimensional staff graph, three dimensional staff graph and three dimensional plot with contour

maps. A communication software through networks between VAX6000/310 and personal computer or workstation (UNIX, VMS) was also developed. Fig. 3 shows a schematic diagram of the communication system. Such communication programs are coded by VAX-FORTRAN and VAX-C. The communication protocols of DECnet is used for VAX, TCP/IP for UNIX machines and DECnet/ PCSA for personal computers.

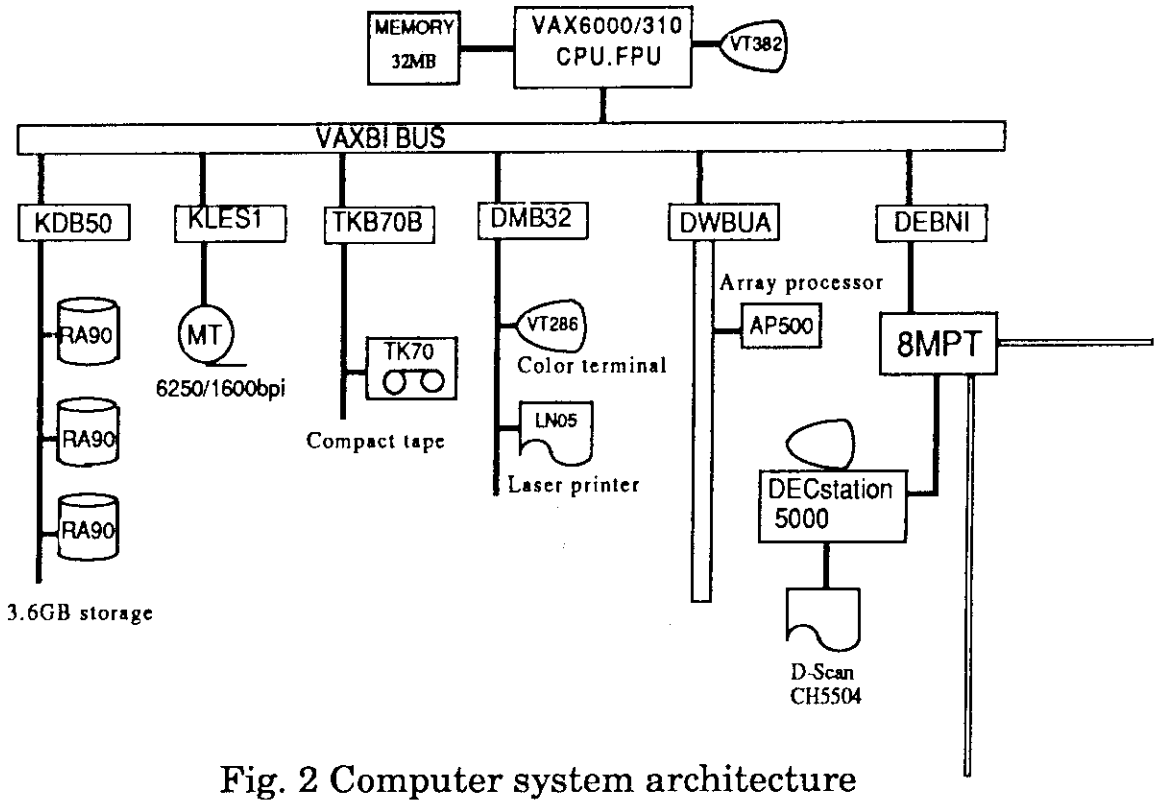

Fig. 2 Computer system architecture

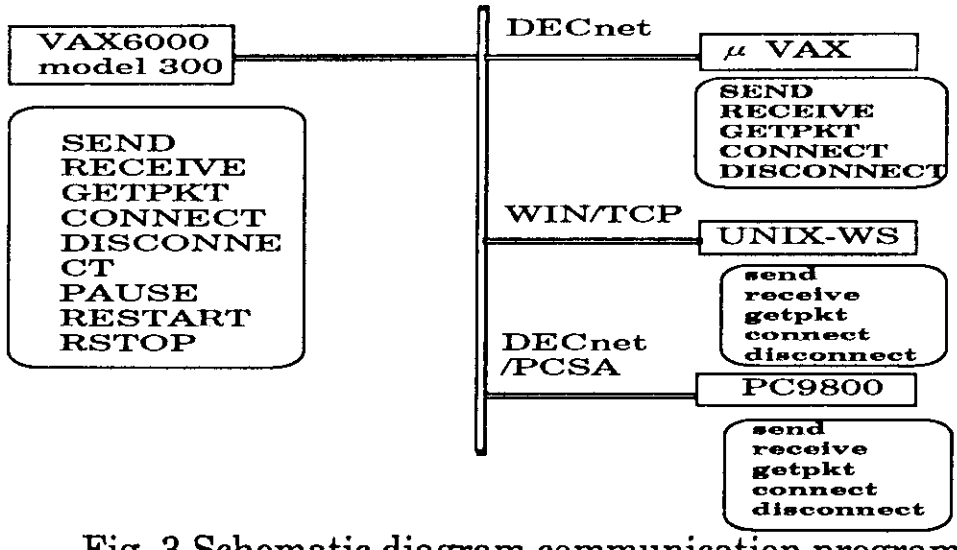

Fig. 3 Schematic diagram communication program

3.2 IRAC : A Code System to Calculate Induced Radioactivity Produced by Ions and Neutrons

[1)]Susumu TANAKA, [1)]Mitsuhiro FUKUDA, [1)]Koichi NISHIMURA,[1)]Watalu YOKOTA, [1)]Tomihiro KAMIYA, [1)]Hiromasa WATANABE,[2)]Tadao SHIRAISHI, [3)]Kentaro HATA and [4)]Naoki YAMANO

[1)]Department of Advanced Radiation Technology,
[2)]Department of JMTR Project,
[3)]Department of Radioisotopes, JAERI,
[4)]Sumitomo Atomic Energy Ind., Ltd.

1. INTRODUCTION

To meet various research plans in the Advanced Radiation Technology(ART) project[1)], four different type ion accelerators were installed in TIARA to cover a wide variety of ion species in different energies from several tens keV to several hundreds MeV. Target chambers and measuring instruments have been installed at the beam course ends of the accelerators to start experiments.

Radioactivity is induced in the accelerator components, the target chambers and target samples irradiated by energetic ions and secondary produced neutron beams. It depends on the projectile energy, beam current and the material of the components and the samples. In the planning stage of experiment, estimation of the induced radioactivity is required for radiation protections to reduce the radioactivity, and to minimize radiation exposure to personnel and the amount of radioactive wastes.

The IRAC and IRAC3D code systems[2)] have been developed in JAERI to provide a comprehensive computational capability to calculate radioactivity and gamma-ray dose rate at TIARA. The IRAC system is applicable to one-dimensional multi-material configurations for general purpose. The IRAC3D system extends the IRAC system capability to three-dimensional multi-material configurations.

This report describes the outline of the IRAC code system.

2. OUTLINE OF THE IRAC CODE SYSTEM

The IRAC code system computes the nuclide transmutations due to nuclear reactions and the consequent decays in plane multi-layered targets. It consists of the functional modules and data libraries for analyzing the induced radioactivity and the gamma-ray dose. The flow chart of the IRAC code system is shown in Fig. 1.

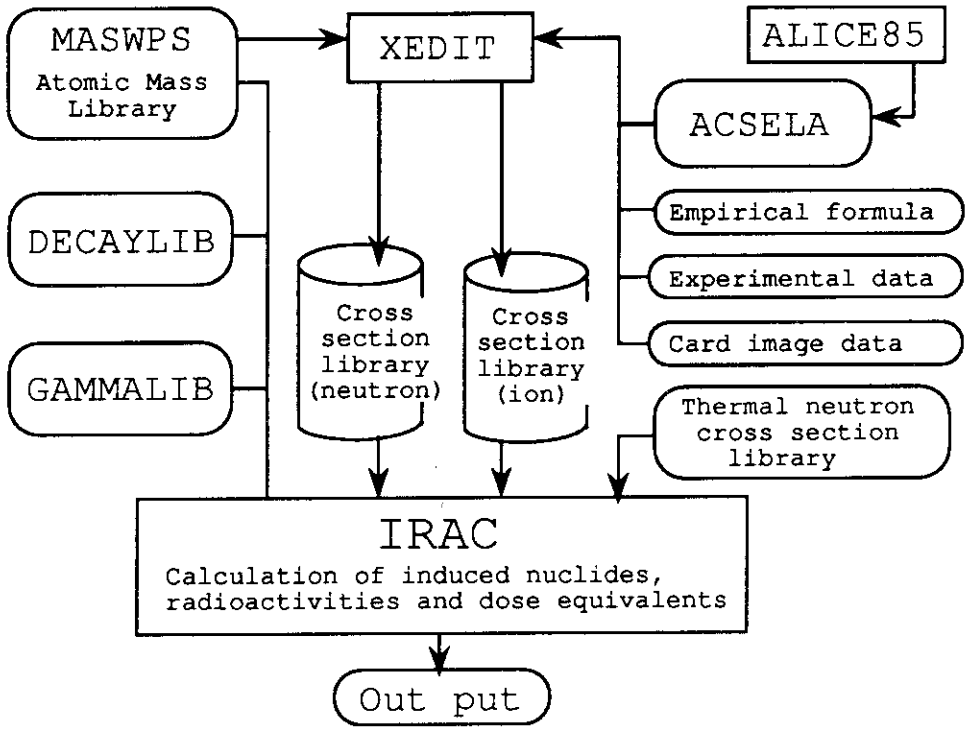

Fig. 1 Flow chart of induced radioactivity calculation in the IRAC code system

1) IRAC : Module for calculation of induced radioactivity

The IRAC(Induced Radioactivity Analysis code) is main functional module in the IRAC code system. The induced nuclides, radioactive nuclides, and gamma-ray dose equivalent rate are computed for the incident particles, ion and/or neutrons, at specified irradiation and cooling periods. Energy degradation of energetic ions in the target material is calculated by using stopping power and projected range obtained by subroutines of OSCAR code[3]. For energy degradation of neutrons, it assumed that the incident energy is kept constant in the target material.

Matrix exponential method adopted in ORIGEN2 code[4] are used to calculate transmutation of nuclides.

2) XEDIT : Module for generating activation cross sections

The XEDIT module is an editing tool for generating ion- and neutron- activation cross section libraries in the IRAC code system. The cross section libraries are obtained by editing a library of ACSELA(Activation Cross Section Library calculated by ALICE85 code[5]), experimental data, data calculated by empirical formula and card image data for specified incident particle and the target nuclides of interest.

3) ACSELA : Activation cross section library

The IRAC code system has a major activation cross section library, ACSELA, calculated with the ALICE85 code. The cross sections for combinations of 7 incident particles and 76 nuclides were calculated. Table 1 lists the incident particles and target nuclides in the library.

Table 1 Incident particles and target nuclides in the cross section library ACSELA

Incident particles	^{1}H, ^{2}H, ^{4}He, ^{12}C, ^{14}N, ^{40}Ar, Neutron	
Target nuclides	H (^{1}H) C (^{12}C, ^{13}C) N (^{14}N) O (^{16}O) Na (^{23}Na) Mg (^{24}Mg, ^{25}Mg, ^{26}Mg) Al (^{27}Al) Si (^{28}Si, ^{29}Si, ^{30}Si) P (^{31}P) S (^{32}S, ^{34}S) Ca (^{40}Ca, ^{44}Ca) Cr (^{50}Cr, ^{52}Cr, ^{53}Cr ^{54}Cr) Mn (^{55}Mn) Fe (^{54}Fe, ^{56}Fe, ^{57}Fe) Co (^{59}Co) Ni (^{58}Ni, ^{60}Ni, ^{62}Ni) Cu (^{63}Cu, ^{65}Cu) Zn (^{64}Zn, ^{66}Zn, ^{67}Zn, ^{68}Zn)	Ga (^{69}Ga, ^{71}Ga) Ge (^{70}Ge, ^{72}Ge, ^{73}Ge, ^{74}Ge, ^{76}Ge) As (^{75}As) Nb (^{93}Nb) Mo (^{92}Mo, ^{94}Mo, ^{95}Mo, ^{96}Mo, ^{97}Mo, ^{98}Mo, ^{100}Mo) Ag (^{107}Ag, 109Ag) In (^{113}In, ^{115}In) Sn (^{112}Sn, ^{114}Sn, ^{115}Sn ^{116}Sn, ^{117}Sn, ^{118}Sn, ^{119}Sn, ^{120}Sn, ^{122}Sn, ^{124}Sn) Ta (^{181}Ta) W (^{182}W, ^{183}W, ^{184}W, ^{186}W) Au (^{197}Au) Pb (^{206}Pb, ^{207}Pb, ^{208}Pb) Bi (^{209}Bi)

4) DECAYLIB : Decay data library

The DECAYLIB provides decay data over 2600 nuclides generated by using Evaluated Nuclear Structure Data File, ENSDF[6]. It contains nuclide half-lives, decay modes, natural abundances, daughter nuclides, and comments for updating histories. It has the same format as the decay data library of the ORIGEN2 code.

5) GAMMALIB : Photon data library

The GAMMALIB generated with the ENSDF gives the photon intensities emitted per 100 disintegrations of each parent nuclide. The photon intensities are classified in 18 energy groups up to 11 MeV. The photon data include annihilation radiation, but dose not include characteristic X-rays.

3. SUMMARY

The IRAC code system has been developed for calculation of the induced radioactivity and gamma-ray dose rate at TIARA. Activation cross sections are not available at present for all the combinations of incident particles with target nuclides. We intend to extend the activation cross section library by calculating with an advanced ALICE code.

REFERENCES

1) M.Maruyama, Proc. 2nd Int. Symp. on Advanced Nuclear Energy Research, Ibaraki, Jan. 24-26(1990)
2) S.Tanaka, M.Fukuda, W.Yokota, T.Kamiya, H.Watanabe, T.Shiraishi, K.Hata and N.Yamano, Autumn Meeting of the Atomic Energy Society of Japan in Sendai, C42(1988)
3) K.Hata and H.Baba, JAERI-M 88-184(1988)
4) A.G.Croff, ORNL/TM-7175(1980)
5) M.Blann, DE87 007443(1987)
6) J.K.Tuli, BNL-NCS-51655-Rev.87(1987)

3.3 Experimental Facilities for Accelerator Shielding and Spectrum Measurement of Monoenergetic Neutron Source

Shun-ichi TANAKA, Hiroshi NAKASHIMA, Susumu TANAKA*,
Ryuichi TANAKA*, Takashi NAKAMURA**, Mamoru BABA**,
Mineo IMAMURA*, Kazuo SHIN**, Hideo HIRAYAMA***

Department of Reactor Engineering, *Takasaki Radiation Chemistry Research Establishment, JAERI,
** Tohoku University, * University of Tokyo,
** Kyoto University,
*** High Energy Physics Research Laboratory

I. INTRODUCTION

A lot of accelerators have been widely used in nuclear physics, material science, medicine, biology and industries. Besides, accelerators are going to become crucial in nuclear energy research and industry. Several accelerator projects; SPring-8 synchrotron radiation facility, ETA high energetic intense proton accelerator for OMEGA project, ESNIT deutron accelerator for material irradiation testing, a free electron lazer facility and a positron factory are under progress and plan to facilitate nuclear energy research and developement in JAERI. These high energy and intense accelerators demand exquisite shielding design in construction of the accelerator building and user's facilities, because many kinds of energetic and intense radiations are produced. The basic data of radiation production by energetic ion beams, nuclear reactions of high energy neutrons, activation cross sections and shielding are essential to develop the shielding design method for accelerators.

Hence, some experiments have been planned by a research group on ion-accelerator shielding under the Research Committee of Advanced Radiation Technology, and experimental facilities and instruments have been prepared to acquire the data from 15 to 90 MeV with respect to the accelerator shielding in the TIARA.

II. EXPERIMENTAL PLAN AND FACILITIES[1]

The following experiments have been designated; A)measurement of neutrons and secondary γ-rays penetrating through typical shielding

materials: iron, concrete and polyethylene, B)measurement of activation cross section of materials used in accelerators, C)measurement of neutron total and double differential cross sections of standard and typical nuclides for shielding calculations, D)measurement of neutron and photon production data by charged particles.

A monoenergetic neutron source facility has been built for the experiments as shown in Fig.1. A proton beam extracted from the cyclotron is focused on a ^{7}Li enriched target in the target changer. The thickness of the ^{7}Li target is selected so that the energy loss of incident protons in the target is about 2 MeV, corresponding to the thickness of 2 mm for 20 MeV and 7 mm for 90 MeV protons. Six different ^{7}Li targets in their thickness are available in the target changer. Residual protons penetrating through the target are bent down to an angle of 50 degree by a clearing magnet and introduced into the beam dump with a Faraday cup. While, the monoenergetic neutrons emitted in the forward direction by the ^{7}Li(p,n) reaction are transported to the experimental room(Ion Room No.3) through a rotary shutter of 100 mm diameter. The experimental space with a cross section of 120 cm x 120 cm is useful for set-up of the shield materials up to the maximum thickness of 230 cm.

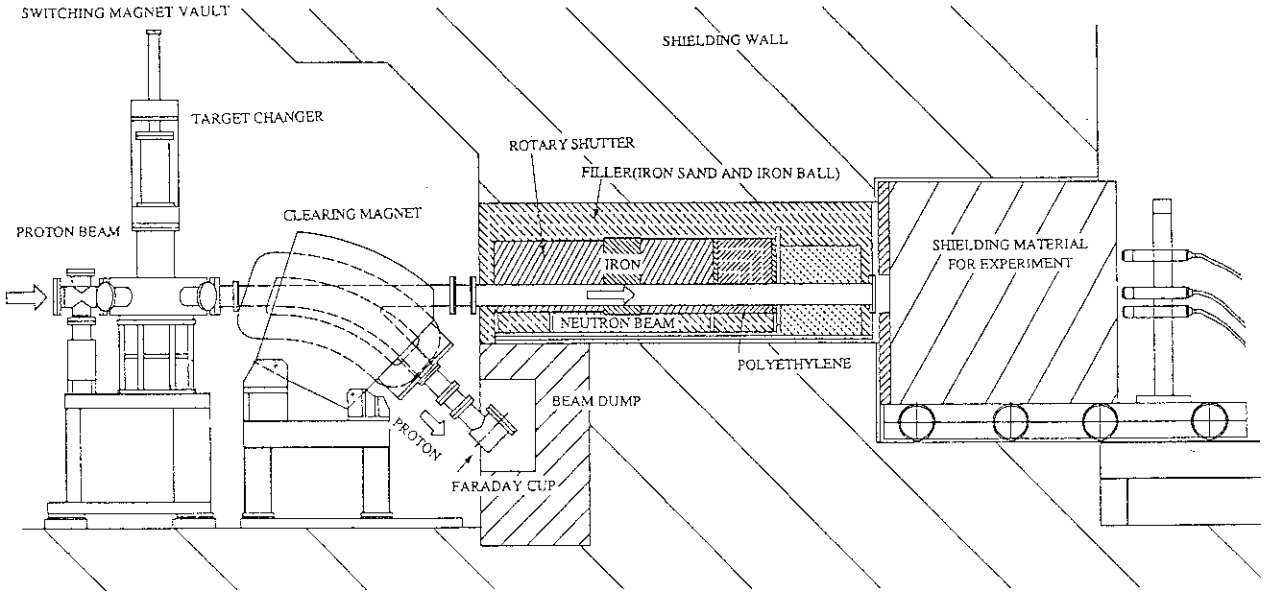

Fig.1 Schematic view of the monoenergetic neutron beam line.

III. Neutron Source Characteristics

The energy spectrum was measured using a recoil-proton telescope detector at the exit of the rotary shutter.[2] An experimental set-up and an arrangement for the measurement are shown in Photo.1 and Fig.2. The counter is composed of a polyethylene radiater Si-SSD(ΔE-detector), and NaI(E-detector), by which the TOF spectrum of recoil protons associated with the H(n,n) reaction is measured.

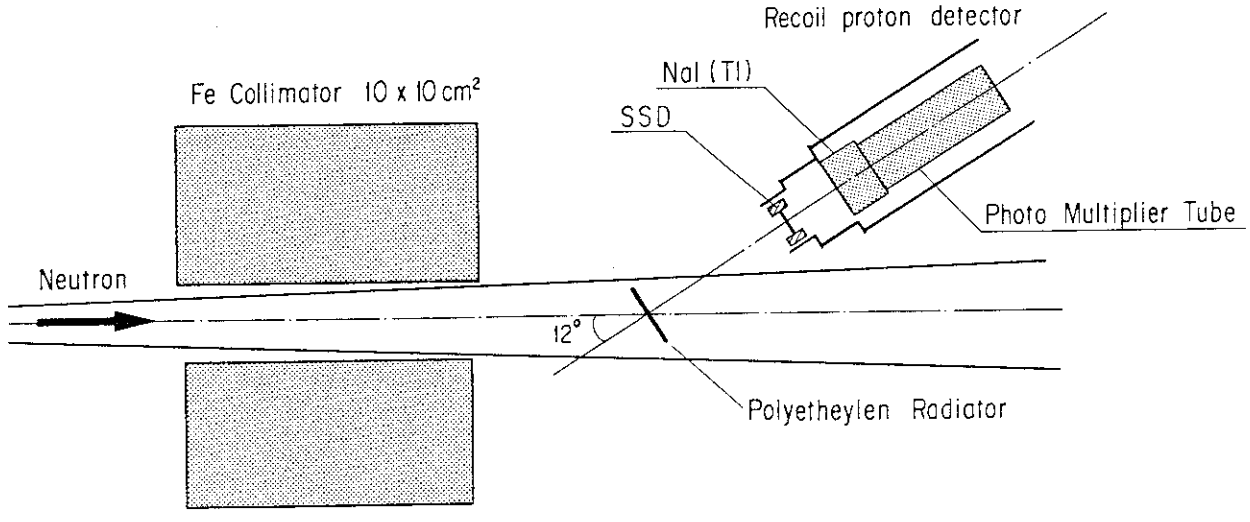

Fig.2 Arrangement of neutron spectrum measurement with the recoil proton telescope.

A neutron spectrum produced with 43 MeV proton beam is exhibited in Fig.3, which has been measured at a position of 5.5 m far from the ^{7}Li-target. The peak intensity at 40.7 MeV was 1.19×10^{4}(±5%) n/cm^{2} per μC, consisting well with 1.12×10^{4} n/cm^{2} per μC estimated from the cross section of ^{7}Li(p,n) reaction, although a continuous component due to the breakup reaction also was observed in lower energy region.

REFERENCES

1) Su.Tanaka et al., Proc. of 2nd Int. Symp. on Advanced Nuclear Energy Research(JAERI), Mito (1990) p.342.
2) M.Yoshioka et al., Autumn Meeting of Atomic Energy Society of Japan, G24 (1992).

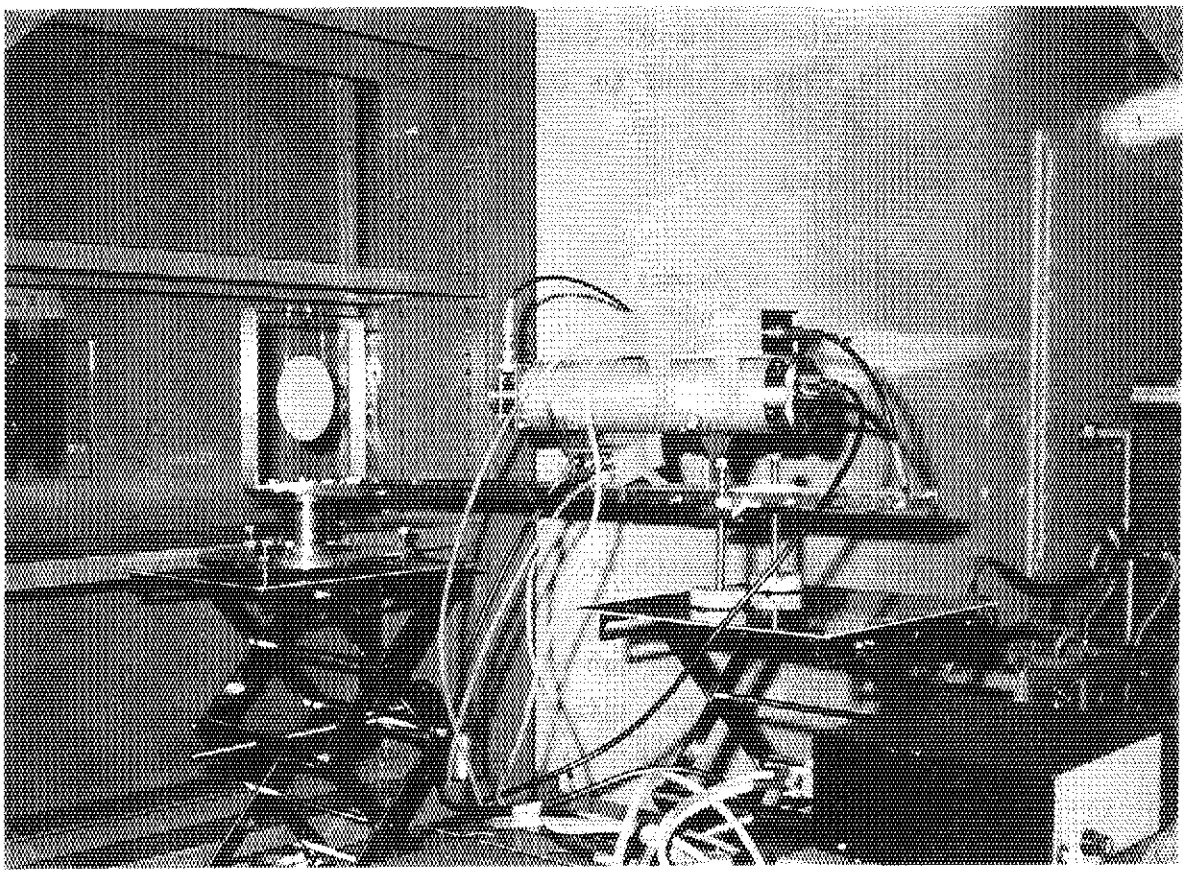

Photo.1 Picture of telescope detector for neutron spectrum measurement.

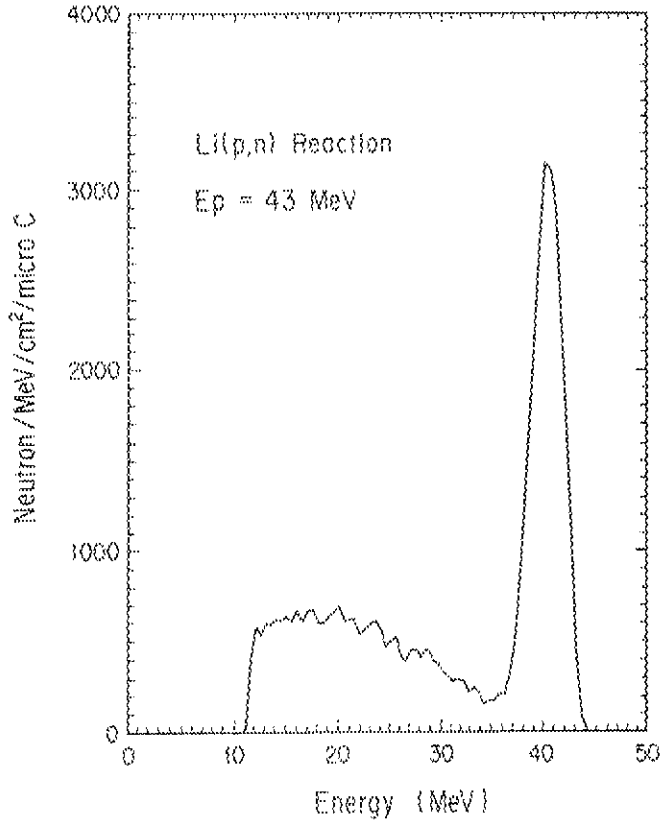

Fig.3 Measured neutron spectrum produced by ^{7}Li(p,n) reaction of 43 MeV proton beam.

3.4 Design and Manufacturing of Slow Positron Beam Line Electrostatically Transported to Double Direction

Sohei OKADA

Department of Material Development, JAERI

I. INTRODUCTION

Ion beam bombardments on solids cause defect production. To investigate and control thus induced defects is one of key techniques in developing materials and devices. Positron annihilation spectroscopy is a powerful tool to detect and analyze vacancy-type defects, which are not directly detectable by other probes.

Energy-tunable positron beams can afford information about arbitrary depths of solids, e.g., surface, interface and inside, separatedly. We manufactured a slow positron beam line named PALADIS (Positron Annihilation Lattice Defect Investigation System)[1] mainly for the depth profiling of defects induced by ion beams. A new configuration of moderators was designed to obtain slow positrons.

II. CONVENTIONAL MODERATOR CONFIGURATION

In almost all slow positron beam lines using ^{22}Na source (β^+ maximum energy:546keV) etc., the source is placed close to a thin tungsten foil moderator, from the oposite side of which reemitted slow positrons are extracted as shown in Fig.1.

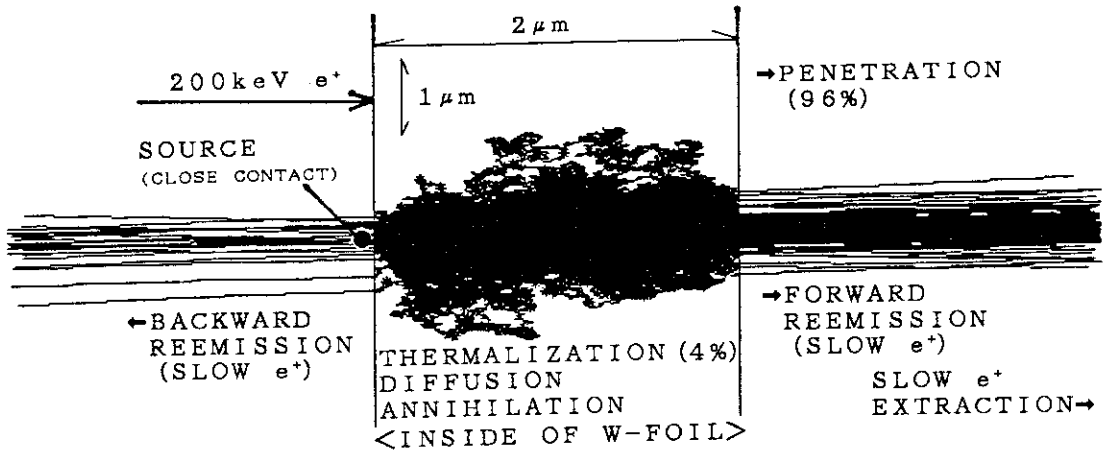

Fig.1. The Monte Carlo simulation on positron behavior in the conventional moderator configuration.

The figure demonstrates penetration, thermalization, diffusion, annihilation and reemission of positrons in such a moderator configuration, which is calculated with a Monte Carlo simulation code SPG (Slow Positron Generation) developed by us[2]. Here is shown an example of 200 keV incident positrons onto a tungsten foil of 2 μm in thickness.

It is clear from the simulation that non-thermalized energetic positrons penetrate the moderator and contaminate the slow positron beam obtained from the reemission process. In usual cases the energetic positrons are eliminated by using a ExB filter and/or a curved solenoid tube during the magnetic transportation.

III. ELECTROSTATICALLY TRANSPORTED SLOW POSITRON BEAM LINE WITH A NEW MODERATOR CONFIGURATION

In PALADIS we adopted a new moderator configuration in order to manufacture a compact beam line electrostatically transported as shown in Fig.2. Reemitted slow positrons are extracted parallel to surfaces of

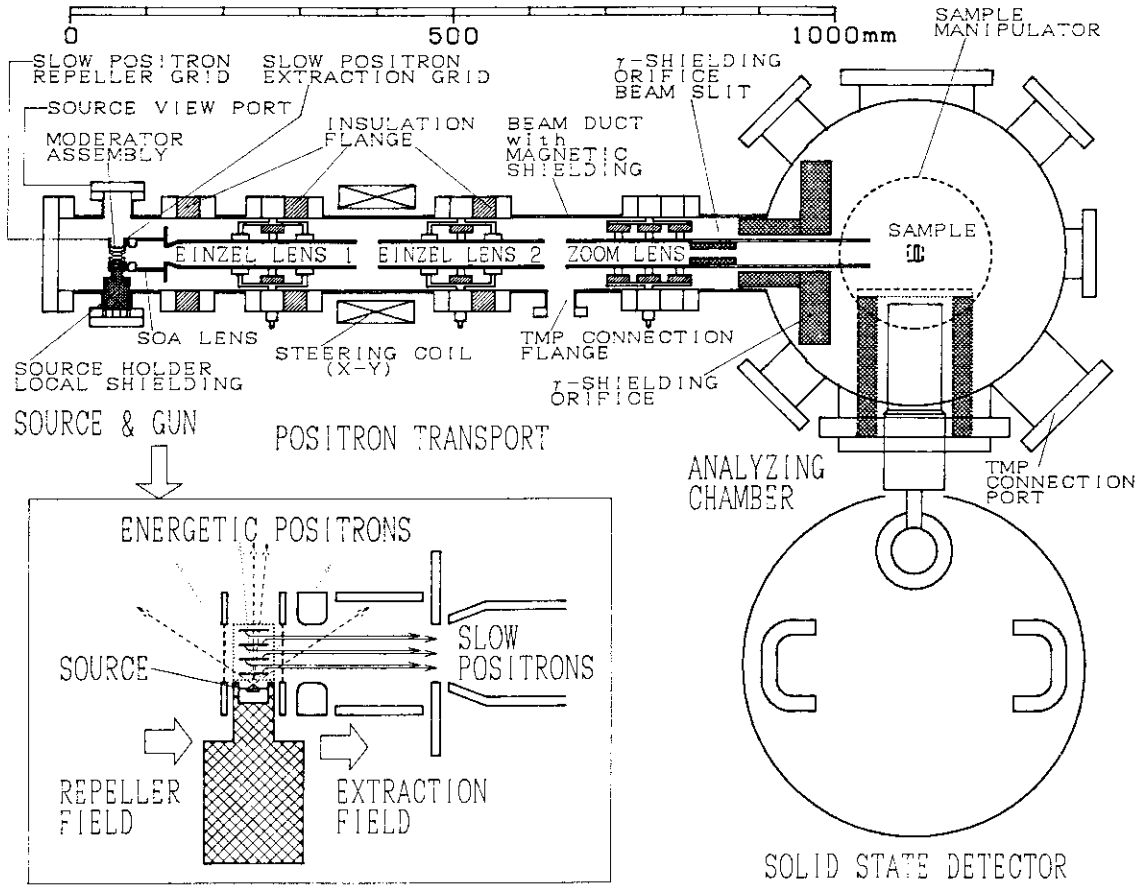

Fig.2. A concept of PALADIS (Positron Annihilation Lattice Defect Investigation System)

multiple tungsten moderator foils placed near to the source as demonstrated in Fig.3. The purpose of this new configuration is to eliminate penetrating energetic positrons at the initial stage of slow positron generation i.e. in the moderator part (left hand side of Fig.2).

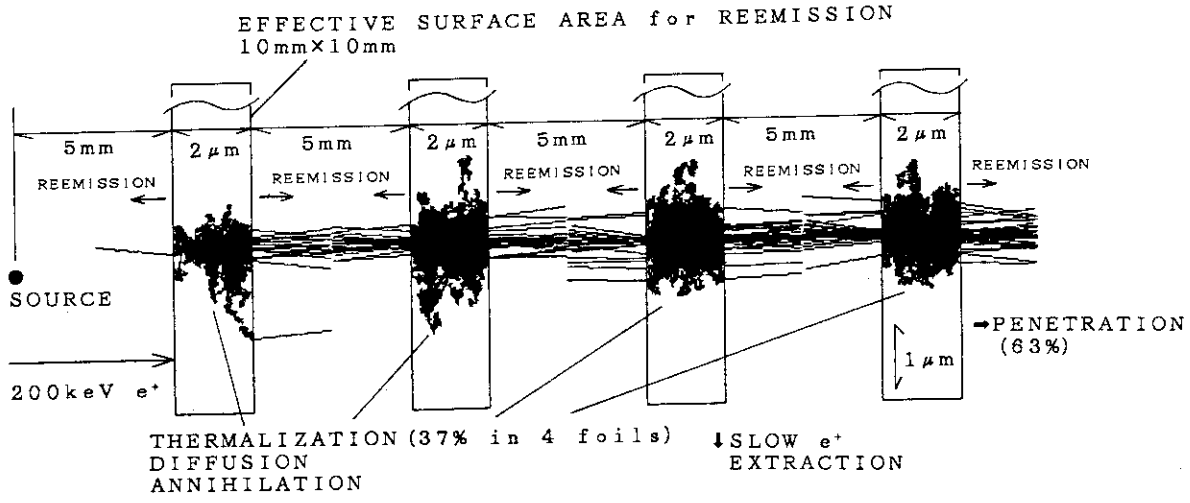

Fig.3. The Monte Carlo simulation on positron behavior in the new moderator configuration in PALADIS.

We evaluated slow positron yields (the number of reemitted slow positrons / the total number of β^+ emission from ^{22}Na) using SPG by varying incident positron energies onto the moderators. The β^+ energy spectrum was approximated to be as follows:

$$F(\varepsilon) \propto (\varepsilon_{max}-\varepsilon)^2(\varepsilon^2+2\varepsilon)^{1/2}(\varepsilon+1). \quad (1)$$

Here ε is kinetic energy in unit of mc^2 (m:rest mass of electron, c:light velocity). Effective solid angles made by the moderator surfaces viewed from the point source and a branching ratio of positron reemission at the surfaces of the tungsten moderators (=1/3) were taken into account. The result is shown in Table 1. It may be concluded that the new configuration gives not less yields than the conventional one.

Table 1. Slow positron yields in the conventional and the new moderator configuration calculated by the Monte Carlo simulation.

THICKNESS OF TUNGSTEN FOIL	CONVENTIONAL CONFIGURATION (1 foil)	NEW CONFIGURATION (4 foils)
200 nm	1.49×10^{-3}	1.37×10^{-3}
2 μm	2.59×10^{-3}	2.08×10^{-3}

The new moderator configuration will provide another slow positron beam line (direction to the left in Fig.2) with only one source by inverting polarities of the electric potentials of the extraction and the repeller grid. The maximum acceleration energy of the slow positron beam is 30 keV. The machine will be open to routine applications from 1993 after installation of a 10 mCi ^{22}Na source. In addition to the depth profiling of defects with Doppler broadening technique, we plan other types of experiments to exploit a special merit that magnetic field does not exist at the point of specimen.

REFERENCES

1)S.Okada, Proc. of the 29th Annual Meeting on Radioisotopes in the Physical Sciences and Industries (Tokyo, June 29-July 1, 1992) p.161 (in Japanese).

2)S.Okada and H.Sunaga, Nucl. Instrum. Methods Phys. Res., Sect.B56/57 (1991)604.

3.5 Heavy Ion Microbeam Apparatus for Single Event Upset Analysis

Tomihiro KAMIYA, Hidenori YUTOH and Ryuichi TANAKA

Department of Advanced Radiation Technology, JAERI

I. INTRODUCTION

A heavy ion microbeam apparatus[1] illustrated in Fig. 1. was installed on a beam line of a 3 MV tandem electrostatic accelerator system. Many high energy microprobe systems have been constructed for ion beam analyses using light ions[2], while this apparatus was designed mainly for study of single event upset (SEU) using high energy heavy ions. SEU occurs when a high-energy single heavy ion hits an integrated circuit and generates a large amount of transient charge. The SEU phenomena depends not only upon hitting particles, but also upon the hit position on the microcircuit. To test the positional dependency with a high spatial resolution of less than 1 μm, the system was designed to meet the following three technical means, (1) a microbeam focusing spot size less than 1 μm, (2) a beam positioning accuracy within 1 μm and (3) a single ion hitting.

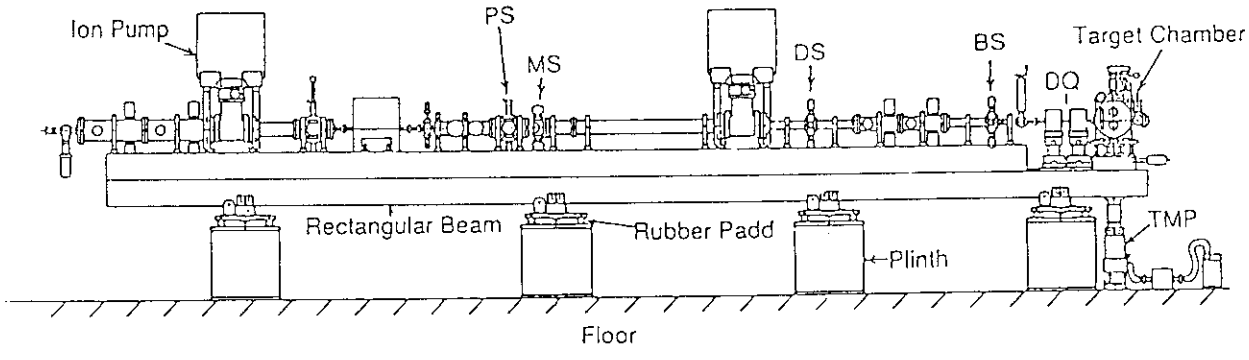

Fig.1 Side view of the heavy ion microbeam system. DQ: precision doublet quadrupole lens PS: preslits, MS: microslits, DS: divergence-defining-slits and BS: baffle slits.

II. MICROBEAM FOCUSING

The precision focusing system consists of preslits (PS), microslits (MS), divergence-defining slits (DS), baffle slits (BS) and a doublet quadrupole lens (DQ). MS have cylindrical tungsten-carbide slit chips. The bore radius and the mechanical pole length of the magnets of DQ is 10 mm and 120 mm, respectively. The object distance from MS to the entrance of DQ is 3750 mm

and the working distance is 200 mm. The demagnification factors in horizontal and vertical planes are 4.6 and 28, respectively.

The beam size measurement was performed using 15 MeV Ni^{4+} beams. Fig. 2 (a) shows a two-dimensional secondary electron image of a Cu mesh (600 lines per inch) over the scanned area of 100 X 100 μm^2. Fig. 2 (b) shows examples of the one-dimensional secondary electron maps of the mesh in the X and Y directions. The sharpness of the varying secondary electron yield at the each edge defines the beam size. The FWHM of each peak in the derivative of the secondary electron profile was evaluated as the beam size using least square fitting.

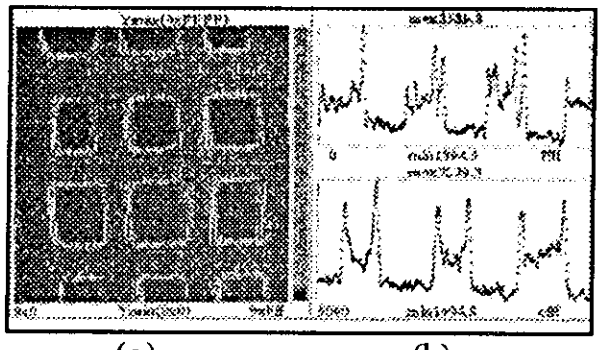

Fig. 2 (a) Two dimensional secondary electron image of the Cu mesh (600 lines / inch) obtained by microbeam scanning over the scan area of 100 X 100 μm^2
(b) One dimensional profiles of secondary electron yield in the horizontal (upper) and vertical (lower) directions.

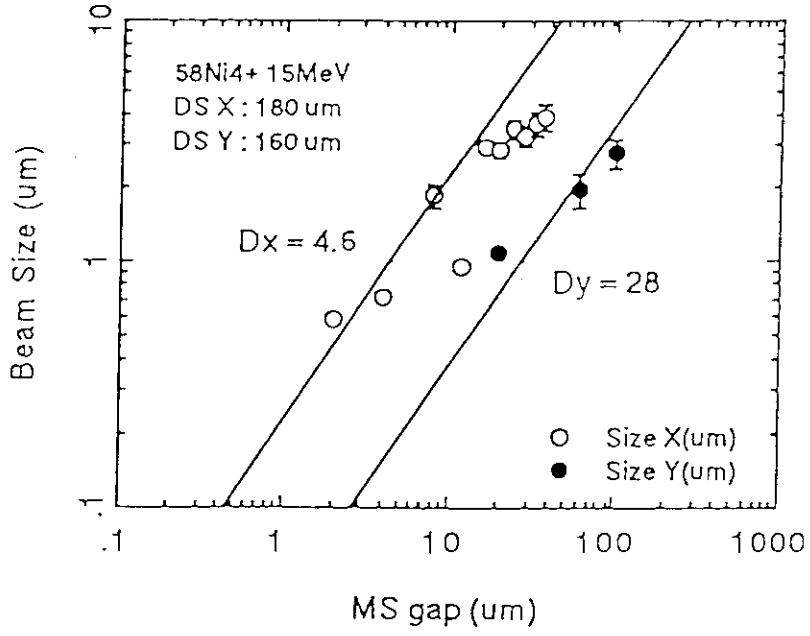

Fig. 3 Beam spot sizes in X and Y directions as functions of MS gaps. Solid lines indicate demagnification factors for each direction.

The beam spot size of 0.70 X 1.1 μm^2 was observed under the condition that the object slit size was 4 X 20 μm^2 and beam current was 8 pA at the target. The designed value of 1 μm for the beam spot size was achieved in this system. Fig. 3 shows a result of the beam size measurement, varying the microslit gaps.

III. BEAM POSITIONING AND SINGLE ION HIT

To avoid radiation damage caused by energetic heavy ions in the secondary electron yield mapping of integrated circuits, a reference point is set outside the sensitive area and an indirect beam positioning[1] is performed before SEU measurement. For accurate beam positioning, the displacement from the reference point to the aimed one is measured by using a scanning electron microscopy (SEM) or a high-resolution optical microscope. Positioning uncertainty of the target-stage and the amplitude of the vibration of the target-holder also affect accuracy of the beam positioning. Those of our test chamber is estimated at a few μm. A new target chamber for SEU analysis is under designing in consideration described above.

A single ion hit system is being developed to make a single ion hit a point within a aimed local area. Fig. 4 shows a block diagram of the single ion hit system. It provides two single ion detectors SE1 and SE2. To eliminate

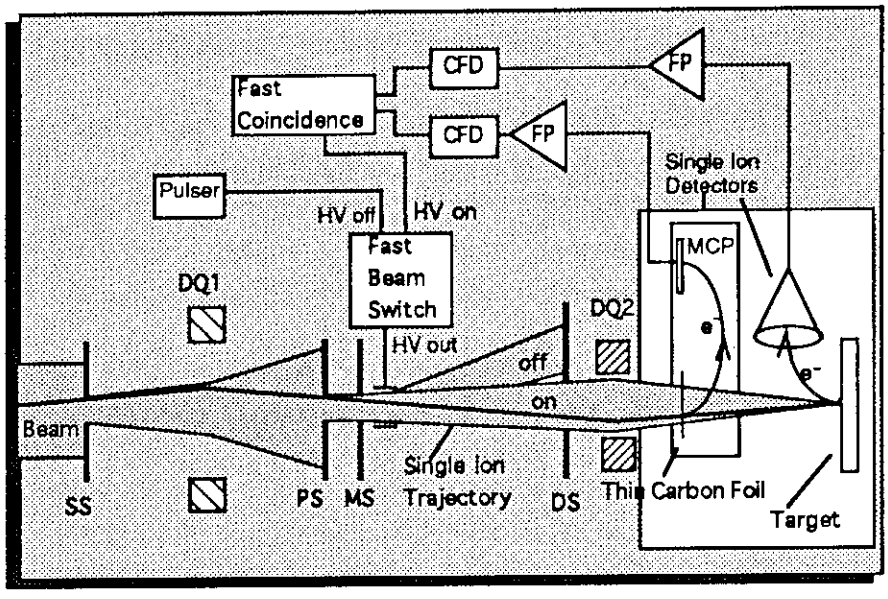

Fig.4 Schematic diagram of single ion hit. SE1: transmission type secondary electron detector, SE2: electron multiplier, FP: fast pre-amp, CFD: constant fraction discriminator, FCM: fast coincidence module.

noise from signals of each detector, a pulse generated by coincident signals from both detectors at the fast coincidence module is used as a trigger for fast beam switch to deflect the beam electrostatically. SE1 is a transmission-type

single ion detector with a thin carbon foil to generate secondary electrons and with a micro-channel plate (MCP) to detect them. The detection efficiency for α-particles from a ^{241}Am source was measured by a silicon surface-barrier detector as a monitor of ion hit. An efficiency of 60% has been obtained so far with 10 μg/cm^2 carbon foil, and higher efficiency will be expected with heavy ions, because of the larger number of secondary electron emission from the foil. However, large mean squared multiple scattering of heavy ions through the foil contributes to decrease the positioning accuracy. Therefore, an ultra-thin foil may be required to reduce the total uncertainty in beam positioning within a reasonable value.

SE2 is an electron multiplier to detect secondary electrons emitted from the target. The fast beam switching system consists of a high-voltage power supplier actuated by a trigger signal from the single ion detection system and an electrostatic beam deflector to prevent further ions from hitting the target after the single hit.

IV. Summary

The beam spot size of 1 μm has been achieved so far in microbeam focusing test using 15 MeV nickel ion beams from a 3MV tandem accelerator. This means that the first requirement for SEU experiment was satisfied in the microbeam apparatus. Our development program is now followed by the development of remaining two techniques, accurate beam positioning and single ion hit.

Preliminary measurement of single-event current transients were made on an n-type silicon diode by 15 MeV carbon and nickel ion microbeams[3]. Beam positioning was tried to make those ions hit a point within a sensitive local area of the test samples. The radiation damage of the diodes induced by high-energy heavy ions was observed clearly after a short exposure of the microbeam. This suggests the single ion hit technique is essential for SEU experiment.

References

[1] T. Kamiya, N. Utsunomiya, E. Minehara, R. Tanaka and I. Ohdomari, Nucl. Instrum. Methods Phys. Res., Sect. B 64 (1992) 362.
[2] K.Traxel, Nucl. Instrum. Methods Phys. Res., Sect. B 50 (1990) 177.
[3] T.Hirao, Y.Morita, S.Nishijima, T.Kamiya, H.Yutoh and R.Tanaka, Proc. of the Int. Workshop on Radiation Effects of Semiconductor Devices for Space Application, Takasaki, Japan (1992) 142

4. MATERIALS FOR SPACE ENVIRONMENT AND NUCLEAR FUSION REACTOR

4.1 Ion Irradiation Chamber Designed for Evaluation of Space Solar Cells and Modification of Semiconductors

Yousuke MORITA AND Isamu NASHIYAMA

JAERI,Takasaki Radiation Chemistry Research Establishment

I. INTRODUCTION

The space solar cells is used as the power source of artificial satellites, and those are directly exposed for protons and electrons under space environment. As satellites have been recently designed with higher power and longer life-time than before, it is important to evaluate the degradation of the space solar cells by irradiation. In TIARA facility, the chamber for the above purpose is prepared, and the intensive studies will be made to evaluate and elucidate the deterioration of electric properties of the space solar cells by ion irradiation.

In addition, the chamber can be also used for very high-energy ion implantation in semiconductors with wide area.

II. DESIGN CONCEPT

In Figure 1 is illustrated the schematic drawing of the chamber which is designed under the following concept.

(1) To study the degradation of the solar cells(min. size $2x2cm^2$) under proton irradiation, or the deep ion implant into semiconductor materials, it is needed to irradiate samples with wide area and uniform dose. There are two types of the sample holders at the center of the chamber as described below.

(a)the sample holder has irradiation area of $10x10cm^2$, and its temperature can be changed from -120 °C to 200 °C.

(b)the sample holder is capable of sequential irradiation of three large specimens($10x10cm^2$) without breaking vacuum at ambient temperature.

At the rear port, there is a sample holder which has irradiation area of $5x5cm^2$, and it is more easier to exchange specimens.

(2) To measure the changes of electrical properties of the solar cells immediately after ion irradiations, a solar simulator(power:140mW/cm^2(1 solar)x100cm^2,spectrum:AM-0) and a I-V measurement system(volt:0-2V,ampere:0-4A) are equipped with the chamber.

(3) To measure ion fluencies in the irradiation, Faraday cup and SSD can be used, and in further, a parallel plate avalanche counter for profiling ion beam and a scintillation counter for the flux of ions will be also provided.

(III) DOSE UNIFORMITY

Beam uniformity was checked by using dosimeters of cellulose triacetate film(CTA) and radiochromic dye film(RCD). Figure 2 shows the intensity profiles of the incident spot and the scanned beams(proton,45MeV) by using CTA dosimeter. In the profile of the scanned beam, the dose in its central part is ca.10% higher

than those in other area. This reflects the feature of beam-scanning magnets. By using this chamber, the specimens with the shape of 10x10cm^2 can be irradiated within the dose uniformity of 3% except the central part(ca. 10%).

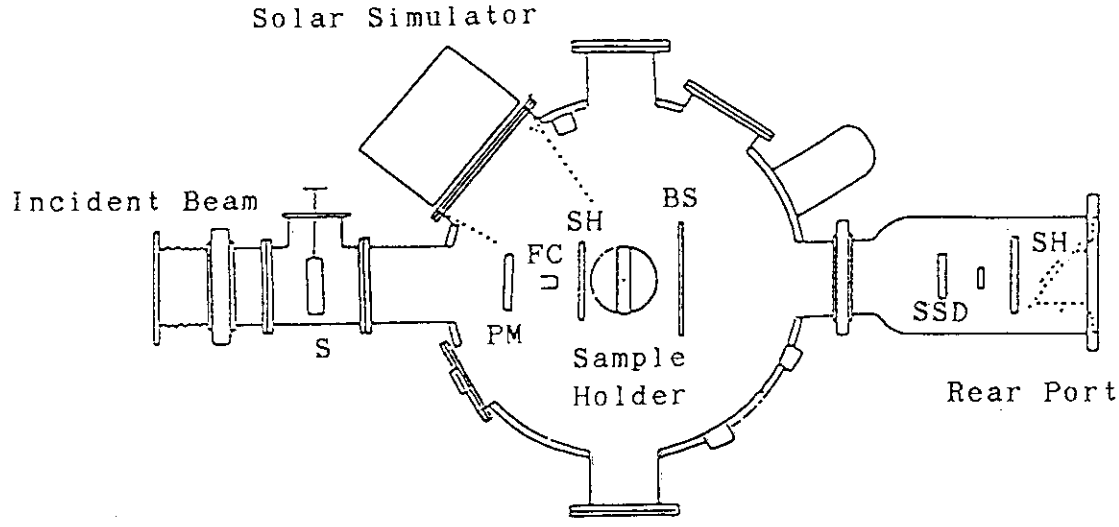

Fig. 1 Schematic Drawing of Chamber for Ion Irradiation of Solar Cells and Semiconductor Materials
S:XY slit, PM:Beam profile monitor, FC:Faraday cup, SH:Beam Shutter, BS:Beam stopper, SSD:Silicon detector

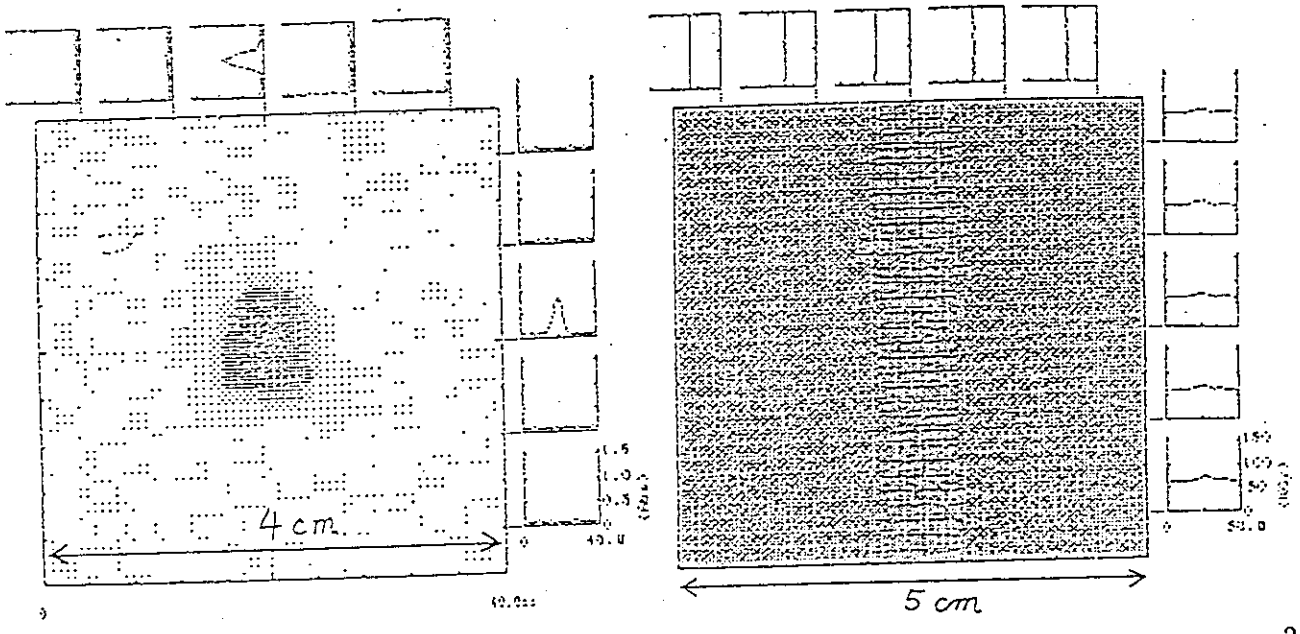

(a) Spot Beam
Irradiation:100nA,50s

(b) Scanned Beam(Central part of 8x8cm^2)
Irradiation:100nA,70min,
Scanned rate:0.5Hz at Y axis
and 50Hz at X axis,
Scanned size:8x8cm^2,
Average dose:67kGy.

Fig. 2 CTA Profile of 45MeV-proton Beam

4.2 Heavy-ion Irradiation System for the Study of Single-event Radiation Effects on Semiconductors by Using AVF-cyclotron

Hisayoshi ITOH, Toshio HIRAO, Yousuke MORITA, and Isamu NASHIYAMA

Department of Materials Development, JAERI

I. INTRODUCTION

Single-event phenomena such as soft-errors, latchup, and burn-out of semiconductor devices are induced by the impingement of a single high-energy ion from the cosmic ray environments in space.[1] These phenomena result from that dense electron-hole pairs generated along the ion track deposit additional charges in memory cells, change current paths in device circuits, and introduce lattice damage in device structures.[2] However, the fundamental processes of the single-event phenomena, e.g., the transient behavior of the dense electron-hole pairs, have not yet been clarified up to now. It is important to reveal those fundamental processes for the complete understanding of the mechanism of the single-event upsets, the prediction of the error rates in electronic devices to be used in space, and the development of error-free devices. In addition, it is indispensable to acquire the data on the single event upsets of the devices fabricated for the space application.

For the basic research of the single-event phenomena and the test of the error rates of electronic devices by energetic ions, we have fabricated an ion irradiation equipment connected to a heavy-ion beam course of JAERI AVF-cyclotron. We study ion irradiation effects on the electrical and the optical properties of semiconductor materials and devices by using this equipment.

II. ION IRRADIATION SYSTEM

The equipment consists of two irradiation chambers HE1 and HE2, which are shown schematically in Figs.1(a) and 1(b), respectively. The typical specification of the equipment is described below.

Each chamber has an ion pump and turbo molecular pump evacuation system. The ultimate vacuum pressure is the order of 10^{-8} Torr. The alignment of the samples to the ion beam is made with an He-Ne laser (λ=0.63μm). The fluence rate of heavy-ions is obtained by detecting the current from the Faraday cups and/or from the sample holders. The approximate beam profile can be observed with an alumina monitor placed at the target

position and TV camera. All the X-Y slits, the Faraday cups, the shutters, and the gate valves are remotely controllable.

The cryostat on the two-axes goniometer is installed in the chamber HE1. The temperature of semiconductor samples can be controlled in the range between 20K and 300K. The incident angle of heavy-ions to the sample surface is varied by rotating the goniometer controlled remotely. The change in the optical properties (reflectivity, transmission, luminescence, etc.) of samples by ion irradiation is measured with the streak camera system (Hamamatsu C1587). From those data, we can get the information about electron-hole pairs and defects induced by the irradiation.

In the chamber HE2, two kinds of goniometers (four-axes and two-axes goniometers) are installed. Both goniometers are also remotely controllable. Thin metal films used as an ion-scatterer are attached to the four-axes goniometer stage. Device samples placed on the two-axes goniometer stage are irradiated with scattered ions which are homogeneous and have a low fluence rate, and the number of the soft-errors occurred in the irradiated devices is counted with a computer system. The energy and the fluence of the scattered ions are detected with an SSD connected with an ion-counting system. The error rates are obtained from those data. The irradiation conditions such as the incident energy, the fluence rate, and the effective LET of ions are variable by the use of different scatterers and by the alternation of the incident angles of ions to the scatterers and to the devices.

REFERENCES

1) E.L.Petersen, in the Text of Tutorial Short Course in IEEE 1983 Nuclear and Space Radiation Effects Conference, held on July 17, 1983, in Gatlinburg, TN, USA.
2) J.C.Pickel, in the Text of Tutorial Short Course in IEEE 1983 Nuclear and Space Radiation Effects Conference, held on July 17, 1983, in Gatlinburg, TN, USA.

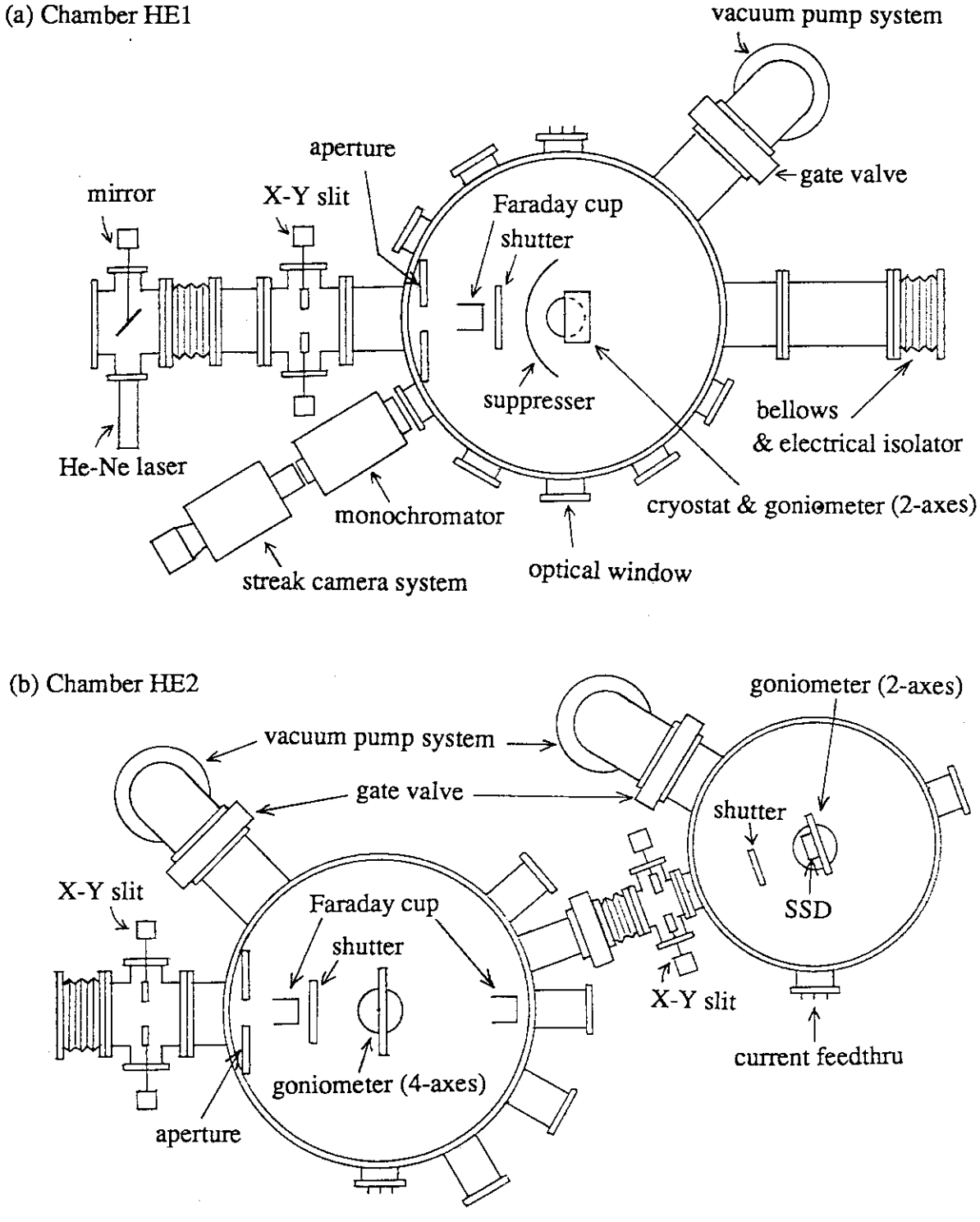

Fig.1 Heavy-ion irradiation system.

4.3 Measurement of Transient Currents Induced by Heavy Ion Microbeams

Toshio HIRAO, Toshiji NISHIJIMA*, Tomihiro KAMIYA, Hidenori YUTOH, Yousuke MORITA, Isamu NASHIYAMA, and Ryuichi TANAKA

Japan Atomic Energy Research Institute
*Electrotechnical Laboratory

1. Introduction

Excess carriers generated by the passage of a single heavy ion in the sensitive region of memory devices can give rise to non-permanent changes in data patterns stored in the memory. This phenomenon is known as a single event upset (SEU). As integrated circuits are scaled down in size, they become more sensitive to SEUs, because the amount of charges which is sufficient enough to trigger the upset becomes lower with increasing junction sizes of the devices.

In recent years, several attempts have been made for the direct measurements of extremely fast transient currents induced by the single ion strikes on the p/n junction, and charge collection mechanisms such as drift, funneling and diffusion effects have been studied (1,2,3). However, these measurements were made only for light and heavy ions with limited ion species and energies.

In the present work, we apply carbon ion microbeams in order to obtained detailed information about the charge collection mechanisms of the SEUs, and pico-second current transients in a p/n junction diode are measured under various bias conditions. Total collected charges are evaluated from the current transients obtained.

2. Experiment

Carbon ion microbeams of approximately 1μm in diameter were provided for the SEU experiments using a microbeam apparatus connected to the 3MV tandem accelerator at JAERI Takasaki (4,5). The method of the experimental setup is schematically shown in Fig.1. The measurements were performed using the microbeams with the energies of 3, 5, 10 and 15 MeV. The samples used in the present experiments were low-capacitance p/n junction diodes

with a n-type base-layer of doping level 2 x 10^{15} cm^{-3}, 50μm$^{\phi}$ junction area, and 250μm x 250μm chip size. The sample diode was mounted on a chip carrier with 50Ω double-ended micro stripline(6).

Transient currents were measured under the bias conditions of 15,10, and 15V using wide-band coaxial cables of 50Ω impedance and a 40 GHz wide-band sampling oscilloscope (Tektronix model CSA803).

Since radiation damage and signal pileup were observed for beam currents above $\sim 1 \times 10^{-12}$ A, we applied the beam currents less than 10^{-14} A for the present experiments.

3. Results and Discussion

Figure 2 shows several waveforms of the transient currents induced by 15 MeV carbon ions in the silicon diode under different bias conditions. The pulse height and total collected charge increases with bias voltage, corresponding to the increase in the depletion layer thickness of the diode. The waveform exhibits a sharp peak followed by a slightly long tail. This current waveform is understood by the superposition of the prompt component with a rise time about 200ps and the delayed component with a nano-second decay time. The prompt component is known to be the sum of the drift and the funneling currents. The former is due to charges collected from the depletion layer of the p / n junction diode. The later is charges collected from the electron-hole plasma column created along the trajectory of incident ions beyond the depletion layer. The slow component is due to diffusion of the excess minority carriers induced around the plasma column. The current perturbation observed at around 3ns after the peak in Fig. 2 is caused by the signal reflection at the cable connectors.

We introduce a funneling factor defined by Q_T / Q_L, in order to make clear the effect of the funneling, where Q_T is the total amount of collected charges which can be obtained from the time integral of the current waveform by applying a correction factor related to an attenuation of the signal intensity through the cable. The ideal amount of charges, Q_L, collected from the depletion layer are theoretically derived by the following equation,

$$Q_L = q \cdot LET \cdot \rho(Si) \cdot L / W = LET \cdot \rho(Si) \cdot L / 22.5 \quad (pC) \qquad (1)$$

where, q is unit charge, LET linear energy transfer in MeV/(mg/cm^2), ρ (Si) the density of silicon in g/cm^3, L the depletion layer thickness, and W the energy necessary for creating one

electron-hole pair in silicon. When the funneling factor is less than unity, charges are collected mostly from the depletion layer. Whereas, when the funneling factor is greater than unity, additional charges are collected from the substrate by the funneling effects.

We obtained funneling factors for various beam energies and bias conditions as shown in Table 1. The funneling factors are 1.7~2.6 for 10 MeV and 15 MeV C ions, indicating that a significant funneling effect exists and the funnel length defined by L · (funneling factor - 1) is 2~4 μm. For 3 and 5 MeV beams, funneling factors are less than unity, which corresponds to the fact that the ion ranges are shorter than the depletion layer.

4. Conclusions

By applying carbon ion microbeams combined with a wide band-width measurement system, transient currents induced by the heavy ion incidence on a silicon diode are measured successfully for the first time. Significant funneling effects were found for the carbon-ion strikes with energies above 10 MeV.

Acknowledgments

The authors would like to acknowledge N.Suzuki of Radiation Application Development Asociation the help of for his assistance in setting up the experiments.

Reference

1) Ronald S.Wagner et al., IEEE Trans. Nucl. Sci. Vol. NS-34, No.6 (1987) 1240.
2) Ronald S.Wagner et al., IEEE Trans. Nucl. Sci. Vol. NS-35, No.6 (1988) 1578.
3) Toshiji Nishijima et al., *Proc. of the Int.Workshop on Radiation Effects of Semiconductor Device for Space Application* (Takasaki, 1992) 138.
4) Tomihiro Kamiya et al., *Proc. of the Int.Workshop on Radiation Effects of Semiconductor Device for Space Application*, Takasaki, Japan (1992) 112.
5) Tomihiro Kamiya et al., *Proc. of the First Meeting on The ION Engineering Society of Japan* (1992) 105.
6) H.R.Kaupp, IEEE Trans. Elec.Com., 185 (1967) 4.

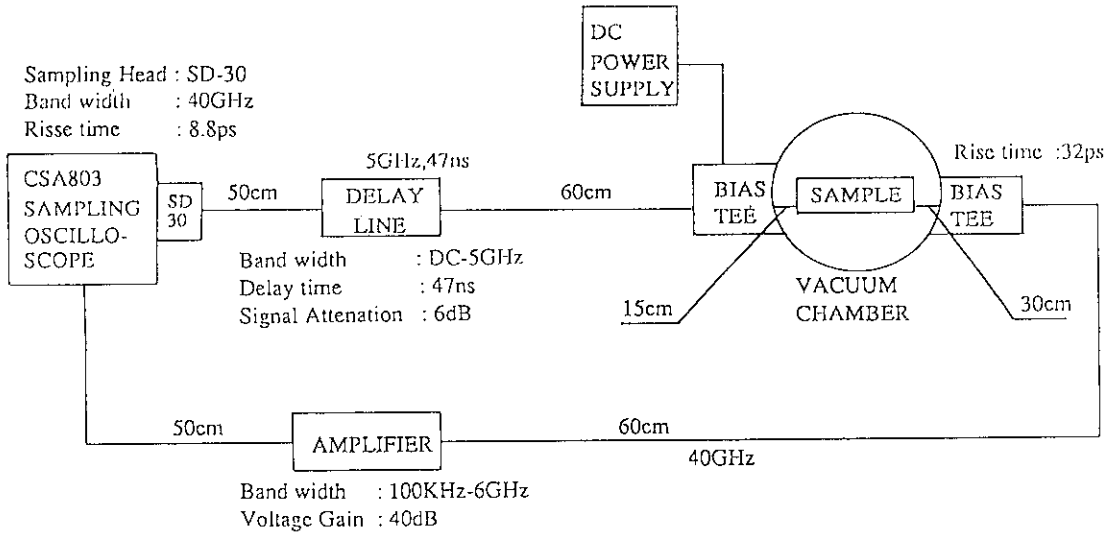

Figure 1. Block diagram of the electronic system for transient current measurements.

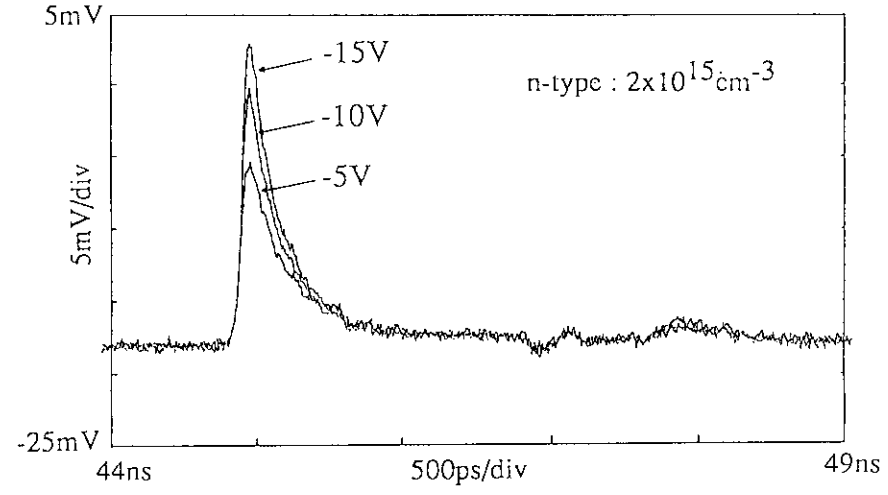

Figure 2. Effect of bias on SEU transient current induced with 15MeV C^{+4} ions.

Table 1. Funneling factors for 3 ~ 15 MeV C^{+4} ion strikes on silicon diodes under various bias voltages.

Funneling Factor

Beam Energy	Bias (V) / Depletion Layer (μm)		
(MeV)	-5/1.96	-10/2.66	-15/3.21
3	0.89	0.58	0.59
5	0.90	0.48	0.46
10	2.25	1.93	1.71
15	2.65	2.57	2.37

4.4 Metal Ion-implantation in Amorphous Silica Glass

Osamau YODA

Department of Materials Development, JAERI

It is well known that metal clusters enclosed in glass show peculiar optical properties; absorption of light in the visible region and hence coloring, and the non-linear optical response to the incident light intensity. If one can create metal clusters with the controlled size, shape and concentration in a transparent matrix such as glass and plastics, those materials would be interesting from the viewpoint of the application to optical devices.

Ion-implantation with the use of an accelerator is one of the most suited techniques for the introduction of foreign particles into materials. The position of implantation and the concentration of metal ions can be controlled quite easily. However, little is known not only about the states of implanted particles and the matrix but about the way to form clusters with the definite size and shape.

With a view to understanding metal ion-implantation in glass and to attempting the formation of regulated clusters in the matrix, the author has started to try implantation experiments by use of a tandem ion accelerator (9SDH-2, NEC) installed recently in JAERI-Takasaki.

So far Au^{2+} and Ni^{2+} ions have been implanted in silica glass (Suprasili®), 0.285mm thick, for a fluence level of $3\times10^{16}/cm^2$ with an acceleration energy of 3MeV. Implanted materials exhibit tints in red and brown by implantation of gold and nickel, respectively. Small-angle X-ray scatterings (SAXS) from as-implanted materials have been measured to investigate inhomogeneities which might be introduced in the expected homogeneous glass matrix.

Figure 1 shows a logarithmic plot of SAXS intensity vs. the momentum transfer k ($= 4\pi \sin\theta / \lambda$) from matrix glass with θ and λ being half the scattering angle and the wavelength of X-rays, respectively. In Fig. 2 are shown SAXS from the glass implanted with gold. Little difference can be observed between these two figures.

The above situation suggests the following possibilities. 1) The implanted metal atoms disperse uniformly in a region limited by the acceleration energy. 2) The concentration of metal particles introduced in glass is insufficient to

reveal adequate contrast in SAXS even though they form clusters.

The slight coloring of the implanted glass mentioned earlier supports the latter possibility. Further implantation is then necessary to determine the size and shape of as-implanted clusters by means of SAXS. After having determined the morphology of as-implanted clusters, the author will attempt to modify the shape and size of the cluster by applying thermal stress as well as magnetic field.

The author would like to thank Drs. H. Naramoto, S. Yamamoto, H. Takeshita and A. Miyashita for help in ion-implantation experiments.

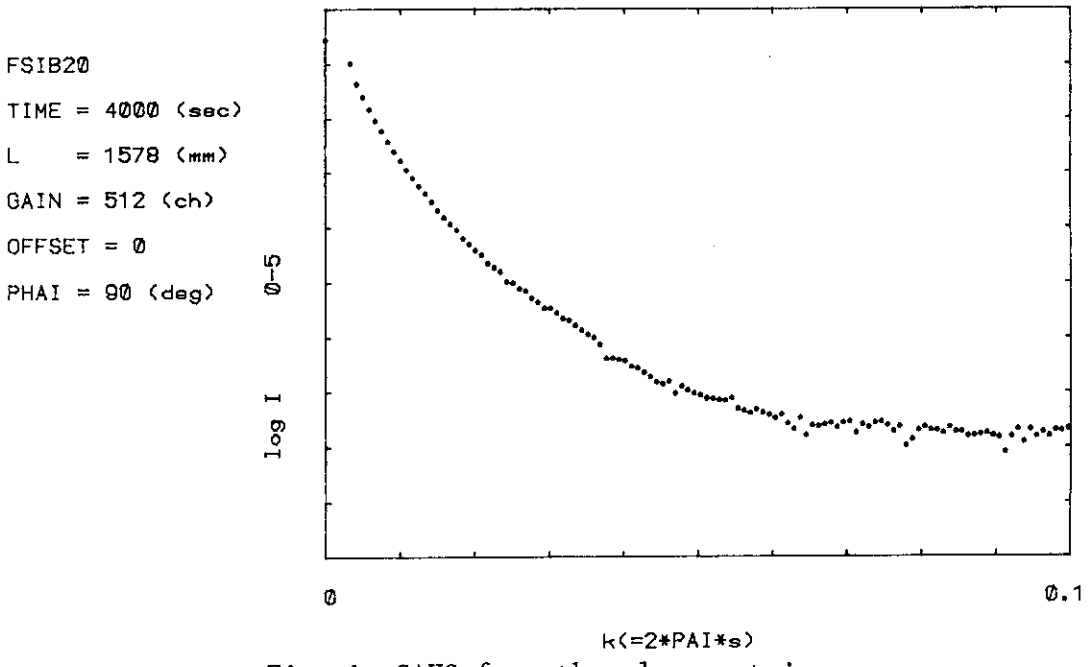

Fig. 1 SAXS from the glass matrix.

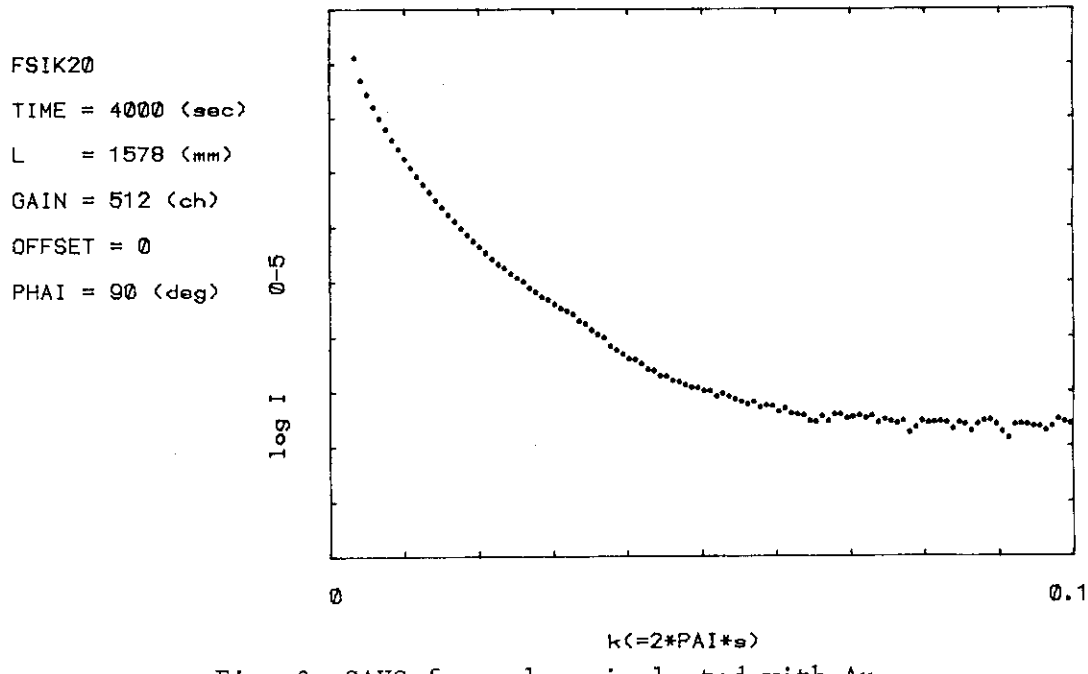

Fig. 2 SAXS from glass implanted with Au.

5. ORGANIC FUNCTIONAL MATERIALS

5.1 Irradiation Apparatus for Preparation of Porous Films by Ion Track Effect

Masaharu ASANO[1], Masaru YOSHIDA[1], Masao TAMADA[1], Hideki OMICHI[1], Ryoichi KATAKAI[2]

[1]Department of Material Development, Takasaki Radiation Chemistry Research Establishment, JAERI, [2]Department of Chemistry, Faculty of Engineering, Gunma University

I. INTRODUCTION

Environmentally responsive polymers have been synthesized and their applications have been investigated[1-3]. As one of the applications of these polymers, we studied, by means of ion beam irradiation on the films, the possibility of making porous films the pore size of which can respond to the changes of such environmental conditions as temperature, electric filed, pH, etc. For this purpose, an irradiation apparatus using heavy ion beams generated from the Takasaki AVF cyclotron was designed and constructed.

In the present paper, the outline of the apparatus and a preliminary experimental result are reported.

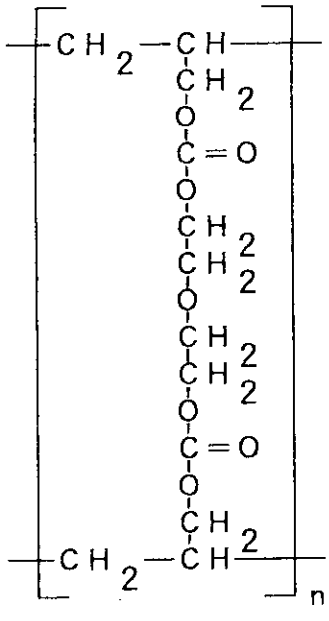

Scheme 1

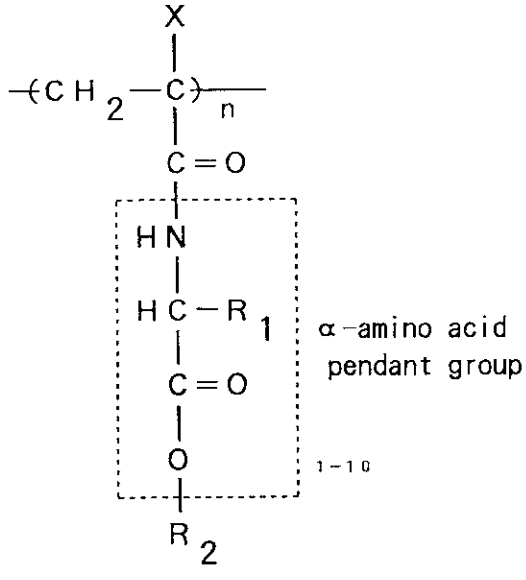

Scheme 2

II PROCEDURES

As a raw material for the above-mentioned porous membrane, we used a copolymer made of polyethylene glycol-bis-allyl carbonate (CR-39®) and acryloyl or methacryloyl monomer containing pendant α-amino acid ester or their oligomers as shown in the schemes 1 and 2, respectively. It is well known that the latter polymer exhibits a characteristic thermal-response in water such as low-temperature swelling and high-temperature shrinkage [4-6]. Accordingly, it is expected that a combination of radiation-sensitive CR-39 and thermally-responsive polymers leads to the porous membrane with an on-off switch function.

Figure 1 shows the scheme for the fabrication of ion track pore in polymer films. The copolymer films were first irradiated by heavy ion beam, followed by a chemical etching to obtain the ion track pore in the copolymer films.

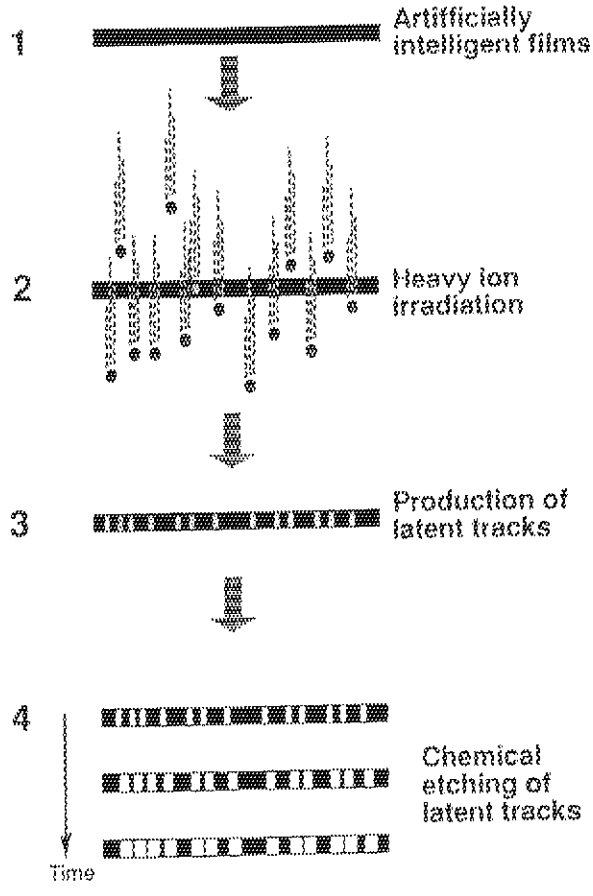

Fig. 1 Scheme for the fabrication of ion track pore in polymer films

III. EXPERIMENTAL

Figure 2 shows the photograph of the irradiation apparatus connected to the ion beam line (HV-1 port) of the AVF cyclotron. The components of this apparatus is as follows: chamber, film roller, turntable, Faraday cup, beam viewer, variable-type slit and vacuum pump.

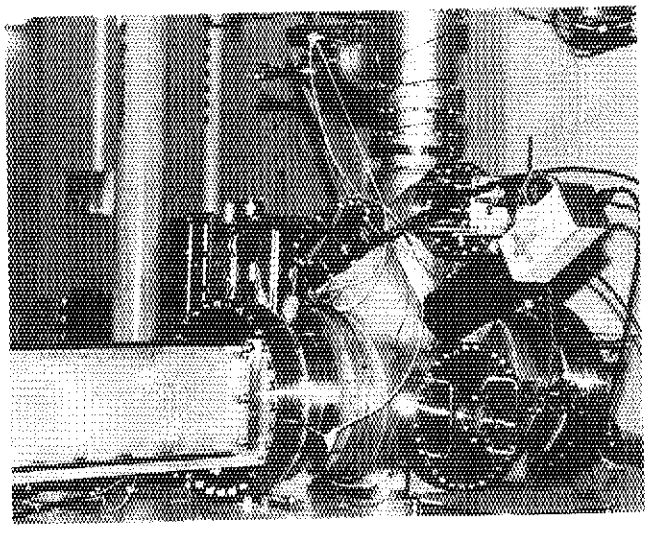

Fig. 2 An irradiation apparatus for the preparation of ion track pore

The vacuum system keeps the vacuum level at 5×10^{-8} Torr.

Figure 3 shows the illustration of the irradiation apparatus. The chamber, 35cm in diameter and 86cm in height, can be used either for the irradiation of small square samples and for the roll of films. For small square film irradiation, six samples of 5cm square can be set on the turntable sample holder. The angle of incident ion beam is controlled by changing the direction of the sample holder. The maximum irradiation width and length of the rolled film are 10cm and a few meter, respectively. In order to irradiate the film homogeneously, the forward movement of the film is synchronized with the movement in the perpendicular direction. In other words, the film proceeds in a zigzag pattern during irradiation.

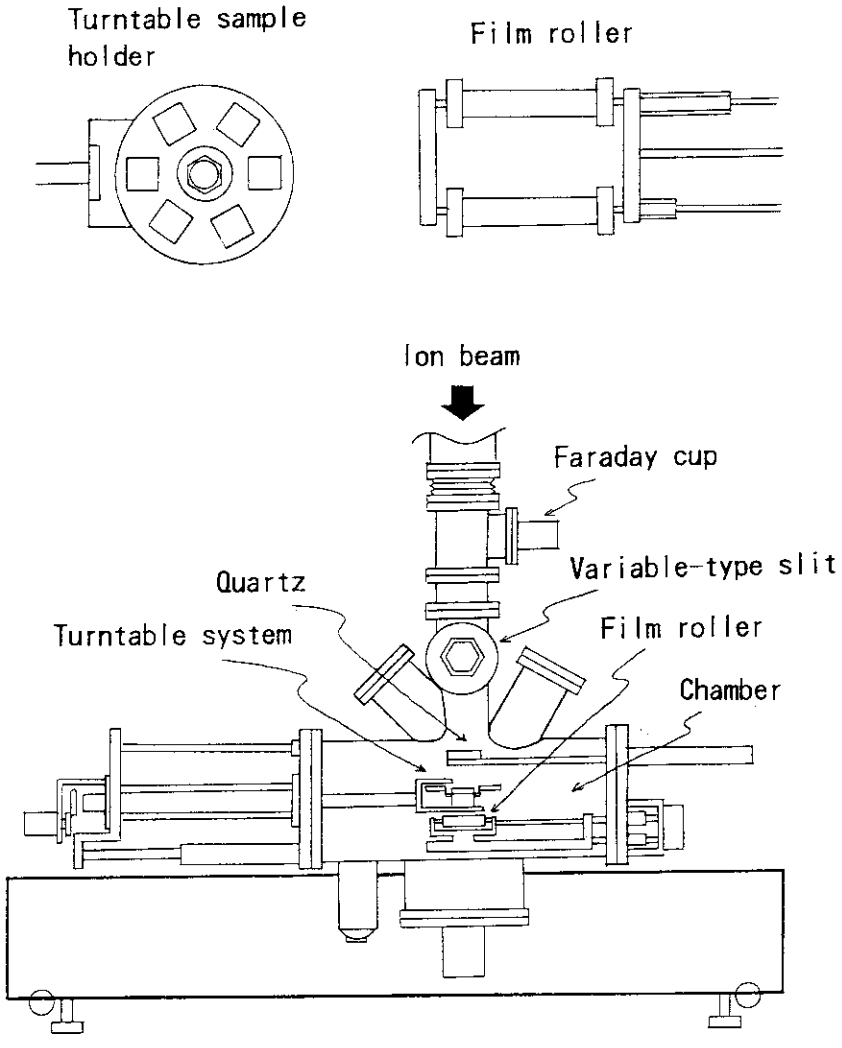

Fig. 3 Illustration of the irradiation apparatus

IV. RESULTS

(1) Ability of irradiation apparatus

Figure 4 shows the efficiency of evacuation for this irradiation apparatus. After 7 min's evacuation with a rotary pump the degree of vacuum reached 5×10^{-3} Torr. Then, a turbo-pump was acutuated. The degree of vacuum reached 8×10^{-6} Torr after 2.5 min and 8×10^{-7} Torr after 20.5 min. It was found that 2.8×10^{-8} Torr or a lower degree of vacuum could be obtained by baking (150℃, 24h). This vacuum level satisfies the specification (5×10^{-8} Torr).

(2) Tests of ion beam irradiation

The ion beam of 50MeV He^{2+} was followed by the current monitor. It was found that the spotted beam position could be controlled by observation of light emitted on quartz target. The shape of the scanned beam was squarein a size of 5cm.

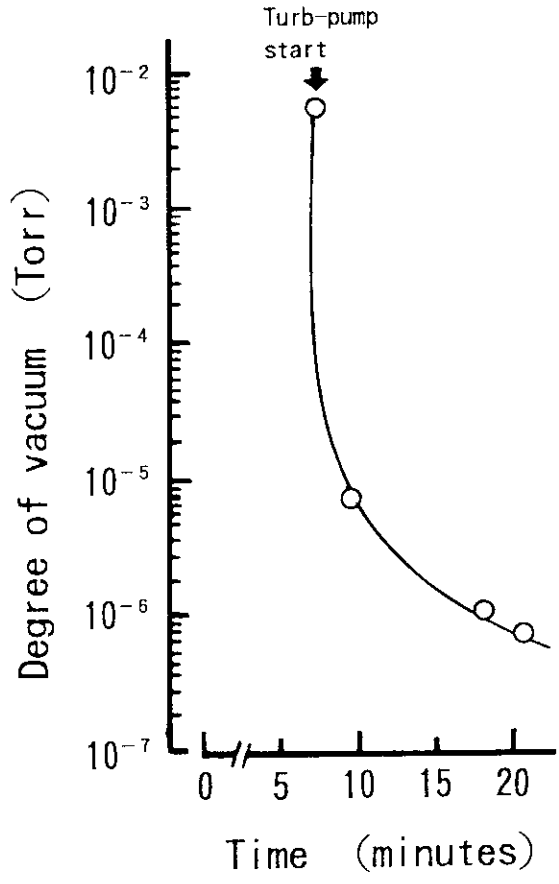

Fig. 4 Efficiency of evacuation for the irradiation apparatus

REFERENCES

1) Y. Okahata, H.J. Lim, G. Nakamura and S. Hachiya, J. Am. Chem. Soc., 105 , 4855 (1983)
2) T. Tanaka, I. Nishio, S.T. Sun and S. Nishio, Science, 218 , 467 (1982)
3) M. Irie, Macromolecules, 19, 2890 (1986)
4) M. Yoshida, M. Asano, and M. Kumakura, Eur. Polymer J., 25, 1197 (1989)
5) M. Yoshida, M. Asano, M. Kumakura, R. Katakai, T. Mashimo, H. Yuasa, and H. Yamanaka, Drug Design and Delivery, 7 , 159 (1991)
6) M. Yoshida, M. Tamada, M. Kumakura, and R. Katakai, Radiat. Phys. Chem., 38, 7(1991)

5.2 Trial Preparation of Phthalocyanine/Copper Hybrid Thin Films Using PVD and IBS Methods

Yoshinobu IZUMI, Fumio HOSOI, Masao TAMADA
and Hideki OMICHI

Funct. Mat. Lab. 1., Dept. Mat. Develop., Takasaki Radiation Chemistry Research Establishment, JAERI

INTRODUCTION

Since the early 1980's, the ideas to synthesize hybrid materials have attracted many scientists in the field of materials development. The hybrid material means the composite material consisting of such plural materials as organic and inorganic materials in the state controlled at a molecular or an atomic level. The plasma polymerization, L-B method, ion beam sputtering (IBS) deposition and ion implantation method have been studied and expected as possible candidates to realize hybrid materials by reason that they are the best methods to hybridize materials in the state controlled at a molecular or an atomic level. It is earnestly expected that the development of such techniques will lead not only to the modification of conventional materials but also to the production of entirely new materials. Hara M. and his co-workers studied the epitaxial growth process of copper phthalocyanine (CuPc) onto various substrates by using OMBE method[1]. Inaoka K. and his co-workers have studied the crystal growth process of metallic layer evaporated onto monocrystalline stearic acid[2], and that of stearic acid evaporated onto inorganic monocrystals[3,4].

Ion implantation is expected as one of the possible methods for hybridizing organic and inorganic materials. Recently, ion implantation into organic materials has been extensively studied. Many of them aimed at the improvement of electrical conductivity of organic materials caused by doping effect. There are some examples in which the electrical conductivity of organic materials was raised by ion implantation method[5,6]. It was concluded, however, that the result was caused by decomposition, degradation or carbonization of organic materials[7].

On the other hand, the deposition of metallic substances onto organic materials by using a low energy IBS technique is expected effective for hybridizing organic and inorganic materials to improve electrical conductivity and optical properties without degradation of organic materials.

We planed to synthesize hybrid thin films without degradation of organic layer using PVD, CVD and IBS methods, and fabricated the apparatus for preparing hybrid thin films. Prior to the study using this apparatus, we made a preparatory experiment of

the low energy IBS for hybridizing H_2Pc and Cu, and compared characteristics of IBS with that of ion implantation. In the present paper, we report an outline of the apparatus for preparing hybrid thin films and the result of the trial experiment.

THE APPARATUS FOR PREPARING HYBRID THIN FILM

Fig. 1 shows the apparatus for preparing hybrid thin films fabricated in September of 1991. This apparatus is equipped with the chambers for laser CVD, surface analysis and IBS deposition. A sample treated in each chamber can be conveyed to another chamber for next process without contacting with air.

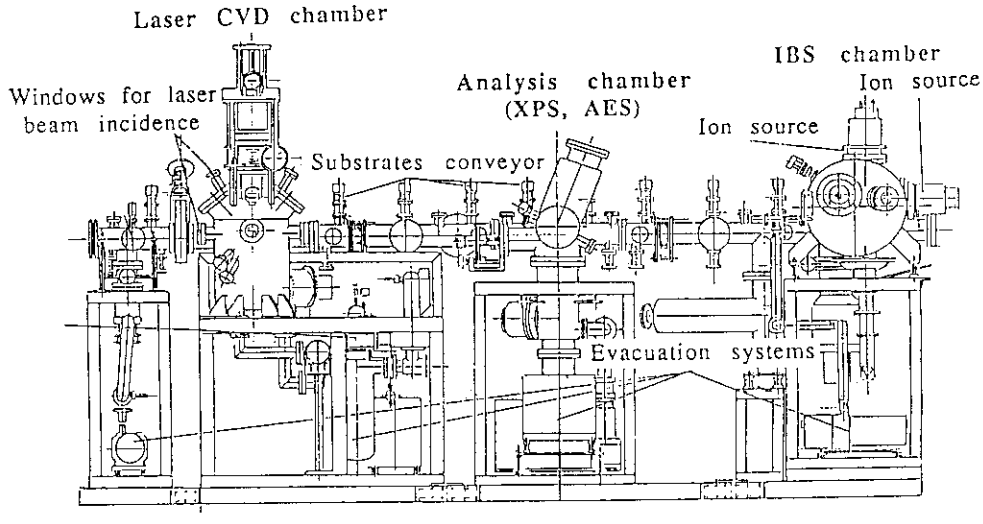

Fig. 1 The apparatus for preparing hybrid thin films

In the laser CVD chamber, orientation-controlled organic thin films can be synthesized by using CVD of organic gas and ablation of polymer. The orientation-controlled organic thin films can also be photopolymerized in this chamber. An excimer laser system (Lambda Physik LPX 105 icc) is equipped as the UV light source for CVD. This laser can radiate ArF (193 nm) and KrF (248 nm) lights with the pulse energy of 200 mJ/pulse and 300 mJ/pulse, respectively. The IBS chamber is equipped with two ion sources for ion beam processing. Both of them can generate Ar^+ and He^+ ion beams with the acceleration energy up to 5.0 kV. Four targets for sputtering can be installed within this chamber. In the analysis chamber, the surface analysis system (Parkin Elmer 255) is equipped, and XPS and AES are employed to analyze on the hybridized thin films.

EXPERIMENTAL

Materials and physical vapor deposition

H_2Pc thin films with a thickness of about 50 nm were prepared by the sublimation from H_2Pc powder onto the glass substrates, Au vapor deposited substrates

and fused silica substrates. During that process, the pressure was kept under 10^{-3} Pa and the substrates were kept at 300 K.

IBS deposition , ion implantation and analyses on the hybridized thin films

H_2Pc PVD thin films were loaded into the chambers for IBS deposition of Cu and Cu^+ implantation. In the case of Cu IBS, Cu target was sputtered by Ar^+ ion beams with an acceleration energy of 0.5-2.0 kV and a current of 225 μA. In the case of implantation, H_2Pc PVD thin films were irradiated with Cu^+ ion beams with an acceleration energy of 10.0-50.0 kV, a current of 5 nA and a fluence of $1x10^{13}$ ion/cm^2. Before and after IBS deposition of Cu and Cu^+ implantation, C_{1s}, N_{1s} and Cu_{2p} photoelectron spectra, UV and FT-IR spectra of the films were measured.

RESULTS AND DISCUSSION

Fig. 2 shows the UV absorption spectra of H_2Pc PVD thin films irradiated with Cu^+ ion beams. Because of the low fluence, the absorption due to Cu was thought negligible, and it was considered that the absorption increase in the region near 500 nm was caused by carbonization of H_2Pc[7]. On the other hand, the decrease in absorption at 210, 330 and 630 nm was caused by dissociation or etching of H_2Pc by Cu^+ ion beams.

Fig. 3 shows the UV absorption spectra of H_2Pc thin films deposited with Cu by IBS method. The absorbance in the region near 500 nm increased similarly to the case in Fig. 2. But this increase in absorbance was due to the absorbance of deposited Cu, so the carbonization of H_2Pc during IBS deposition process can be regarded negligible. Three absorption peaks did not change in intensity in this case. In other cases with depositions at higher Ar^+ acceleration energy, on the other hand, the kinetic energy of sputtered Cu particles is higher, and the etching of

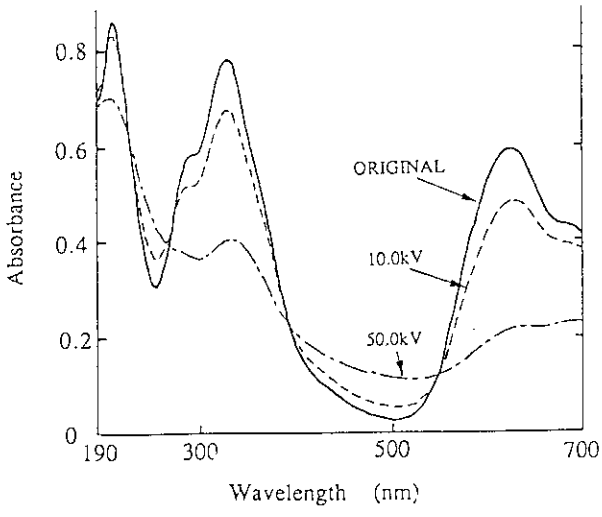

Fig. 2 UV absorption spectra of H_2Pc PVD thin films irradiated with Cu^+ ion beams. Cu^+ fluence = $1x10^{13}$ ion/cm^2.

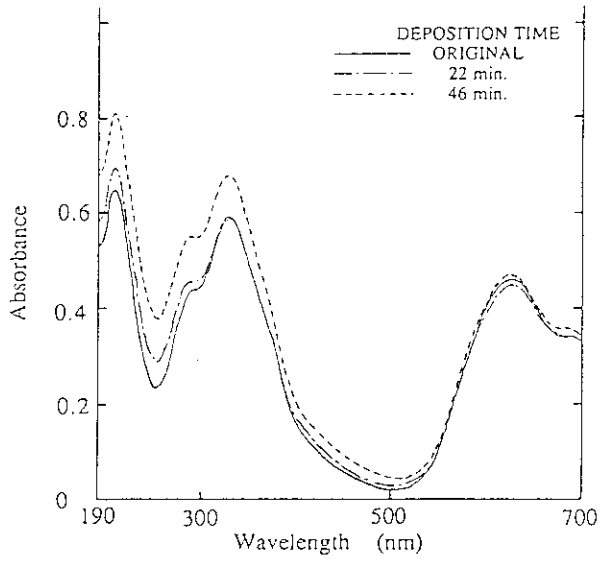

Fig. 3 UV absorption spectra of H_2Pc PVD thin films deposited with Cu by IBS method. Ar^+ ion energy = 0.5 kV.

H_2Pc layer was caused. Therefore, the deposition of Cu particles with the energy as low as possible is indispensable in order to avoid the destruction of organic layer, and the IBS method is superior to ion implantation method as the means for hybridizing H_2Pc and Cu.

CONCLUSIONS

We have studied the low energy ion beam sputtering (IBS) for hybridizing H_2Pc and Cu, and compared with ion implantation. In the case of Cu^+ ion implantation, H_2Pc PVD thin film was degraded and etched. On the other hand, the degradation and etching of samples were not induced by Cu IBS deposition. The deposition of Cu particles with the energy as low as possible is indispensable in order to avoid the destruction of organic materials, and the IBS method is superior to ion implantation method as the means for hybridizing H_2Pc and Cu.

REFERENCES

1) Hara M., Sasabe H., Yamada A. and Garito A. F., Jpn. J. Appl. Phys., 28 (1989) L306.

2) Inaoka K., Yase K. and Okada M., Vacuum, 30 (1987) 853.

3) Matsuzaki F., Inaoka M., Okada M. and Sato K., J. Cryst. Growth, 69 (1984) 231.

4) Inaoka K., Kobayashi M., Okada M. and Sato K., *ibid.*, 87 (1988) 243.

5) Forrest S. R., Kaplan M. L., Schmidt P. H., Venkatesan T. and Lovinger

A. J., Appl. Phys. Lett., 41 (1982) 708.

6) Robinet S., Salvi M. and Clarisse C., Nucl. Instrum. Methods Phys. Res., B53 (1991) 46.

7) Robinet S., Gauneau M. Salvi M., Clarisse C., Delamar M. and Leclerc M.,Thin Solid Films, 200 (1991) 385.

5.3 Construction of a Wide Area Irradiation Chamber for Polymeric Materials and Dose Uniformity

Tsuneo SASUGA, Hisaaki KUDHO and Tadao SEGUCHI
Department of Material Development, JAERI Takasaki

I. Introduction

Fiber reinforced plastics (FRP) and polymer films are used in space environment as the structural materials and thermal insulator of artificial satellites and space station. These materials are subjected to irradiation of electrons, protons and heavy ions like iron under low and high temperature. For selection and application of the materials used in space, knowledge about the ion irradiation effects is necessary.

Glass fiber reinforced plastics (GFRP) are expected to be used as an insulator for super conducting magnets of a fusion reactor. In this environment, GFRP is irradiated by 14 MeV neutrons and gamma rays under cryogenic condition. It is well known that neutron irradiation effects of organic materials is caused by recoiled protons created by collision of the incident neutrons to the hydrogen atoms in medium[1]. So that, neutron irradiation effects could be simulated by proton irradiation.

On the scientific view point, the effects of linear energy transfer (LET) on polymer degradation is an interesting matter. The LET effects on chemical reaction and products have been extensively studied, but the reports of the LET effects on the mechanical properties of polymeric materials are very few[2-4].
We constructed a chamber to irradiate specimens widely and uniformly as possible to measure mechanical properties. In this paper, the design concept of the chamber and the characteristic of the dose uniformity are presented.

II. Design concept

(1) In order to measure the changes in mechanical properties of materials, uniform irradiation on wide area of the sample is essential. The chamber is mounted on a port where ion beam can be scanned to 100 mm x 100 mm.

(2) In irradiation of organic materials, a lot of gas evolution is unavoidable. So, the chamber is composed of the to the two vacuum vessels having individual exhaust systems, and these vessels can be isolated each other by metal foil inserted between

the vessels, if required.

(3) Providing for several kinds of irradiation mode, like ambient temperature, low temperature and in situ irradiations, three types of sample holder modules are equipped.

(a) Ambient irradiation module: Four sample holders and one empty hole used to observe beam profile are aligned on the turret made of aluminum. The sample holder have graphite beam stopper and cooling water jacket just behind them. So that, four samples can be irradiated sequentially whiteout breaking vacuum.

(b) Low temperature irradiation module: The sample can be irradiated below -100 C. Sample is cooled down by liquid nitrogen flow through the thermal conduction jacket.

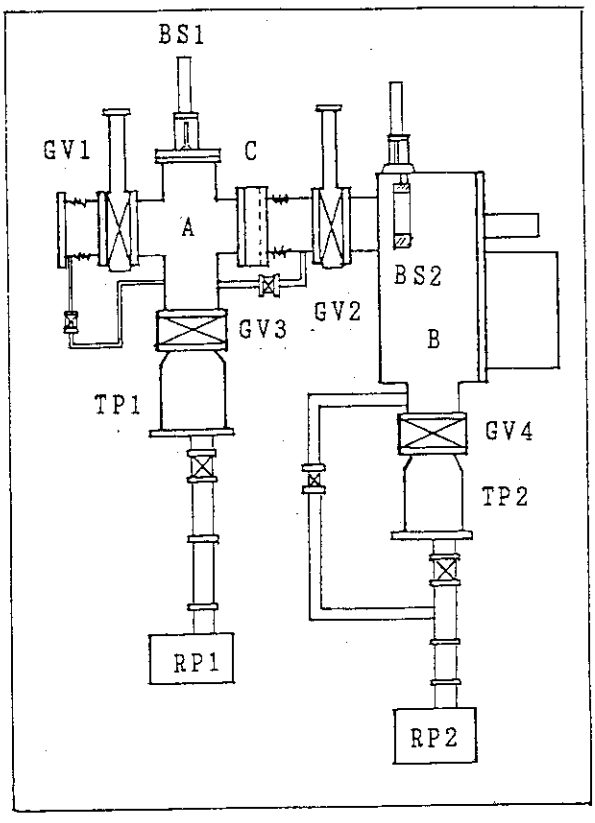

Figure 1. Illustration of Chamber.

A: Vacuum vessel 1,
B: Vacuum Vessel 2,
RP: Rotary pump, TP: Turbo pump,
GV: Gate valve, BS1; Beam shutter,
BS2: Gate type beam stopper for beam trimming

(c) Stress relaxation module: The module is used to measure stress relaxation under irradiation at ambient temperature.

(4) Other equipments: Beam shutter (used during change of sample), several view and assist ports, and gate type beam stopper for trimming the edge of scanned beam are available.

The chamber constructed on the basis of above concept is illustrated in Figure 1.

III. Dose uniformity

Dose uniformity was checked by using a cellulose tri-acetate film dosimeter (CTA, 100 mm x 100 mm, 0.125 mm thickness). Figure 2 show the incident spot beam profile in the irradiation by 45 MeV proton with the current of 100 nA for 50 seconds. The diameter of beam is approximately 10 mm and the optical density becomes to

reduced toward outside. As the optical density reflects absorbed dose, it means the higher in dose toward the center.

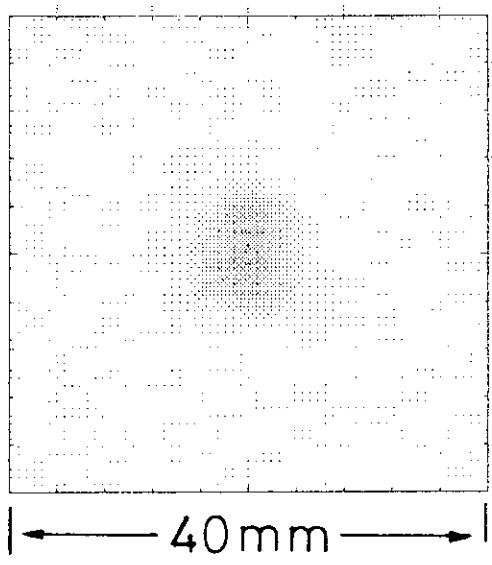

Figure 2. The profile of spot beam (45 MeV proton).

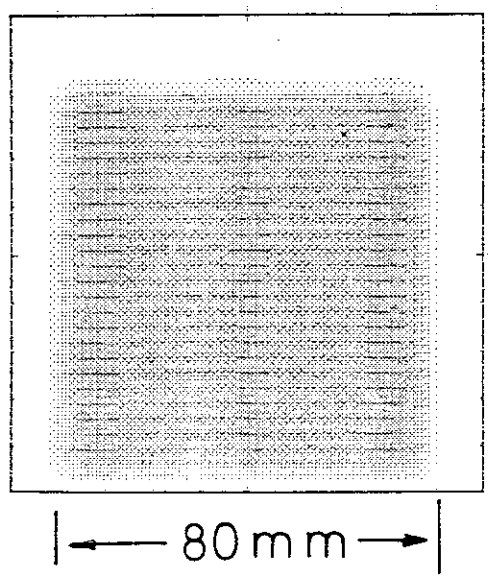

Figure 3. Scanning beam profile.

The dose profiles obtained by the scanning of this spot beam to 80 mm x 80 mm is shown in Figure 3. The scanning rate of the spot beam is 50 Hz for horizontal direction (x-direction) and 0.5 Hz for vertical direction (y-direction). It can be seen that the dose distribution is uniform for y-direction, but the dose at the edges of beam turning and at the center are high. Figure 4 shows the dose profile at the left side edge (the area is indicated in the Figure). The dose is calculated to 67.3 kGy by average and the edge of beam is 81.0 kGy, i.e., 20 % higher than the average. Figure 5 shows the profile at the center area (50 mm x 50 mm) of CTA film. The dose is 66.6 kGy by average and the one at the center part (about 10 mm width) is 75.4 kGy (13 % higher).

These dose distribution is brought about by the performance of power source of scanning facility. So, reduction of ununiformity at the center is unavoidable, but at the edges can be improved by over scanning and trimming of beam edge by beam slit. By using the gate type beam stopper shown in Figure 1, the specimens with the size of 100 mm x 100 mm can be irradiated uniformly except the center part.

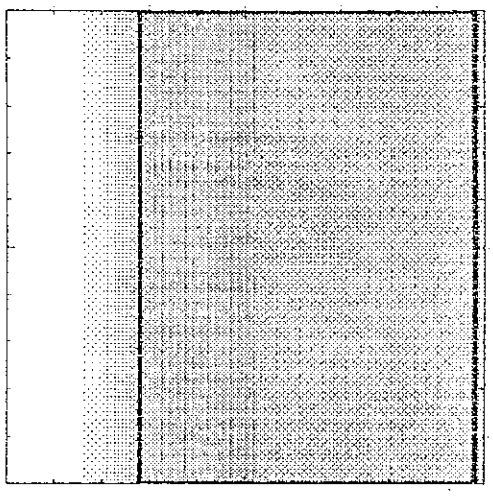

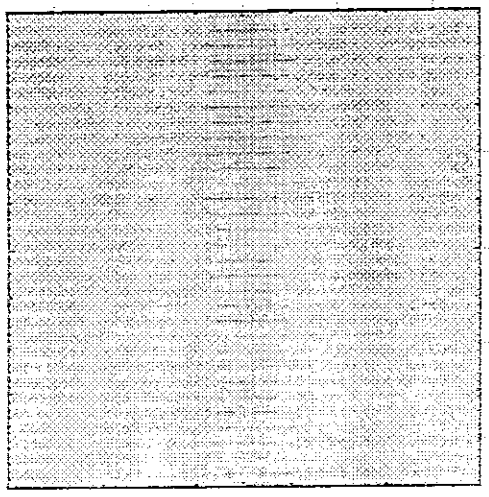

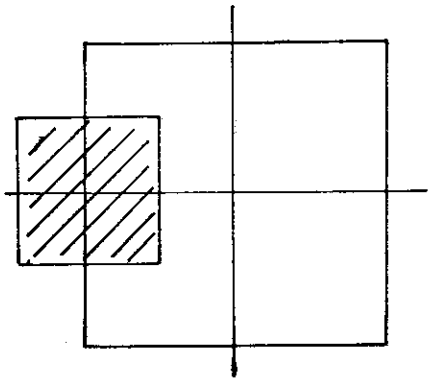

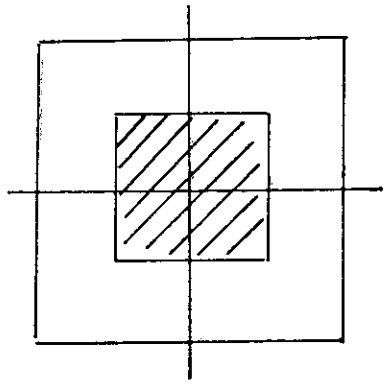

Figure 4. Scanning beam profile at the left side edge.

Figure 5. Scanning beam profile at the center part.

Reference

1) For example, J.W.T. Spinks and R.J. Woods, "An Introduction to Radiation Chemistry", John Wily & Sons Inc., New York(1964).
2) Wang Guang-how, PAN Guo-qiang, Dou Lie, Yu Run-xin, Zhang Teng, Jiang Shan-gen and Dai Qing-lai, Nucl. Instrum, Meth. Phys. Res., B27, 410(1987).
3) D.R. Culter, M.V. Smith, Fundow Tasy, A. Gupta, and R.E. Fornes, J. Appl. Polym. Sci., 30, 1753(1985).
4) T. Sasuga, S. Kawanishi, M. Nishii, T. Seguchi, I. Kohno, Polymer, 30, 2054(1989).

5.4 Radiation-induced Adhesion at fe-PTFE Interfaces-I

Mufamad GAFARI , Hidetoshi YAMABE*, Yoji NAKAMURA**, Teruya SHINJYO*** , Nobuyosi HOSOITO***, Hidefumi TAKESHITA****, Yasushi AOKI****, Shunnya YAMAMOTO****, Hiroshi NARAMOTO****,

Nisshin Steel, Steel R&D Laboratories, Osaka 592 Japan
* Nisshin Steel, Steel R&D Laboratories, Chiba 272 Japan
** Faculty of Science and Technology, Ryukoku University, Otsu 520 Japan
*** Institut for Chemical Research, Kyoto University, Uji 611 Japan
****Takasaki Radiation Chemistry Research Establishment, JAERI, Takasaki, Gunma, 370-12, Japan

I. INTRODUCTION

Interest in Teflon-Metal has been encouraged by the observation that irradiation of Fe-Teflon with ion beams in the electronic stopping region results in a significant adhesion enhancement at the Fe-Teflon interfaces. This discovery may have a technological significance in applications, such as corrosion protection and thin film technology. Therefore, it is of fundamental interest to understand the reason for the improvement of the adhesion at the interfaces. Microscopic methods, such as Mössbauer spectroscopy could contribute to the understanding of the complicated structure in the interfaces. In present paper, we will demonstrate the usefulness of Conversion Electron Mössbauer Spectroscopy (CEMS) for identification of different components located in the interface.

II. MATERIALS AND METHODS

The specimens were prepared by sequentially vapor deposition of 25 Å ^{57}Fe and 155 Å ^{56}Fe onto the Teflon substrates using electron-beam heating of the source materials. The pressure in the deposition chamber was 10^{-9} and 10^{-8} Torr before and during deposition, respectively. The evaporation rate (as measured by quartz-crystal oscillator) was 1 Å/min. ^{57}Fe atoms behave as probes at the interface between Teflon and Fe. The layer of ^{56}Fe

acts as protective coating material for ^{57}Fe. The irradiations of samples were performed with 15 MeV S ions. The samples were bombarded to doses ranging from 10^{14} to 10^{15} ions/cm^2. The beam current was kept at about 9 nA/cm^2. The CEMS was used for the characterization of interfaces in the surface region within the range of 7.3 KeV conversion electrons.

Ⅲ. RESULTS AND DISCUSSION

Fig.1 shows the Mössbauer spectra of ^{57}Fe atoms on the Teflon. Before irradiation, the ^{57}Fe atoms located in the interface consist of metallic iron and Fe^{3+}. The irradiation at different doses, however, alters the shape of the spectra. The analysis of Mössbauer spectra of irradiates that iron atoms located in the interface are mainly in Fe^{3+} and Fe^{2+} charge state. Fe^{3+} charge state is due to formation of Fe-O compounds. The Fe^{2+}charge state, however, is mainly due to the formation of Fe-F and Fe-F-C compounds. The formation of the Fe-F and Fe-F-C compounds at the Fe-Teflon interfaces leads to the adhesion enhancement. In other words, the induced Fe-F and Fe-F-C compounds at the Fe-Teflon interfaces is correlated to the adhesion enhancement.

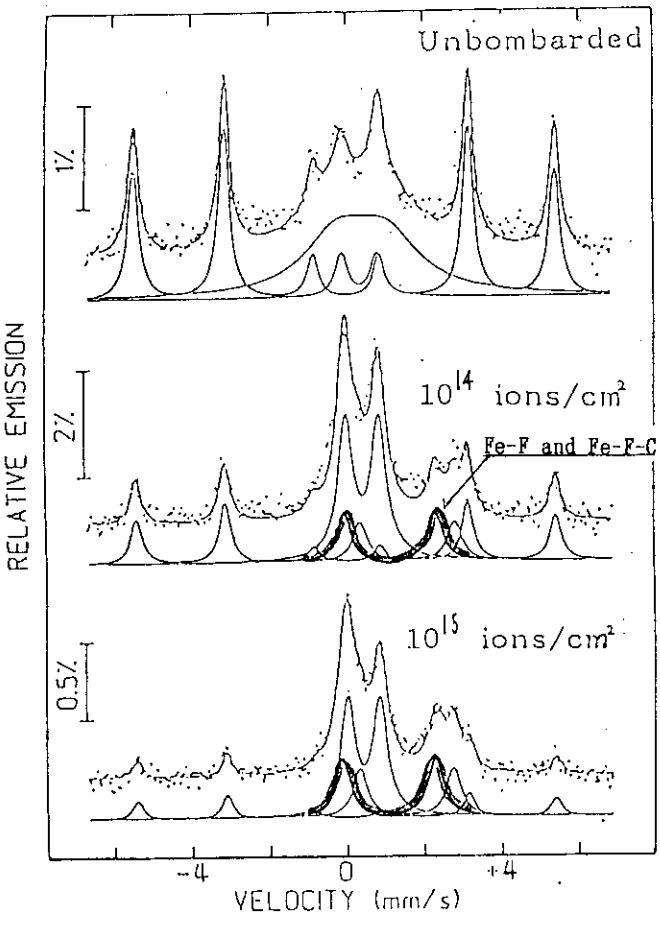

Fig.1 Mössbauer spectra of ^{57}Fe atoms on Teflon before and after irradiation

6. INORGANIC FUNCTIONAL MATERIALS

6.1 In-situ Observation of Damage Evolution in Sic Crystals During He+ and H2+ Dual-ion Beam Irradiation

K. Hojou[1], S. Furuno[1], H. Otsu[1] and K. Izui[2]

1 Department of Chemistry, Japan Atomic Energy Research Institute, Tokai-mura, Ibaraki 319-11, Japan
2 Faculty of Education, Nagasaki University, 1-14, Bunkyo-machi, Nagasaki-shi, Nagasaki 852, Japan

1 Introduction

In-situ observation of damage evolution in ion irradiated materials is important for simulating plasma-wall interaction as well as 14MeV neutron irradiation damage in a fusion reactor[1,2].

We constructed an in-situ observation system consisting of 100kV electron microscope linked with a 10kV ion accelerator and a parallel electron energy loss spectrometer(Parallel-EELS)[3]. Using this system, we have observed the dynamical processes of structural changes in SiC crystals irradiated with helium [4] and hydrogen ions [5] at various temperatures and found various irradiation conditions under which amorphization and bubble formation occurred. Furthermore, compositional changes in SiC due to hydrogen ion irradiation at room temperature were found with parallel-EELS[6].

Recently we have developed a new system of in-situ observation and chemical analysis of materials during dual-ion beam irradiation within a 400kV electron microscope [7,8], aiming to promote simulation experiments to match more complex situations in which ions of more than two species are simultaneously injected.

In the present experiments, effects of simultaneous He^+ and H_2^+ ion irradiation were examined and the results were compared with that obtained by He^+ ion irradiation after H_2^+ pre-irradiation.

2 Experimental procedures

The specimens used in the present work were SiC sintered polycrystals containing beryllia(BeO) powder less than 1wt%, which were supplied from Hitachi Research Ltd. The structure of SiC crystals were hexagonal 6H type. Disks with about 3mm diameter were cut out from a plate by ultrasonic machining and a center part of the disk was polished to a thickness of 10-20μm with a dimple grinder to form concave lens shape. Thin films suitable for electron microscopy were then made by 2.5keV Ar^+ ion bombardment with etching angle of about 20° at room temperature.

The in-situ observation during ion irradiation was made by using a 400kV transmission electron microscope of JEM-4000FX type combined with two sets of ion accelerator. These ion accelerators were connected to the electron microscope from the left and right side, as shown in Fig.1[7,8]. Results of in-situ observation during dual or successive ion irradiation were recorded with a VTR through a CCD camera and the electron micrographs were taken on films at some intervals.

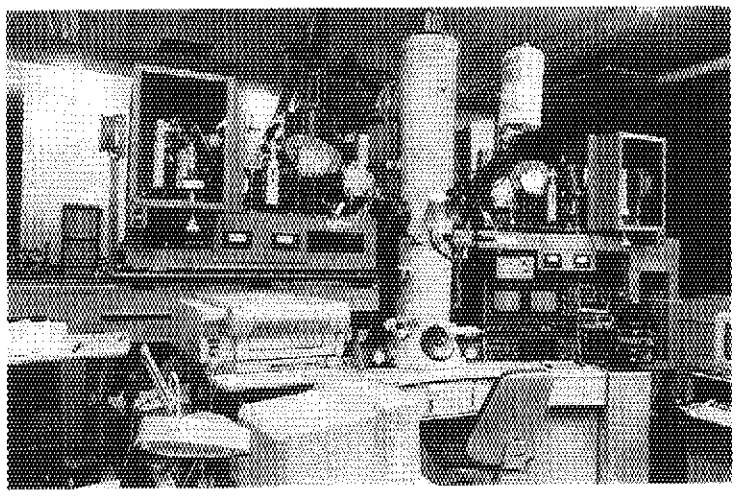

Fig.1 400kV electron microscope with analytical equipments of EDS and parallel-EELS, combined with two sets of 40keV ion accelerator.

A mass selected ion beam is incident at each angle of 60° to the surface of the specimen. In the present experiments, the energies of H_2^+ and He^+ions were taken to be 15kV and 12kV, respectively so that the range of each ions has the same value, about 120nm, on the basis of TRIM-cord calculation. The damage density in SiC amorphous structure was also calculated by TRIM-cord for 7.5keV hydrogen atoms and 12keV helium atoms of a fluence of 2.7×10^{17}(H,He)/cm^2. The damage density due to 12keV helium atom irradiation is about ten times larger than that due to 7.5keV hydrogen atom irradiation. To examine the effect of hydrogen atom injection on bubble formation in He^+ ion irradiated SiC crystals, the following experiments of two kinds were performed .

(1) 15keV H_2^+ ion irradiation with the flux of 1×10^{14}(H)/cm^2/s after pre-irradiation of 12keV He^+ ions with the flux of 1×10^{14}(He)/cm^2.

(2) Simultaneous irradiation with both 12keV He^+ and 15keV H_2^+ ions, with atom fluxes of 1×10^{14} (H,He)/cm^2/s, respectively.

3 Experimental results and Discussion

Dual-ion beam irradiation experiment in SiC crystals H_2^+ and He^+ dual-ion irradiation experiments were performed on thin foils of SiC crystals using the above mentioned equipment. In parallel with VTR observation and recording, electron micrographs were taken on films for some time intervals using the standard method of an electron microscope. The result of simultaneous dual beam irradiation was compared with that of successive and alternative single ion beam irradiation with two kinds of ions. In both of these experiments, irradiation fluxes of each ion were set to be equal so that the number of implanted atoms become equal for both cases of irradiations.

Figures 2 (a) and (b) show the structural changes in SiC produced by simultaneous H_2^+

and He^+ dual ion beam irradiation at room temperature. The flux of H_2^+ ions was $1x10^{14}$ (H)/cm^2/sec and that of He^+ ions was $1x10^{14}$(He)/cm^2/sec so that the implantation rate of each kind of atoms, H and He, is the same. After 30 minutes irradiation amorphization occurred, as shown in fig. 2 (a), but bubbles were not observed at this stage of irradiation. After 45 minutes irradiation, bubbles formation was remarkable in the amorphous structure of SiC, as shown in fig. 2 (b).

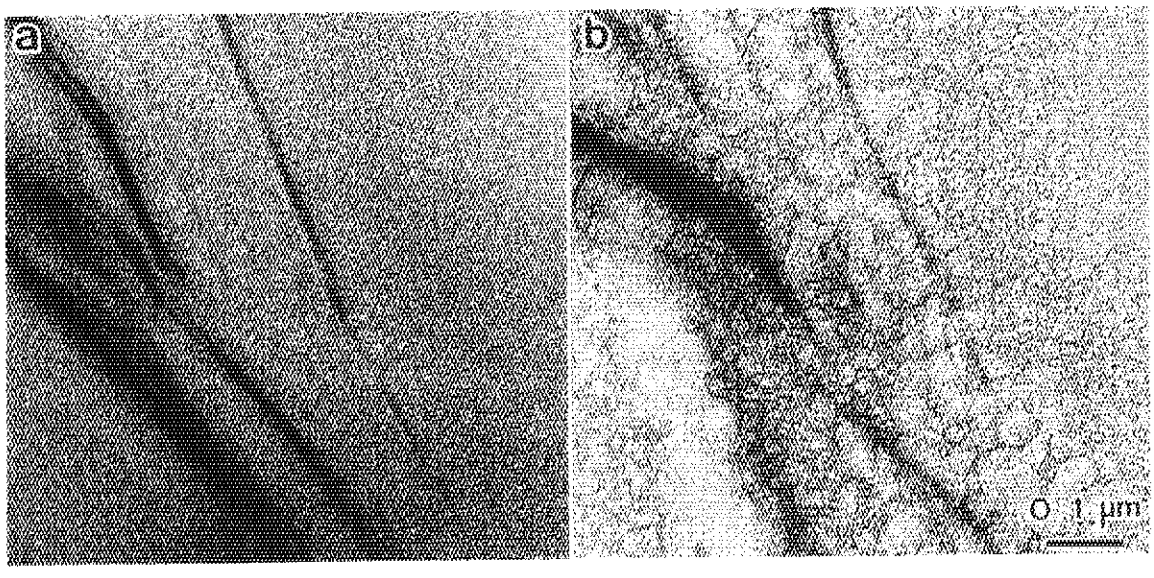

Fig.2 Structural changes of SiC during 15keV H_2^+ and 12keV He^+ simultaneous dual ion irradiation. The atomic fluxes of both hydrogen and helium were about $1x10^{14}$(H,He)/cm^2. fluence:(a) $1.8x10^{17}$(He)/cm^2 + $1.8x10^{17}$(H)/cm^2,(b) $2.7x10^{17}$(He)/cm^2 + $2.7x10^{17}$(H)/cm^2.

Fig. 3 (a) and (b) show the results of successive and alternative single ion beam irradiation, firstly with He^+ ions for 45 minutes and secondly with H_2^+ ions for 45 minutes, at room temperature. After 30 minutes irradiation, bubble formation occurred as well as amorphization, as shown in fig. 3 (a). After 90 minutes irradiation (He^+: 45 minutes, H_2^+: 45 minutes), bubbles were largely grown, as shown in fig. 3 (b). From the comparison of fig. 2 (a) with fig. 3 (a) it is clearly seen that the simultaneous implantation of H atoms in addition to He atoms has the effect of suppressing bubble formation in comparison with the case of the single He atom implantation.

By the present experiments it was revealed that hydrogen atoms gave quite a different effect on the formation of helium bubbles according as whether they were pre-injected or simultaneously injected in addition to helium atom injection. This behavior of hydrogen atoms seems peculiar but very important in the stand point of simulation experiments on plasma-wall interaction. The reason for this remarkable behavior of hydrogen atoms is not clear at the present stage. It should be pointed out that this phenomena occurred in an amorphous structure formed by the ion irradiation. Interaction of hydrogen or helium atoms with dangling bonds in an amorphous structure would play an essential role in the formation of bubbles[5]. Further systematic studies are needed to solve this problem, including

temperature dependence.

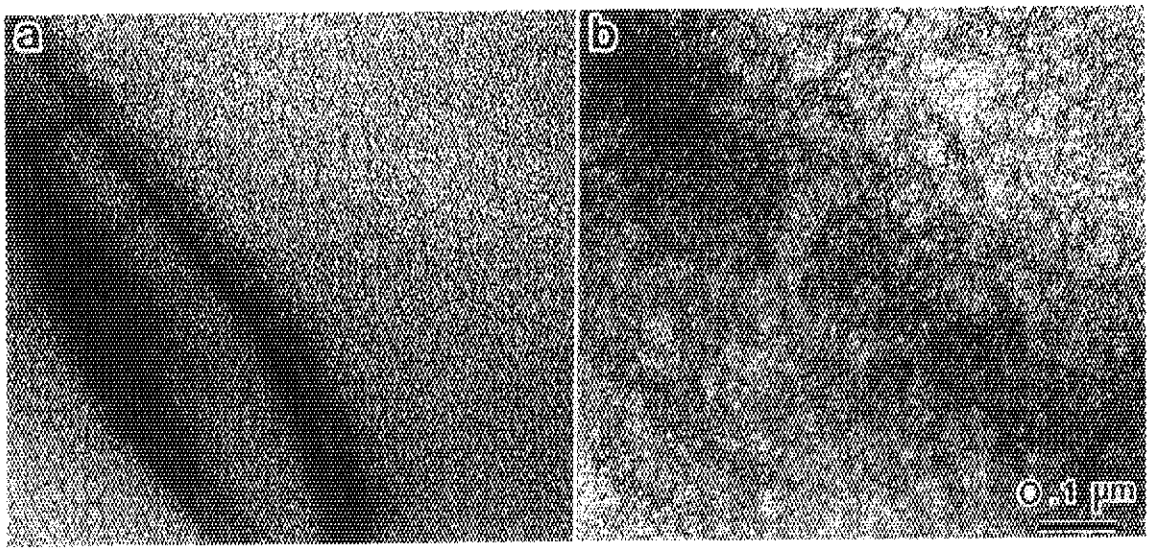

Fig.3 Structural changes of SiC during successive and alternative He^+ and H_2^+ ion irradiation. The atomic fluxes of both hydrogen and helium were about $1x10^{14}$(H,He)/cm^2/sec. fluence:(a) $1.8x10^{17}$(He)/cm^2 (b) $2.7x10^{17}$(He)/cm^2 + $2.7x10^{17}$(H)/cm^2.

4 Conclusions

The effects of hydrogen atom injection on bubble formation in He^+ ion irradiated SiC crystals were examined at room temperature by the following experiments of three kinds : (1) 15keV H_2^+ ion irradiation after pre-injection of 12keV He^+ ions. (2) Simultaneous 12keV He^+ and 15keV H_2^+ ion irradiation.

The obtained result is that the simultaneous implantation of H atoms in addition to He atoms has the effect of suppressing bubble formation in comparison with the case of the single He atom implantation.

References

[1] S.Ishino, H.Kawanishi, K.Fukuya and T.Muroga, IEEE Trans. Nucle. Sci. NS-30 (1983) 1255.
[2] T.Takayama, S.Ohonuki and H.Takahashi, J. Nucl. Mater. 133&134 (1985) 571.
[3] K.Hojou, S.Furuno, H.Otsu, K.Izui and T.Tsukamoto, J.Nucl.Mater.155-157(1988)298.
[4] K.Hojou and K.Izui, J.Nucl.Mater. 160 (1988) 147.
[5] K.Hojou, S. Furuno and K. Izui, J.Electron Microsc., 40(1991) 157.
[6] K.Hojou, S.Furuno, T.Soga and K.Izui, J.Nucl.Mater. 179-181 (1991) 411.
[7] S.Furuno, K.Hojou, H.Otsu, K.Izui, T.A.Sasaki, T.Tsukamoto and T.Hata, Electron Microscopy, 4 (1990) p538.
[8] S.Furuno, K.Hojou, H.Otsu, K.Izui, T.A.Sasaki, T.Tsukamoto and T.Hata, J.Electron Microsc.,41,(1992) 273.

6.2 An Ultra－low Energy Ion Beam Deposition Apparatus for Thin Film Growth

Hideki OHNO* and Siro NAGAI
Takasaki Radiation Chemistry Research Establishment, JAERI
*Department of Physics, Meisei University

1. INTRODUCTION

Extensive studies have been carried out on thin film growth by the use of the ion beam deposition (IBD) technique employing low energy (< 1 keV) ion beams. The advantages of the IBD technique are (1) epitaxial growth of crystalline films and (2) synthesis of metastable phase materials like diamond[1]. On the other hand, some films grown by this method have been reported to contain some defects that may be associated with carbon atoms incorporated during IBD[2]. These advantages and problems involved, however, have been found from the studies using practical ion beam deposition systems where it was difficult to define and control experimental parameters such as ion energy and substrate temperature, for thin film growth.

The IBD technique is expected to be one of the promising techniques that allow the film growing process to be controlled at the levels of atoms and molecules. To approach this goal, it seems most important to relate the nature and structure of the deposited thin film with the deposition parameters using a highly sophisticated ion beam deposition apparatus combined with in-situ surface analysis equipment. The principal requirements for such apparatus are:

(1) The apparatus can deliver highly uniform, mass-resolved ion beam with current densities greater than 1 $\mu A/cm^2$ over areas of a few cm^2,

(2) Ultra-high vacuum (UHV) of the order of 10^{-9} Torr can be maintained in the target chamber during ion beam deposition,

(3) The target is at earth potential for convenience of in-situ surface analysis,

and

(4) The target chamber is equipped with multiple surface analysis equipments which allow in-situ, desirably real-time, analysis of growing thin films.

An apparatus meeting the requirements listed above, manufactured

by VSW Scientific Instruments Ltd., GB, on the basis of the technologies developed by Prof. D.G.Armour and his co-workers at the university of Salford[3], has recently been installed at our institute. The outline of the apparatus and the results of a preliminary experiment on carbon ion deposition are described below.

2. APPARATUS

A plan view of the ultra-low energy ion beam deposition apparatus is shown in Fig. 1. The apparatus consists of ion source, beam transport, beam focusing and deceleration, and irradiation/analysis systems. The ion source is of a Freeman type equipped with a high temperature oven. The ions extracted from the ion source are accelerated to the transport voltage at -10 kV with respect to the ion source voltage. The electromagnet selects ion with the required mass to charge ratio and focuses them on the resolving slit. The focus lens/neutral trap is used to increase the beam current density at the target. In the target chamber is housed a single gap deceleration lens which retards the ion beam to the required low energy down to 10 eV just prior to the target. The target is at earth potential, mounted on a precision five motion

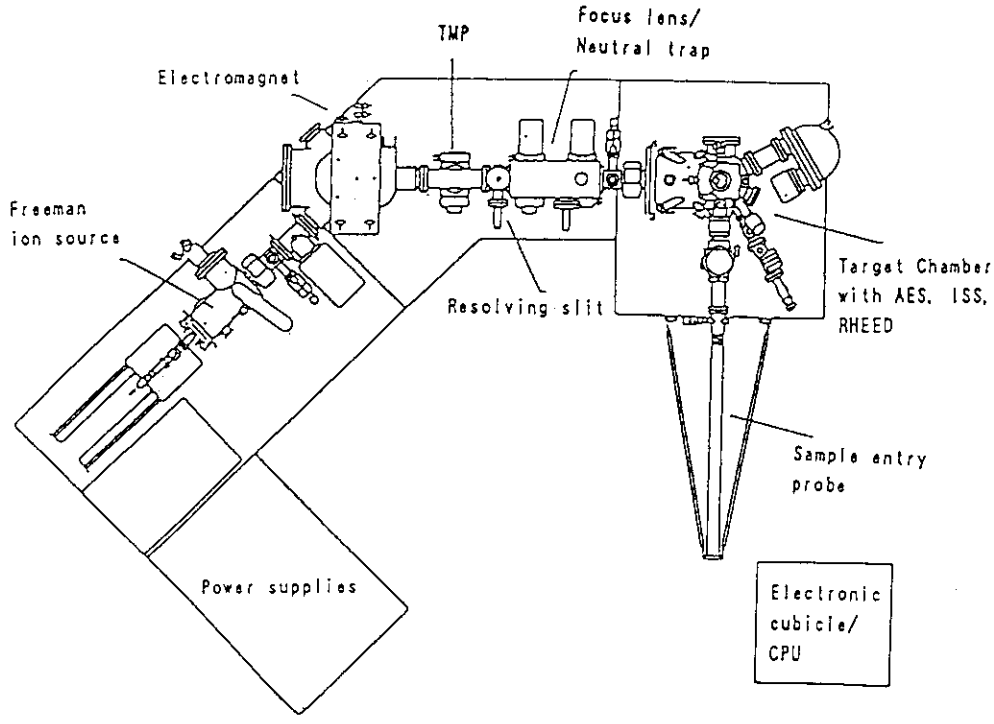

Fig.1 Plan view of the ultra-low energy ion beam deposition system

manipulator. Temperature of the target can be varied either by heating with electron back-bombardment or by cooling with drawing liquid nitrogen through the reservoir placed close to the target.
A small-apperture (1 mm^2) screened Faraday collector is used to obtain the ion beam profiles in horizontal and vertical axes. In addition, the target chamber is equipped with RHEED (Reflection High Energy Electron Diffraction), ISS (Ion Scattering Spectroscopy) and AES (Auger Electron Spectroscopy) for in-situ surface analysis of deposited thin films. The vacuum system includes six differential pumped stages to enable UHV of the order of 10^{-10} Torr to be maintained in the target chamber during IBD.

3. PRELIMINARY EXPERIMENT ON CARBON ION DEPOSITION

The performance of the apparatus was tested with 200-10 eV Ar^+ and C^+ beams. The results showed that the current density measured by the Faraday collector exceeded 1.0 $\mu A/cm^2$ at the ion energy down to 10 eV for both ions without deterioration of the vacuum 10^{-9} Torr in the target chamber. Fig. 2 shows an example of the beam profiles obtained for Ar^+ and C^+ ions.

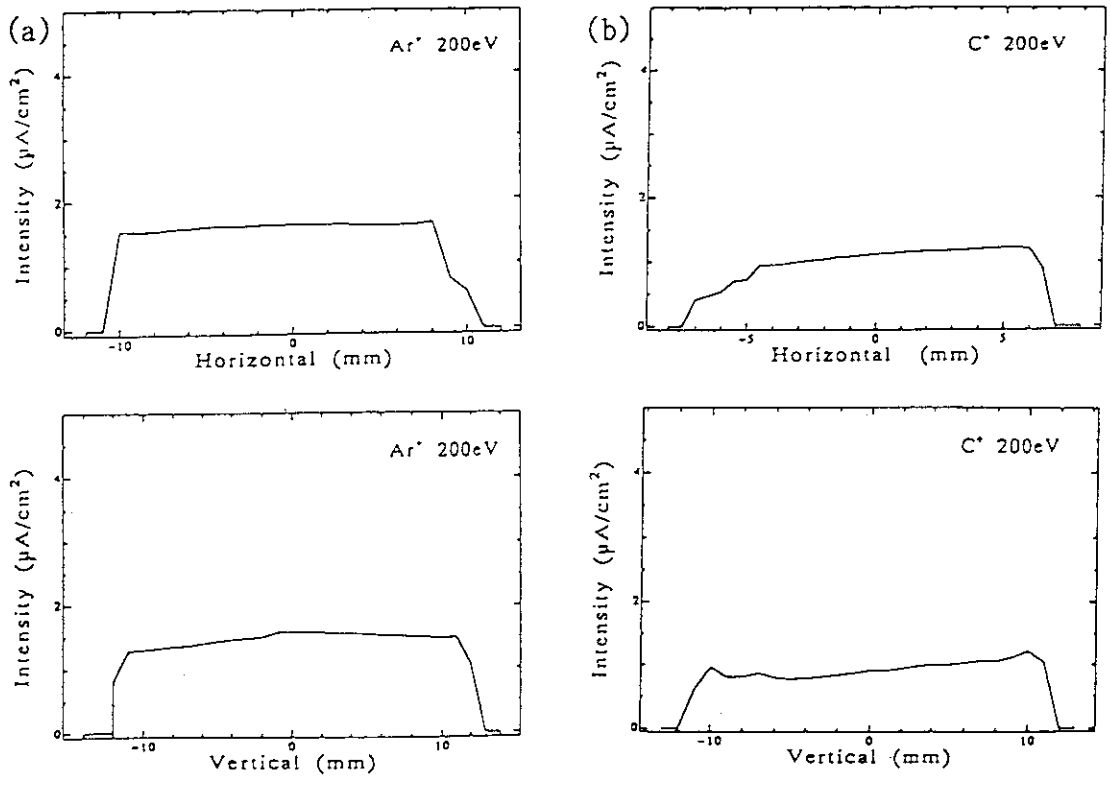

Fig.2 Beam profile for 200 eV (a) Ar^+ and (b) C^+

A preliminary experiment on carbon film growth was carried out using this apparatus. In this experiment, 10 eV C^+ ion beams were deposited on poly-aluminium for 4 hrs. The AES spectra of the deposited carbon film shown in Fig. 3 suggest that the film contains a graphite structure. On the other hand, the Raman spectrum of the film shown in Fig. 4 indicates the film to be diamond-like carbon structure[4]. By taking into account that the diameter of the probing area by AES employed in this study was ca. 100 μm while that by Raman spectroscopy was ca. 2 μm, the results obtained imply that the deposited carbon film contains a small diamond-like carbon in graphite framework.

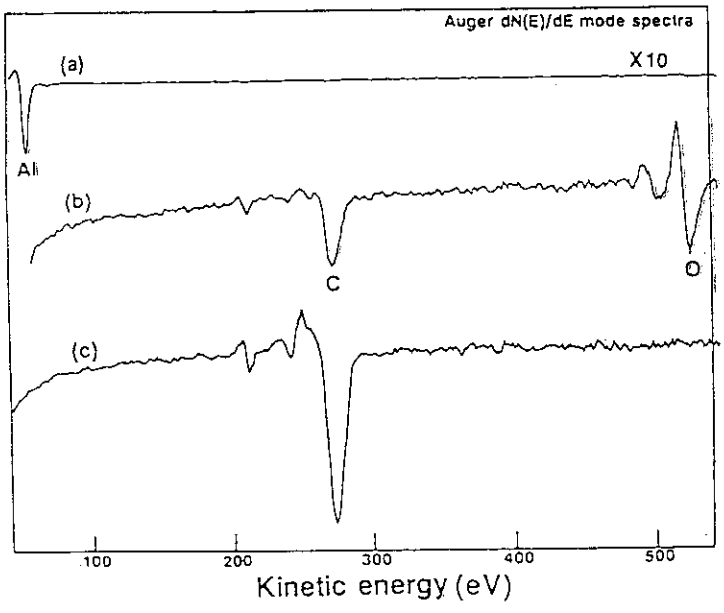

Fig.3 AES spectra of the carbon film deposited on poly-aluminium
(a) Substrate
(b) Film formed after 10 eV C^+ deposition for 1 hr
(c) Film formed after 10 eV C^+ deposition for 4 hrs

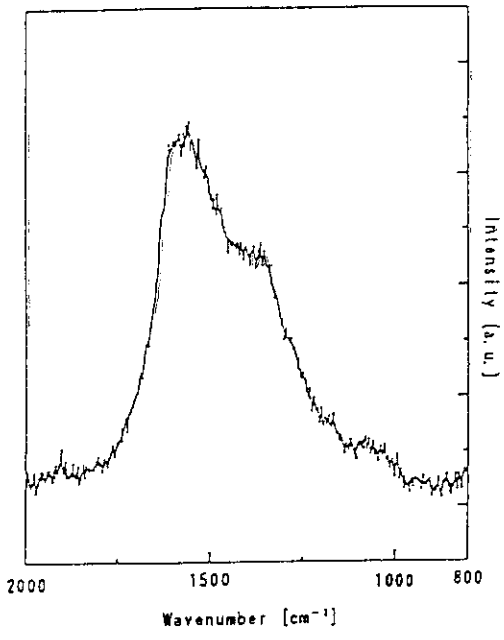

Fig.4 Raman spectrum of the carbon film deposited on poly-aluminium

REFERENCES

1) Y.Lifshitz, S.R.Kasi and J.W.Rabalais, Phys. Rev., B41, 10468(1990).
2) D.G.Armour, A.H.Al-Bayati and J.S.Gordon, Proc. Intern. Conf. on Evolution in Beam Applications, Takasaki (1991), p. 25.
3) K.G.Orrman-Rossiter, R.S.Baht, R.J.Badheka, M.J.Wadsworth and D.G.Armour, Nucl. Instr. Meth., B36, 446(1989).
4) J.N.Kidder,Jr. and W.J.Varhue, J. Vac. Sci. Technol., A10, 1414(1992).

6.3 Time-resolved X-ray Absorption Spectroscopy Apparatus

Atsumi MIYASHITA, Osamu YODA, Kouichi MURAKAMI*,
Takasumi OHYANAGI*, Sadao AOKI** and Naohiro YAMAGUCHI***

JAERI Takasaki, Institute of Materials Science*, Institute of Applied Physics**, Plasma Research Center***, University of Tsukuba

1. Introduction

Soft X-rays emitted from laser produced plasma have many interesting properties when used as a source of time-resolved X-ray absorption spectroscopy. 1) The X-ray intensity per pulse is high enough to perform the single shot measurement[1]. 2) The X-ray pulse width is as short as or shorter than incident laser pulse width, which makes it easy to get short X-ray pulse[2]. 3) The X-ray energy distribution depends on the electronic structure of the target material, which makes it easy to get both line radiation and continuum spectra by choosing an appropriate target. 4) The X-ray energy range is from about 100eV to a few keV, which covers K-absorption edges of low-Z elements such as carbon, nitrogen, oxygen, aluminum and silicon, and L-absorption edges up to medium-Z elements. Therefore, the soft X-rays emitted from laser produced plasma are quite an attractive X-ray source for the dynamic investigation of materials composed of light elements.[3]

2. Constitution of the Apparatus

Figure 1 shows a schematic diagram of our spectrometer. The apparatus is composed mainly of two parts: the laser system and the spectrometer. A 20J Q-switched Nd:YAG/glass laser (Continuum K.K.) is used both to produce soft X-rays and to irradiate samples. The FWHM of the laser pulse is about 12ns. The fundamental laser pulse of 1064nm is frequency-doubled with the use of second harmonics generators (SHGs). The first SHG(SHG_1) generates 7J, 532nm beam, and the partial fundamental wave passes through the SHG_1, which is again frequency-doubled with SHG_2 and 1J 532nm beam is generated and converged on the sample with a lens(L_2). The delay circuit (10~100ns) is installed in the 7J beam path to adjust the timing between sample irradiation and probing. The 7J beam is focused on the cylindrical target, 40mm in diameter and 25mm long, with a condenser lens(L_1). The focus size is about 100μm in diameter. In this case, the laser energy density on the target reaches $7\times10^{12}W/cm^2$, and hence hot and dense laser plasma generates soft X-rays on the target. A 7 channel X-ray diode (XRD: KMS Fusion Inc.) is installed in the target chamber for measurements of the total X-ray yield in wide energy passbands and the X-ray pulse shape. To measure the angular distribution of the X-ray yield, the XRD can be attached to flanges located at every 15° from 30°

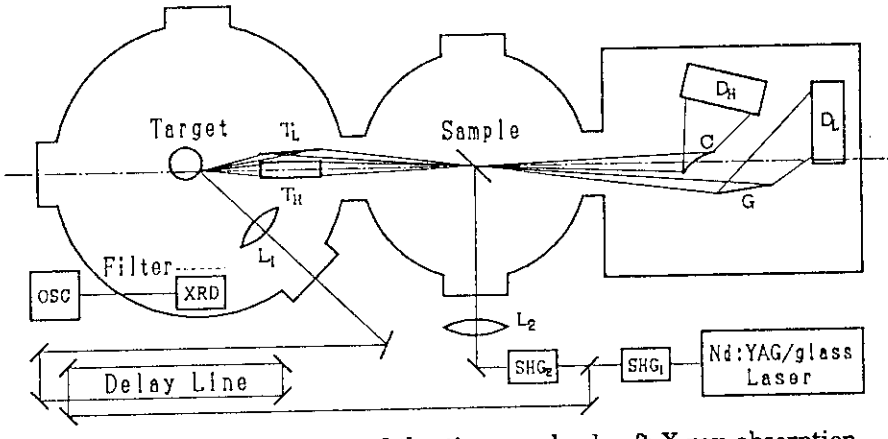

Fig.1 A schematic diagram of the time-resolved soft X-ray absorption spectroscopy apparatus using laser produced plasma X-rays.

to 90° with respect to the target normal. To select an energy range, a filter can be attached on the each channel of XRD.

Our spectrometer was originally designed to observe X-ray absorption fine structure (XAFS) in a rather wide energy range, from 90eV to 3keV. However, it was found difficult to analyze such a wide energy range by a simple polychromator. We have provided two sets of X-ray optical systems[4], one for lower energy region, from 90eV to 1000eV, and the other for higher energy region, from 1keV to 3keV. Both energy regions, toroidal mirrors(T_L,T_H) collect and converge X-rays on the sample, and X-rays are absorbed by the sample, then arrive at the polychromator. In the lower energy region, we use a grazing incident flat field grating(G) as an energy analyzer, and a 1024 channel MCP-PCD(D_L) as an X-ray detector. In the higher energy region, a convex curved KAP crystal(C) and MCP-PCD(D_H) are used.

3. Results and Discussion

3.1. X-ray intensity

The X-ray pulse shape and total X-ray yield were measured by XRD with a 0.5μm thick polycarbonate (PC) filter and a 0.25μm thick nickel foil filter. The former has X-ray sensitivity between 100 and 300eV. Figure 2 shows pulse shapes of the laser and X-rays. The laser pulse was measured with a photo-transistor by detecting laser light transmitted through a 90° reflection mirror. The FWHM of the X-ray pulse is about 12ns which is the same or narrower than that of the laser pulse.

In order to estimate the total X-ray yield, angular distributions of emitted X-rays were measured. In Fig.3, x-axis, the detecting angle from the target normal is scaled in the cosine function. The X-ray yield decreases clearly in a cosine-like law with increasing angle. Based on this, the total X-ray intensity is estimated. Table 1 shows the X-ray

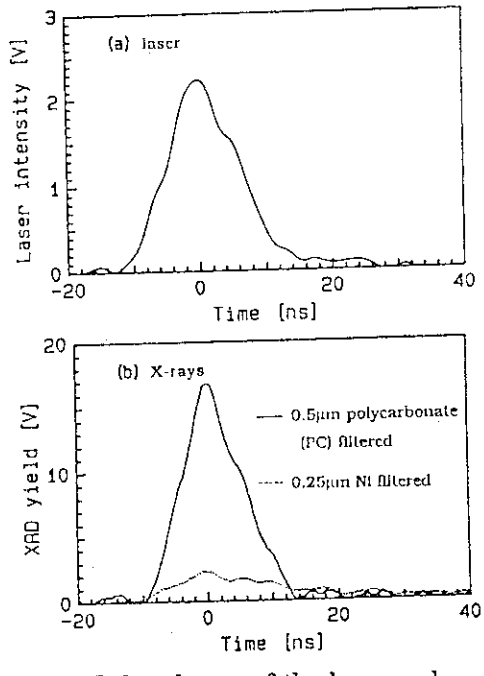

Fig.2 Pulse shapes of the laser and generated X-rays.

Table 1 The X-ray intensity and the conversion efficiency of the laser energy to soft X-rays. (PC filter)

	Total X-ray intensity [photons/pulse]	Conversion efficiency [%]	X-ray intensity on the sample [photons/pulse]
Au	1.0×10^{16}	4.6	1.8×10^{11}
Cu	8.2×10^{15}	3.7	1.5×10^{11}
Mo	7.6×10^{15}	3.4	1.3×10^{11}
Ti	5.3×10^{15}	2.4	9.5×10^{10}

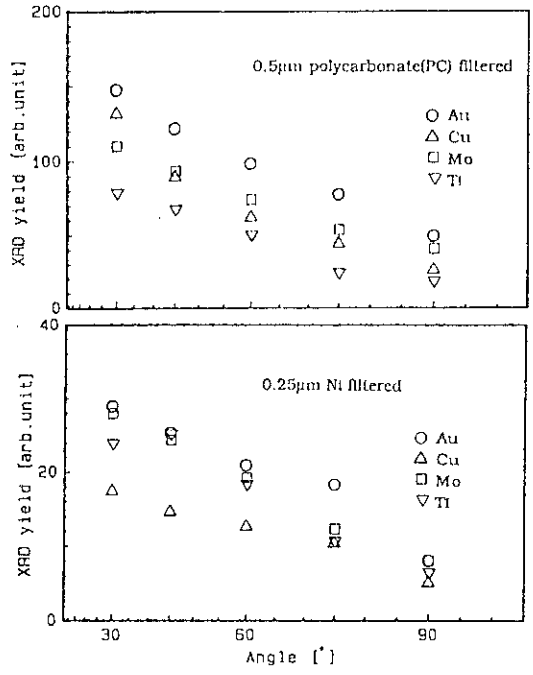

Fig.3 Angular distributions of the emitted X-ray intensity.

intensity and the conversion efficiency of various target materials. Among them, gold emits the most intense X-rays. The total amount of emitted X-ray intensity is reached to 1.0×10^{16} photons/pulse and the conversion efficiency of the laser to X-rays is 4.6%. The number of photons incident on the sample is evaluated to be about 1.8×10^{11}photon/pulse; this is enough to measure absorption spectra by only one single pulse of the laser produced plasma X-rays.

3.2. Source X-ray spectra

Figure 4 shows typical source X-ray spectra in the low energy region. Each spectrum was obtained by a single shot with a laser irradiance of 1×10^{13}W/cm^2. X-ray spectra of various targets differ from each other. In general, X-ray spectra of low-Z materials, like carbon, contain many sharp line radiations from multi-charged ion species, whereas those from high-Z materials, like gold, exhibit rather continuum energy distributions. Thus, high-Z materials are suitable for the soft X-ray source of the absorption spectroscopy.

For the energy calibration and the determination of the energy resolution of the spectrometer, a simulation spectrum was synthesized by convoluted transition line of a given target material in various ionization states by a Gaussian instrumental function with the width

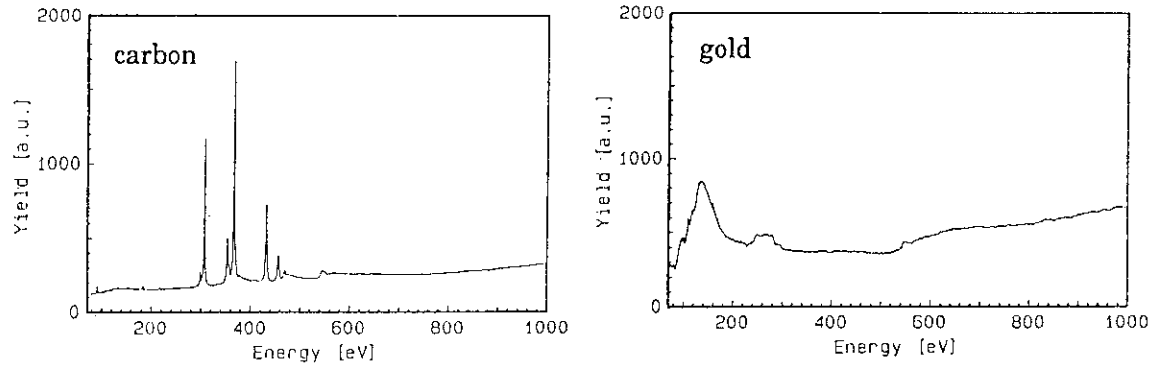

Fig.4 The source X-ray spectra from carbon and gold in the lower energy region.

of the broadening function as a resolution parameter. Simulated spectrum was compared with the observed spectrum, and made best fit by changing the resolution parameter. An example is shown in Fig.5 for aluminum. Thus, energy resolutions of our spectrometer are found to be 0.8eV, 2.0eV, 10eV and 8eV in energy ranges of 100~200eV, 200~500eV, 500~1000eV, 1~3keV, respectively.

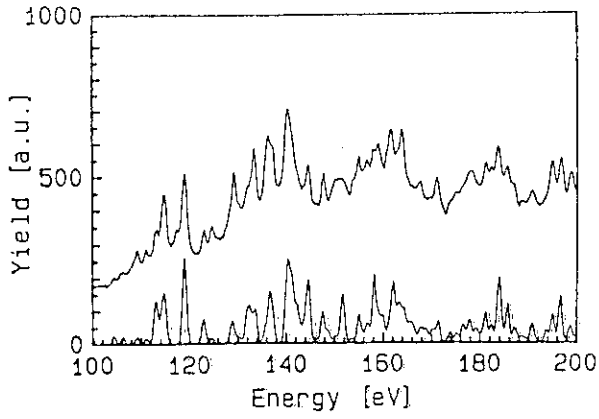

Fig.5 Comparisons of the observed (upper) and simulated (lower) spectra of aluminum. The width of the broadening function is 0.8eV.

3.3. Spatial dependence of ablated carbon

The energy range of our spectrometer covers K-absorption edges of low-Z elements. We observed spatial dependent X-ray absorption spectra of ablated carbon (Fig.6). The energy density of the laser for ablation on the sample is about 10J/cm^2 and the delay time between laser irradiation and X-ray probing is 100ns. The spectra exhibit a main absorption edge and peaks with fine structures. The absorption edge at 296.5eV originates in 1s to vacuum level transition of neutral carbon, and the three peaks, 284eV, 288eV and 293.5eV are radiation from 1s-2p transitions of neutral carbon atom (CI), singly ionized carbon(CII) [5] and doubly ionized carbon(CIII) ions, respectively. The spectra from neutral carbon (CI and K-absorption edge) decrease with increase distance from the surface. On the other hand, the radiation peaks from highly ionized species(CIII) are observed far from the surface. Therefore, it is suggested that the speed of highly ionized species is faster than neutral atoms.

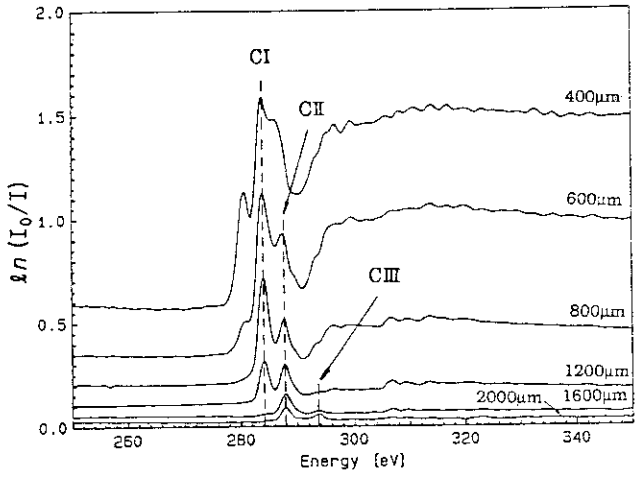

Fig.6 The X-ray absorption spectra of ablated carbon for various distance from the surface.

References

1) H.C.Gerritsen, H. van Brug, F.Bijkerk and M.J. van der Wiel, J.Appl.Phys. 59(1986)2337.

2) D.J.Nagel, Adv.X-ray Anal. 1(1975)1.

3) K.Murakami, H.C.Gerritsen, H. van Brug, F.Bijkerk, F.W.Saris and M.J. van der Wiel, Phys.Rev.Lett. 56(1986)655.

4) A.Miyashita and O.Yoda, JAERI-M Report 88-212(1988).

5) E.Jannitti, P.Nicolosi and G.Tondello, Physica Scripta 41(1990)458.

6.4 Ion Beam Analysis System for Materials Development in JAERI/Takasaki

Hiroshi NARAMOTO, Hidefumi TAKESHITA, Yasushi AOKI
and Shunya YAMAMOTO

Department of Materials Development, JAERI/Takasaki

1. Ion Beam Analysis in "Advanced Radiation Applications(ART)" Project

In the ART project, the creation of new materials with novel functions is one of the important research themes. In this research, various kinds of ions different in their energies and species can be used to process and to analyse the surface layer of potential materials. The use of energetic beam gives us an advantage of non-equalibrium processing in the synthesis of new phases. Thus, the processing temperature is a key factor to control the microstructure obtained. It has been planned that the beam lines from 400 kVimplantor, 3 MV tandem and 3 MV single-ended electrostatic accelerators are connected with each other to use the ion beams in a multiple mode. Our group has designed "Dual Beam Analysis System" which can be used both for the implantation and for the analysis of implants and induced defects, simultaneously or successively even at low temperatures.

In advance of installing the dual beam system, the preparatory experiments have been initiated since last year using "Baby BAS" which is a simple ion beam analysis system connected with a 3 MV tandem accelerator. Here in this report, some typical studies are introduced which have been made in "Baby BAS" with the illustration of that system. Are also described briefly the main features of Dual Beam Analysis Systems, and the research programs.

2. "Baby BAS" System for Ion Beam Analysis

This system has been designed to perform the ion beam analysis on surface layer of crystalline materials in combination with channeling. A beam collimating system is arranged so as to confine the beam divergence less than 0.01 degrees for the channeling experiment. This system is also used for ion implantation over larger area by changing an aperture in the collimating system, followed by the channeling analysis to detect the microstructural change induced by ion implantation. An arrangement of this sys-

tem is illustrated in Fig. 1, which makes it possible to perform a variety of spectroscopic experiments by setting detectors, from particle detectors for RBS, ERDA and NRA to photon detectors for PIXE analysis and resonance-type NRA. For the low temperature ion processing, a liquid helium cooling unit can be connected, but the carefull attention is needed to avoid the surface contamination by cooling the thermal shroud around a specimen stage to liquid nitrogen temperature at least. For channeling experiment, a three axis goniometer system(Panmure Instrument Ltd) is set up in the analysis chamber, and is controlled automatically using a computer.

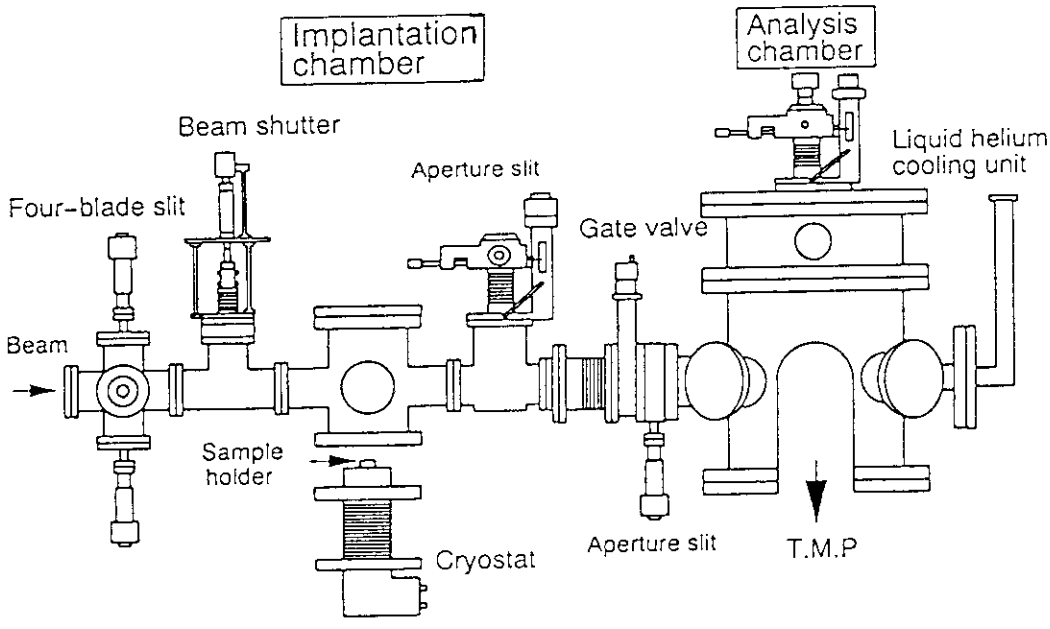

Fig. 1 Schematic Illustration of Ion Beam Analysis System(Baby BAS)

An implantation chamber placed up beam-stream is designed for the measurement of electrical properties at low temperatures using a cryogenic system, which is most suitable for the study of the radiation effects on superconducting oxides.

3. Collaborative Studies Performed in This Period(Oct.'91-Mar.'92)

In this period, the preparative experiments have been made in confirmation of the good beam quality(divergence, uniformity, etc.) and the proper operation in beam collimator and goniometer systems. Table 1 summarizes the experiments made in Baby BAS. In a tandem accelerator, the beam current

of helium ions is supposed to be small because of the difficulty in preparing negative ions, but our beam collimator assured the rather reasonable intensity of incident beam without increasing its divergence, which was examined in the channeling experiment under axial and planar conditions. Most of the studies here were successful, and one of the most promising experiments is the analysis on the charge state of moving fast ions in solids by detecting the secondary electrons emerged under channeling conditions in Si crystal. This study leads to determining the density of valence electrons especially in the covalent crystal lattice.

Table 1: Experiments Performed Using "Baby BAS"(Oct.'91-Mar.'92)

Incident Ions	Research Items	Samples	Collaboration
2MeV ^{4}He	RBS/Chanelling	(110)Si	within JAERI
3.05MeV ^{4}He	Resonant Elastic Scattering/Chanelling	Oxydized Layer of Si	JAERI/Shin-Etsu
9MeV ^{58}Ni	Surface Modification	Oxide Crystals	within JAERI
0.9MeV p	Nuclear Reaction	^{15}N in Cubic SiC	JAERI/ETL
1.25MeV d	Nuclear Reaction /Chanelling	(100)Diamond	within JAERI
3 and 7.2MeV ^{197}Au	Ion Implantation for Surface Modification	High Pure Fe	within JAERI
9MeV ^{58}Ni	Charge State Analysis	Ceramic Crystals	within JAERI
20MeV ^{58}Ni 21MeV ^{197}Au	Radiation Effects (TEM Analysis)	FCC Metals(Cu,Ni)	Nagoya Univ. /JAERI
2.5MeV p 3.75MeV p 18MeV ^{16}O	Secondary Electron Spectroscopy under Chanelling Condition	(110)Si	Tsukuba Univ. /JAERI
15MeV ^{32}S	Ion Mixing(electronic)	^{57}Fe/Teflon	Nisshin Steel/JAERI
3MeV ^{197}Au 3, 6MeV ^{58}Ni	Ion Implantation for Surface Modification	SiO_2	within JAERI
2MeV ^{4}He	RBS	Cu/Si(IBAD etc)	Kyoto Univ./JAERI
0.8MeV ^{12}C	Self Ion Irradiation	(100)Diamond	within JAERI

The ion implantations were made by employing various kinds of ions. For the light ion implantation, it is easier to prepare the uniform beams by detecting lights emitted through electronic excitation associated with

energetic ion irradiation. For the heavy ion implantation, on the contrary, it is very difficult to obtain uniform beam because of its remarkable deterioration of light-emission even after the short exposure to the ions. The interface mixing with high energy ions was successful in an ^{57}Fe/Teflon system, and the examination of microstructure using Mössbauer spectrometer gives the evidence for the formation of new chemical products by electronic excitation.

4. Dual Beam Analysis System and Future Research Programs

In Dual Beam Analysis System, two kinds of ion beam analysis chambers are prepared. One is connected with 3 MV tandem accelerator and 400 kV implantor, and the other with 3 MV single-ended electrostatic accelerator and 400 kV implantor. A 6 axis goniometer system which can be cooled down to 15 K can be accomodated in the above system, and both of the implantation and the ion beam analysis can be performed without warming up the implanted specimens. These chambers are evacuated up to 10^{-10} Torr, which makes it possible to prepare the clean surface of single crystals in combination with a laser illuminating system.

In a chamber connected with a tandem accelerator, the Rutherford back scattering spectrometry and the nuclear reaction analysis using heavy ions will be employed to separate the implanted heavy element, and to detect light elements like hydrogens in a high Z matrix. The detection of anisotropic vibration of hydrogens just at the surface will become possible in this system by making the low temperature channeling experiment combined with the nuclear reasonance such as $H(^{15}N, \alpha, \gamma)^{12}C$ reactions. A specially designed x-ray spectrometer with the high resolution is equiped with the above chamber, and the chemical shift in emitted x-ray spectrum from compounds will be detected under the energetic heavy ion irradiation.

In a chamber connected with 3 MV single-ended electrostatic accelerator, the detailed analysis on the interactions between implants and induced defects can be accomplished as a function of implantation temperature. A study of the ion-mixing is also suitable in this system, and the athermal component can be separated from the thermally activated one through the ion mixing experiment at low temperatures. In a special case, the verification of discrete energy loss process will become possible by using resonance nuclear reactions induced by the ions with the extremely high stability from 3 MV single-ended electrostatic accelerator.

6.5 Study of Charge States of Fast Ions in Solids by Means of Ion-induced Secondary Electron Spectroscopy

Hiroshi KUDO, Hidefumi TAKESHITA*, Yasushi AOKI*,
Shunya YAMAMOTO*, Hiroshi NARAMOTO* and Susumu KUWABARA**

Institute of Applied Physics, University of Tsukuba,
*Department of Materials Development, JAERI, ** Isobe R&D Center, SEH Co.

I. INTRODUCTION

When fast ions are incident on a solid target, high-energy secondary electrons are produced as a result of close encounter collisions between the ions and the target electrons. Since such close-encounter processes can be reasonably treated by the binary encounter approximation[1], a simple Z_1^2-scaling character is observed for the energy spectra of high-energy secondary electrons.[2,3]

Because of this simplicity in the production mechanism of the electrons, the binary-encounter electron spectroscopy (BEES) is useful for observing ion-beam shadowing phenomena which occur when the ion beam is incident in an axial or a planar direction of a crystal. In the present case, we treat the effective "shadow" inherent to the motion of MeV or higher-energy ions, which developes along atomic rows or planes as a result of small-angle multiple scatterings of ions by the aligned atoms.

Under channeling incidence conditions, the decrease in the electron yield can be interpreted in terms of the localized production of the primarily scattered electrons near the surface, resulting from the shadowing effect.[2-5] In this case, the electron yield simply comes from the unshadowed part of the two-dimensional electron distribution projected on the plane perpendicular to the beam direction. This effect is applicable to the determination of the charge states of heavy ions in solids. Actually, a small change in the shadowing effect due to the ion's screened nuclear charge can be well detected by analyzing the ion-induced secondary electrons under channeling incidence conditions.

In BEES analysis, it is necessary to compare the spectrum yields for various equal-velocity ions. However, it is generally difficult to obtain equal-velocity ions (for example, H to S ions) from one Tandem accelarator. For this reason, we have started the Takasaki-Tsukuba collaboration in

which the two Tandem Accelerators at Takasaki and Tsukuba are used complementally to cover a wide energy range (terminal voltage 0.4-12 MeV).

II. METHOD OF ANALYSIS

When fast ions are incident on a solid target, an equilibrium charge-state distribution is quickly established as a result of the balance between electron capture and loss processes. Actually, the inner-shells of MeV/u heavy ions in solids should be partly filled with captured electrons. In this case, the ion-beam shadowing effect can be reduced by the presence of the projectile's bound electrons which screen the ion's nuclear charge. The reduced shadowing effect can be observed sensitively by BEES under channeling conditions, and therefore, the charge states of fast heavy ions can be determined[3]. The important aspect of this method is that the charge states *in* the solid can be measured, which is essentially different from the case of the transmission experiments in which the charge states of all *emergent* ions is measured.

The charge states in solids are determined from a simple comparison of the shadowing effect for the heavy ions and for the equal-velocity light ions that are fully stripped in the crystal. If the heavy ions such as Si or S ions are fully stripped in the crystal, the shadowing effect for those ions must be the same as that for the equal-velocity deuterons or alpha particles because for both cases the shadow cone radius, R, given by

$$R=(8Z_1 Z_2 e^2 d/M_1 v^2)^{1/2}, \qquad (1)$$

are the same, where Z_1 and Z_2 are the atomic numbers of the ion and target atom, respectively, M_1 is ion's mass, v is the ion velocity, e is the electronic charge, and d is the interatomic distance along the atomic row. Therefore, in this case the ratio of the binary-encounter electron yield for the channeling and random (nonchanneling) cases should be the same. However, if the inner shells of the heavy ions are filled with captured electrons, Z_1 in Eq.(1) must be replaced by the effective nuclear charge Z_{eff} ($\leq Z_1$), taking into account the screening effect. This indicates that the yield ratio for the screened heavy ions is larger than for the fully stripped light ions.

In the above analysis, unshadowed electrons in the target crystals must be taken into account since those electrons contribute to the spectrum yield under channeling incidence conditions. The average number of unshadowed electrons per target atom can be estimated from the secondary electron yield for H^+ beams, using the Z_1/M_1 dependence of R in Eq.(1).[6] Therefore, the measurements for H^+ is particularly important in the determination of the charge states of ions in solids.

III. SPECTROMETER SETUP

Because of the smooth shape of the energy spectrum of inary-encounter electrons, the electron spectrometer for BEES does not require high energy resolution (typically $\Delta E/E=10\%$ in our measurements). However, in the spectrometer the stray electrons which increase the spectrum background must be suppressed before reaching the electron multiplier. Furthermore, the electrons emitted at 180° with respect to the beam direction must be analyzed since in this case the electron yield is independent of the angle between the beam direction and the surface normal of the sample.

To satisfy these conditions, we have refined a 45° parallel-plate electrostatic spectrometer of the mirror-symmetry type having a variable energy acceptance by adjusting the window slit from outside the target chamber. This mechanism is useful for the channeling experiments since the choice of a wide energy acceptance enables quick alignment of the crystal direction under high count rate of the electron yield. Because of its compact design, the spectrometer can be quickly set up inside the "Baby BAS" to carry out BEES measurements.

IV. RESULTS AND DISCUSSION

Figure 1 shows energy spectra of secondary electrons induced by 2.5-MeV H^+ under <100> and random conditions. We see in Fig.1 that the ratio of channeling to random yield are constant in a wide energy range below the binary-peak energy, E_B. From the yield ratio for H^+ and for heavier ions, we can determine the average number of unshadowed electrons per target atom, N, in the axial direction of the target crystal.

The principle of the method is similar to that used in the determina-

tion of Z_{eff},[3] but in this case the yield ratios for protons and for equal-velocity deuterons (or alpha particles) are compared. Since below E_B the ratio of channeling to random yield should have a contribution of $\mu(=N/Z_2)$, the ratios for protons and for the others, $W(p)$ and $W(d,\alpha)$, respectively, may be related by

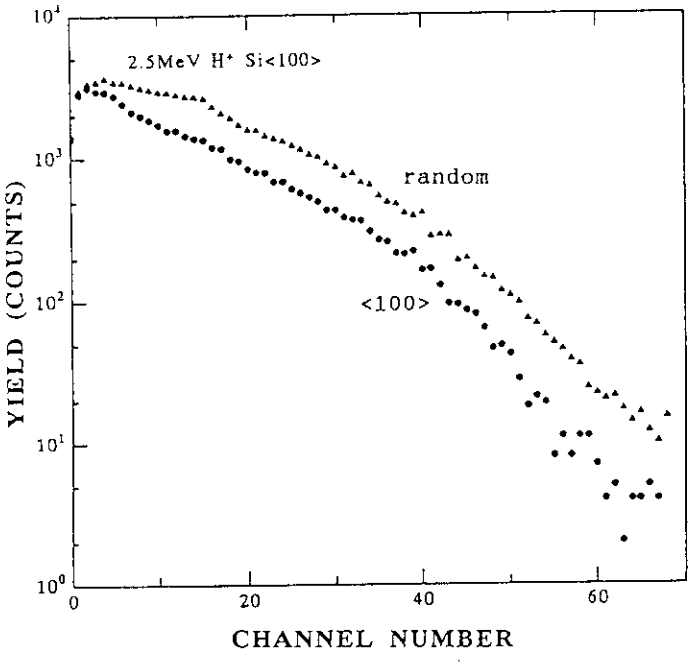

Fig.1 Energy spectra of secondary electrons induced by 2.5-MeV protons under <100> and random incidence conditions, measured at 180° with respect to the beam direction. The width of 1 channel corresponds to 0.096 keV.

$$[W(d,\alpha)-\mu]/[W(p)-\mu] = \sqrt{2}, \quad (2)$$

where $\sqrt{2}$ comes from the R-dependence of the effective thickness ($\propto R$) over which the inner shells are fully shadowed [2,3]. By using Eq.(2), we have obtained that $N \simeq 3.5$-5 for 2.5 and 3.5 MeV/u ions incident in the Si<110> and Si<100> directions.

The corresponding measurements for 2.5- to 3.5-MeV/u heavy ions (He to Cl ions with various initial charge states) is now under way at the University of Tsukuba. The charge states of those ions in Si will be determined for the first time, by using the values of N thus determined.

REFERENCES

1) C.L.Cocke, in *Methods of Experimental Physics*, edited by L.Marton and C. Marton (Academic, NewYork, 1980), Vol.17, Chap. 7.
2) H. Kudo et al, Phys. Rev. B43(1991)12729.
3) H. Kudo et al, Phys. Rev. B43(1991)12736.
4) H. Kudo et al, Phys. Rev. B38(1988)44.
5) H. Kudo et al, J. J. Appl. Phys., 31(1992)L1284.
6) H. Kudo et al, Phys. Rev .B(1992) in press.

6.6 Channeling Examination of Crytalline Materials Using Ion Beam Analysis in JAERI／Takasaki

Shunya YAMAMOTO, Hidefumi TAKESHITA, Yasushi AOKI,
Hiroshi NARAMOTO and Susumu KUWABARA*

Department of Material Development, JAERI/Takasaki
*Isobe R&D Center,Shin-etsu Handotai Co, Ltd.

I. Introduction

Ion beam analysis has been demonstrated to be a powerful technique for sensitive measurements of material composition and structure, for characterization of atomic scale of surface, interface and thin layers.

The RBS(Rutherford backscattering spectrometry)/channeling method can be used for the lattice site location of foreign atoms, the determination of thermal vibration amplitudes, the depth profiling and annealing of damage instance (for due to ion implantation), and the location of misfit dislocation network and superlattices in strained layers. These information is necessary to design the new functional materials.

Recently, We have installed an ion beam analysis system named "Baby BAS" connected with a 3MeV tandem accelerator at JAERI Takasaki. As the first step, the channeling measurements were carried out for Si, diamond, and Nb single crystals. The measured critical half-angles and minimum yields for axial channeling are compared with those derived from the continuum theory, to examine the proper operation of collimating and automated goniometer systems.

II. Experimental

Experiments were carried out using a 3MV tandem accelerator,NEC 9SDH-2, in TIARA. The analysing beam of ^{4}He ions with energy of 2.0-3.05MeV was incident on a sample. The size of the beam was about 1mm in diameter and the beam current was about 3nA typically. Backscattered particles were energy-analysed by a standard surface-barrier detector(EG&G ORTEC) placed 120mm from the target at 165 degrees to the incident beam. In order to suppress secondary electrons, the negative potential of 350V was applied to a copper ring in front of the target.

Samples used were (110)Si, (100)diamond and (100)Nb single crystals. The samples were mounted on a 3-axis goniometer(Panmure Instruments Ltd.) which was modified for the remote operation by a personal computer.

III. Results and Discussion

Fig.1 shows a typical example of angular yield profiles for 3.05MeV ^{4}He ions incident along the <110> axis of Si. The critical half-angle($\phi_{1/2}$) and the minimum yield(χ_{min}) were found to be 0.45° and 1.9%, respectively. These values are good agreement with the calculated ones. The experimental values of $\phi_{1/2}$ were determined from the angular profiles by the half-width at a level halfway between the minimum yield and the random level. The critical half-angles were calculated according to the formulas given in the ion beam handbook[1]. The measured and calculated values in other samples are presented in Table 1,where $\phi_{1/2}$ are in good agreement with the calculated ones, but the minimum yields in Nb and diamond were larger than the calculated ones. The reason for this discrepancy may be attributed to the presence of lattice imperfection in the near surface region. Fig.2 shows a typical spectrum obtained from (100) diamond sample for ions incident along a random direction and along the <100> axis. Because the integrated yield of $^{12}C(d,p)^{13}$ nuclear reactions is larger than the backscattered yield, the alignment of ion beam with a specific crystallographic direction can be made easily in carbon-rich materials. In the nuclear reaction spectra, double peaks are formed reflecting the energy dependence of the reaction cross-sections. In the aligned spectrum,the peak intensity at higher energy region is relatively decreased.

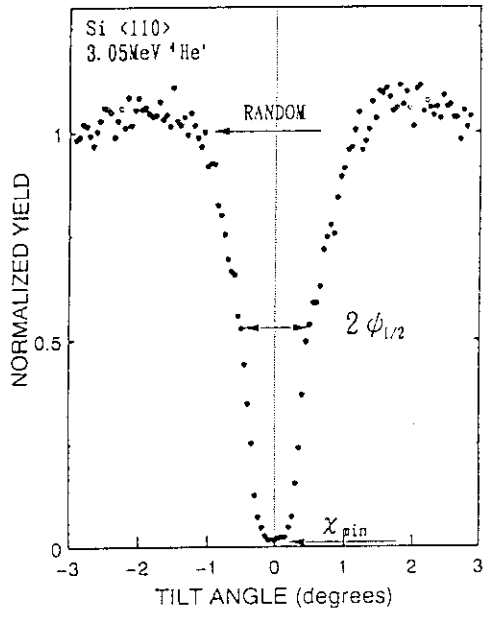

Fig. 1. Angular profiles for 3.05MeV ^{4}He ions incident along <110> axis of Si.

Table 1 Comparison of calculated and measured values of $\phi_{1/2}$ and χ_{min} for axial channeling.

Target	Energy (MeV)	$\phi_{1/2}$ (deg.) Calculated	$\phi_{1/2}$ (deg.) Measured	χ_{min} (%) Calculated	χ_{min} (%) Measured
Nb <100>	2.0	0.81	0.71	2.2	6.7
Si <110>	2.0	0.51	0.53	2.1	2.1
	3.05	0.41	0.45	2.1	1.9
C <100>	2.0	0.53	0.59	0.13	3.8

It is reasonably interpreted that the channeled ions lose their energy through electronic excitation without inducing nuclear reactions in the higher energy region.

Fig.3 shows angular profiles for diamond crystal, (a) from RBS-channeling, and (b) from NRA-channeling. The RBS measurements were performed using a beam of 2.0MeV ^{4}He ions, while for the NRA measurements a 1.25 MeV D^{+} beam was used to induce $^{12}C(d,p)^{13}C$ nuclear reactions. The values of $\phi_{1/2}$ for RBS and NRA are 0.59° and 0.36°, respectively.

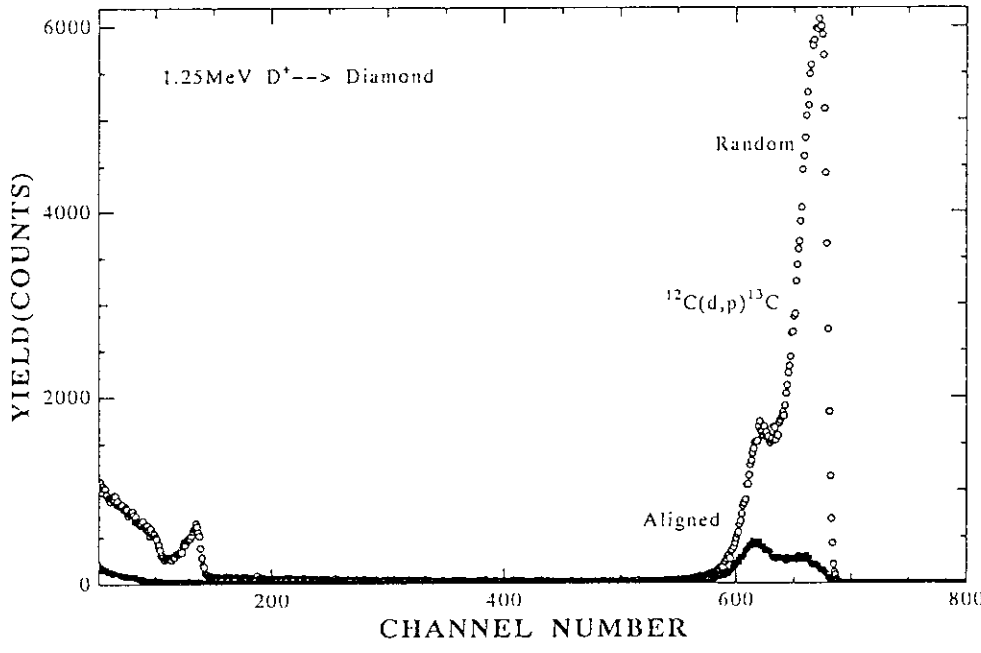

Fig. 2. NRA spectrum from (100) diamond crystal for D^{+} beam incident along a random direction and along the <100> axis.

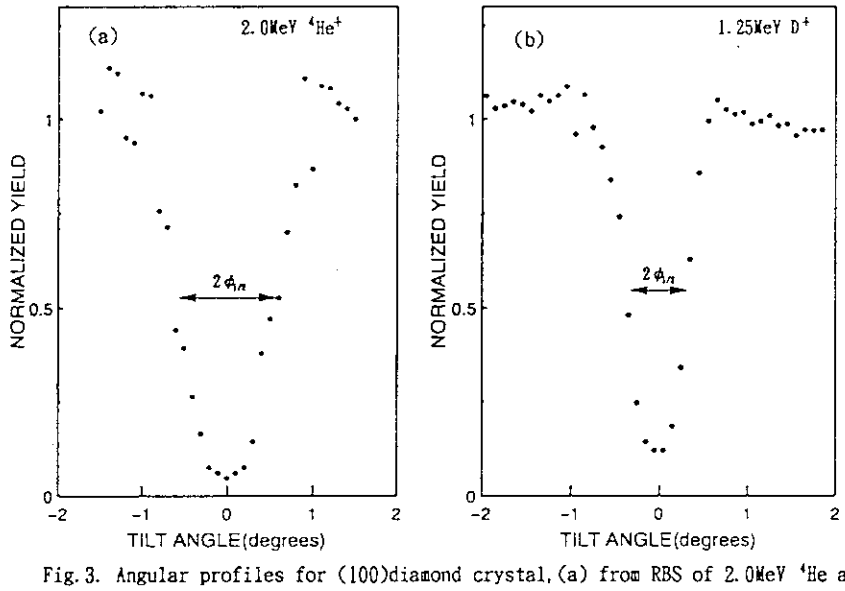

Fig. 3. Angular profiles for (100)diamond crystal, (a) from RBS of 2.0MeV ^{4}He and (b) from NRA of 1.25MeV D.

The critical half-angle for NRA measurement is much larger than the calculated one, which is due to the difficulty of depth-sensitive data-collection in the NRA measurement.

IV. Conclusive Remarks

Through these channeling studies, it is confirmed that an integrated goniometer system at JAERI/Takasaki shows the proper operation. This computer-based operation makes it possible to take a true random spectrum without rotating a specimen around the surface-normal.

The beam intensity of He ions from a tandem accelerator is low, and it is obliged to use the focusing system which causes slight change in incident beam direction. This, however, does not give the critical influence on the channeling features under the condition that the beam trajectory should not be changed during the experiment.

REFERENCES

1) J.W.Mayer and E.Rimini, eds. Ion beam handbook for material analysis (Academic Press, New York, 1977)

6.7 Some Applications of Nuclear Reaction to Light Element Analysis

Hidefumi TAKESHITA, Yasushi AOKI, Shunya YAMAMOTO,
Hiroshi NARAMOTO and Susumu KUWABARA *

Department of Materials Development, JAERI,
*Isobe R&D Ceneter, Shin-Etu Handohtai Co.

Studies about inorganic functional materials such as thin films and superlattices currently attract considerable attention because of their unusual and unique physical properties. In these studies it is indispensable to characterize surface or near-surface region of nano- to micro-meter in depth. Materials analysis based on high energy ion beam probe is a powerful tool for this purpose.

In this light, Rutherford backscattering spectrometry(RBS), one of the most commom ion beam analysis(IBA) techniques, has been widely used. RBS allows one to obtain composition depth profiles nondestructively. Especially, the advantage of RBS has been presented in the analysis of heavy elements in the matrix of light element. In the reverse case, RBS is not practicable becasue of insufficient sensitivity.

Nuclear reaction analysis(NRA) is a reasonable solution to improve the sensitivity to light elements including hydrogen without compromise of the capability of depth profile analysis, which is the case for particle-induced x-ray emission(PIXE) analysis.

In this report, we demonstrate the usefulness of NRA technique by presenting some applications to the analysis of typical light elements such as oxygen, carbon and nitrogen.

Ion Beam Analysis System

An apparatus for the ion beam analysis has been installed at Takasaki Ion Accelerators facility, TIARA. For the moment, one beam line is available from 3MV tandem accelerator, NEC 9SDH-2. This accelerator has two negative ion sources(SNICS for solid source material and Alphatross for noble gas). Our IBA system, named Baby BAS, has been placed at the beam line of 30 ° from the switching magnet. The details of Baby BAS has been described elsewhere[1] .

Oxygen Analysis

In most of reactive metals, it is almost impossible to avoide surface contamination from oxygen. The well-known resonant elastic collision between ^{16}O and ^{4}He is a suitable reaction to evaluate the degree of oxygen surface contamination. A distinct strong resonance peak of scattering cross section is known at energy around 3.0MeV for ^{4}He incident on ^{16}O [2] . Fig.1 shows RBS spectra for a silicon single crystal under random and aligned conditions, respectively. The silicon sample was chemically etched to remove any surface oxide just before sample setting. Thus, any surface oxygen was not observable even for the alighned spectrum. Effectiveness of the above resonance reaction for the detection of oxygen is shown in Fig.2, where surface oxygen was clearly revealed in the aligned spectrum. Oxygen atoms in Fig.2 corresponds to a SiO_2 layer with several angstroms thickness.

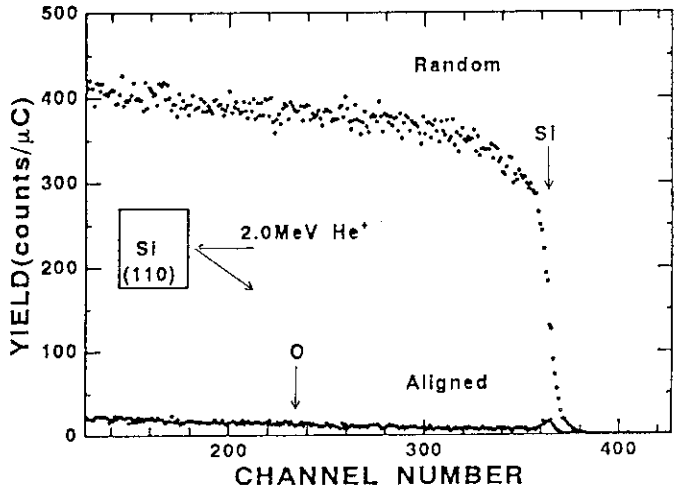

Fig.1 Energy spectra for 2.0MeV He incident on Si(100) under random and aligned conditions

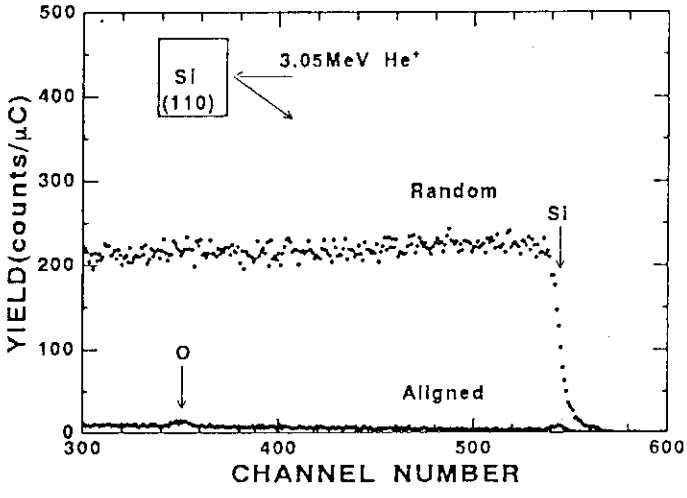

Fig.2 Energy spectra for 3.05MeV He incident on Si(100) under random and aligned conditions

Carbon Analysis

Like oxygen, carbon is also one of the common elements as contaminant in most materials processing. As mentioned above, normal RBS does not give high sensitivity enough to make a quantitative analysis about a trace amount of carbon. Here again, the sensitivity of carbon can be remarkably increased by using NRA. An example is shown in Fig.3, where the reaction of $^{12}C(d,p)^{13}C$ was applied to the detection of carbon. The sample was diamond and the probe beam was 1.25MeV deuteron. A large peak at higher energy region was due to proton emitted through this reaction. The cross section of this reaction becomes three times as large as that of the corresponding elastic scattering. A yield curve at lower energy region corresponds to the elastic collision. In the spectrum shown in Fig.3, a shoulder in the proton yield and a dip in the deuteron yield reflect the energy dependence of the respective cross sections.

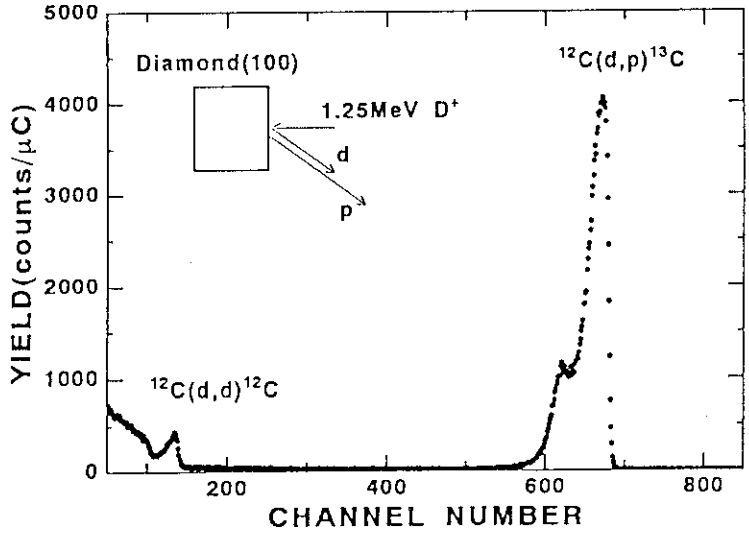

Fig.3 Energy spectrum for 1.25MeV D^+ incident on a diamond(100) surface under a random condition

Nitrogen Analysis

This application illustrates the special usage of NRA that isotopes can be distinguished. A sample was an epitaxial film of silicon carbide, 3C-SiC, grown by the CVD technique on a substrate of silicon single crystal. An impurity of nitrogen has been considered to be an origin of residual carriers in semiconductor SiC. Therefore, understanding of a mechanism for the nitrogen contamination is a key issue to improve a quality of SiC film. ^{15}N-enriched nitrogen, in which ^{15}N was contained as much as 99%, was intentionally added up to 70ppm into a raw gas mixture used for SiC synthesis in order to check how a product SiC was contaminated from nitrogen impurity in a gas atmosphere.

Analysis of ^{15}N was made by using the nuclear reaction of $^{15}N(p, \alpha_0)^{12}C$. A particle detected was alpha emitted with an energy of about 4MeV. In the measurement, a detector was covered with an Al-coated Kapton film of 12.5 μm thickness to eliminate excess incidence of scattered protons. For the calibration of ^{15}N content, a Si_3N_4 film of 6000 Å thickness, which was made of natural nitrogen, was used as a reference. The resulting spectrum for the reference Si_3N_4 is shown in Fig.4. It is seen from this figure that the alpha peak is well separated from a spectrum due to the scattered proton. The result of the ^{15}N-doped SiC film is shown in Fig.5. Because of large thickness of the SiC film, the alpha peak has a tail to a lower energy side. Based on these results, a concentration, N/Si, of nitrogen impurity in the SiC sample was roughly estimated to be 20ppm.

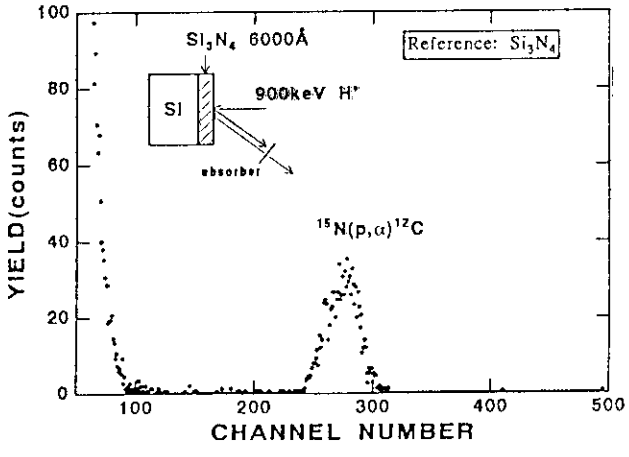

Fig.4 Energy spectrum for 900keV H incident on Si_3N_4 film

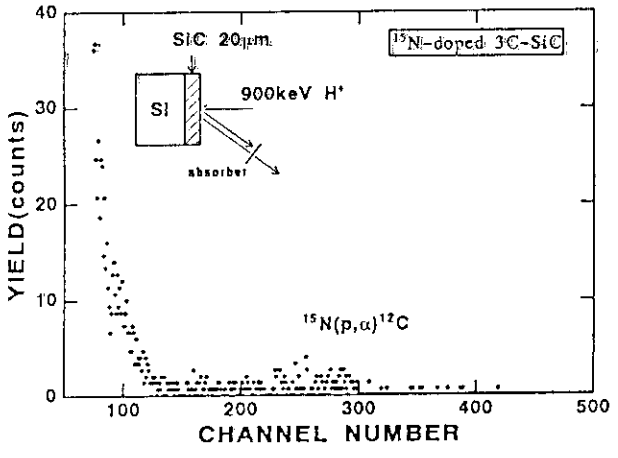

Fig.5 Energy spectrum for 900keV H incident on ^{15}N-doped SiC

The examples demonstrated above are only a part of the capability of NRA technique for light elements analysis. NRA technique is expected to be quite effective for the research of inorganic functional materials, where the behavior of light elements such as oxygen, carbon and nitrogen is one of the main concerns.

REFERENCES

1) H.Takeshita, Y.Aoki, S.Yamamoto and H.Naramoto, Proc. of the International Conference on Evolution in Beam Applications, Takasaki, Japan, Nov.5-8 (1991) p.129.

2) L.C.Feldman and J.W.Mayer, Fundamentals of Surface and Thin Film Analysis(Elsevier Science Publishing, New York, 1986) p.28.

6.8 Charge States of Cr Ions Implanted in Ceramics

Tsuneji FUTAGAMI, Yasushi AOKI, Osamu YODA, and Siro NAGAI

Takasaki Radiation Chemistry Research Establishment, JAERI, Watanuki-machi 1233, Takasaki, Gunma 370-12, Japan

I. INTRODUCTION

Understanding of physical and chemical effects on ceramics induced by ion implantation is fundamental to the study of its surface modification by ion beams. The change in the crystal structure of ceramics by ion implantation has been investigated by means of RBS-Channeling measurements and TEM observation: The surface of α-Al_2O_3 becomes amorphous by high dose implantation (10^{17}/cm^2) of Fe [1], while spinel or magnetite is formed by annealing of MgO implanted with Fe[2]. On the other hand, the charge states of implanted atoms can bring information on their chemical environments, which is complementary to information on structural change. The charge states of implanted atoms have extensively been investigated on Fe ions implanted in α-Al_2O_3 and MgO by means of conversion electron Mössbauer spectroscopy[1),3),4)], but only a few studies have been performed on other ions. In this study, the charge states of Cr implanted into single crystals of α-Al_2O_3 and MgO were investigated by X-ray photoelectron spectroscopy (XPS). The analysis is based on the chemical shift depending on the charge state of atoms: The chemical shift of Cr $2p_{3/2}$ is 2.2 eV between Cr metal and Cr^{3+} (Cr_2O_3). Information on lattice defects created by ion implantation can possibly elucidate the charge states of implanted atoms, because a portion of implanted atoms may be associated with some lattice defects[3]. Optical absorption measurements on Cr implanted crystals were performed in order to study the structure of created lattice defects.

II. EXPERIMENTAL PROCEDURES

Single crystals of (100) MgO and (0001) α-Al_2O_3 with an optical grade polish were used. Implantation was performed at room temperature by an ion implanter (Danphysik). Energy was 200 keV and fluences were 4×10^{16}Cr/cm^2,

$8x10^{16}Cr/cm^2$, and $4x10^{17}Cr/cm^2$ for MgO, and $8x10^{16}Cr/cm^2$, and $4x10^{17}Cr/cm^2$ for $\alpha-Al_2O_3$. Current densities ranged from 0.6 μA/cm^2 to 2.4 μA/cm^2. During the implantations, the sample surfaces were inclined by about 5° in order to avoid channeling effects. Ion beams were scanned for uniform implantation over the sample surfaces (10mmx5mm). XPS measurements were performed by an ESCA LAB-MKII (VG Scientific Co.). Depth profiles were measured, by successive etching of implanted samples by a 4 keV Ar ion gun under the pressure of $1x10^{-7}$Torr. Optical absorption measurements on Cr implanted $\alpha-Al_2O_3$ and MgO crystals were also performed using a Shimadzu UV-365. For this measurement, samples were implanted to $5x10^{15}/cm^2$, $1x10^{16}/cm^2$, $2x10^{16}/cm^2$, $4x10^{16}/cm^2$, $8x10^{16}/cm^2$, and $2x10^{17}/cm^2$. Unimplanted samples were used as references in measurements.

III. RESULTS AND DISCUSSION

(1) XPS measurements

The XPS spectra of Cr $2p_{3/2}$ and Cr $2p_{1/2}$ for $\alpha-Al_2O_3$ implanted to $4x10^{17}Cr/cm^2$ are shown in Fig. 1a. They were recorded at the depth of the maximum Cr concentration. The peak center of Cr $2p_{3/2}$ agrees with the binding energy (574.3eV) for Cr $2p_{3/2}$ in the metallic state (Cr^0). The XPS spectra for $\alpha-Al_2O_3$ implanted to $8x10^{16}Cr/cm^2$ shown in Fig. 1b show the presence of another peak overlapping on the high energy side of the peak for Cr^0. The difference in energy between the two peaks is 2.4 eV which agrees well with the difference in binding energy between Cr^0 and Cr^{3+}. Therefore, the high energy peak is attributed to Cr^{3+}. On the basis of these assignments, the concentrations of Cr^0 and Cr^{3+} relative to the concentration of Al atoms in the target at various depths were obtained from the XPS spectra recorded during etching of the sample by Ar ions. The results indicate that the concentration of Cr^0 increases nearly linearly with the concentration ratio of implanted Cr atoms to Al atoms (Cr/Al), while the Cr^{3+} concentration saturates with $Cr^{3+}/Al=0.04$ for Cr/Al greater than 0.05. The XPS spectra of Al 2p, on the other hand, showed that a portion of Al was reduced from Al^{3+} to Al^0. The depth analysis showed that the concentration of Al^0 increased with the Cr^{3+} concentration, which implies that charge exchange occurred between implanted Cr atoms and Al ions in $\alpha-Al_2O_3$. From the RBS-Channeling measurements of Cr implanted $\alpha-Al_2O_3$, it was reported that a portion of implanted Cr atoms substitutes the lattice sites of Al atoms in $\alpha-Al_2O_3$[5]. Therefore, the Cr^{3+} detected by XPS can be attributed to the Cr atoms substituting the Al sites.

The XPS spectra of Cr $2p_{3/2}$ and Cr $2p_{1/2}$ in MgO implanted with the dose of $4x10^{17}Cr/cm^2$ are shown in Fig. 2. The Cr $2p_{3/2}$ spectrum consists of two peaks due to Cr^0 and Cr^{3+}. For the MgO samples implanted to doses of $4x10^{16}/cm^2$ and $8x10^{16}/cm^2$, single peak due to Cr^{3+} was observed. The depth analysis for MgO implanted to $4x10^{17}Cr/cm^2$ indicates that the Cr^0 concentration increases with Cr/Mg ratio while the Cr^{3+} concentration tends to saturate at high Cr/Mg ratios. The saturation occurred with Cr^{3+} /Mg=0.25 for Cr/Mg greater than 0.3. Both ratios are about six times as large as the corresponding ratios found for $\alpha-Al_2O_3$, indicating that much more Cr^{3+} are stabilized in MgO than in $\alpha-Al_2O_3$.

(2) Optical absorption measurements

In Cr implanted MgO crystals, absorption peaks due to F or F^+ centers, F_2 centers, and V^- centers were observed at 250 nm, 365 nm, and 565 nm, respectively. In addition to these peaks, an unidentified absorption peak at 330 nm was also observed when irradiation dose exceeds $1x10^{16}/cm^2$.

Some of the detected lattice defects may be associated with implanted atoms[3]. The V centers produced in Cr implanted MgO, for instance, may possibly be associated with Cr^{3+}, but no evidence for this has yet been obtained.

IV. SUMMARY

The Cr atoms implanted into $\alpha-Al_2O_3$ and MgO are stabilized as Cr^0 and Cr^{3+}. The concentration of Cr^0 increases with the increase of the concentration of implanted Cr atoms while the concentration of Cr^{3+} saturates when the concentration ratio of implanted Cr atoms to metal atoms of the target exceeds 0.05 for $\alpha-Al_2O_3$ and 0.30 for MgO.

REFERENCES

1)C.J.McHargue, P.S.Sklad, and C.W.White, Nucl. Instr. Meth. B46 (1990) 79.

2)A.Perez, M.Treilleux, L.Fritsch, and G.Marest, Nucl. Instr. Meth. 182/183 (1981) 747.

3)A.Perez, G.Marest, B.D.Sawicka, J.A.Sawicki, and T.Tyliszczak, Phys. Rev. B 28 (1983) 1227.

4)C.J.McHargue, G.C.Farlow, P.S.Sklad, C.W.White, A.Perez, N.Kornilios, and G. Marest, Nucl. Instr. Meth. B19/20 (1987) 813.

5)H.Naramoto, C.W.White, J.M.Williams, C.J.McHargue, O.W.Holland, M.M.Abraham, and B.R.Appleton, J. Appl. Phys. 54 (1984) 683.

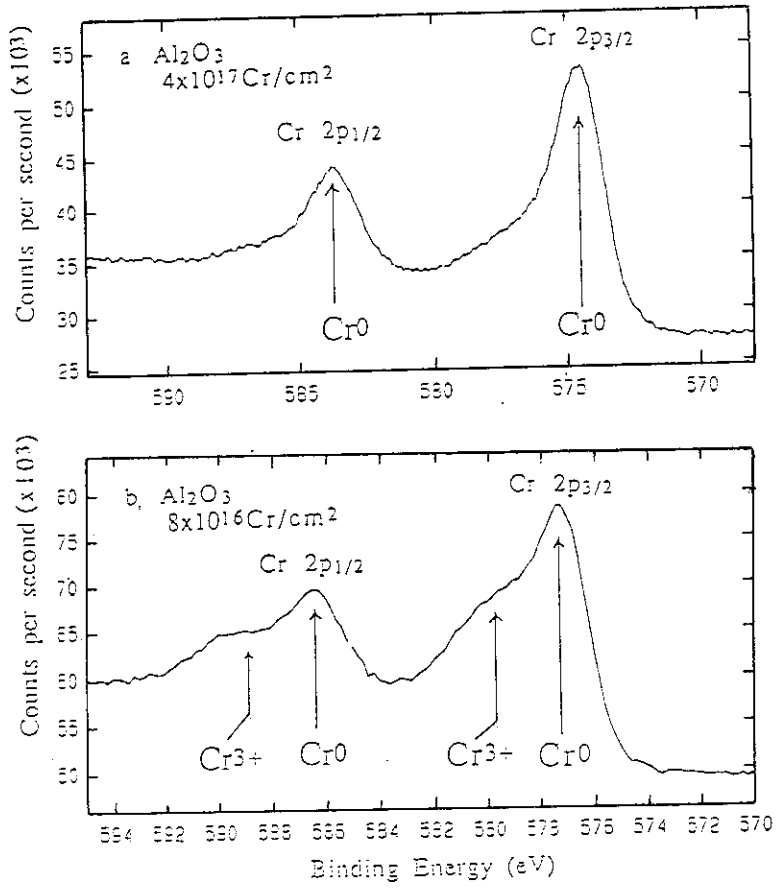

Fig. 1 Cr $2p_{3/2}$ and Cr $2p_{1/2}$ spectra from the implanted α-Al_2O_3 crystals. The peaks in b shift to higher energy due to charging up of the sample surface during XPS measurement.

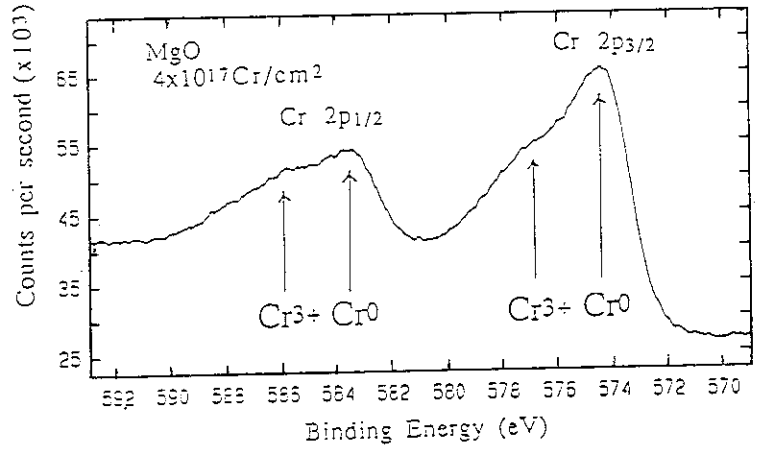

Fig. 2 Cr $2p_{3/2}$ and Cr $2p_{1/2}$ spectra from the implanted MgO crystal.

7. BIOLOGY, MEDICINE AND RADIATION CHEMISTRY

7.1 Ion Beam Irrasdiation Apparatus for Biological Samples

Masahiro KIKUCHI, Atsushi TANAKA, Yasuhiko KOBAYASHI,
Ranko NOZAWA and Hiroshi WATANABE

Department of Radiation Research for Environment and Resources, JAERI

I. INTRODUCTION

The irradiation condition for biological samples should be selected according to their composition, size and so on. Bacterial spore, plant seed and freeze-dried cell treated under special condition are so tolerant to dryness that they can be irradiated *in vacuo* by ion beams. For the irradiation of most biological samples in a living state, however, it is essential to irradiate samples in air. In this paper the outline of apparatuses which were made up for ion irradiation of various biological samples in air are described.

II. MATERIALS AND METHODS

(1) Irradiation Apparatuses

JAERI prepared two apparatuses for biological samples. One is Irradiation Apparatus for Cell (IAC) which has been connected to a horizontal beam line of 3MV tandem accelerator. The other is Irradiation Apparatus for Seed (IAS) which has been connected to a vertical beam line of AVF cyclotron.

(2) RCD Dosimetry

A radiochromic dosimeter (RCD) produced by Far West Technology, FWT60-20 (15x15cm sheet), was used. The thickness is 50.8μm. Measurement of absorbance of RCD was performed either by a spectrophotometer (Beckman DU-65) for spot measurement and by a scanning spectromicrophotometer (NLM-301) developed by JAERI for the two dimensional measurement.

(3) Irradiation of RCD at IAC

RCD (1x1cm) attached on a petri dish of a hexagonal column was irradiated by 6MeV helium ion beam (78enA at the Faraday cup of tandem accelerator) scanned with 3.2cm width (2kVp-p). The hexagonal column was passed 20 times with 120cm/min across beam window and then the absorbance was measured.

III. RESULTS AND DISCUSSION

(1) Outline of IAC and IAS

Figure 1 shows an outline of IAC. It is an apparatus to irradiate relatively small samples up to 30μm. Choosing appropriate ion species and energy, only the surface of biological samples can be irradiated by this apparatus. Ion beams can be taken out through a kapton film of 8.5μm thickness from vacuum chamber. A differential vacuum system was installed for keeping high vacuum at the upstream beam line. A guard system composed of a fast acting valve and three gate valves is provided as a countermeasure for the break of vacuum caused by the destruction of the kapton film. Biological samples are irradiated on the hexagonal column which can carry 12 pieces of disposable petri dishes. The samples are irradiated uniformly by moving the column at a constant speed and by scanning ion beams.

Figure 2 shows an outline of IAS. It is an apparatus to irradiate samples with high energy ions from the AVF cyclotron. This apparatus is available for irradiating such large samples in the range of 100μm to several mm as seeds, seedlings, parts of mature plants, fertilized eggs, tissues, culture with medium and cells in buffer. For plant bleeding which requires a treatment of large quantities of seeds, this apparatus is connected to vertical beam line that ion beam is scanned over 5cm, and has a conveyor system to treat samples successively.

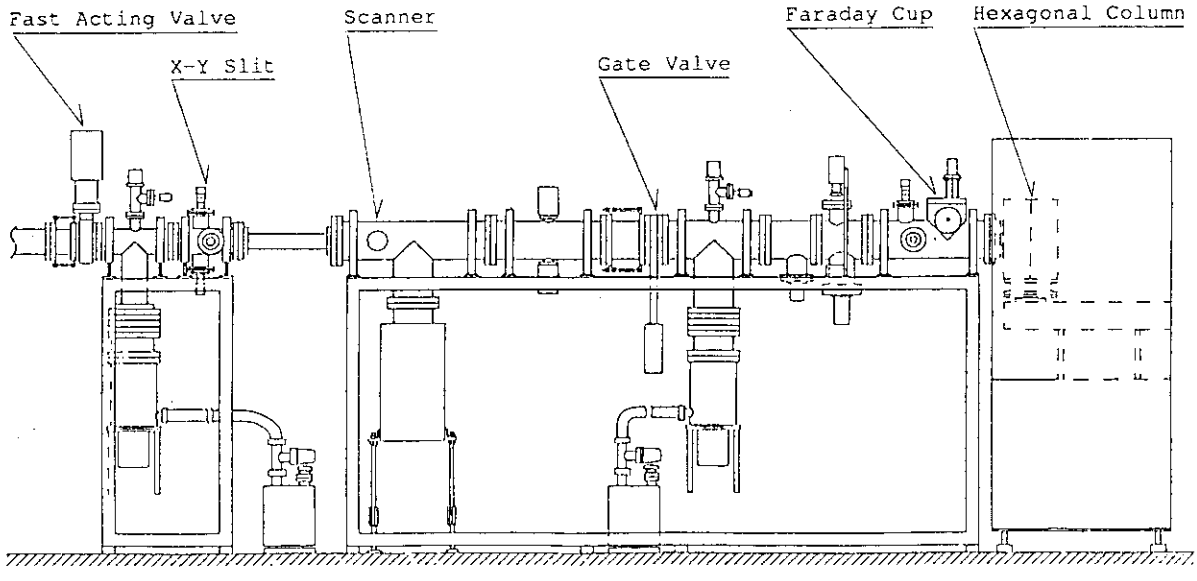

Figure 1. Irradiation Apparatus for Cell

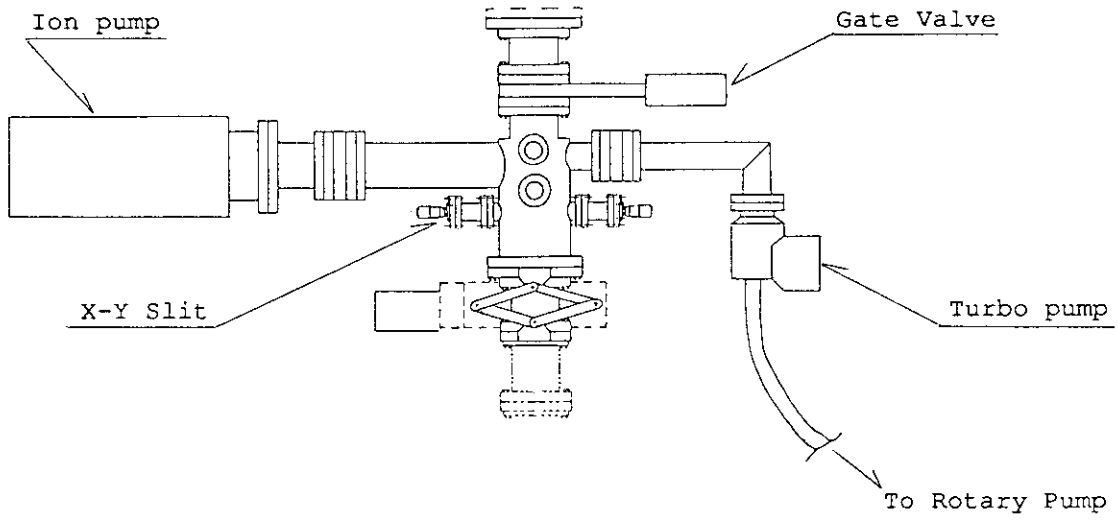

(a) Beam Line

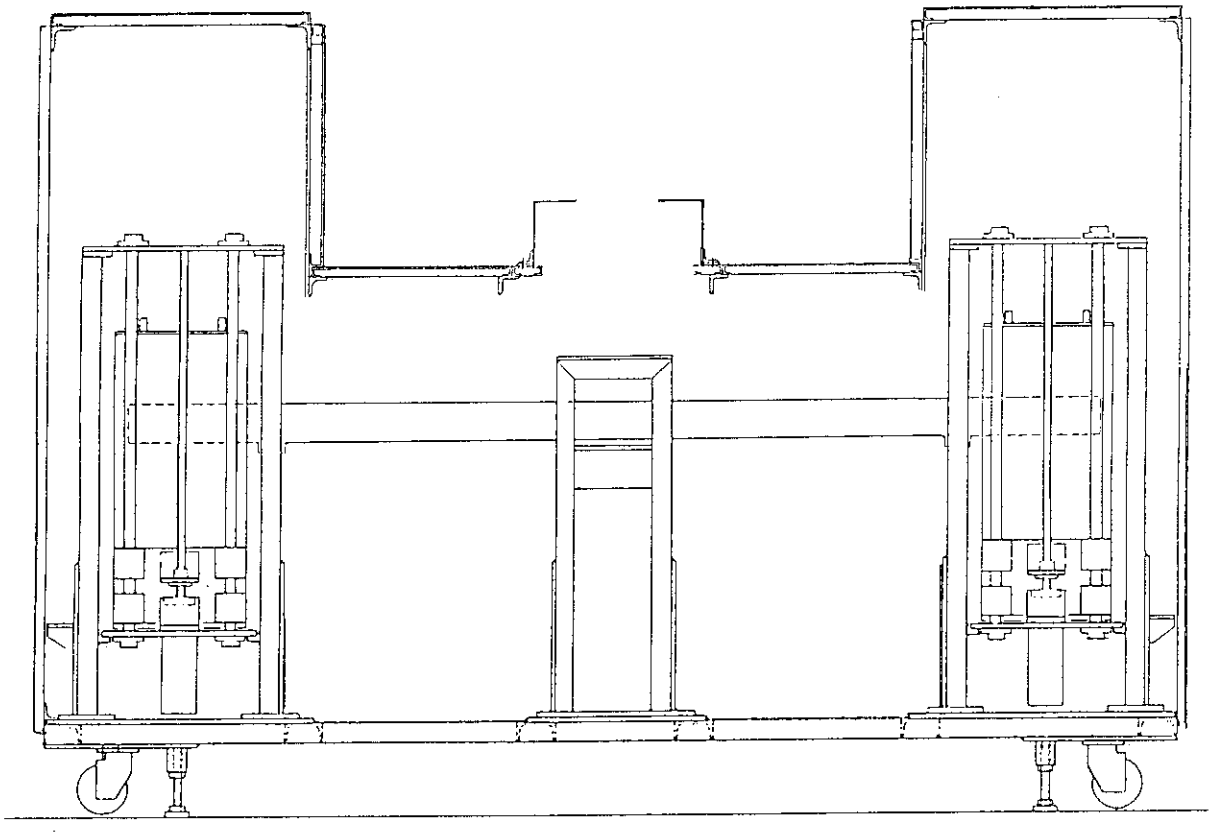

(b) Conveyor System

Figure 2. Irradiation Apparatus for Seed

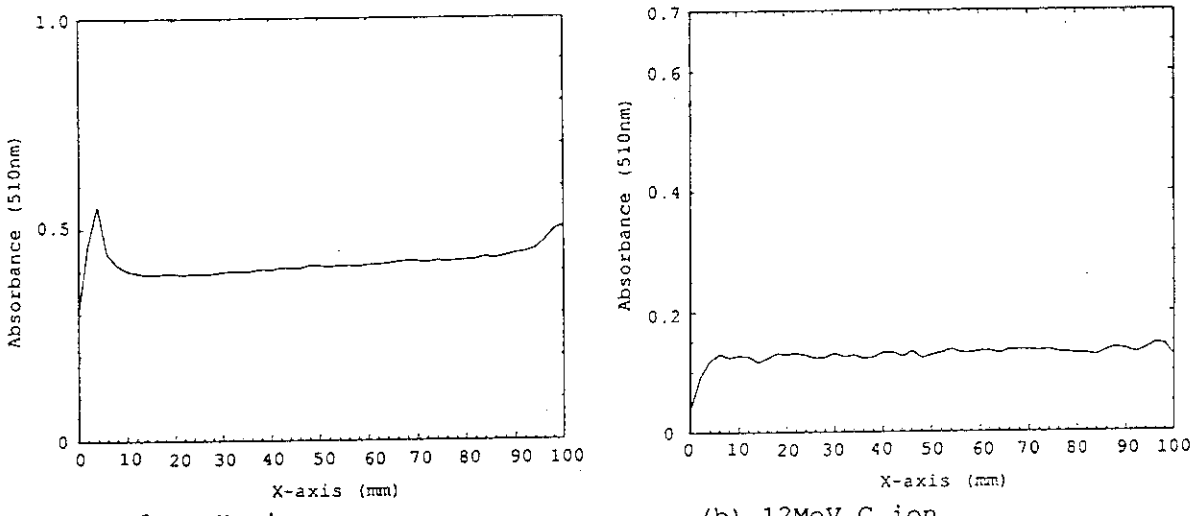

(a) 6MeV He ion (b) 12MeV C ion

Figure 3. Dose Distribution

(2)Dose Uniformity

Figures 3 shows dose distribution of 6MeV Helium ion and 12MeV Carbon ion in IAC. Both beams were scanned to 10cm. The dose uniformity at both edges of scanning was low, but comparatively high in the range of 10-90mm at X-axis. This range appears to be available to irradiate biological samples.

(3)Range of Ion Beam

Figure 4 shows a comparison of a range between calculated value and experimental value. The ranges of ion beam were calculated with the ELOSS code which was developed in JAERI for calculation of the lost energy of ion beam along trucks. The residual energy of ions which means the energy coming out to air through the kapton film was also calculated with ELOSS code. The range of 6MeV Helium ion was consistent with the calculated range with 4% error.

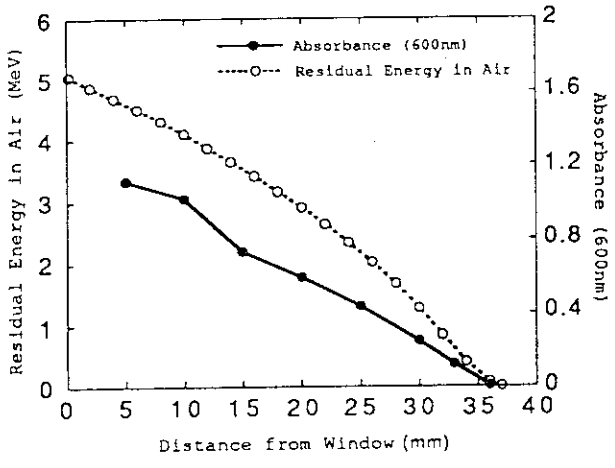

Figure 4. The Range of 6MeV He Ion

7.2 Experimental Apparatus for Basic Radiation Chemistry with Heavy Ions

Hideki NAMBA, Yasushi AOKI, Mitsumasa TAGUCHI
and Katsutoshi FURUKAWA*

Department of Radiation Research for Environment and Resources,
JAERI, *Department of Chemistry, JAERI

I. INTRODUCTION

It is well known that the radiation effect (e.g., lethal effect in biology) of high energy ion or neutron beam is different from that of γ-ray or electron beam. The biological or chemical effects induced by radiation are occurred through the energy deposition or energy transfer (Physical Process), formation of unstable components and the reaction of them with matters (Chemical Process), and finally they appear as "radiation effects". We have been doing fundamental research works on peculiar radiation effects by high energy ion beams. For that purpose, we have installed new experimental apparatus for basic radiation chemistry with heavy ions (EA-BRACHI) at HX1 port of AVF cyclotron in TIARA.

II. EA-BRACHI

Fig.1 shows a schematic diagram of EA-BRACHI, which is connected to a vertical beam port of AVF cyclotron. It has 7 meters length and was installed in Second Heavy Ion Irradiation Room. It is consist of three irradiation chambers. All most all the functions of EA-BRACHI are possible to operate from a neighboring operation room named Heavy Ion Preparation Room as well as from Second Heavy Ion Irradiation Room.

(1) First Chamber

Heavy ion beams from the cyclotron are introduced to the first chamber of the EA-BRACHI through a bending magnet of HX1 port. Irradiated position and shape of the beam are monitored by a MgO beam monitor. A fast acting valve (NEC VS2F) to protect the beam line is put up adding to usual gate valve. A tantalum collimator with 5mmϕ aperture is set on a remote-controlled XY-stage (Ozak XYG) with an accuracy of 5μm. The intensity of the ion beams are measured by a Faraday cup. Beam pick up system with thin carbon foil and MCP (micro channel plate) is installed to detect pulsed ion beam. The chamber is evacuated by a magnet-floating type turbo-molecular pump (Osaka Vacuum TG360M) and a rotary pump. The pressure in the chamber is measured or monitored by

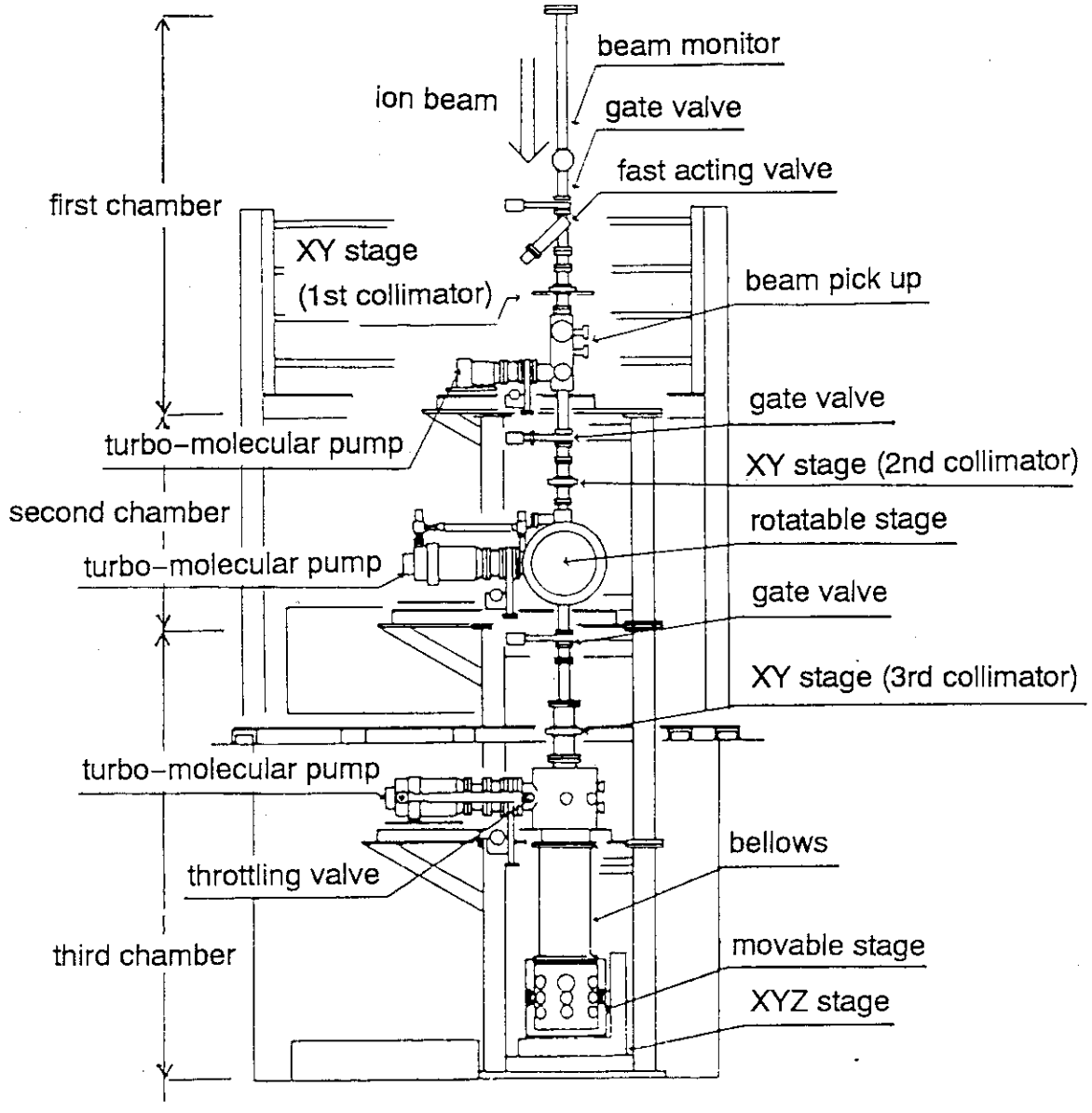

Fig.1 Schimatic diagram of EA-BRACHI

three vacuum gages, one of which is used as a sensor for the fast acting valve.

(2) Second Chamber

The ion beams through the first chamber are introduced to the second chamber passing through second gate valve. A tantalum collimator with 0.5mmϕ aperture is set on a remote-controlled valve that is possible to put in or out with vacuum-tight condition in order to accomplish two different experiments. The valve with the collimator is fixed on the XY-stage that is the same as in the first chamber. The intensity of the ion beams through the collimator are measured by a Faraday cup. An 300mmϕ rotatable stage is installed in

the chamber for solid sample irradiation . The stage has twenty irradiation ports for 10mmϕ samples, three beam monitors and a Faraday cup. The chamber is evacuated by a turbo-molecular pump (Osaka Vacuum TG600M) and a rotary pump. The vacuum condition is monitored by a Q-mass detector (ANELVA QIG-066), an ionization gage and a thermo-couple gage.

Quartz windows are set on the side of the chamber to detect the light from the sample for the experiment of ion beam pulse radiolysis.

(3) Third Chamber

The ion beams through the second chamber and the third gate valve are hit to another tantalum collimator with 0.05mmϕ aperture, which is set on the XY-stage that is the same as in the first and the second chamber. A copper made irradiation stage, which is possible to control the temperature between +100 °C ~ -196 °C, and two small ionization chambers are set in the lower part of the chamber that is connected to the upper part with huge bellows seals (320mmϕ and 700mmϕ L). This lower part, whose weight is about 500kg, is set on a XYZ stage to move all the directions with an accuracy of 5μm.

The third chamber is evacuated by a turbo-molecular pump (Osaka Vacuum TG1000M) and a rotary pump those are connected to the upper part of the chamber. The vacuum condition is monitored by an ionization gage and a thermocouple gage. The pressure control system combined with pressure sensors (MKS Baratron 122A and 127A), pressure controller (MKS113A), mass flow controller (MKS 147B) and throttling valve (MKS 253A-2-4CF-2) is also set in the chamber for the experiment of microdosimetry.

(4) Differential pumping system

EA-BRACHI has three stage differential pumping system that consists of three sets of pumps, three collimators and pressure control system. It is possible to control the pressure in the third chamber between 760 to 10^{-3} Torr with this system during ion beam irradiation. Gaseous sample is introduced to the third chamber with controlling its flow rate by mass flow controller . The pressure of the gas is measured and controlled by pumping through throttling valve connected to the turbo-molecular pump in the third chamber. Fig. 2 shows the relationship between the amount of pressure increase in each chamber and the pressure in the third chamber. The pressure in the chambers was increased by increasing the pressure in the third chamber. However, the amount of increase in the first chamber was still less than 6 X 10^{-8} Torr even at 760 Torr in the third chamber. That means we can introduce the ion beams safely to the gaseous or liquid samples at one atmosphere by this differential pumping system.

(5) Beam alignment

A light from He-Ne laser, which had been installed on the bending magnet of HX1 port, is used for the alignment of EA-BRACHI and ion beams. Main part of EA-BRACHI was carefully set up along with the laser beam line during the construction with the accuracy of 0.5mm.

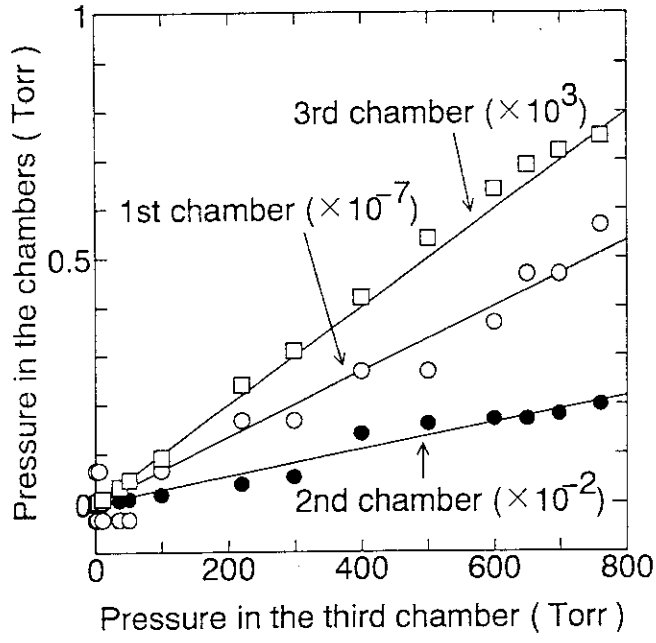

Fig.2 The relationship between the amount of pressure increase in three chambers and the controlled pressure of the third chamber.

Before each irradiation experiment, the position of the laser beam line is monitored at three different positions, namely by alumina beam monitor in a beam diagnosis station, which is exist between bending magnet and EA-BRACHI, by MgO beam monitor in the first chamber and by three monitors (Quartz, Alumina and Desmarquest) in the second chamber. All the positions are monitored by three TV cameras and marked on TV monitors. Ion beam from the cyclotron is adjusted its positions and shapes on the beam monitors to be the same as those marked by the laser beam. Fine alignment tunings are done by the XY stages in the chambers to get maximum beam current.

III. Research Items

Three research works, namely microdosimetry, pulse radiolysis and radiation effect on polymers and biological materials, will be done by EA-BRACHI. In the study of microdosimetry, the amount of energy deposition and its spatial distribution that is transferred from heavy ion beam by irradiation will be investigated. The produced intermediates by pulsed heavy ion beams will be studied by pulse radiolysis. Radiation effects and radiation quality on polymers and biological materials will be investigated by ion beam irradiation with the experimental apparatus.

ACKNOWLEDGEMENT

The authors wish to express their thanks to the members of "Research Group for Radiation Chemistry with Heavy Ions" for their helpful suggestions to construct this Experimental apparatus.

8. RADIOISOTOPE PRODUCTION AND NUCLEAR CHEMISTRY

8.1 An ISOL System in TIARA

Toshiaki SEKINE, Shin-ichi ICHIKAWA* and Yuichi HATSUKAWA

Department of Radioisotopes, *Department of Chemistry, JAERI

INTRODUCTION

An ISOL (Isotope Separator On-Line) connected to an accelerator is a powerful tool for studying unstable radioisotopes far from the stability line. An ISOL mass-separates nuclear reaction products immediately after nuclear reaction and produces a low-energy radioisotope ion beam, although an adequate ion source is needed for ionization of reaction products of interest. In JAERI, an isotope separator has been connected on-line to a tandem accelerator, and, by taking advantage of its capability of rapid separation, the decay of short-lived radioisotopes has been investigated[1,2]. To extend further this kind of study and develop fields of application of low-energy radioisotope-ion beams, an ISOL has been constructed at the cyclotron facility in TIARA.[3]

The TIARA cyclotron equipped with an ECR ion source in addition to a multicusp ion source delivers heavy-ion beams as well as light-ion beams. With these beams, radioisotopes to be obtainable

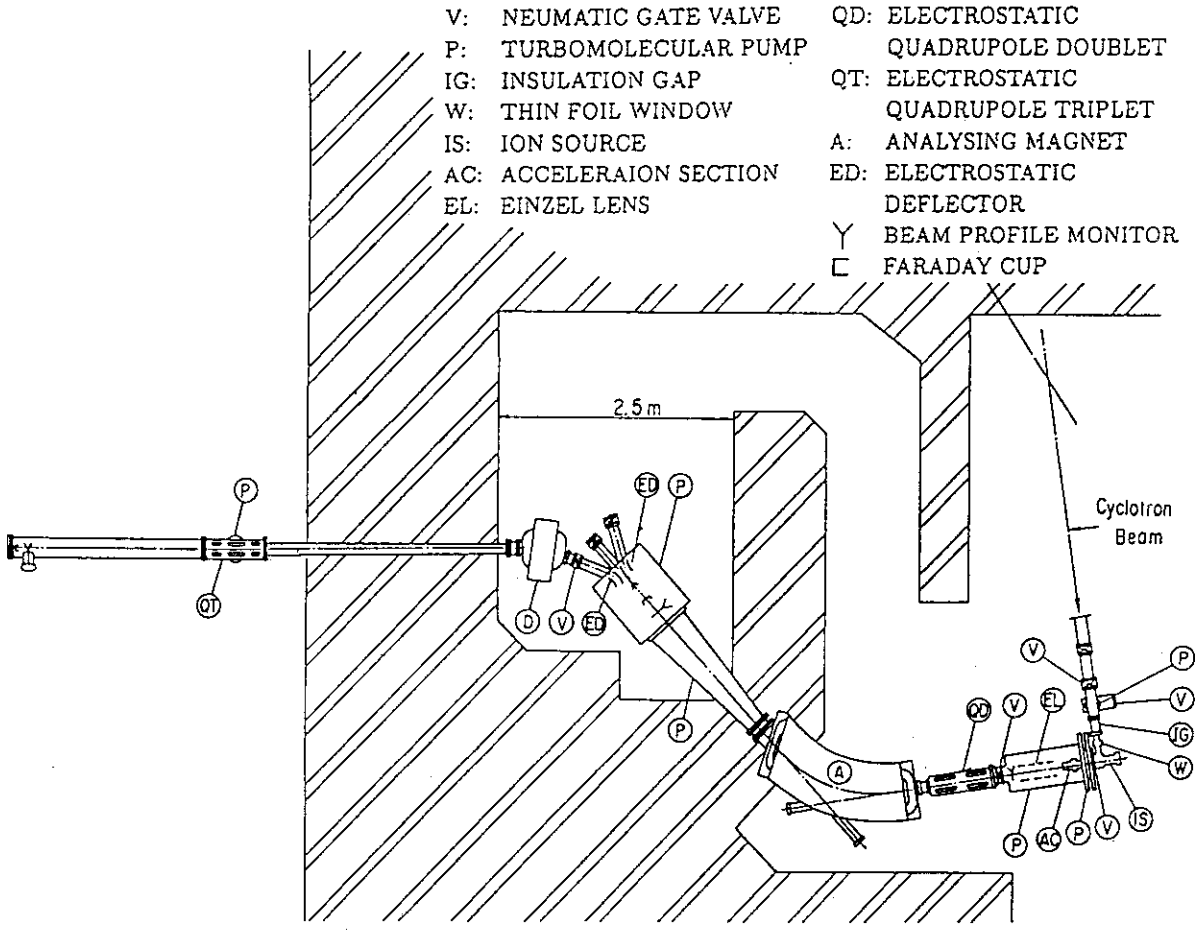

Fig. 1 The ISOL installed in TIARA.

covers a broad range in the nuclear chart. Heavy-ion beams, such as ^{36}Ar beam which is not available with a tandem accelerator, are expected to extend the present investigation of neutron deficient isotopes locating near the proton drip line toward more unstable isotopes. Meanwhile, light-ion beams produce rather long-lived radioisotopes to be used mainly for application of radioisotopes. These radioisotopes can be mass-separated in an off-line operation of the ISOL and implanted into a sample material; spectroscopic studies are possible with the samples, when a nuclide adequate to the spectroscopy is implanted.

The ISOL in TIARA

The ISOL installed in TIARA is an ISOLDE type isotope separator[4] supplied by Danfysik. As shown in Fig. 1, the ISOL system consists of the following components: an ion source, an extraction electrode system, a quadrupole triplet lens, an analyzing magnet, a beam dispersion chamber, a collection chamber and an electrostatic beam transport line. The ion source connects the isotope separator with the AVF cyclotron and produces ions of nuclear reaction products. A parallel beam of the ions is formed by an einzel lens in the extraction electrode system and introduced into a 55° sector magnet. The use of the electrostatic quadrupole doublet lens before the analyzing magnet gives high resolution and high transmission. The mass-separated beams are focussed horizontally and vertically on the focal plane in the collection chamber. With an electrostatic deflector and a dipole magnet, the mass fraction of interest is introduced into a beam transport line. The basic characteristics of the ISOL are summarized in Table 1. Figure 2 shows a mass spectrum of Xe obtained using a Nielsen-type ion source; the mass resolution was found to be 1350±120.

Table 1 Basic characteristics of the ISOL

Analyzed mass range:	1 to 270 amu
Analyzing magnet:	Double focusing R=1500 mm B_{max}=5 kG.
Resolving power $M/\Delta M$: (M=mass number)	1000 or greater
Maximum current: at high resolution mode	1 mA $300/M^{1/2}$ μA
Dispersion:	1500 mm/M
Collection range $(M_{max}-M_{min})/M_{min}$:	30%
Acceleration voltage:	10 – 100 kV
Number of beam transport line:	1 (Maximum: 3)
Beam size at the end of the beam transport line:	less than 3.5 mm
Pumping system:	Magnetic suspension type TMP

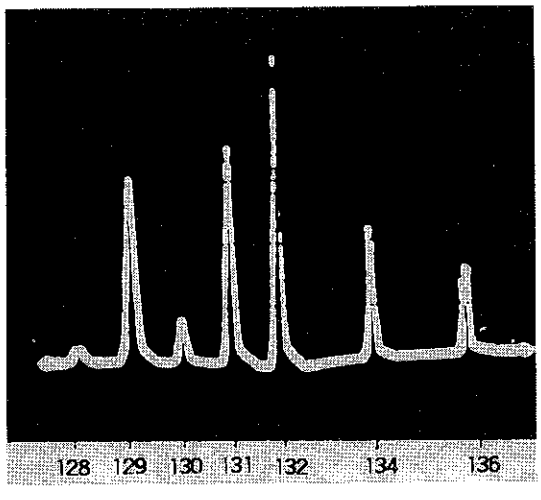

Fig. 2 Mass spectrum of Xe obtained with the ISOL.

Although the ISOL in TIARA has almost the same basic characteristics with the ISOL in Tokai, new features have been given to the part of ion source; the ion source is the most important component of an ISOL to develop a

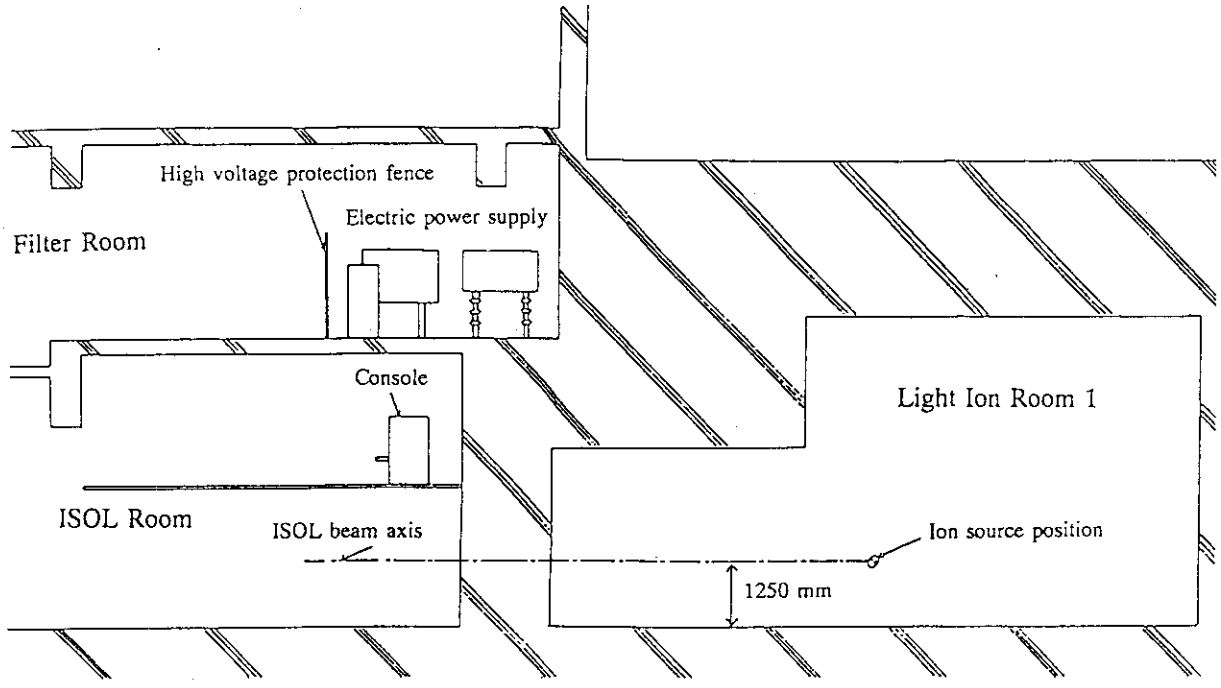

Fig. 3 Arrangement of the ISOL system.

frontier of unstable nuclei. As seen from Fig. 1, windows are constructed in the analyzing magnet. The windows will be used to introduce laser beams for a laser ion source, which applies the multistep photoionization of atoms. The laser ion source is expected to enable element-selective mass-separation. Another feature is that the ISOL is equipped with an automated handling apparatus for a Nielsen-type ion source which is used in an off-line operation. This apparatus enables us to load easily the ion source with a sample and can work in combination with the target transfer line[5] which carries an ion-source component containing a sample between a shielded cell in the hot laboratory and the terminal located by the ion source position.

The Nielsen type ion source is an arc discharge type and ionizes atoms in a plasma formed by a Xe support gas. This ion source ionizes atoms with rather high ionization potential like rare gas atoms. For atoms with low ionization potential, a surface ionization source is useful. High-temperature surface ionization sources are available for on-line and off-line operation. The release characteristics of Cs^+, Ba^+, La^+, LaO^+, Ce^+, CeO^+, Pr^+ and Nd^+ ions from the surface ionization source were studied by the present authors.[6]

The ISOL is integrated in the radioisotope production facility, as described elsewhere.[5] Figure 3 presents schematically the arrangement of the ISOL system. The ion source is placed at the port LE-1 in Light Ion Room 1. The mass-separated beam reaches ISOL Room for a low-background radiation measurement. An iron deck is constructed in ISOL Room. The area of the deck is 50 m^2 and that of the ground floor is 65 m^2 At the deck, the console of the ISOL is placed and a data acquisition system

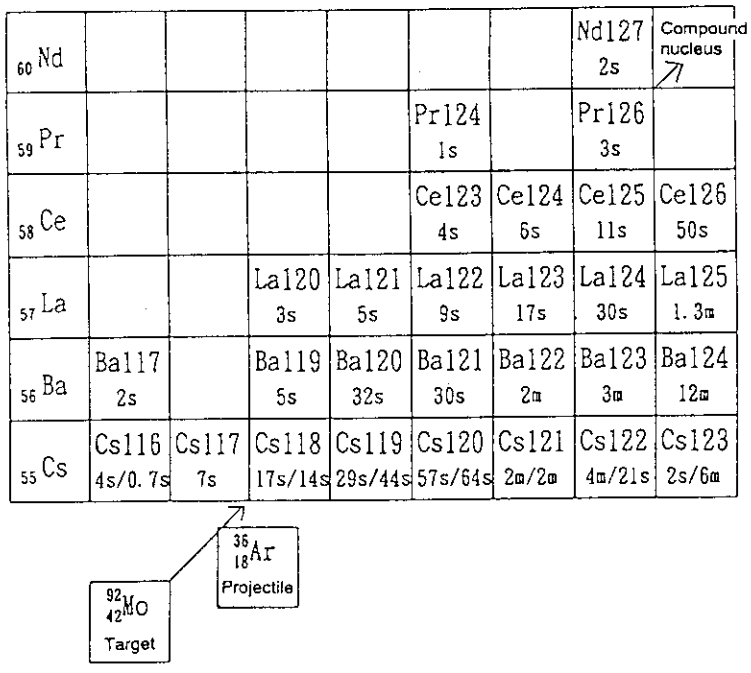

Fig.4 Part of the nuclear chart. The compound nucleus in the reaction $^{36}Ar+^{92}Mo$ is indicated. This region is located around the proton drip line. The white block is an unknown nuclide.

will be installed. The electric power supply is located in Filter Room (waste-gas treatment facility) over ISOL Room.

Studies using the TIARA ISOL

Evolution of nuclear shape is of great interest as a nuclear collective motion. The nuclei indicated in Fig. 4 are known to be in a transitional region of nuclear deformation from a sphere to a ellipsoid. In addition, the degree of freedom of triaxial deformation is involved in this region. Using the ISOL in Tokai, the decay of Cs, Ba and La isotopes has been studied; the isotope ^{121}La was newly identified[7] and it was found from the decay study of La isotopes that ^{122}Ba is the most deformed nucleus in known Ba isotopes.[2] To extend this study, different ion beams are needed. As seen from Fig. 4, the ^{36}Ar beam is useful for the production of unstable Ce, Pr and Nd isotopes. As mentioned before, this beam is available in TIARA. To produce more unstable La isotopes than ^{121}La, metallic ion beams like ^{64}Zn beam will be needed.

REFERENCES

1) S. Ichikawa, T. Sekine, M. Oshima, H. Iimura and Y. Nakahara, Nucl. Instr. Methods, B70, 93 (1992).

2) T. Morikawa, M. Oshima, T. Sekine, Y. Hatsukawa, S. Ichikawa, H. Iimura, A. Osa, M. Shibata and A. Taniguchi, Phys. Rev. C46, R6 (1992).

3) T. Sekine, S. Ichikawa and Y. Hatsukawa, Proc. Int. Symp. on Advanced Nuclear Energy Research -Evolution by Accelerators-, (Mito, Jan. 24-26, 1992).

4) B.R. Nielsen, Nucl. Instr. Methods, 186, 457 (1981).

5) M. Izumo, T. Sekine, S. Motoishi, H. Matsuoka, K. Kobayashi, K. Hashimoto, Y. Hatsukawa, N. Shigeta, F. Miura, T. Sorita, T. Moriya, H. Kudo, H. Umezawa and H. Watanabe, paper in this volume.

6) S. Ichikawa, T. Sekine, H. Iimura, and M. Oshima, Nucl. Instr. Methods, B70, 156 (1992).

7) T. Sekine, S. Ichikawa, M. Oshima, H. Iimura, Y. Nagame, K. Hata, N. Takahashi and A. Yokoyama, Z. Phys. A331, 105 (1988).

8. 2 A Radioisotope Production FAcility Utilizing Ion Beams from AVF Cyclotron

Mishiroku IZUMO, Toshiaki SEKINE, Shoji MOTOISHI, Hiromitsu MATSUOKA, Katsutoshi KOBAYASHI, Kazuyuki HASHIMOTO, Yuichi HATSUKAWA, Noriko SHIGETA, Fuminori MIURA, Takami SORITA, Takashi MORIYA, Hiroshi KUDO, Hirokazu UMEZAWA and Hiromasa WATANABE*

Department of Radioisotopes, *Department of Advanced Radiation Technology, JAERI

INTRODUCTION

JAERI has established production techniques of a variety of radioisotopes mainly utilizing nuclear reactors and supplied products across Japan for medical, industrial and scientific use. For several isotopes produced by charged-particle reactions, production methods have been developed with proton and deuteron beams from a tandem accelerator[1,2,3]. The demand for radioisotopes produced by charged-particle reactions is increasing; these radioisotopes are a positron emitter and/or a product in high specific activity with a rather short half-life for nuclear medicine, life science, engineering and research of the environment.

At TIARA/JAERI, an AVF cyclotron has been constructed for advanced radiation technology research. From the cyclotron equipped with a multicusp ion source and ECR ion sources, beams of light ions and heavy ions are available for production of a broad range of radioisotopes. In particular, light-ion beams like proton with energies up to 90 MeV as well as deuteron, ^{3}He and ^{4}He are useful for radioisotope production. For development of potentially useful radioisotopes and labelled compounds, a radioisotope production facility utilizing these ion beams has been constructed in TIARA.[4]

The facility consists of an irradiation apparatus, a solid-target transfer system, shielded cells for solid target and shielded cells for labelled-compound synthesis with gas and liquid targets. For chemical processing of α-ray emitters a glovebox is installed. These instruments are placed in a target room, called

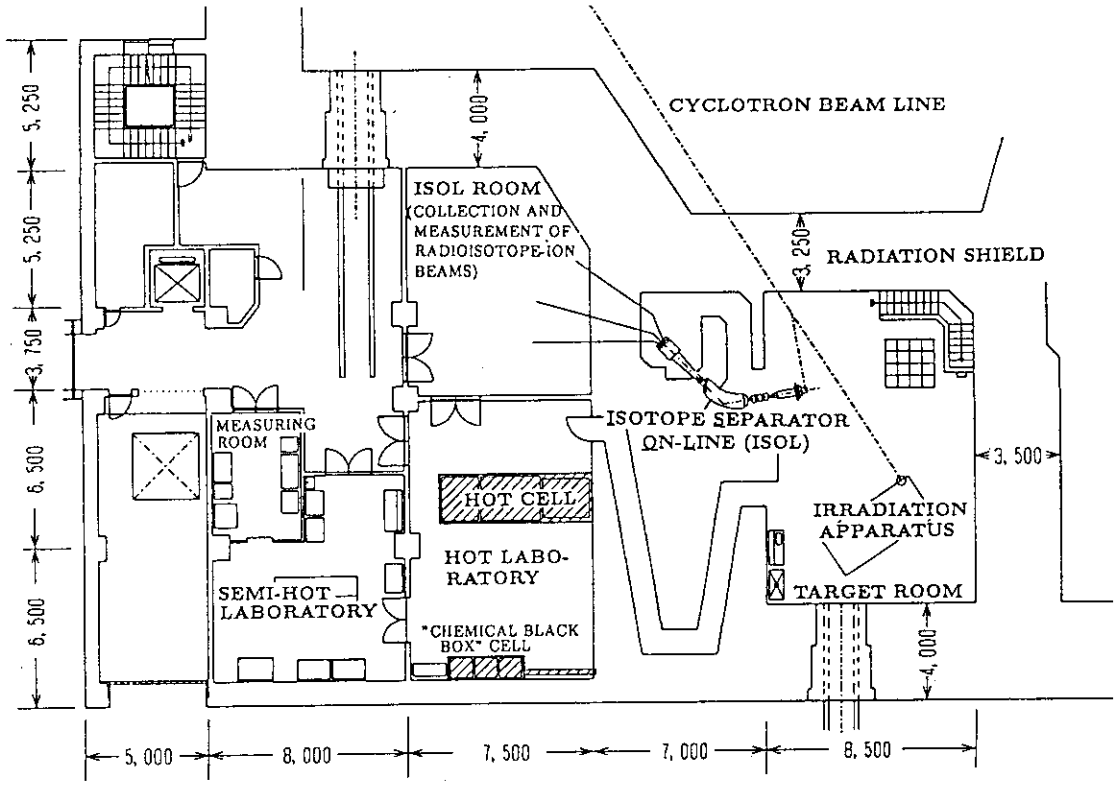

Fig.1 The radioisotope production facility in TIARA/JAERI utilizing ion beams from AVF cyclotron.

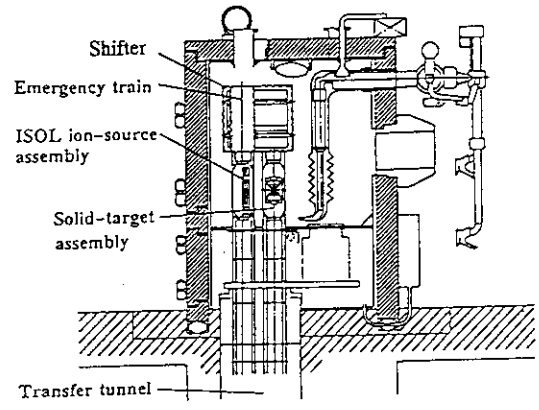

Fig. 4 The shielded cell connected to the solid-target transfer line.

of the beam line with an air cylinder. In external irradiation, the space between the metal window at the end of beam line and the solid-target surface (or the metal window of a gas and liquid target holder) is cooled with a He gas chilled at 5 - 10 °C. The back of the target is also cooled with water chilled at 5 - 10 °C. A gas or liquid target is supplied to the target holder through a thin tube from the hot laboratory and, after irradiation, collected through the tube to the shielded cells for labelled compound synthesis. Also, the irradiation of flowing gas and liquid targets is possible. For solid target, a solid target transfer system is installed to carry a target assembly between the shielded cell and the irradiation position, as described in detail later. A procedure of the above operation on the target supply, irradiation and collection is programmed in a sequential circuit.

SOLID-TARGET TRANSFER SYSTEM

The solid-target transfer system, as shown in Fig. 3, consists of monorail lines, trains and terminals handling a target assembly. The monorail lines begin from the terminal in a shielded cell and end at two terminals located at the irradiation apparatus and an isotope separator on-line (see Fig.1). The length of the rail line to the irradiation apparatus is 35 m. On the rail line, a train having a load of 3 kg can run at 36 m/min in a horizontal part and 24 m/min in a vertical part. The rail line is equipped with detectors to recognize the running train, train stoppers and a rail shifter for future extension.

For safety of the system, fire protection shutters are installed along the rail line. Further, another train working as a wrecker for a troubled train stands by at the terminal in the shielded cell. The control of the system is performed by a sequential program or manually.

SHIELDED CELLS FOR SOLID TARGET

Three shielded cells are installed in a hot laboratory to treat high level radioactivity produced in a solid target. These shielded cells are interconnected; a target and a product are carried by a train moving under the floor of the cells (see Fig. 5). Each of the cells is furnished with a pair of manipulators, water supply, drainage and electricity supply.

The first cell, depicted in Fig. 4, has the terminal of the solid-target transfer system. In this cell, the irradiated target is unfixed and the radioactivity of the target is measured with an ionization chamber. To bring in high level radioactivity soon after irradiation, radiation shielding is thickest in this cell. Its shielding material is 20 cm thick lead. The inside of the cell is 1.9 m in length, 1.6 m in width and 2.4 m in height. This cell is ventilated 30 times an hour and kept at a negative pressure of 10 mm Aq to the outside, although this cell is not airtight.

In the second cell, a solid target is processed chemically, where a chemical-processing unit for production of an isotope of interest will be placed. The radioactive waste after processing can be kept inside during a certain period for cooling. The solidification of the radioactive waste is also possible in this cell. Its shielding material is 18 cm thick iron. This cell has an inner box, being airtight to prevent volatile radioactivity from escaping to the workroom. The inside of the cell is 2.4 m in length, 1.5 m in width and 1.6 m in height. This cell is ventilated 40 times an hour. The inner box is kept at a negative pressure of 30 mm Aq. Its airtightness was found to be 0.1 v/o/h.

From the third cell, a product is taken out after its radioactivity is inspected. This cell is not airtight and

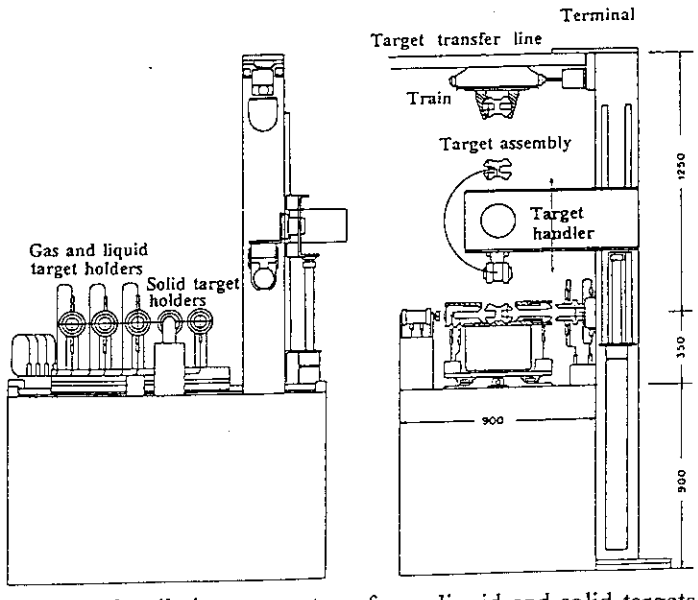

Fig.2 The irradiation apparatus of gas, liquid and solid targets and the terminal of solid-target transfer line equipped with a manipulator of solid target assembly.

Light-Ion Room No.1, and a hot laboratory, as shown in Fig.1. The present paper describes main instruments in the facility.

IRRADIATION APPARATUS

At the irradiation apparatus, targets of solid, gas and liquid are bombarded by an accelerator beam. A solid target is irradiated in a vacuum (internal irradiation) or outside the vacuum (external irradiation). For external irradiation, a thin Ti foil is placed at the end of the vacuum line. The Faraday cup in the vacuum line is inserted periodically and the beam current is integrated in the irradiation. When the current integrated reaches the preset value, the irradiation stops.

As shown in Fig.2, target holders of solid, gas and liquid targets are set on a movable plate. By moving the plate, the target holder retaining a target to be irradiated is placed at the beam position and fixed to the end

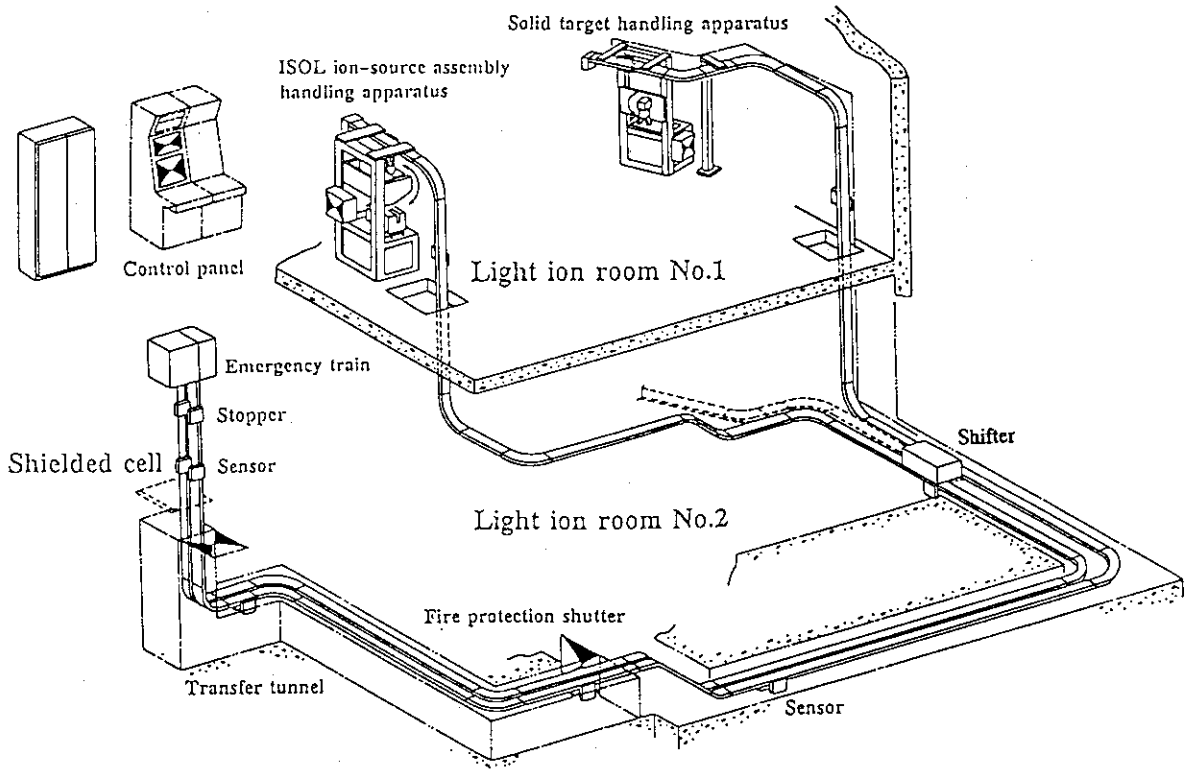

Fig. 3 Solid-target transfer system between the shielded cell and two ports: the irradiation apparatus and the isotope separator on-line.

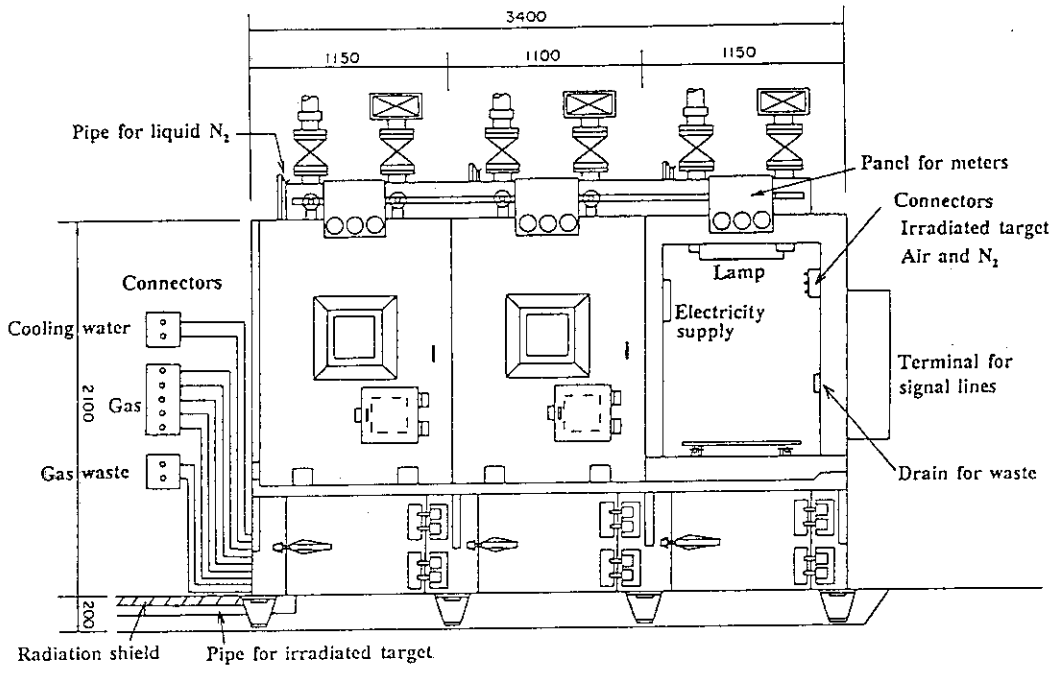

Fig. 5 The CBB cells in which CBBs for labeled compound synthesis are placed.

the shielding material is the same as the second one. The inside of this cell is 1.4 m in length, 1.6 m in width and 2.4 m in height.

SHIELDED CELLS FOR LABELED COMPOUND SYNTHESIS

Units of labeled compound synthesis, called CBB ("Chemical Black Box"), are installed in the shielded cells named CBB cells. In a CBB, a compound will be automatically labeled with short-lived positron emitters like ^{11}C, ^{13}N, ^{15}O and ^{18}F, produced from gas and liquid targets. The CBB cells are furnished with tubing for collection of irradiated targets, compressed air and nitrogen, electricity supply and wiring for signals to control the CBBs. Three CBB cells are interconnected, as shown in Fig. 5. Their radiation shield is equivalent to 10 cm thick lead. The inside of the CBB cells is 1.0 m in length, 0.9 m in width and 1.2 m in height. In the front of the CBB cells, there are two movable radiation shields; this means that two of the three CBB cells are shielded. Behind the front shields, doors made of lucite are placed to suppress the flow of the air from inside to outside.

REFERENCES

1) M. Izumo, T. Sorita, Y. Nagame, K. Hata, T. Sekine, H. Matsuoka, R. Motoki and S. Baba, JAERI-M 90-102 (1990).
2) M. Izumo, T. Sorita, H. Matsuoka, Y. Nagame, K. Hata, T. Sekine and S. Baba, JAERI-M 90-156 (1990).
3) M. Izumo, H. Matsuoka, T. Sorita, Y. Nagame, T. Sekine, K. Hata and S. Baba, Appl. Radiat. Isot. **42**, 297 (1991).
4) M. Izumo, T. Sekine, S. Motoishi, H. Matsuoka, K. Kobayashi, K. Hashimoto, Y. Hatsukawa, N. Shigeta, F. Miura, T. Sorita, T. Moriya, H. Kudo, H. Umezawa and H. Watanabe, Proc. Int. Conf. on Evolution in Beam Applications (Takasaki, Nov. 5-8, 1991) p.552.

9. PUBLICATIONS

9.1 Publications in Journal

1. S.Furuno, K.Houjou, H.Otsu, K.Izui, T.A.Sasaki, T.Tsukamoto and T.Hato,
System for *in situ* observation and chemical analysis of materials during dual-ion beam irradiation in an electron microscope
J. Electron Microsc.(Tokyo) 41 (1992) 273.
O

2. S.M.Gorbatkin, R.Zuhr, J.Roth and H.Naramoto,
Damage formation and substitutionality in $^{75}As^{++}$-implanted diamond
J. Appl. Phys. 70 (1991) 2986.
O

3. S.Ichikawa, T.Sekine, H.Iimura and O.Oshima,
Measurement of hold-up times in a thermal ion source for metallic and monoxide ions of lanthanum and cerium
Nucl. Instrum. Methods Phys. Res., Sect. B 70 (1992) 156.
O

4. I.Ohdomari, M.Sugimori, K.Koh, K.Noritake, H.Shimizu, R.Tamaka, T.Kamiya and N.Utsunomiya,
Ion microprobe system combined with scanning electron microscope for high precision aiming
Nucl. Instrum. Methods Phys. Res., Sect. B 54 (1991) 71.
O

5. H.Kudo, K.Shima, K.Masuda and S.Seki
Secondary electrons induced by fast ions under channeling conditions. I. Production and emissions of secondary electrons
Phys. Rev., B 43 (1991) 12729.
O

6. H.Kudo, K.Shima, S.Seki and T.Ishihara
Secondary electrons induced by fast ions under channeling conditions. II. Screening of fast heavy ions in solids
Phys. Rev., B 43 (1991) 12736.
O

7. H.Kudo, K.Shima, K.Masuda, T.Ishihara and S.Seki
Binary encounter electron spectroscopy under channeling incidence conditions
Radiat. Eff. Defects Solids 117 (1991) 85.
O

8. A.Miyashita, O.Yoda, K.Murakami, T.Ohyanagi, S.Aoki and N.Yamaguchi,
Time-resolved soft X-ray absorption spectroscopy apparatus using laser produced plasma X-ray
Laser Adv. Mater. Proces. 2 (1992) 1029.
O

9. H.Naramoto, K.Kawatsura, M.Sataka, Y.Sugizaki, Y.Nakai, K.Ozawa, S.Yamaguchi, Y.Fujino and M.Aoki,
Lattice Location of deuterium in Nb-Mo with ion beams
Nucl. Instrum. Methods Phys. Res., Sect. B 33 (1988) 595.
O

10. T.Morikawa, M.Oshima, T.Sekine, Y.Hatsukawa, S.Ichikawa, H.Iimura, A.Osa, M.Shibata and A.Taniguchi,
Lifetime measurement of the first 2^+ state in ^{122,124,126}Ba
Phys. Rev., C 46 (1992) R6.
O

11. S.Okada and H.Sunaga,
Design of an intense slow positron beam production system using a 100 kW electron linac for the positron factory
Nucl. Instrum. Methods Phys. Res., Sect. B 56/57 (1991) 604.
O

12. O.Oshima, T.Sekine, S.Ichikawa, Y.Hatsukawa, I.Nishinaka and T.Morikawa,
Status report of the JAERI on-line isotope separator
Nucl. Instrum. Methods Phys. Res., Sect. B 70 (1992) 93.
O

13. O.Oshima, T.Sekine, S.Ichikawa, Y.Hatsukawa, I.Nishinaka and T.Morikawa,
Development of a laser-enhanced ion-guided ion source
Nucl. Instrum. Methods Phys. Res., Sect. B 70 (1992) 241.
O

14. R.Tanaka,
Plan of ion beam application in JAERI-Takasaki
J. Atomic Energy Society of Japan 33 (1991) 1018 (in Japanese).
C,T

9.2 Publications in Proceedings

1. T.Agematsu, S.Okumura, W.Yokota, K.Arakawa, T.Murakami, T.Okumura,
   Knowledge based operation assist system for JAERI AVF cyclotron
   Proc. of the International Conference on Evolution in Beam Applications
   (Takasaki, Nov. 5-8, 1991) p.280.
   C

2. K.Arakawa, Y.Nakamura, W.Yokota, M.Fukuda, T.Kamiya, T.Nara, T.Agematsu,
   S.Okumura, I.Ishibori, R.Tanaka and M.Murayama,
   Construction of the JAERI AVF cyclotron
   Proc. of the International Conference on Evolution in Beam Applications
   (Takasaki, Nov. 5-8, 1991) p.264.
   C

3. K.Arakawa, Y.Nakamura, W.Yokota, M.Fukuda, T.Kamiya, T.Nara, T.Agematsu,
   S.Okumura, I.Ishibori, R.Tanaka, M.Murayama, T.Tachikawa, Y.Hayashi,
   K.Ishii and T.Satoh,
   Construction and present status of the JAERI AVF cyclotron
   Proc. of the 8th Symposium on Accelerator Science and Technology
   (Saitama, Nov. 25-27, 1991) p.34.
   C

4. M.Fukuda, K.Arakawa, Y.Nakamura, W.Yokota, T.Kamiya, T.Nara, T.Agematsu,
   S.Okumura, I.Ishibori, R.Tanaka, T.Karasawa, A.Shimizu, Y.Kumata,
   Y.Fukumoto,
   RF System of the JAERI AVF cyclotron
   Proc. of the 8th Symposium on Accelerator Science and Technology
   (Saitama, Nov. 25-27, 1991) p.138.
   C

5. S.Furuno, K.Hojou, H.Otsu, K.Izui, T.A.Sasaki, T.Tsukamoto and T.Hata,
   A new system for in-situ observation of dynamic process of structural
   and chemical changes during dual ion beam irradiation in a 400 keV
   electron microscope
   Electron Microscopy, 4 (1990) 538.
   O

6. S.Furuno, K.Hojou, H.Otsu, K.Izui, T.A.Sasaki, T.Tsukamoto and T.Hata,
   In-situ observation system for dual ion irradiation damage
   Proc. of the International Conference on Evolution in Beam Applications
   (Takasaki, Nov. 5-8, 1991) p.741.
   O

7. S.Hamada, K.Hojou and A.Hishinuma,
In-situ observation of weld joint of austenitic stainless steel due to helium irradiation
Proc. of the International Conference on Evolution in Beam Applications (Takasaki, Nov. 5-8, 1991) p.753.
O

8. T.Hirao, Y.Morita, S.Nishijima, T.Kamiya, H.Yutoh and R.Tanaka,
Single-event current transients with heavy ion micro-beam
Proc. of the International Workshop on Semiconductor Devices for Space Application (Takasaki, Feb. 25-26, 1992) p.142.
C

9. K.Hojou, S.Furuno, K.N.Kushita, H.Otsu, K.Izui, Y.Ueki and T.Kamino,
Electron energy loss spectroscopy of SiC crystals implanted with hydrogen and helium dual ion beam
Electron Microscope (EUREM 92) (1992) p.261.
O

10. K.Hojou, K.N.Kushita, S.Furuno and H.Otsu,
Effects of single- and dual-ion irradiation on graphite and silicon carbide studied by an analytical electron microscopy
Material Chemistry (1992) p.449.
O

11. F.Hosoi, Y.Izumi and H.Ohmichi,
An apparatus for preparation of hybrid thin films using low energy ion beams
Proc. of the 4th Workshop on Tandem Accelerator Facility and Technology (Takasaki, July 11-12, 1990) p.138.
O

12. M.Izumo, T.Sekine, S.Motoishi, H.Matsuoka, K.Kobayashi, K.Hashimoto, Y.Hatsukawa, N.Shigeta, F.Miura, T.Sorita, T.Moriya, H.Kudo, H.Umezawa and H.Watanabe,
A radioisotope production facility utilizing ion beam from AVF cyclotron
Proc. of the International Conference on Evolution in Beam Applications (Takasaki, Nov. 5-8, 1991) p.552.
C

13. T.Kamiya, N.Utsunomiya, E.Minehara, R.Tanaka and I.Ohdomari,
Microbeam system for study of single event upset of semiconductor devices
Proc. of the 10th International Conference on Ion Beam Analysis (Eindhoven, July 1-5, 1991) Nucl. Instrum. Methods Phys. Res., Sect. B 64 (1991) 362.
T

14. T.Kamiya, N.Utsunomiya, E.Minehara, R.Tanaka, M.Ohmura, K.Kohno and E.Iwamoto
Heavy ion microbeam system for study of single event effect
Proc. of the International Conference on Evolution in Beam Applications (Takasaki, Nov. 5-8, 1991) p.286.
T

15. T.Kamiya, H.Yutoh and R.Tanaka,
JAERI heavy ion microbeam system and single ion hit technique
Proc. of the International Workshop on Semiconductor Devices for Space Application (Takasaki, Feb. 25-26, 1992) p.112.
T

16. M.Koh, M.Sugimori, K.Noritake, T.Matsukawa, K.Hara, Y.Takiguchi, T.Kamiya, N.Utsunomiya, E.Minehara, H.Shimizu, R.Tanaka and I.Ohdomari,
Development of ion microprobe system at Waseda University
Proc. of the International Workshop on Semiconductor Devices for Space Application (Takasaki, Feb. 25-26, 1992) p.105.
O

17. H.Kudo, E.Yoshida, K.Shima and T.Ishihara,
Ion beam analysis using ion-induced secondary electrons
Proc. of the International Conference on Evolution in Beam Applications (Takasaki, Nov. 5-8, 1991) p.156.
O

18. K.N.Kushita, K.Hojou and S.Furuno,
Structure modification of electron-irradiation graphite at low temperature observed by EELS
Electron Microscope (1992) p.146.
O

19. H.Ohno and S.Nagai,
Low energy ion beam system combined with in-situ surface analysis system
Proc. of the 35th Symposium of Radiation Chemistry (Takasaki, Oct. 6-8, 1992) p.75.
T

20. S.Okada,
Design and manufacturing of slow positron beam line electrostatically transported to double direction
Proc. of the 29th Annual Meeting on Radioisotopes in Physical Sciences and Industries (Tokyo, June 29 - July 1, 1992) p.161 (in Japanese).
O

21. S.Okumura, T.Agematsu, W.Yokota, T.Kamiya, M.Fukuda, Y.Nakamura, T.Nara, I.Ishibori, K.Arakawa, M.Murayama, K.Iso, K.Hoshika, M.Tachibana, T.Murakami and T.Okamura,
Control system of the JAERI AVF cyclotron
Proc. of the 8th Symposium on Accelerator Science and Technology (Saitama, Nov. 25-27, 1991) p.356.
C

22. S.Okumura, T.Agematsu, W.Yokota, T.Kamiya, M.Fukuda, Y.Nakamura, T.Nara, I.Ishibori, M.Murayama, K.Iso, K.Hoshika and M.Tachibana,
Control system of the JAERI AVF cyclotron
Proc. of the International Conference on Evolution in Beam Applications (Takasaki, Nov. 5-8, 1991) p.275.
C

23. Y.Nakamura, K.Arakawa, K.Mizuhashi, W.Yokota, M.Fukuda, T.Kamiya, T.Nara, T.Agematsu, S.Okumura, I.Ishibori, R.Tanaka, M.Sano, K.Hoshika, T.Satoh, T.Torii, K.Suzuki and H.Watanabe,
Vacuum system of the JAERI AVF cyclotron
Proc. of the 8th Symposium on Accelerator Science and Technology (Saitama, Nov. 25-27, 1991) p.194.
C

24. H.Naramoto,
Materials analysis by combined use of RBS/NRA/PIXE
Proc. of the International Conference on Evolution in Beam Applications (Takasaki, Nov. 5-8, 1991) p.138.
O

25. T.Saga, A.Ushirokawa, S.Matsuda and Y.Morita,
Radiation effects on silicon single crystal solar cells and plan for multi-beam irradiation tests
Proc. of the International Workshop on Semiconductor Devices for Space Application (Takasaki, Feb. 25-26, 1992) p.73.
C,T

26. S.Sato
The Advanced Radiation Technology Project using ion beams in JAERI-Takasaki
Proc. of the International Conference on Evolution in Beam Applications (Takasaki, Nov. 5-8, 1991) p.239.
C,T

27. S.Sato
Ion beam facilities and Advanced Radiation Technology Project in JAERI-Takasaki
Proc. of the International Workshop on Semiconductor Devices for Space Application (Takasaki, Feb. 25-26, 1992) p.3.
C,T

28. T.Sekine, S.Ichikawa, O.Oshima, H.Iimura, T.Morikawa, A.Osa, W.H.Chung and Y.Hatsukawa,
Decay spectroscopy of ^{122,124,126}La isotopes by means of heavy-ion nuclear reaction and isotope separator
Proc. of the International Conference on Evolution in Beam Applications (Takasaki, Nov. 5-8, 1991) p.531.
O

29. T.Tachikawa, Y.Hayashi, K.Ishii, T.Satoh, Y.Nakamura, W.Yokota, M.Fukuda, T.Kamiya, T.Nara, T.Agematsu, S.Okumura, I.Ishibori and K.Arakawa,
First results of beam generation test for JAERI AVF cyclotron
Proc. of the International Conference on Evolution in Beam Applications (Takasaki, Nov. 5-8, 1991) p.270.
C

30. S.Tajima, I.Takada, K.Mizuhashi, Y.Saito, K.Yotsumoto and R.Tanaka,
Construction and first operation of the JAERI 3MV tandem accelerator
Proc. of the 4th Workshop on Tandem Accelerator Facility and Technology (Takasaki, July 11-12, 1990) p.27.
T

31. Su.Tanaka, T.Nakamura, M.Baba, M.Imamura, H.Hirayama, K.Shin, Sh.Tanaka and R.Tanaka,
Research plan of radiation shielding for accelerator facility and monoenergetic neutron source
Proc. of the 2nd International Symposium on Advanced Nuclear Energy Research - Evolution by Accelerator - (Mito, Jan. 24-26, 1990) p.342.
C

32. R.Tanaka,
Ion accelerators and their application to materials science research
Proc. of the 20th Japan Conference on Radiation and Radioisotopes (Tokyo, Nov. 12-14, 1991) p.839.
C,T

33. R.Tanaka and T.Kamiya,
Preliminary study on very high energy heavy-ion microbeam
Proc. of the International Workshop on Semiconductor Devices for Space Application (Takasaki, Feb. 25-26, 1992) p.118.
T

34. H.Takeshita, Y.Aoki, S.Yamamoto and H.Naramoto,
Molecular-beam epitaxial growth and ion-beam analysis system for functional materials research
Proc. of the International Conference on Evolution in Beam Applications (Takasaki, Nov. 5-8, 1991) p.129.
T

35. O.Yoda, A.Miyashita, K.Murakami, S.Aoki and N.Yamaguchi,
Time resolved X-ray absorption spectroscopy apparatus using laser plasma as an X-ray source
SPIE Semin. Proc., 1503 (1991) 463.
O

36. M.Yoshikawa, Y.Morita, H.Itoh, I.Nashiyama, S.Misawa, H.Okumura and S.Yoshida,
Irradiation effects of cubic silicon carbide metal-oxide-semiconductor structure
Proc. of the International Workshop on Semiconductor Devices for Space Application (Takasaki, Feb. 25-26, 1992) p.32.
T

37. H.Watanabe, Y.Kobayashi, M.Kikuchi, R.Nozawa and S.Inaba,
Effect of ion beam on dry cells of *D.radiodurans*
Proc. of the International Conference on Evolution in Beam Applications (Takasaki, Nov. 5-8, 1991) p.599.
O

38. W.Yokota, K.Arakawa, Y.Nakamura, M.Fukuda, T.Kamiya, T.Nara, T.Agematsu, S.Okumura, I.Ishibori, R.Tanaka, M.Maruyama, T.Tachikawa, Y.Hayashi, K.Ishii, K.Iso and T.Satoh,
Operation of ECR and Multi-cusp ion sources for the JAERI AVF cyclotron
Proc. of the 8th Symposium on Accelerator Science and Technology (Saitama, Nov. 25-27, 1991) p.70.
C

10. PERSONNEL AND COMMITTEES

10. 1 Consultative Committee

(for fiscal year 1991)

1. Consultative Committee for The Advanced Radiation Technology

Chairman	Yoneho	Tabata	(Tokai University)
Members	Teruhiko	Beppu	(Tokyo University)
	Masao	Doyama	(West Tokyo University)
	Kenkichi	Ishigure	(Tokyo University)
	Hiromiti	Kamitsubo	(Inst. of Phy. Chem. Res. (Riken))
	Itaru	Mita	(Japan Dow Corning Research Center)
	Susumu	Namba	(Nagsaki Inst. Appl. Sci.)
	Koki	Sato	(Nat. Inst. Radiol. Sci., STA)
	Kenji	Sekido	(NEC Corporation)
	Masayuki	Shimodaira	(Nat. Space Development Agency of Japan)
	Haruki	Shiraishi	(National Res. Inst. for Metals, STA)
	Takio	Tomimasu	(Free Electron Laser Res. Inst., Inc.)
	Akio	Ushirokawa	(Tokyo University)
	Hikoyuki	Yamaguchi	(Komazawa University)
	Masashi	Iizumi	(JAERI)
	Isao	Ishigaki	(JAERI)
	Tatsuo	Kondo	(JAERI)
	Michio	Maruyama	(JAERI)
	Shoichi	Sato	(JAERI)
	Susumu	Shimamoto	(JAERI)
	Enzo	Tachikawa	(JAERI)
	Hirokazu	Umezawa	(JAERI)
Secretaries	Hideo	Osono	(JAERI)
	Ryuichi	Tanaka	(JAERI)
	Satomi	Yambe	(JAERI)

2. Subcommittee - Accelerator Facilities

Chairman	Hiromiti	Kamitsubo	(Inst. of Phy. Chem. Res. (Riken))
Members	Manabu	Fujioka	(Tohoku University)
	Akira	Isoya	(Tokai University)
	Miroru	Miwa	(Nat. Inst. Radiol. Sci., STA)
	Takashi	Nakamura	(Tohoku University)
	Hideo	Sakairi	(Inst. of Phy. Chem. Res. (Riken))
	Akira	Shimizu	(Osaka University)

	Seiichi	Tagawa	(Tokyo University)
	Yukio	Kazumata	(JAERI)
	Chiaki	Kobayashi	(JAERI)
	Ryuichi	Tanaka	(JAERI)
	Hiromasa	Watanabe	(JAERI)
	Keiichi	Yotsumoto	(JAERI)

3. Subcommittee - Radiation Resistant Materials for Space Development

Chairman	Akio	Ushirokawa	(Tokyo University)
Members	Toshifumi	Arimitsu	(NEC Corporation)
	Masahiko	Ikeda	(Hitachi Corporation)
	Toshihiko	Kanayama	(Electrotechnical Laboratory, MITI)
	Kenji	Maeguchi	(Toshiba Co.)
	Sumio	Matsuda	(Nat. Space Development Agency of Japan)
	Atsuo	Morio	(Reliability Center for Electronic Components of Japan)
	Isamu	Nashiyama	(Electrotechnical Laboratory, MITI)
	Iwao	Ohdomari	(Waseda University)
	Kazunori	Ohnisi	(Nihon University)
	Yasuhiko	Onodera	(Mitsubishi Electric Co.)
	Noboru	Shiono	(Nipp. Teleg. & Teleph. Pub. Corp.(NNT))
	Katsuyuki	Ara	(JAERI)
	Isao	Ishigaki	(JAERI)
	Yosuke	Morita	(JAERI)

4. Subcommittee - Biotechnology

Chairman	Hikoyuki	Yamaguchi	(Komazawa University)
Members	Yasuo	Asada	(Fermentation Res. Inst., MITI)
	Kensuke	Furukawa	(Kyushu University)
	Tadaaki	Hori	(Nat. Inst. Radiol. Sci., STA)
	Tatsuo	Ido	(Tohoku University)
	Isao	Karube	(Tokyo University)
	Kazuhiko	Kinoshita	(Keio University)
	Akira	Kira	(Inst. of Phy. Chem. Res. (Riken))
	Isao	Kohno	(Inst. of Phy. Chem. Res. (Riken))
	Kenji	Ohmasa	(Nat. Inst. for Environmental Studies)
	Katsuo	Ohyama	(Inst. of Radiation Breeding, MAFF)
	Ysuhito	Sasaki	(Tokyo University)
	Koki	Sato	(Nat. Inst. Radiol. Sci., STA)
	Mamoru	Tamura	(Hokkaido University)
	Mitsuteru	Yoshida	(Tokyo University of Science)
	Takashi	Fujimura	(JAERI)

	Shinichi	Ohno	(JAERI)
	Takashi	Moriya	(JAERI)
	Hiroshi	Watanabe	(JAERI)

5. Subcommittee - Functional Materials

Chairman	Susumu	Namba	(Nagsaki Inst. Appl. Sci.)
Members	Masakazu	Aono	(Inst. of Phy. Chem. Res. (Riken))
	Junzo	Ishikawa	(Kyoto University)
	Akira	Ishitani	(Toray Research Center, Inc.)
	Masaya	Iwaki	(Inst. of Phy. Chem. Res. (Riken))
	Kozo	Masuda	(Tsukuba University)
	Shoji	Noda	(Toyota Central R & D Labs., Inc.)
	Iwao	Ohdomari	(Waseda University)
	Kazuo	Saito	(Nat. Res. Inst. for Metals, STA)
	Masayuki	Tsukioka	(Inorganic Materials Laboratory, STA)
	Siro	Nagai	(JAERI)
	Hiroshi	Naramoto	(JAERI)
	Hideki	Omichi	(JAERI)
	Hideo	Ohno	(JAERI)
	Sohei	Okada	(JAERI)
	Osamu	Yoda	(JAERI)

6. Subcommittee - the Positron Factory Project

Chairman	Masao	Doyama	(West Tokyo University)
Members	Toshinobu	Chiba	(Inorganic Materials Laboratory, STA)
	Masayuki	Hasagawa	(Tohoku University),
	Yoshihide	Honda	(Osaka University)
	Yasuo	Ito	(Tokyo University)
	Hitoshi	Kobayashi	(Nat. Lab. for High Energy Physics (KEK))
	Tomohisa	Mikado	(Electrotechnical Laboratory, MITI)
	Nobuhiro	Shiotani	(Tokyo Univiversity of Fisheries)
	Osamu	Sueoka	(Yamaguchi University)
	Shoichiro	Tanigawa	(Tsukuba University)
	Yusuke	Ujihira	(Tokyo University)
	Miyuki	Hagiwara	(JAERI)
	Sohei	Okada	(JAERI)
	Jiro	Okamoto	(JAERI)
	Teikichi	Sasaki	(JAERI)
	Saburo	Takamura	(JAERI)

10.2 TIARA Program Committee

1. General Program Committee

Chairman	Susumu	Namba	(Nagsaki University of Sciences)
Members	Fumio	Imai	(National Space Development Agency of Japan)
	Kenkichi	Ishigure	(Tokyo University)
	Michihiko	Mamba	(Kyoto University)
	Kozo	Masuda	(Tsukuba University)
	Kazuo	Sadamitsu	(Furukawa Electric Co.)
	Yasuhito	Sasaki	(Tokyo University)
	Koki	Sato	(Nat. Inst. of Radiat. Res., STA)

Mitsuhiko	Ishii	(JAERI)	Michio	Maruyama	(JAERI)
Isao	Ishigaki	(JAERI)	Susumu	Shimamoto	(JAERI)
Waichiro	Kawakami	(JAERI)	Enzo	Tachikawa	(JAERI)
Tatsuo	Kondo	(JAERI)	Hirokazu	Umezawa	(JAERI)

Secretaries

Ryuichi	Tanaka	(JAERI)	Hiroshi	Watanabe	(JAERI)
Hiromasa	Watanabe	(JAERI)	Satomi	Yambe	(JAERI)

2. Program Advisory Committee (PAC)

Chairman	Waichiro	Kawakami	(JAERI)
Members	Tatsuo	Ido	(Tohoku University)
	Takeshi	Uwozumi	(Tokyo University)
	Chiken	Kinoshita	(Kyushu University)
	Kenji	Morita	(Nagoya University)
	Yosuke	Katsumura	(Tokyo University)
	Haruki	Shiraishi	(Nat. Res. Inst. for Metals, STA)
	Sumio	Matsuda	(National Space Development Agency of Japan)

Yutaka	Anazawa	(JAERI)	Kenji	Noda	(JAERI)
Michio	Maruyama	(JAERI)	Hideki	Omichi	(JAERI)
Yosuke	Morita	(JAERI)	Tadao	Seguchi	(JAERI)
Takashi	Moriya	(JAERI)	Ryuichi	Tanaka	(JAERI)
Hiroshi	Naramoto	(JAERI)	Hiroshi	Watanabe	(JAERI)

10.3 Advisory Groups

(m* : manager)

1. Microbeam Technology

	Akira	Isoya	(ToKai University)
	Misao	Kageyama	(Terada Inc.)
	Shunji	Nishijima	(Electrotechnical Laboratory, MITI)
	Iwao	Odomari	(Waseda University)
	Hiroyoshi	Sekiguchi	(Electrotechnical Laboratory, MITI)
	Mikio	Takai	(Osaka University)
	Eisuke	Minehara	(JAERI)
m*	Ryuichi	Tanaka	(JAERI)

2. Shielding of Ion Accelerators

	Mamoru	Baba	(Tohoku University)			
	Hideo	Hirayama	(Nat. Lab. for High Energy Physics (KEK))			
	Kazuo	Hata	(Kyoto University)			
	Mineo	Imamura	(Tokyo University)			
	Takashi	Nakamura	(Tohoku University)			
	Ryuichi	Tanaka	(JAERI)	Shunichi	Tanaka	(JAERI)
m*	Susumu	Tanaka	(JAERI)			

3. Radiation Effects on Semiconductors

	Kunihiko	Kasama	(NEC)			
	Sumio	Matsuda	(Nat. Space Development Agency of Japan)			
	Isamu	Nashiyama	(Electrotechnical Laboratory, MITI)			
	Shunji	Nishijima	(Electrotechnical Laboratory, MITI)			
	Kazunori	Onishi	(Nihon University)			
	Noburu	Shiono	(LSI Lab., NTT)			
	Michio	Tajima	(Inst. Space Sci., Min. Ed.)			
	Yasukiyo	Takami	(Rikkyo University)			
	Kiyoshi	Toriyama	(Mitsubishi Electric Co.)			
	Kikuo	Watanabe	(Hitachi Corporation)			
	Ichiro	Yoshii	(Toshiba Corporation)			
	Katsuyuki	Ara	(JAERI)	Yousuke	Morita	(JAERI)
	Isao	Ishigaki	(JAERI)	Ryuichi	Tanaka	(JAERI)
m*	Hisayoshi	Ito	(JAERI)	Masato	Yoshikawa	(JAERI)
	Waichiro	Kawakami	(JAERI)			

4. Radiation Resistance of Electronic Devices

	Mikio	Ikeda	(Hitachi)
	Mikio	Kuboyama	(Nat. Space Development Agency of Japan)
	Susumu	Mituishi	(NEC)
	Sizuhiko	Murakami	(Fujitsu)
	Tatsuo	Saga	(Sharp)
	Mikio	Shibuya	(Toshiba)

	Mari	Tsugami	(Mitsubishi Electric)
	Toshio	Hirao	(JAERI)
m*	Yousuke	Morita	(JAERI)

5. Radiation Damage I

	Eiichi	Kuramoto	(Kyushu University)
	Yasuji	Maeda	(Tokyo University)
	Shigeo	Okuda	(Tsukuba University)
	Keiai	Suzuki	(Tokyo University)
m*	Tadao	Iwata	(JAERI)

6. Radiation Damage II

	Yudai	Kato	(Tokyo University)
	Hikaru	Kayama	(Tokyo University)
	Chiken	Kinoshita	(Kyushu University)
	Naoki	Kishimoto	(Inst. of Metals, STA)
	Naoto	Sekimura	(Tokyo University)
	Haruki	Shiraishi	(Inst. of Metals, STA)
	Michitaka	Terasawa	(Himeji Inst. Tech.)
	Shozo	Hamada	(JAERI)
m*	Akimichi	Hishinuma	(JAERI)

Kenji	Noda	(JAERI)

7. Compound Materials

	Kazuo	Kawakami	(Mitsubishi Electric)
	Norihiko	Nakano	(Res. Inst. Polymers & Textiles, MITI)
	Shigehiro	Nishijima	(Osaka University)
	Isamu	Ohsawa	(Tokyo University)
	Hiromi	Shibata	(Tokyo University)
	Noriaki	Sugawara	(Fuji Heavy Industry)
	Hiroo	Takeda	(Tokyo University)
	Hideo	Nakajima	(JAERI)
m*	Tsuneo	Sasuga	(JAERI)

Takashi	Udagawa	(JAERI)

8. Gene Resources

	Kensuke	Furukawa	(Kyushu Univ.)
	Shigeru	Inaba	(Tokyo Univ. of Agriculture)
	Masayoshi	Inoue	(Kyoto Prefectural University)
	Hirokazu	Nakai	(Shizuoka University)
	Koki	Sato	(Nat. Inst. of Radiological Sciences, STA)
	Shigemitsu	Tano	(Tokyo University)
	Takeshi	Uozumi	(Tokyo University)
	Osamu	Yato	(Inst. for Radiation Breeding, MAFF)
m*	Hiroshi	Watanabe	(JAERI)

9. Radiation Chemitry with Heavy Ions

	Shuichi	Hashimoto	(Gunma College of Technology)
	Hiroshi	Hiratsuka	(Gunma University)

	Akira	Ito	(Inst. Cancer Research)		
	Kazuie	Kimura	(Inst. of Phys. and Chem. Res. (RIKEN))		
	Masahiro	Saito	(Kyoto Uneversity)		
	Seiichi	Tagawa	(Tokyo Uneversity)		
	Yasushi	Aoki	(JAERI)	Shinichi	Ohno (JAERI)
m*	Hideki	Namba	(JAERI)		

10. Biological Functinal Materials (until March 1991)

	Hiroshi	Morisaki	(Univ. Electro-Communications)		
	Hidetoshi	Nakayama	(Gunma University)		
	Kiyoshi	Takahashi	(Tokyo Inst. Tech.)		
	Mamoru	Tamura	(Hokkaido University)		
	Takashi	Fujimura	(JAERI)	Isao	Kaetsu (JAERI)
m*	Minoru	Kumakura	(JAERI)		

11. Organic Functional Materials II. (from April 1991)

	Masami	Fujii	(Inst. Space & Astronautical Sci., Min. Ed.)		
	Ryoichi	Katakai	(Gunma University)		
	Minoru	Kumakura	(West Tokyo University)		
	Koichi	Ogura	(Nihon University)		
	Rikio	Yokota	(Inst. Space & Astronautical Sci., Min. Ed.)		
	Mutsuhide	Komaki	(JAERI)	Hideki	Omichi (JAERI)
m*	Masaru	Yoshida	(JAERI)		

12. Advanced Measurement of Functions in Living Bodies

	Shigeru	Inaba	(Tokyo Agricul. Univ.)
	Tomio	Ishihara	(Gunma Univ.)
	Hirotake	Kamei	(Electrotechnical Laroratory, MITI)
	Harumichi	Kobashi	(Gunma Univ.)
	Akihiro	Kusumi	(Tokyo Univ.)
	Fumiyuki	Mitsmori	(Nat. Inst. for Environmental Studies)
	Kuniaki	Nagayama	(JEOL)
	Norio	Nakatsuji	(Meiji Milk Products Co.)
	Junkichi	Soma	(Kangawa University)
	Tadashi	Suzuki	(Gunma Univ.)
	Katsumi	Tomiyoshi	(Gunma Univ.)
m*	Takashi	Fujimura	(JAERI)

13. Nuclear Chemistry

	Masato	Asai	(Nagoya University)
	Toyokazu	Endo	(Showa Pharmac. Univ.)
	Manabu	Fujioka	(Tohoku University)
	Takayoshi	Horiguchi	(Hiroshima University)
	Toshiro	Kato	(Nagoya University)
	Kiyoshi	Kawade	(Nagoya University)
	Taichi	Miura	(Nat. Lab. for High Energy Physics (KEK))
	Hisakazu	Muramatsu	(Shinshu University)

Akihiko	Osa	(Nagoya University)			
Hiroshi	Yamamoto	(Nagoya University)			
Kazuyuki	Hashimoto	(JAERI)	Hiromitsu	Matsuoka	(JAERI)
Yuichi	Hatsukawa	(JAERI)	Takashi	Moriya	(JAERI)
Mishiroku	Izumo	(JAERI)	Shouji	Motoishi	(JAERI)
Katsutoshi	Kobayashi	(JAERI)	m* Toshiaki	Sekine	(JAERI)
Mitsumasa	Koizumi	(JAERI)	Niriko	Shigeta	(JAERI)
Hiroshi	Kudo	(JAERI)	Hirokazu	Umezawa	(JAERI)

14. Organic Functional Materials I.

Hideomi	Koinuma	(Tokyo Inst. Tech.)
Katsuhiko	Nakamae	(Kobe University)
Katsuo	Orihara	(Yamagata University)
Tatsuo	Wada	(Inst. of Phys. and Chem. Res. (RIKEN))
Fumio	Hosoi	(JAERI)
m* Hideki	Omichi	(JAERI)

15. Inorganic Functional Materials

Chiken	Kinoshita	(Kyushu University)			
Kazuo	Sato	(Institute for Metals)			
Shigemi	Furuno	(JAERI)	m* Hiroshi	Naramoto	(JAERI)
Kiichi	Hojou	(JAERI)	Kensuke	Shiraishi	(JAERI)
Hideo	Ohno	(JAERI)	Hidefumi	Takeshita	(JAERI)

16. Semiconductor Functional Materials

Toshihiko	Kanayama	(Electrotechnical Laboratory, MITI)
Satoru	Matsumoto	(Keio University)
Koichi	Murakami	(Tsukuba University)
Hiroki	Takita	(Tsukuba University)
m* Osamu	Yoda	(JAERI)

EXAFS Working Group

Sadao	Aoki	(Tsukuba University)
Koichi	Murakami	(Tsukuba University)
Naohiro	Yamaguchi	(Tsukuba University)
Atsumi	Miyashita	(JAERI)
m* Osamu	Yoda	(JAERI)

17. Ion Beam Analysis Technology

Kiyoshi	Kawatsura	(Kyoto Inst. Technology)
Kenichi	Komaki	(Tokyo University)
Hiroshi	Kudo	(Tsukuba University)
Kenji	Morita	(Nagoya University)
Shinji	Nagata	(Tohoku University)
Isao	Sakamoto	(Electrotechnical Laboratory, MITI)
Katsumi	Takahiro	(Tohoku University)
Hiroshi	Watanabe	(Electrotechnical Laboratory, MITI)

	Sadae	Yamaguchi	(Tohoku University)			
	Yasushi	Aoki	(JAERI)		Teikichi	Sasaki (JAERI)
	Yukio	Kazumata	(JAERI)		Shunya	Yamamoto (JAERI)
m*	Hiroshi	Naramoto	(JAERI)			

18. Positron Beam Application Technology

Working Group 1 (Construction Planning)

	Toshio	Hyodou	(Tokyo University)			
	Yasuo	Ito	(Tokyo University)			
	Hitoshi	Kobayashi	(Nat. Lab. for High Energy Physics (KEK))			
	Tomohisa	Mikado	(Electrotechnical Laboratory, MITI)			
	Shoichiro	Tanigawa	(Tsukuba University)			
	Katsuo	Mashiko	(JAERI)		Hiroyuki	Tachibana (JAERI)
m*	Sohei	Okada	(JAERI)		Keiichi	Yotsumoto (JAERI)
	Hiromi	Sunaga	(JAERI)			

Working Group 2 (Positron Beam Technology)

	Takashi	Akabane	(Nat. Inst. Res. in Inorg. Mat., STA)
	Hideo	Hirayama	(Nat. Lab. for High Energy Physics (KEK))
	Yoshihide	Honda	(Osaka University)
m*	Yasuo	Ito	(Tokyo University)
	Ikuzo	Kanazawa	(Tokyo Gakugei University)
	Hitoshi	Kobayashi	(Nat. Lab. for High Energy Physics (KEK))
	Susumu	Nanao	(Tokyo University)
	Nobuhiro	Shiotani	(Tokyo Univ. of Fisheries)
	Yasuyuki	Suzuki	(Mie University)
	Sohei	Okada	(JAERI)

Working Group 3 (Research Theme)

	Toshinobu	Chiba	(Nat. Inst. Res. in Inorg. Mat., STA)
	Masayuki	Hasagawa	(Tohoku University)
	Hikaru	Ishii	(Tottori University)
	Osamu	Sueoka	(Yamaguchi University)
m*	Shoichiro	Tanigawa	(Tsukuba University)
	Sohei	Okada	(JAERI)
	Saburo	Takamura	(JAERI)

19. Low Energy Ion Beam Technology

	Junzo	Ishikawa	(Kyoto University)
	Minoru	Kojima	(Osaka University)
	Eiji	Kamijo	(Ryukoku University)
	Masuhiro	Ogoma	(Sophia University)
	Minoru	Tsuda	(Chiba University)
m*	Siro	Nagai	(JAERI)

10.4 Personnel

I. Department of Advanced Radiation Technology

Deputy Director: Isao Ishigaki

1. Ion Beam Research Administration Division

General Manager	Hiromasa	Watanabe		
Administrative Staff	Satomi	Yambe	Akihisa	Sakumoto *[1]
	Katsuyuki	Tomatsuri	Rie	Hayakawa *[1]
	Masamitsu	Washino *[1]		
Scientific Staff	Michio	Maruyama §	Takashi	Fujimura #[2]
	Yousuke	Morita #[2]	Siro	Nagai #[2]
	Okihiro	Tokunaga #[2]	Sohei	Okada #[2]
	Hiroshi	Watanabe #[3]		
Technical Staff	Nobuyoshi	Akiyama	Koichi	Nishimura
	Susumu	Tanaka		

2. Ion Accelerator Division

General Manager	Ryuichi	Tanaka		
Scientific Staff	Akio	Ozawa	Yuichi	Saito
	Watalu	Yokota	Nobuhiro	Utsunomiya*[4]
	Mitsuhiro	Fukuda	Hidenori	Yutoh *[4]
	Tomihiro	Kamiya	Eisuke	Minehara #[5]
	Susumu	Okumura		
Technical Staff	Keiichi	Yotsumoto	Kiyoshi	Mizuhashi
	Satoshi	Tajima	Takayuki	Nara
	Kazuo	Arakawa	Takashi	Agematsu
	Isao	Takada	Ikuo	Ishibori
	Yoshiteru	Nakamura		

II. Department of Administrative Services

Safety Division

General Manager	Yutaka	Anazawa
Administrative Staff	Takashi	Watanuki
Technical Staff	Yukio	Iwaya
	Kazuhiro	Sato

---

§ : Invited Researcher

* : detatched from [1] Radiation Application Development Association and [4] Nissin High Voltage Co., respectively.

\# : additional post, the main post being at [2] Dept. Material Development, [3] Dept. Radiat. Res. for Environment & Resources and [5] Department of Physics, respectively.